DETERMINATION OF FLUID VISCOSITIES FROM BICONICAL-ANNULAR GEOMETRIES: EXPERIMENTAL AND MODELLING STUDIES

A Dissertation

by

NOLYS JAVIER RONDON ALFONZO

Submitted to the Office of Graduate Studies of
Texas A&M University
in partial fulfillment of the requirements for the degree of

DOCTOR OF PHILOSOPHY

May 2008

Major Subject: Petroleum Engineering

DETERMINATION OF FLUID VISCOSITIES FROM BICONICAL-ANNULAR GEOMETRIES: EXPERIMENTAL AND MODELLING STUDIES

A Dissertation

by

NOLYS JAVIER RONDON ALFONZO

Submitted to the Office of Graduate Studies of
Texas A&M University
in partial fulfillment of the requirements for the degree of

DOCTOR OF PHILOSOPHY

Approved by:

Chair of Committee,	Maria Barrufet
Committee Members,	Thomas A. Blasingame
	Victor Ugaz
	Peter Valko
Head of Department,	Stephen A. Holditch

May 2008

Major Subject: Petroleum Engineering

ABSTRACT

Determination of Fluid Viscosities from Biconical-Annular Geometries: Experimental and Modeling Studies. (May 2008)

Nolys Javier Rondon Alfonzo, B.S., Universidad Central de Venezuela; M.Eng., Texas A&M University

Chair of Advisory Committee: Dr. Maria Barrufet

Knowledge of viscosity of flow streams is essential for the design and operation of production facilities, drilling operations and reservoir engineering calculations. The determination of the viscosity of a reservoir fluid at downhole conditions still remains a complex task due to the difficulty of designing a tool capable of measuring accurate rheological information under harsh operational conditions. This dissertation presents the evaluation of the performance of a novel device designed to measure the viscosity of a fluid at downhole conditions.

The design investigated in this study addresses several limitations encountered in previous designs. The prototype was calibrated and tested with fluids with viscosities ranging from 1 to 28 cp under temperatures ranging from 100 to 160^{o}F. Viscosity measurements were validated with independent measurements using a Brookfield viscometer. We proposed a mathematical model to describe the performance of the device for Power-law fluids. This model describes the response of the device as a

function of the rheology of the fluid and the physical dimensions of the device. Experimental data suggests the validity of the model to predict the response of the device under expected operating conditions. This model can be used to calculate optimal dimensions of the device for customized target applications.

This is dedicated to my mother and father: Maria and Euclides and my sisters Janeth, Marialex and Virginia

ACKNOWLEDGMENTS

I would like to express my most sincere appreciation and gratitude to my committee chair, Dr. Maria Barrufet, for her continuous support and guidance throughout my time as a graduate student at Texas A&M University. I truly appreciate the dedication and heart she put into guiding me to achieve my goal. Thank you, Dr. Barrufet.

I also would like to thank Dr. Thomas Blasingame for his support, guidance and words of wisdom and for serving on my committee. Thank you.

I am also very thankful to my committee members, Dr. Peter Valko and Dr. Victor Ugaz, for the superb advice, comments and suggestions for the development of this work.

I wish to thank my mother and father for their never-ending support and encouragement during my studies, my sisters Janeth and Marialex for their support, and Virginia, for her incredible help during my graduate studies. I also would like to thank my friends since college, Jose Rivero and Meiling, who were my family while in College Station and helped me achieve this goal.

I also wish to thank Dr. Gary Lehring for his friendship, his wit, and his help with the preparation of my dissertation, and Dr. Terry Honan for his tremendous help and contribution to this work.

TABLE OF CONTENTS

Page

CHAPTER Page

Page

LIST OF FIGURES

Page

Page

Page

Page

Page

Page

LIST OF TABLES

Page

Page

Page

CHAPTER I

INTRODUCTION

The study of rheological properties of fluids is a key aspect in many fields of engineering. Knowledge of the viscosity of flow streams in petroleum engineering is essential to the proper design and operation of production facilities, startup pumping requirements, drilling operations and reservoir engineering calculations. Fluid viscosity is usually measured by taking and testing fluid samples under conditions that might be very different from the actual flow conditions in the pipelines or the reservoir. Real time monitoring of viscosity under actual flowing conditions has a number of potential applications in fluid characterization, well control, mud logging, and fracture fluid analysis.

The objective of this study is to assess the potential of a new device with a tapered conical geometry as an online sensor to monitor viscosity in real time. This device was recently designed and patented by Halliburton with the purpose of being used as an online sensor for petroleum engineering applications. A secondary objective is to

---

This dissertation follows the style of *SPE Journal.*

develop a fundamental model to evaluate the rheological behavior of the fluid in a conical annular geometry and to use this model to improve the design of the tool for different applications.

1.1 Definition of the Problem

Viscosity is a property that describes the resistance of the fluids to flow. Measuring it with accuracy is fundamental to many industrial applications because it defines the very nature of the flow. In the oil and gas industry, knowledge of this property at actual flowing conditions is extremely important. Particularly in drilling operations, with the emphasis on directional drilling and ultra deep wells, there is a need for instrumentation that allows for careful monitoring of mud quality and rheological properties at downhole conditions. The effects of pressure, temperature and composition in the rheology of highly non-newtonian drilling and fracturing fluids can be difficult to measure unless highly specialized laboratory equipment is used.

Several devices and methods have been used to measure downhole information during drilling of wells. These tools are typically known as measurement-while-drilling (MWD) tools. The main objective of these tools is to capture information about the rock formation and the physical condition of the wellbore. However, most measurements taken for fluid rheology are conducted by analyzing samples collected from the fluid in the surface. These measurements result in rheological parameters that may not accurately represent the nature of the fluid at downhole conditions and can lead to

erroneous estimations and predictions. Therefore, there is definitely a need for methods and devices specially designed to accurately determine the viscosity of a reservoir fluid in situ.

More importantly, there is a need to understand, recognize and characterize the flow behavior of any type of fluid to be able to assess the impact of different flow variables (rate, type of fluid) and geometrical characteristics on the device response. This fundamental modeling of the design will allow optimization and fluid characterization for Newtonian and non-Newtonian fluids.

1.2 Importance of the Study

The determination of the viscosity of a reservoir fluid at downhole conditions still remains a complex task. There is the difficulty of designing a tool that is capable of withstanding the demands of high pressure and high temperature operating conditions.

The design investigated in this study addresses several of these issues and provides measurements that can be used to monitor the rheological properties. Information from the viscosity sensor can be processed by a downhole processor or by a computer at the surface. A surface computer can then display the pressure responses that are processed to obtain the rheological information in a tabular of graphical form. This research will describe the performance of the device and develop a generalized model to characterize

Newtonian and non-Newtonian fluids alike and offer recommendations on future improvements on this design.

1.3 Objectives

There are two basic objectives in the proposed research. The first is to evaluate experimentally the performance of the device as a sensor by validating its resolution and accuracy against fluids with known viscosity values. A second objective is to optimize the physical dimensions of the device depending on the desired application. With this intention, we will derive a mathematical model that describes the pressure response of the device under a variety of flow scenarios, fluids types and geometrical features.

To accomplish each one of these objectives we will carry out the following stages:

Conduct a systematic evaluation of the sensor by designing selective experimental tests to:

- Design and construct a flow loop to conduct experiments and data acquisition software
- Calibrate the sensor
- Evaluate sensor performance with different types of fluids
    - Newtonian
    - Non-Newtonian (power-law)

Facilitate the evaluation and optimization of the sensor dimensions based on the anticipated range of flow and type of fluid by:

- Developing a fundamental model of the response of the sensor including geometrical variables.
- Generalizing this response to Newtonian and Non-Newtonian fluids

The first objective of this research is aimed at obtaining a basic envelope of the sensor performance, that is, the pressure response to changes in flow rate. We conducted preliminary experiments using Newtonian fluids, and the results suggest that the device produces consistent and repeatable measurements under laminar flow regime. Therefore, the natural progression in the investigation is to use non-Newtonian fluids following the power-law model in order to expand the usefulness of the sensor.

Apart from testing the basic response of the sensor, the experimental setup can be used to investigate the sensitivity of the measurements to changes of fluid viscosity caused by contamination. Preliminary experiments show the sensitivity of the sensor to detect changes in viscosity of oil mixtures as a function of different blending ratios.

For our second objective we will use the known sensor geometry and develop a mathematical model that describes the pressure drop as a function of flow rate and the sensor geometry. Our goal is to provide a model that is portable and easy to use.

1.4 Deliverables

We believe that the results obtained in this research validate the basic performance of the sensor design. All valuable experimental data of viscosity and the computer codes developed in this research are certainly useful for further study and continuous improvement of this solution.

In specific in this research, we present the following products:

- Complete description of sensor performance for Newtonian and non-Newtonian fluids (power law).
- Development of a simple model to determine the rheological parameters for Newtonian and Power Law fluids in the sensor.
- Generation of curve types, simplified models for quick estimation of the response of the sensor.
- Software to model analytically and numerically the response of the sensor, using several approximations.
- Provide optimization criteria (geometry, operating conditions) for specific applications.

1.5 Organization of the Dissertation

The outline of the proposed dissertation is as follows:

- Chapter I- Introduction
    - Definition of the Problem
    - Importance of the Study

- Objectives
- Deliverables
- Organization of the Dissertation

- Chapter II– Background Research
  - Literature Review
  - Rheology Basics
  - Finite Element Method
  - Rheometry Measurements
- Chapter III- Description of the Solution
  - Description of the Sensor Design
- Chapter IV Experimental Evaluation of the Sensor Response
  - Experimental Methodology
  - Experimental Procedure
  - Effect of spring Mechanism on Sensor Response
  - Experimental Results, Characterization, Dilution Tests, non-Newtonian fluids
- Chapter V- Simulation of the Sensor Response
  - Approximation as Concentric Cylinders
  - Slot Flow Approximation
  - Finite Element Method Solution
- Chapter VI- Discussion of Results
- Chapter VII- Conclusions and Recommendations for Future Work
  - Conclusions
  - Recommendations
- Nomenclature
- References
- Appendix
- Vita

CHAPTER II

BACKGROUND RESEARCH

2.1 Literature Review

It is our interest in this section to give an overview of the experiences reported in the literature in obtaining viscosity data from online viscometers.

Maglione, Robotti and Romagnoli[1-2] investigated the use of the drilling well as a viscometer and determined the in-situ rheological parameters and behavior of drilling mud circulating in the well using the pump flow rate and stand pipe pressure. The Hershel-Bulkley rheological parameters obtained from the laboratory measurements differed substantially from the parameters derived from the readings taken at the well. The disagreement between laboratory and field can be explained when looking at the experimental procedures. The rheological parameters are estimated using rotational viscometers simulating rotational flow, while in the well; the flow is purely axial flow or a combination of both rotational and axial flow. Their results suggest that the viscosity is sensitive to changes to the mud structure, pressure and temperature. The authors recommend the use of drilling well data to obtain the true effective rheological behavior of the mud.

Chen *et al*[3,4] discuss the experimental procedure to investigate the rheological behavior of a series of polymer based drilling foams. The characterization was done using a single-pass pipe viscometer and a rotational viscometer. For this type of fluid, wall slip effects are present and the rheological parameters are derived with pipe viscometer data with a correction for the slip effects.

Kalotay[5] described the use of Coriolis mass flowmeters as in-situ viscosity sensors. Using the capillary viscometry principles it is possible to measure Newtonian viscosity using this device. The application of the technique for non-Newtonian fluids is suggested but not described.

Dealy[6], Tucker[7] and O'Connor[8] presented very detailed literature reviews describing the state of the art in process control and viscosity measurement in the food industry. Tucker[7] affirms that the importance of these measurement systems is to provide values of viscosity as a means to monitor product quality and controlling intermediate processes. The use of traditional laboratory viscometers is limited since a number of these devices cannot be operated a high temperatures and pressures or are suitable for harsh operating conditions. Tube viscometers

O'Connor[8] describes in great detail the use of real time pipe viscometers to measure rheological properties in the dairy industry. The author presents a concise step by step methodology to select the appropriate viscometer for real time measurements. The

author points out the need for improved technologies for integrated plant control capable of making good use of the viscosity information for process control, specially the integration of viscosity data with temperature.

Zimmer, Haley and Campanella[9] investigated the performance of rotational and tube type in-line viscometers with Newtonian and non-Newtonian fluids. The authors concluded that the devices could not measure rheological properties accurately without additional calibration efforts. The authors affirm that different calibration functions may be necessary depending on the shear rates applied.

Steffe[10] published a very detailed literature review on experimental rheological measurements and techniques in the food industry. He lists the most important sources of error in operating tube viscometers such as kinetic energy loses, end effects, turbulence effect and wall effects.

Enzendonfer *et al*[11] described the characterization of foam rheology using a small-scale pipe viscometer with five pipe diameters. The discrepancies in the results suggested that wall slip effects affected the measurements. The authors used the Oldroyd-Jastrzebski slip correction and obtained corrected flow curves.

For analytical methods to model the flow in geometries similar to the viscosity sensor, we are interested in analytical models developed for non Newtonian flow in geometries similar to the geometry of the viscosity sensor.

Fredrickson and Bird[12] presented the first exact solution of the laminar flow of a non-Newtonian fluid in concentric annuli. They showed analytical derivations for power-law and Bingham fluids and derived type curves to approximate the solution for drilling engineering applications.

Hanks and Larsen[13] presented a simple algebraic solution for the problem of power-law fluid in laminar flow in concentric annuli. The solution is valid for all values of the flow behavior index and is simpler to calculate.

Prasanth and Shenoy[14] presented a generalized expression to calculate the flow profile of a power-law fluid in a concentric annulus in both axial and tangential flow. The solution is a further development of the solution presented by Hanks and Larsen.

Tuoc and McGiven[15] proposed a simpler analytical derivation by matching the Mooney-Rabinowitsch equation between the limiting cases of flow in cylindrical pipes and flow between parallel plates by using the concept of equivalent diameter and a shape factor to account for the difference in geometry. The obtained experimental data matches the proposed model with good agreement.

Escudier, Oliveira and Pinho[16, 17] presented extensive results of numerical simulations of laminar flow of power-law and Hershel-Bulkley fluids in annuli, including effects of eccentricity and rotation of the inner cylinder. The numerical results were compared with experimental data for shear thinning fluids in concentric and eccentric annuli and found good agreement even when neglecting viscoelastic effects.

Vatistas and Ghaly[18] presented an analytical derivation and numerical solution for the flow of Newtonian fluids in conical gaps with common apex. The authors demonstrate that at low Reynolds number and narrow conical passages, the flow is similar to the parabolic profile of Poiseuille's flow.

Ulev[19,20] presented a different solution to the problem of flow of Newtonian fluids at low Reynolds number between conical surfaces. The solution presented allows for the calculation of flow profiles for annuli formed between coaxial cones with and without a common apex. The solution is also extended to conical gaps with variable cross section.

Shenoy[21] presents a review of different types of annular flow models for power-law fluid. He presents approximate solutions to model power-law flow inside conical annular dies which are derived from concentric cylinder solutions.

To fully model the flow of non-Newtonian fluids, another approach is to solve the equations of motion and continuity in order to determine the pressure and velocity field of the fluid. There is a substantial volume of work developed in many decades of research in this area and as a result, a wide variety of tools and open source numerical codes are readily available for modification. Of our particular interest are the tutorials and codes provided by Nassehi[22] Huang *et a*l[23] and Heinrich and Pepper[24]. These codes provide the foundation block ready to modify and reuse to develop the model for the sensor.

2.2 Rheology Basics

Rheology is the study of deformation and flow of matter. It attempts to describe the relationship between force on a material, and its resulting deformation. This chapter presents the basic terms, equations and experimental techniques used to determine the viscous properties of fluids, with emphasis in those that are of interest for petroleum engineering applications.

The measurement of rheological properties of fluids requires the definition of the parameters that describe deformation and flow behavior. Let us consider the flow between two large parallel plates as shown in **Fig. 2.1**. One plate is fixed and the other moves with velocity v_x in the x direction by a force **F** acting parallel to the plate.

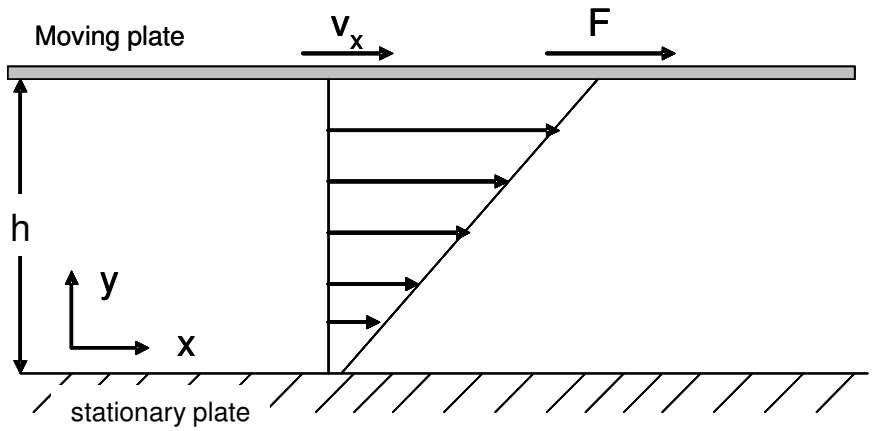

Fig. 2.1— Simple shear.

In this simplified geometry known as simple shear, the fluid deformation resembles a stack of layers. The ratio of the force *F* per unit area of the surface being subjected to the force is known as *shear stress*, defined by Eq. 2.1

$$\tau = \frac{F}{A}. \quad \text{..... (2.1)}$$

The *shear rate* is the change in velocity of the fluid with the distance from one plate to another.

$$\dot{\gamma} = \frac{dv_x}{dy}. \quad \text{..... (2.2)}$$

It is then clear that the shear rate will be a function of the distance *y* as well as of any other variables that describe the velocity of the fluid v_x. To finish the description of the flow in this geometry, it is necessary to obtain a mathematical relationship between the shear rate and the shear stress. These expressions are known as rheological models.

Newtonian Model

The simplest model describing the flow behavior of a liquid is a linear relationship between shear rate and shear stress:

$$\tau = \mu\dot{\gamma}. \quad \text{..... (2.3)}$$

The constant μ is known as *viscosity,* and it is commonly used to characterize the fluid's resistance to flow. The typical units of viscosity are dyne-sec/cm^2 or poise. 1 poise = 100 centipoise. In the metric system, viscosity is expressed as Pa-sec.

The flow behavior of a large number of substances, such as water, mineral and vegetal oils and other low molecular weight fluids can be modeled accurately with the Newtonian model. Other complex fluids, such as emulsions, suspensions or fluids with long molecular chains, such as polymers, cannot be accurately described with this model, therefore, more complex models have been created to describe complicated behaviors

Bingham Model

This model describes plastic materials that behave as solids, unless a stress greater than the *yield stress* τ_y is applied:

$$\tau - \tau_y = \mu_p\dot{\gamma}. \quad \text{..... (2.4)}$$

This model can describe the flow of fluids such as cement slurries and certain drilling muds for a limited range of shear rates. The viscosity for these fluids is known as *plastic viscosity* μ_p.

Power Law Fluid Model

For most fluids, the relationship between shear stress and shear rate is not the linear form shown in Eq. 2.3. Many fluids show rapid changes in viscosity as a function of the shear rate. For some of these fluids, the following expression is used:

$$\tau = k\dot{\gamma}^n . \quad \text{..... (2.5)}$$

The exponent n is known as the flow behavior index and it describes the degree of non-newtonian behavior of the fluid. The consistency index k is a measure of the fluid consistency analogous to viscosity.

For power law fluids, $n < 1$ indicates that the viscosity decreases as shear rate increases. This is called a shear thinning fluid, or pseudoplastic fluids. Fluids with $n > 1$ are known as shear thickening or dilatant fluids. These fluids will show an increase in viscosity as the shear rate increases. For a Newtonian fluid, $n = 1$ and the power law model reduces to Eq.2.3. **Fig. 2.2** shows the different rheological models.

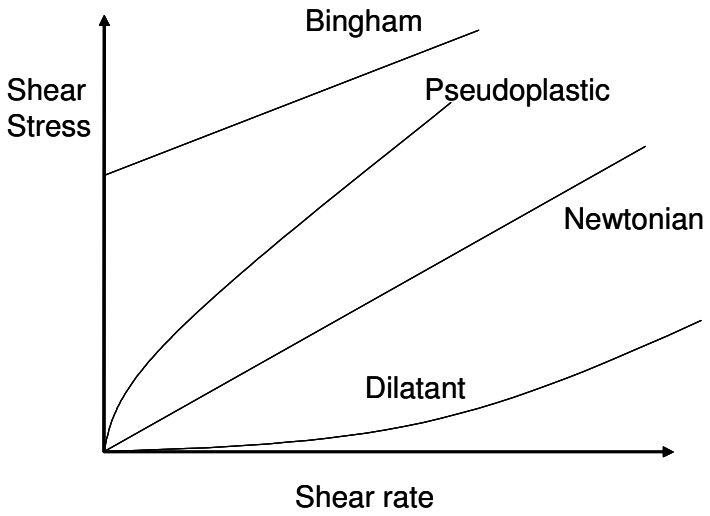

Fig. 2.2— Rheological behavior of Newtonian and non-Newtonian fluids.

A large number of rheological models have been proposed to model flow behavior of different materials. For example:

Herschel-Bulkley Model

$$\tau = \tau_0 + k\dot{\gamma}^n . \quad \text{..... (2.6)}$$

In this model for $\tau < \tau_0$ the material does not flow.

Robertson and Stiff Model

$$\tau = A(\dot{\gamma} + C)^B , \quad \text{..... (2.7)}$$

where *A, B* and *C* are model parameters. *A* and *B* are analogous to *k* and *n* of the power law model.

Casson Model

$$\dot{\gamma} = 0 , \quad \text{for } \tau < \tau_c , \quad \text{..... (2.8)}$$

$$\tau^{\frac{1}{2}} = \tau_c^{\frac{1}{2}} + \mu_c^{\frac{1}{2}} \dot{\gamma}^{\frac{1}{2}}, \quad \text{for } \tau > \tau_c . \quad \text{..... (2.9)}$$

where τ_c is the Casson yield stress and μ_c is the Casson plastic viscosity. This model was developed to describe the behavior of suspensions

Ellis Model

$$\tau = c_1 \dot{\gamma} + c_2 \dot{\gamma}^n , \quad \text{..... (2.10)}$$

where c_1 and c_2 are model parameters. This model shows Newtonian behavior at low stress and power law behavior at high stress.

Several other complex fluids like polymers show other rheological phenomena such as recoil and stress relaxation that are not possible to model as viscous fluids. These fluids show a behavior that is a combination of properties of elastic solids and viscous fluids and have been studied extensively as well.

2. 2. 1 Deformation and Stress Tensor

Stress is the internal distribution of force per unit area or traction that balances and reacts to external loads applied to a body. Traction is a vector quantity. The deformation produced by a force **F** acting on or within a body is a function of the magnitude of such force per unit area; it does not depend on the magnitude of the force itself. To characterize the state of stress at any point in a body, the stress tensor **T,** is used.

To better illustrate the stress tensor, **Fig 2.3** shows a force **F** acting on a body. Around point P, we set up three perpendicular orthogonal planes aligned with a Cartesian coordinate system. This allows the stress state at point *P* to be described relative to *x*, *y*, and *z* coordinate directions. The stress at point P can be represented by an infinitesimal cube with three stress components on each of its six sides.

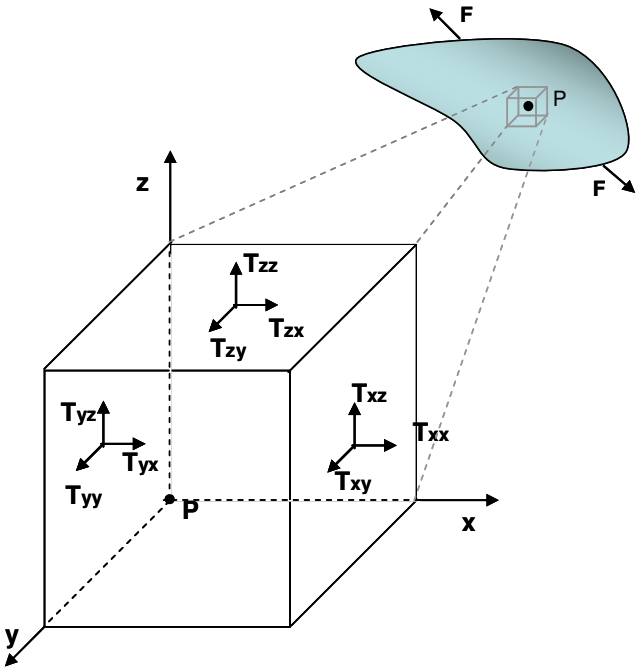

Fig. 2.3—Stress tensor components acting on perpendicular faces of a cube.

These components can be arranged in matrix notation as

$$\mathbf{T} = \begin{bmatrix} T_{xx} & T_{xy} & T_{xz} \\ T_{yx} & T_{yy} & T_{yz} \\ T_{zx} & T_{zy} & T_{zz} \end{bmatrix}. \quad \text{..... (2.11)}$$

The traction or surface stresses acting on an internal datum plane, are typically decomposed into three mutually orthogonal components. The component normal to the surface is known as normal stresses: T_{xx}, T_{yy}, T_{zz} . The other two components tangential to the surface represent the shear stresses.

If $\mathbf{t_n}$ is the stress induced by a force acting on a surface perpendicular to an arbitrary unit vector **n,** then

$$\mathbf{t}_n = \mathbf{n} \cdot \mathbf{T}. \quad \text{..... (2.12)}$$

When a fluid is not in motion, the only stress acting on it is a uniform normal stress called hydrostatic pressure *p*. The stress tensor for the fluid in this rest condition is:

$$\mathbf{T} = \begin{bmatrix} -p & 0 & 0 \\ 0 & -p & 0 \\ 0 & 0 & -p \end{bmatrix}, \quad \text{..... (2.13)}$$

or

$$\mathbf{T} = -p\boldsymbol{\delta}, \quad \text{..... (2.14)}$$

where $\boldsymbol{\delta}$ is the unit tensor:

$$\boldsymbol{\delta} = \begin{bmatrix} 1 & 0 & 0 \\ 0 & 1 & 0 \\ 0 & 0 & 1 \end{bmatrix}. \quad \text{..... (2.15)}$$

The minus sign convention is because compression is considered to be negative.

When the fluid is in motion, there are extra stresses added to the hydrostatic pressure. We can write the stress tensor for the fluid in motion as the sum of two components:

$$\mathbf{T} = -p\boldsymbol{\delta} + \boldsymbol{\tau}. \quad \text{..... (2.16)}$$

The tensor $\boldsymbol{\tau}$, is known as the extra stress tensor.

The deformation of materials follows the relationship between stress and deformation, as well as the law of conservation of mass and the conservation of momentum.

2.2.2 Equation of Continuity

The continuity equation describes the law of conservation of mass. **Fig. 2.4** shows a control volume V. the velocity **v** is the flux velocity of the mass in and out of the control volume.

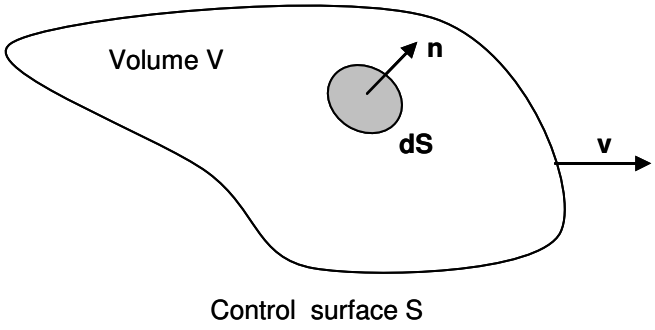

Fig. 2.4—Mass balance in a control volume V.

The mass of the body can be calculated as the integral of the density ρ over the volume V as:

$$m = \int_V \rho dV \ . \quad \text{..... (2.17)}$$

The rate of change of the mass in the control volume must be the same as the net flux of mass across the surface S.

$$\frac{dm}{dt} = \frac{d}{dt}\int_V \rho dV = \text{mass flux across } S \ . \quad \text{..... (2.18)}$$

According to the Reynolds transport theorem, if the volume integral of the field $f(\mathbf{x},t)$ is

$$F(t) = \int_V f(\mathbf{x},t) dV \ , \quad \text{..... (2.19)}$$

then the substantial derivative of $F(t)$ can be expressed as

$$\frac{dF(t)}{dt} = \int_V \frac{\partial}{\partial t} f(\mathbf{x},t) dV + \int_S f(\mathbf{x},t)\mathbf{v}\cdot\mathbf{n} dS \ , \quad \text{..... (2.20)}$$

where **v** is the flux velocity and **n** is the vector normal to the surface as indicated in Fig 2.4.

Using Eq. 2.19 then Eq. 2.18 is :

$$\frac{d}{dt}\int_V \rho dV = \int_V \frac{\partial}{\partial t}\rho dV - \int_S \rho \mathbf{v}\cdot\mathbf{n} dS \,. \quad \text{..... (2.21)}$$

The vector - **n** is used because we want the mass flux going into the volume.

If the density does not change with time then

$$\frac{d}{dt}\int_V \rho dV = -\int_S \rho \mathbf{v}\cdot\mathbf{n} dS \,. \quad \text{..... (2.22)}$$

Using the divergence theorem

$$\frac{d}{dt}\int_V \rho dV = -\int_V (\nabla\cdot\rho\mathbf{v}) dV \,. \quad \text{..... (2.23)}$$

Rearranging:

$$\int_V \left(\frac{\partial\rho}{\partial t} + \nabla\cdot\rho\mathbf{v}\right) dV = 0 \,. \quad \text{..... (2.24)}$$

Since the control volume is arbitrary, then it follows that

$$\frac{\partial\rho}{\partial t} + \nabla\cdot(\rho\mathbf{v}) = 0 \,. \quad \text{..... (2.25)}$$

If the fluid is considered incompressible, the density is constant and we can further simplify this expression as:

$$\nabla\cdot\mathbf{v} = 0 \,. \quad \text{..... (2.26)}$$

Or in terms of cartesian coordinates:

$$\frac{\partial u}{\partial x}+\frac{\partial v}{\partial y}+\frac{\partial w}{\partial z}=0 \ . \quad \text{..... (2.27)}$$

Eq. 2.26 is also known as the incompressibility constraint.

2.2.3 Equation of Motion

The momentum of the body is its mass times velocity. From Eq. 2.17:

$$m\mathbf{v}=\int_V \rho\mathbf{v}dV \ . \quad \text{..... (2.28)}$$

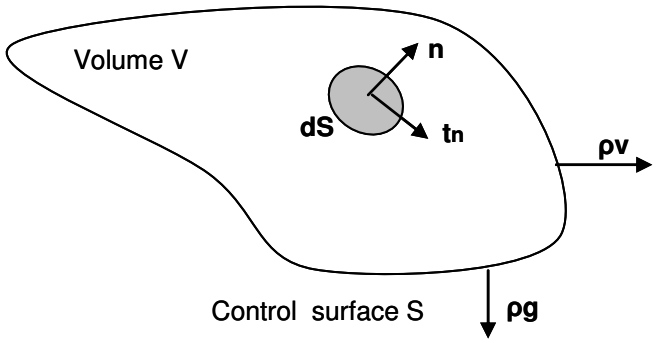

Fig. 2.5—Momentum balance on control volume V.

In the control volume shown in **Fig.2.5,** The momentum caused by the flow across the surface *S* is $\rho\mathbf{v}(\mathbf{n}\cdot\mathbf{v})dS$. The momentum due to the stress vector $\mathbf{t}_n$ acting on the surface *S* is $\mathbf{t}_n=\mathbf{n}\cdot\mathbf{T}$ and the momentum change due to gravity is $\rho\mathbf{g}dV$

Applying a momentum balance**,** and integrating, we obtain:

$$\frac{d}{dt}\int_V \rho\mathbf{v}dV=-\int_S \rho\mathbf{v}(\mathbf{n}\cdot\mathbf{v})dS+\int_S(\mathbf{n}\cdot\mathbf{T})dS+\int_V \rho\mathbf{g}dV \ . \quad \text{..... (2.29)}$$

Using the divergence theorem

$$\int_V \frac{\partial \rho \mathbf{v}}{\partial t} dV = -\int_V (\nabla \cdot \rho \mathbf{v}) \mathbf{v} dV + \int_V (\nabla \cdot \mathbf{T}) dV + \int_V \rho \mathbf{g} dV \,. \quad \text{..... (2.30)}$$

Since the control volume is arbitrary, it follows that

$$\rho \frac{\partial \mathbf{v}}{\partial t} = -\nabla \cdot \rho \mathbf{v}\mathbf{v} + \nabla \cdot \mathbf{T} + \rho \mathbf{g} \,. \quad \text{..... (2.31)}$$

$$\rho \frac{\partial \mathbf{v}}{\partial t} + \rho \mathbf{v} \cdot \nabla \mathbf{v} = \nabla \cdot \mathbf{T} + \rho \mathbf{g} \,. \quad \text{..... (2.32)}$$

The equation of motion is the law of conservation of momentum. This expression is:

$$\rho \frac{\partial \mathbf{v}}{\partial t} + \rho \mathbf{v} \cdot \nabla \mathbf{v} = \nabla \cdot \mathbf{T} + \rho \mathbf{g} \,. \quad \text{..... (2.33)}$$

Using Eq. 2.16 into Eq. 2.33 then the equation of conservation of momentum can be written as:

$$\rho \frac{\partial \mathbf{v}}{\partial t} + \rho \mathbf{v} \cdot \nabla \mathbf{v} = -\nabla p \boldsymbol{\delta} + \nabla \cdot \boldsymbol{\tau} + \rho \mathbf{g} \,, \quad \text{..... (2.34)}$$

where p is the hydrostatic pressure, $\boldsymbol{\delta}$ is the unit tensor and $\boldsymbol{\tau}$ is the extra stress tensor.

2.2.4 Velocity Gradient

The velocity of the fluid is considered to be a function of position and time $\mathbf{v}(\mathbf{x}, t)$. The velocity gradient tensor expresses the degree of change in velocity from one point to another in the fluid. The velocity gradient tensor in index notation is defined as

$$\nabla \mathbf{v} = \frac{\partial v_j}{\partial x_i}. \quad \text{..... (2.35)}$$

. In Cartesian Coordinates it is

$$\nabla \mathbf{v} = \begin{bmatrix} \frac{\partial v_x}{\partial x} & \frac{\partial v_y}{\partial x} & \frac{\partial v_z}{\partial x} \\ \frac{\partial v_x}{\partial y} & \frac{\partial v_y}{\partial y} & \frac{\partial v_z}{\partial y} \\ \frac{\partial v_x}{\partial z} & \frac{\partial v_y}{\partial z} & \frac{\partial v_z}{\partial z} \end{bmatrix}, \quad \text{..... (2.36)}$$

2.2.5 Rate of Deformation Tensor

In general, while in motion, the fluid experiences a combination of translational and rotational motion which is related to the deformation. The velocity gradient tensor can be decomposed into two parts

$$\nabla \mathbf{v} = \frac{1}{2}\left(\nabla \mathbf{v} + (\nabla \mathbf{v})^T\right) + \frac{1}{2}\left(\nabla \mathbf{v} - (\nabla \mathbf{v})^T\right). \quad \text{..... (2.37)}$$

The first term in the right hand side is called the rate of deformation tensor. This tensor is symmetric

$$\mathbf{D} = \frac{1}{2}\left(\nabla \mathbf{v} + (\nabla \mathbf{v})^T\right). \quad \text{..... (2.38)}$$

The components of this tensor are, in index notation:

$$D_{i,j} = \frac{1}{2}\left(\frac{\partial v_i}{\partial x_j} + \frac{\partial v_j}{\partial x_i}\right). \quad \text{..... (2.39)}$$

The second term in the right hand side is called the rotation or vorticity tensor. This tensor is antisymmetric.

$$\boldsymbol{\Omega} = \frac{1}{2}\left(\nabla \mathbf{v} - (\nabla \mathbf{v})^T\right). \quad \text{..... (2.40)}$$

The components of this tensor are, in index notation:

$$\Omega_{i,j} = \frac{1}{2}\left(\frac{\partial v_i}{\partial x_j} - \frac{\partial v_j}{\partial x_i}\right) \quad \text{..... (2.41)}$$

For flows that have no rotational motion, the velocity gradient tensor $\nabla \mathbf{v}$ is symmetric and the vorticity tensor $\boldsymbol{\Omega}$ is zero.

2.2.6 Constitutive Equations

A constitutive equation is an expression that relates the extra stress tensor and the rate of deformation of a fluid when it is flowing. Several constitutive equations have been developed to describe the flow of many complex fluids. However, for most petroleum engineering applications the following are the most commonly used.

Newtonian Fluids

For a Newtonian fluid, the extra stress tensor is proportional to the deformation tensor **D**. The scalar μ is a proportionality constant known as viscosity.

$$\boldsymbol{\tau} = 2\mu\mathbf{D}. \quad \text{..... (2.42)}$$

Or

$$\mathbf{T} = -p\boldsymbol{\delta} + 2\mu\mathbf{D}. \quad \text{..... (2.43)}$$

For example, for the simple shearing flow shown in Fig. 2.1, the velocity gradient tensor is

$$\nabla \mathbf{v} = \begin{bmatrix} 0 & 0 & 0 \\ \dot{\gamma} & 0 & 0 \\ 0 & 0 & 0 \end{bmatrix}. \quad \text{..... (2.44)}$$

The deformation tensor is then

$$D = \frac{1}{2}\begin{bmatrix} 0 & \dot{\gamma} & 0 \\ \dot{\gamma} & 0 & 0 \\ 0 & 0 & 0 \end{bmatrix}. \quad \text{..... (2.45)}$$

The stress tensor is:

$$\mathbf{T} = -p\begin{bmatrix} 1 & 0 & 0 \\ 0 & 1 & 0 \\ 0 & 0 & 1 \end{bmatrix} + \mu\begin{bmatrix} 0 & \dot{\gamma} & 0 \\ \dot{\gamma} & 0 & 0 \\ 0 & 0 & 0 \end{bmatrix}, \quad \text{..... (2.46)}$$

$$\mathbf{T}_{xy} = \tau_{xy} = \mu\dot{\gamma}. \quad \text{..... (2.47)}$$

This is the same as Eq. 2.3.

Generalized Viscous Fluids

For many fluids such as polymers and emulsions, the relationship between the stress tensor and the rate of deformation tensor is far more complex than the Newtonian constitutive model in Eq. 2.42. However, the stress is still a strong function of the rate of deformation only. A general expression describing this behavior is:

$$\mathbf{T} = -p\boldsymbol{\delta} + \eta_1\left(II_{2D}, III_{2D}\right)2\mathbf{D} + \eta_2\left(II_{2D}, III_{2D}\right)(2\mathbf{D})^2, \quad \text{..... (2.48)}$$

where II_{2D} and III_{2D} are the second and third invariant of the stress tensor and η_1 and η_2 are constants.

Both Newtonian model and power law model can be shown to be just special cases of the generalized model in Eq. 2.48. For example, for a Newtonian fluid, imposing $\eta_1(II_{2D}, III_{2D}) = \mu$ and $\eta_2 = 0$ we obtain the Newtonian model of Eq. 2.42.

For a power law fluid, the extra stress tensor is defined as:

$$\boldsymbol{\tau} = 2k\left|II_{2D}\right|^{\frac{(n-1)}{2}}\mathbf{D}, \quad \text{..... (2.49)}$$

where, *k* is the consistency index for the fluid in power law and *n* is the flow behavior index.

For the simple shearing flow of Fig. 2.1, the second invariant is

$$\left|II_{2D}\right| = \dot{\gamma}^2. \quad \text{..... (2.50)}$$

Then:

$$\mathbf{T} = -p\begin{bmatrix}1 & 0 & 0\\ 0 & 1 & 0\\ 0 & 0 & 1\end{bmatrix} + k\dot{\gamma}^{(n-1)}\begin{bmatrix}0 & \dot{\gamma} & 0\\ \dot{\gamma} & 0 & 0\\ 0 & 0 & 0\end{bmatrix}, \quad \text{..... (2.51)}$$

$$\mathbf{T}_{xy} = \tau_{xy} = k\dot{\gamma}^n. \quad \text{..... (2.52)}$$

This is the same as Eq. 2.5.

For a power law fluid, the extra stress tensor is defined as:

$$\boldsymbol{\tau} = 2k\left|II_{2D}\right|^{\frac{(n-1)}{2}}\mathbf{D}. \quad \text{..... (2.53)}$$

The momentum equation and the continuity equation can be written in a Cartesian coordinate system as follows:

$$\rho\left(\frac{\partial v_x}{\partial t}+v_x\frac{\partial v_x}{\partial x}+v_y\frac{\partial v_x}{\partial y}\right)=-\frac{\partial p}{\partial x}+\left(\frac{\partial \tau_{xx}}{\partial x}+\frac{\partial \tau_{yx}}{\partial y}\right)+\rho g_x,\ldots \quad (2.54)$$

$$\rho\left(\frac{\partial v_y}{\partial t}+v_x\frac{\partial v_y}{\partial x}+v_y\frac{\partial v_y}{\partial y}\right)=-\frac{\partial p}{\partial y}+\left(\frac{\partial \tau_{xy}}{\partial x}+\frac{\partial \tau_{yy}}{\partial y}\right)+\rho g_y,\ldots \quad (2.55)$$

$$\frac{\partial v_x}{\partial x}+\frac{\partial v_y}{\partial y}=0\,. \quad \ldots\ldots\ldots\ldots\ldots\ldots\ldots\ldots\ldots\ldots\ldots\ldots\ldots\ldots\ldots\ldots\ldots\ldots \quad (2.56)$$

In most situations of practical interest, these non-linear partial differential equations cannot be solved analytically; and numerical methods of solution are necessary. For engineering purposes, some degree of approximation is acceptable. Therefore, a common approach when solving fluid flow problems is to seek to simplify the original differential equations by removing those terms whose influence on the total fluid motion is sufficiently small. The resulting simplified equation is then solved.

For steady state conditions, the velocity field does not change with time. In the case of viscous flows at low velocities it is possible to simplify the momentum equation even further, by assuming that the inertial terms $\mathbf{v}\cdot\nabla\mathbf{v}$ are negligible.

$$-\nabla p+\nabla\cdot\boldsymbol{\tau}+\rho\mathbf{g}=0\,, \quad \ldots\ldots\ldots\ldots\ldots\ldots\ldots\ldots\ldots\ldots\ldots\ldots\ldots\ldots\ldots\ldots\ldots\ldots \quad (2.57)$$

This flow is described as creeping flow and it is suitable for description of viscous flows at low Reynolds number[22].

In a Cartesian coordinate system in two dimensions (x, y), the equations of motion for steady state low Reynolds are:

$$-\frac{\partial p}{\partial x}+\frac{\partial \tau_{xx}}{\partial x}+\frac{\partial \tau_{yx}}{\partial y}=0\,, \quad \text{..... (2.58)}$$

$$-\frac{\partial p}{\partial y}+\frac{\partial \tau_{xy}}{\partial x}+\frac{\partial \tau_{yy}}{\partial y}=0\,, \quad \text{..... (2.59)}$$

$$\frac{\partial v_x}{\partial x}+\frac{\partial v_y}{\partial y}=0\,. \quad \text{..... (2.60)}$$

2.3 Finite Element Method

The mathematical expressions describing viscous flow are a system of nonlinear partial differential equations. These equations generally cannot be solved using analytical techniques, except in the simplest problems. As a rule, these equations must be solved using numerical methods.

The numerical simulation of non Newtonian fluid flow consists in the formulation of a mathematical model consisting of the equations describing the relationship between the rate of deformation and flow, —conservation of mass and momentum, and the rheological model which describes the constitutive behavior of the fluids. This system of

equations defined over the domain of flow and coupled with well posed boundary conditions can then be solved using numerical methods.

Thanks to the availability of modern computational fluid dynamic codes and hardware resources, it is possible to model a wide range of practical fluid flow problems with a reasonable degree of accuracy. These tools and solvers are used in many industries to design, develop and enhance new products and industrial processes. To solve the differential equations commonly found in engineering, the problem is solved by discretization of the domain. This can be done using several methods, such as the finite differences method or the finite element method. The discreet problem is then solved for the limited number of points in the domain of interest. Finite element modeling is particularly attractive for flow problems because it is very flexible for modeling complex and boundary conditions. Nevertheless, this method is computationally very demanding[22].

The steps to solve a differential equation using the finite element method consist in the following:

1. Discretization of the solution region
2. Selection of Interpolation functions.
3. Assembly of element equations
4. Solution of the global system of equations
5. Calculation of additional results.

In order to solve the system of equations, the velocity variables and the pressure are considered as primary variables and are solved simultaneously. The flow equations are:

$$\nabla \cdot \mathbf{v} = 0, \quad \text{..... (2.61)}$$

$$\rho \frac{\partial \mathbf{v}}{\partial t} + \rho \mathbf{v} \cdot \nabla \mathbf{v} = -\nabla p \delta + \nabla \cdot \tau + \rho \mathbf{g}. \quad \text{..... (2.62)}$$

The pressure and velocities are approximated using shape functions:

$$\begin{aligned} \overline{\mathbf{v}} &= \sum_{i=1}^{n} N i v_I \\ \overline{p} &= \sum_{l=1}^{n} M_L p_L \end{aligned} \quad . \quad \text{..... (2.63)}$$

The weighted residual of the continuity and the equation of motion over an element in the mesh can be expressed as:

$$\begin{aligned} &\int_{\Omega_e} M_L \nabla \cdot \overline{\mathbf{v}} \, \mathrm{d}\Omega_\mathrm{e} = 0 \\ &\int_{\Omega_e} N_J \left(\rho \frac{\partial \overline{\mathbf{v}}}{\partial t} + \rho \overline{\mathbf{v}}^0 \cdot \nabla \overline{\mathbf{v}} \right) \mathrm{d}\Omega_\mathrm{e} = \int_{\Omega_e} N_J \left(-\nabla \overline{p} \boldsymbol{\delta} + \nabla \cdot \overline{\boldsymbol{\tau}} + \rho \mathbf{g} \right) \mathrm{d}\Omega_\mathrm{e} \end{aligned} \quad (2.64)$$

M_L and N_J are the weight functions. Ω_e is an element in the mesh. $\overline{\mathbf{v}}^0$ is the velocity from the previous iteration. For the system described in Eq. 2.64, the elements used to integrate in the system of equations must satisfy the stability condition known as the Babuska-Brezz condition, which states that the interpolating function for the pressure must be of a lower order than that of the velocities. If this condition is not satisfied, the

resulting solution may show mesh locking and oscillations in the pressure field. Different shapes of elements, such as triangles and quadrilateral are typically used to discretize the flow region and satisfy this condition.

2.3.2 Penalty Method

The penalty method is based on the expression of pressure in terms of the incompressibility condition, or continuity equation as

$$p = -\lambda(\nabla \cdot \mathbf{v}), \quad \text{..... (2.65)}$$

where λ is a very large number called the penalty parameter. Eq. 2.65 can be considered as a form of the continuity equation that can be applied to slightly compressible flow regimes. This formulation is very useful since it allows solving the flow equations by eliminating the pressure variable, reducing the size of the system of equations and therefore requires less computing resources.

Substituting the pressure in Eq. 2.65 in Eq. 2.62

$$\rho \frac{\partial \mathbf{v}}{\partial t} + \rho \mathbf{v} \cdot \nabla \mathbf{v} = -\nabla(-\lambda(\nabla \cdot \mathbf{v}))\delta + \nabla \cdot \tau + \rho \mathbf{g}, \quad \text{..... (2.66)}$$

then:

$$\int_{\Omega_e} M_L \nabla \cdot \bar{\mathbf{v}} \, d\Omega_e = 0, \quad \text{..... (2.67)}$$

$$\int_{\Omega_e} N_J \left(\rho \frac{\partial \bar{\mathbf{v}}}{\partial t} + \rho \bar{\mathbf{v}}^0 \cdot \nabla \bar{\mathbf{v}} \right) \mathrm{d}\Omega_\mathrm{e} = \int_{\Omega_e} N_J \nabla \left(\lambda \nabla \cdot \mathbf{v} \right) \boldsymbol{\delta} \mathrm{d}\Omega_\mathrm{e} +$$

$$+ \int_{\Omega_e} N_J \nabla \cdot \bar{\boldsymbol{\tau}} \, \mathrm{d}\Omega_\mathrm{e} + \int_{\Omega_e} N_J \rho \mathbf{g} \, \mathrm{d}\Omega_\mathrm{e} \, . \quad \text{..... (2.68)}$$

The value of the penalty parameter is normally set to the highest value that the computer can handle, which is limited by the word length of the computer. Typically most commonly accepted values[22, 23] are in the range of 10^7-10^9. If the penalty parameter is set too high, the system of equations may become ill-conditioned. If the parameter is set too low, the conservation of mass equation will not be satisfied.

2.4 Online Rheometry Measurements

Steffe[10] classifies the instrument to measure rheological properties according to the type of shear flow they induce. **Fig. 2.6** shows his proposed classification for these instruments.

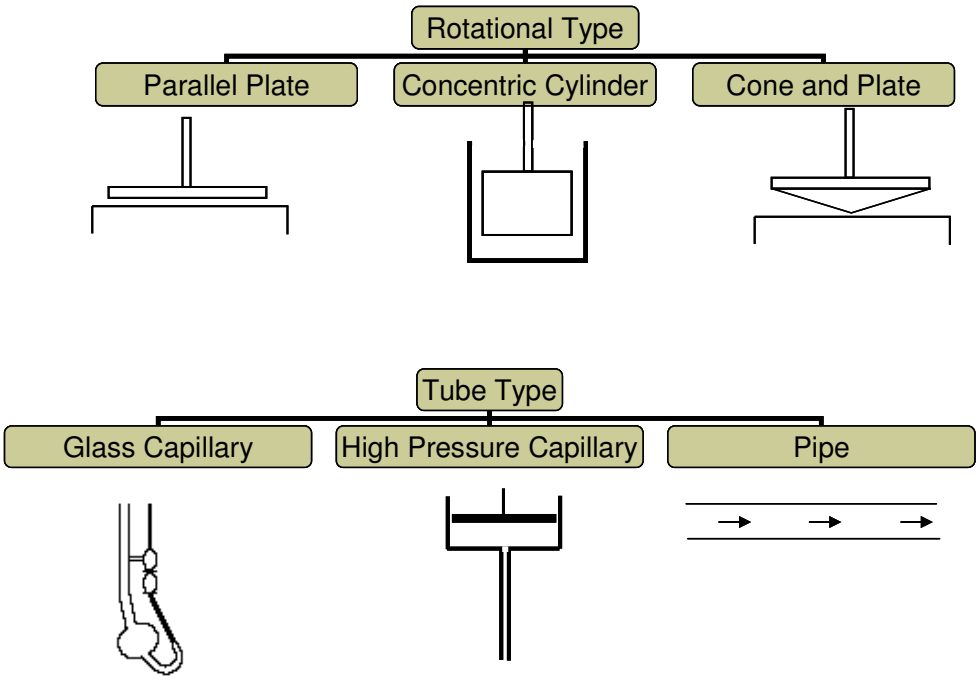

Fig. 2.6— Typical rheological instrument. (from Steffe[10]).

Common instruments capable of measuring fundamental rheological properties of fluids may be placed into two general groups, rotational type and tube type devices.

Rotational systems such as parallel plates, concentric cylinders and cone and plate rheometers are used to investigate time dependent behavior. They can be operated in steady shear or in dynamic mode. These systems are expensive in general and require careful calibration and maintenance.

Tube type systems include glass capillary tubes, high pressure capillaries and pipe systems. These devices are simpler to operate and are less expensive. High pressure

capillaries can operate at high shear rates and pipe viscometers can be built to handle large volumes of fluids in challenging operating environments.

Online viscometers are widely available in the market. These devices have been extensively used in process control in many industries, Food, cosmetics, inks and others have extensive experience dealing with viscosity measurements under process conditions. These systems can be installed directly in the process line or can make measurements on a side stream or bypass loop. The vast majority of online viscometers used correspond to concentric cylinders, vibrational and falling piston viscometers. These instruments are typically installed in a process line and will remain installed permanently.

Pipe viscometers use the relationship between volumetric flow and pressure drop to estimate viscosity[25]. This relationship applies to single phase fluids in fully developed laminar flow through a straight pipe of uniform cross-sectional area. End effects are negligible and there is no slip at the walls. The sensors required for tube viscometry are two or more pressure transducers to measure the pressure drop across a length of pipe and a volumetric flow meter to measure the flow rate, making their construction very easy. The operation of pipe viscometers is well documented. Steffe[10] and Macosko[25] present an extensive treatment of these devices.

The main disadvantage of these systems is that long pipes may be necessary to create a pressure drop large enough to be measurable. This can make them unpractical if space is limited. Also, the data acquisition electronics placement can be difficult. In addition depending on the particular installation and type of fluids, end effects, wall effects, solid deposition and the lack of temperature control can affect the results and make operation difficult.

CHAPTER III

DESCRIPTION OF THE SOLUTION

3.1 Description of the Sensor Design

The physical basis for the viscosity sensor is the measurement of differential pressure over a region for which the flow regime is laminar. The viscosity sensor consists of a downhole tool in which the viscosity of reservoir fluids can be determined according to Poiseuille's Law. The isothermal laminar flow of a Newtonian fluid through a straight tube with circular cross sectional area is described as:

$$\Delta P = \frac{128L}{\pi D^4}\mu Q, \quad \text{..... (3.1)}$$

where Q is the flow rate, ΔP is the differential pressure, L is the length of the tube, D is the diameter of the pipe and μ is the viscosity. **Eq. 3.1** is considered valid for laminar flow, which occurs at Reynolds numbers less than 2100. The Reynolds number for a pipe is calculated as:

$$N_{\mathrm{Re}} = \frac{v\rho D}{\mu}, \quad \text{..... (3.2)}$$

where ρ is the fluid density and v is the fluid velocity.

At the entrance of the pipe the flow regime may not be laminar; however, if the pipe is sufficiently long, the entrance effects can be neglected. The minimum length to ignore the effects can be evaluated from the following expression[10]:

$$\frac{X_e}{D} = 0.55 + 0.055 N_{\mathrm{Re}} . \quad \text{..... (3.3)}$$

Where X_e is the distance required to achieve 98% of fully developed flow. Additionally there will be an additional pressure loss caused by sudden changes in geometry at the opening of the tube and the exit.

Assuming that these additional pressure losses are small and that the flow regime inside the sensor is laminar we can then rearrange Eq. 3.1 to describe the pressure drop as a function of viscosity and flow rate.

$$\Delta P = f \mu Q , \quad \text{..... (3.4)}$$

where

$$f = \frac{128L}{\pi D^4} . \quad \text{..... (3.5)}$$

The parameter f reflects the particular geometry of the cross section of flow passage, in this case a straight tube with circular cross sectional area. However, Eq. 3.4 can be used

to describe the pressure drop for flow geometries with a hydraulic diameter that preserves a laminar flow regime.

The parameter *f* can be calculated using the hydraulic diameter of the system or can be determined experimentally by measuring the response of pressure drop as a function of the flow rate for a fluid of known viscosity.

Since the materials used in construction of the sensor are subject to thermal expansion and contraction, *f* will also be a function of temperature.

The method[26] for determining the viscosity of a reservoir fluid consists then in connecting the sensor to a stream of the fluid at its actual flow conditions and measuring the pressure differential between the inlet and outlet. Alternately, one could impose a pressure differential, and observe the flow rate. The value of viscosity can be calculated using Eq. 3.4.

To hinder the development of deposits inside the sensor and prevent the sensor from being plugged, it is necessary to sustain high flow velocity in the laminar flow region of the sensor. However, at the same time, the Reynolds number must be kept low enough to preserve the laminar flow regime where Eq. 3.4 is valid. One solution is to force the fluid through an annulus with a narrow gap, such as that provided by concentric

cylinders or conical elements of nearly the same radii. **Fig. 3.1** shows the annular gap of the sensor.

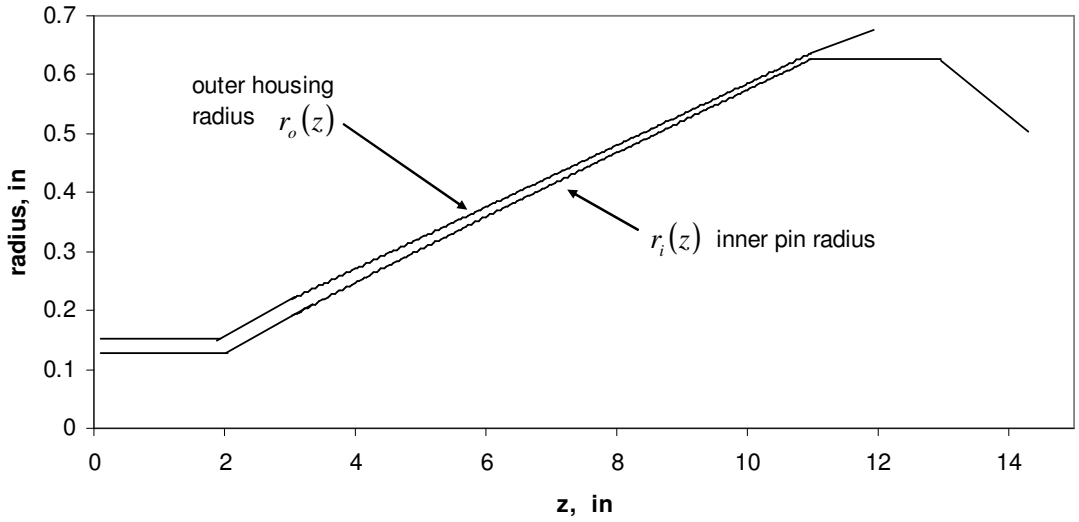

Fig. 3.1— Schematic of the prototype laminar flow viscosity sensor. Flow passage.

The prototype sensor consists of a conical inner member and an outer member whose inner surface is described by a function such that the annular area is constant throughout the active length of the sensor. This results in a constant average flow velocity through the sensor. **Fig. 3.2** describes the geometry of the sensor.

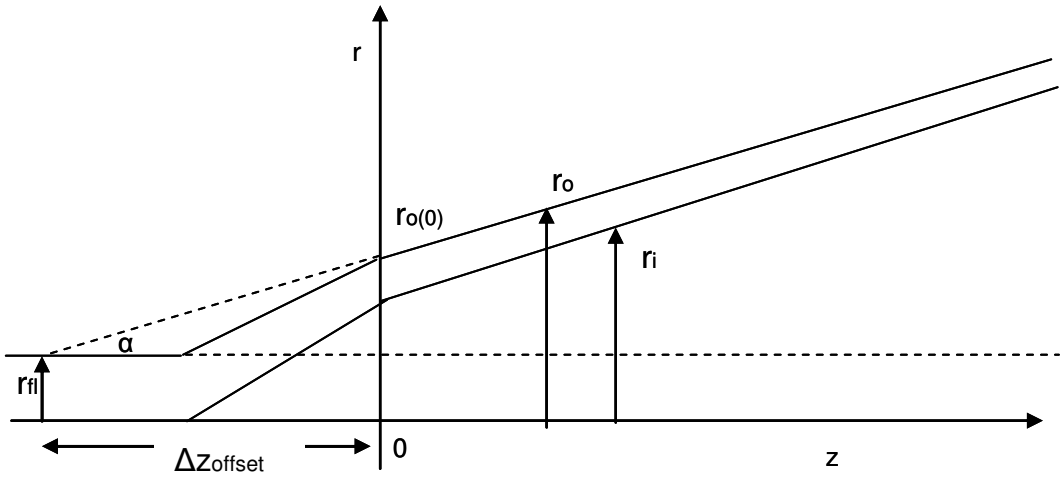

Fig. 3.2— Geometrical configuration of the prototype laminar flow viscosity sensor.

Since the annular area is constant between the surfaces of the inner pin and outer casing, then:

$$\pi r_{fl}^{\,2} = \pi\left[r_o(z)^2 - r_i(z)^2\right], \quad \text{..... (3.6)}$$

$$r_{fl}^{\,2} = r_o(z)^2 - r_i(z)^2 . \quad \text{..... (3.7)}$$

Where r_{fl} is the flow line radius, r_o is the outer housing radius, r_i is the internal radius of the inner pin respectively, as shown in Fig. 3.2.

The offset length Δz is:

$$\Delta z = \frac{r_o(0) - r_{fl}}{\tan(\alpha)}. \quad \text{..... (3.8)}$$

The initial outer housing radius $r_o(0)$ is a design parameter. The outer housing surface radius r_o function is then is described as:

$$r_o(z) = r_{fl} + (z + \Delta z)\tan(\alpha). \quad \text{..... (3.9)}$$

The inner conical pin surface radius r_i is described as:

$$r_i(z) = \sqrt{\left(r_{fl} + (z + \Delta z)\tan(\alpha)\right)^2 - r_{fl}^{\,2}}. \quad \text{..... (3.10)}$$

This geometry is desirable because it allows a certain degree of self-cleaning and prevents the deposition of solids along the annular passage A schematic drawing of sensor and its full assembly is provided in **Fig. 3.3**. The inner pin of the prototype is mounted on a spring with a known load. If the sensor is plugged by solids larger than the narrowest gap, the differential pressure increases. When the pressure exceeds the load on the spring the inner pin is forced to move downwards, opening the radial gap and clearing the solids.

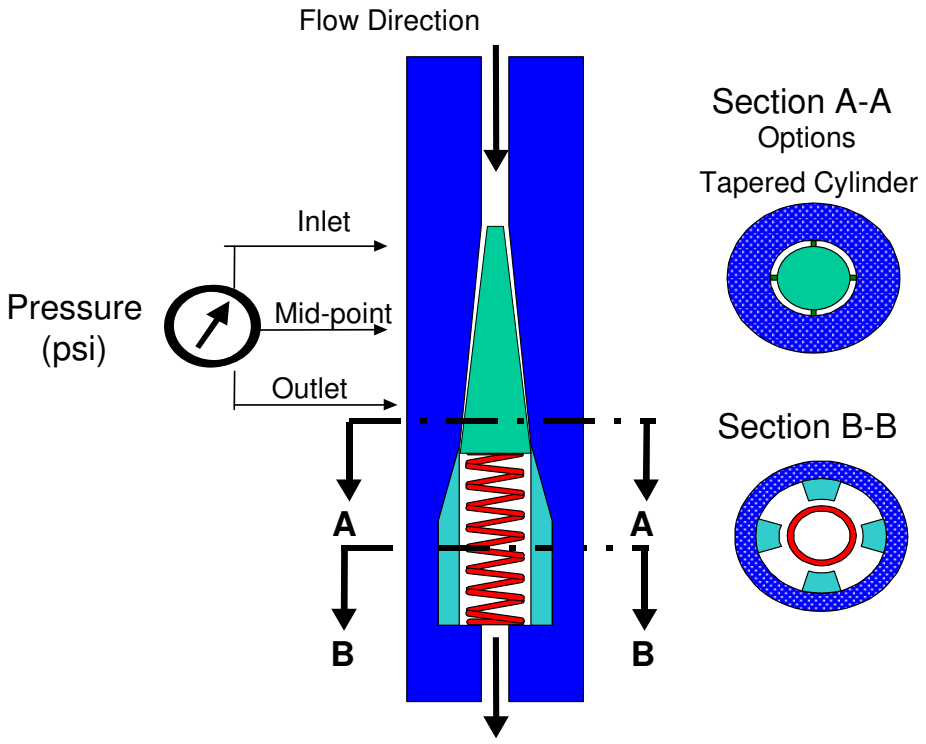

Fig. 3.3— Diagram of the prototype laminar flow viscosity sensor.

The dimensions of the prototype sensor of this investigation are compatible with those of the Reservoir Description Tool (RDT). The annular cross section is approximately equal to that provided by the 0.556 cm (0.219in) ID flow-line of the RDT. This produces a flow cross section of 0.243 cm^2 (0.0377 in^2). The length of the laminar flow region where the pressure measurements are taken was designed. A length of 8.0 in was selected to obtain a measurable pressure drop across the sensor for a fluid with a viscosity of at least 0.5 cp. This resulted in a design in which the gaps between the inner and outer flow surfaces are 840 μm (0.033 in) and 360 μm (0.014 in), at the inlet and outlet pressure taps, respectively. The dimensions of conical inner pin are shown in **Fig. 3.4**. A picture of the prototype, with external housing and inner pin is shown in **Fig. 3.5**

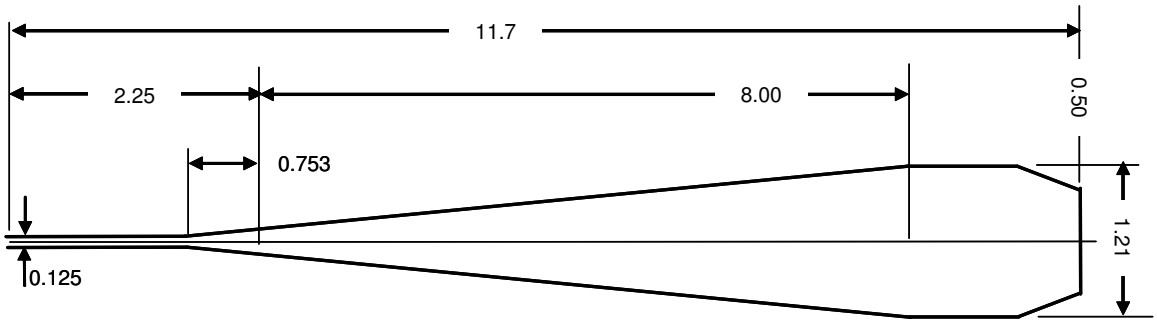

Fig. 3.4—Dimensions of the inner conical pin.

Fig. 3.5—Inner pin and outer casing f the prototype laminar flow viscosity sensor.

To prevent erosion and retard the deposition of large solids, it is possible to filter the fluid by attaching a screen. The particle screens in the RDT are either 304.8 μm or 457.2 μm. Even without a screen, the sensor should function under a modest stream of solid particles larger than the minimum gap. In case the sensor starts to become plugged the force exerted on the inner pin will push it downwards, opening the gap.

CHAPTER IV

EXPERIMENTAL EVALUATION OF THE SENSOR RESPONSE

The main objective of this chapter is to present the results of a series of experiments with the purpose of evaluating the performance of the viscosity sensor in a laboratory setting, in order to make an assessment on the feasibility of using it to measure rheological properties for Newtonian and non-Newtonian fluids.

Our primary objectives in this stage are to estimate how reliable the sensor is to measure rheological properties and how sensible it is to detect changes in these properties. We assembled an experimental flow loop in which we tested different Newtonian and non-Newtonian fluids whose properties were already known. These fluids allow us to compare the measurements obtained from the sensor and estimate the accuracy and sensibility of the viscosity sensor in the laboratory.

4.1 Experimental Methodology

4.1.1 Description of the Flow Loop

Simplified Flow Loop

The original flow designed flow loop was built initially for preliminary tests using water, glycerin and non volatile fluids. This simplified preliminary loop was quick to build and

proved useful for setting up the data acquisition system and calibration. This flow loop did not allow for temperature control. A picture of this initial set up is shown in **Fig 4.1** and **4.2**.

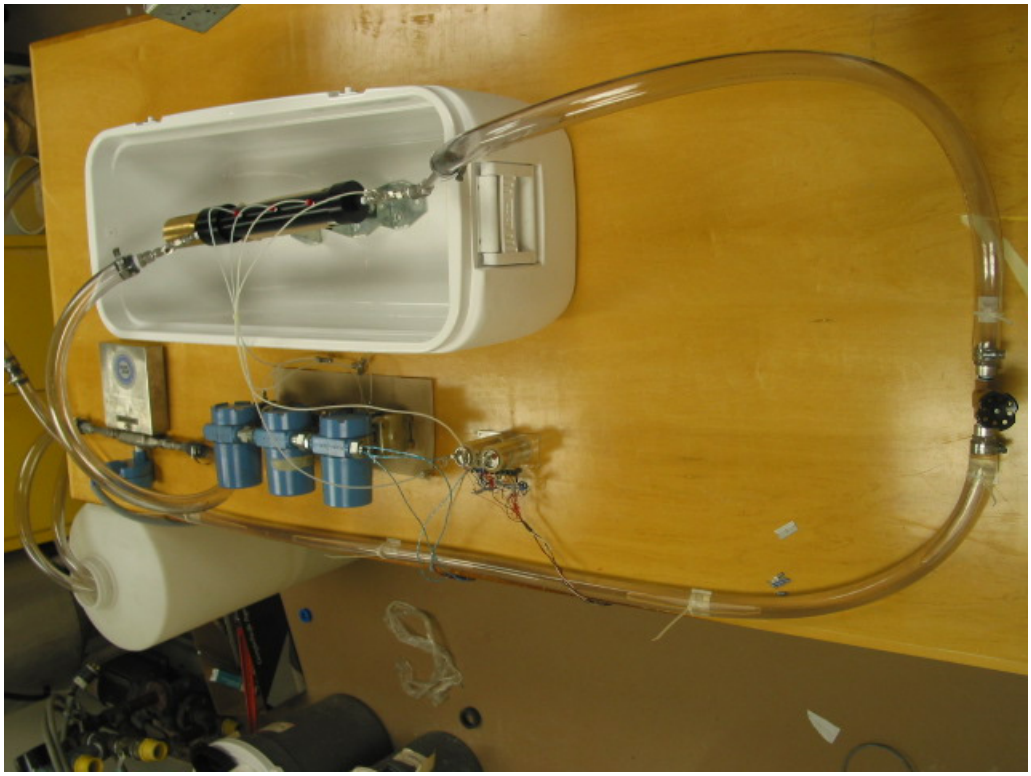

Fig. 4.1—Preliminary experimental flow loop.

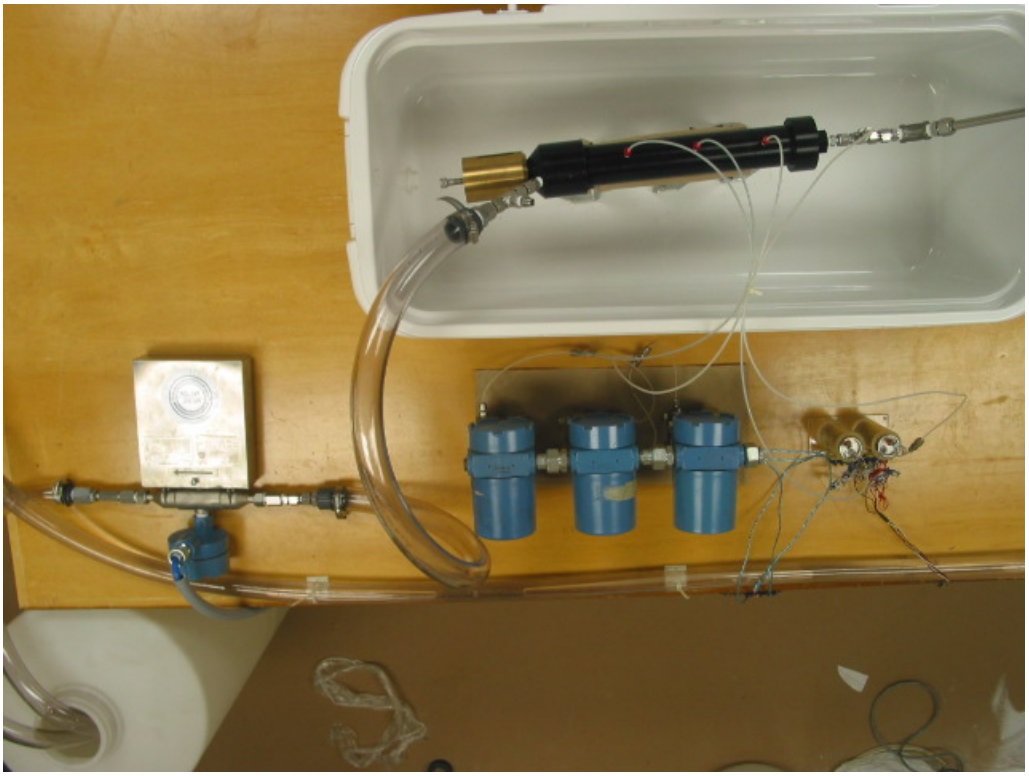

Fig. 4.2—Viscosity sensor, flow meter and pressure transducers installed the preliminary experimental flow loop.

In this preliminary setup, the pump propels the fluid from the recollection tank, into a plastic hose. The fluid enters the viscosity device. We measure the pressure drop and temperature change of the fluid within the device. The fluid exits the device and enters a flow meter, where we measure the flow rate. Then the fluid is dropped into the recollection tank.

The viscosity device is located inside a cooler, with the objective of keeping a constant temperature. We initially installed 5 pressure transducers—Two Paroscientific digital transducers, and three analog Rosemount transducers. We used the analog Rosemount

transducers to measure the pressure at the inlet, outlet and differential pressure. However, due to the limitations of the data acquisition card, we could not use all three analog devices at the same time. A bypass line from the pump back to the recollection tank was installed to allow us to modify the rate of fluid.

The data acquisition system and software was provided by Halliburton and modified accordingly to our experimental set up successfully. The hardware-software solution is described in Appendix B. Once we were comfortable with the operation of the flow loop and the data acquisition equipment was properly set up and operational and the flow meter and transducers were calibrated, we performed a series of preliminary tests to ensure that the system was working as expected.

This flow loop was used to take measurements using non volatile fluids. We used water and glycerin solutions. However, this loop offered no means to control the temperature of the fluid during the test and the volumes of sample required to start flow were in excess of 3 gallons. Since we were interested in making experiments at different temperatures, we decided to build a new flow loop, with considerable less volume of liquid, so that we could achieve a more effective control in the temperature and reduce the volume of sample required for each test. For this loop stainless steel tubing substitutes the plastic hosing. This will be described in the next section.

Generalized Flow loop

The generalized experimental apparatus used to evaluate the performance of the sensor consisted of a closed flow loop. **Fig. 4.3 and 4.4** show the schematic of the experimental setup. It consists of the following components:

- 6-gallon capacity liquid phase storage and mixing tank. The tank is used to store the fluids. This volume was selected because it is small enough to minimize the use of sample fluid in the flow loop.
- Dayton 6K580A centrifugal pump. It pumps the liquid from the 6-gallon tank into the loop. The fluid is pumped over a long period of time to completely fill the pipe, remove any air pockets from the loop and achieve a stable fluid temperature.
- 1/2-in. I.D sized stainless steel pipe. A total of 12 ft of pipe was used to assemble the loop.
- Heating-cooling system. Temperature variation was achieved by submerging the viscosity sensor inside a Precision Scientific Model 186 Heated Bath. For additional heating and cooling capacity, an extra Lauda RCS20-D Temperature Bath was attached to the system.
- The sensor was attached to two Omega K-type thermocouples to measure the inlet and outlet temperature of the fluid. The thermocouples can measure a range of –200°C to 1250°C with a maximum standard error of 2.2 °C or 0.75% above 0 °C.

- Micromotion DS025S119 sensor. This device measures flow rate in the range of 1-3 gal./min and density with an accuracy of ±0.15% of the reading.. The flow rate data is displayed and logged using a Micromotion RFT9712-IPNU transmitter.
- A Rosemount 1151 pressure transmitter was used to measure the pressure differential in the viscosity sensor. The range of the scale was set to 0-15 psia and accuracy of ±0.2%.
- Isco syringe pump with a capacity of 300 cc. This pump is used to inject fluids in the storage tank.
- Data acquisition system. All of the sensors provided a current to the Agilent 34970A DAQ Unit through an Agilent 34901A 20-Channel Multiplexer. The unit then provided the data to a LabVIEW code sampling every 30 seconds.

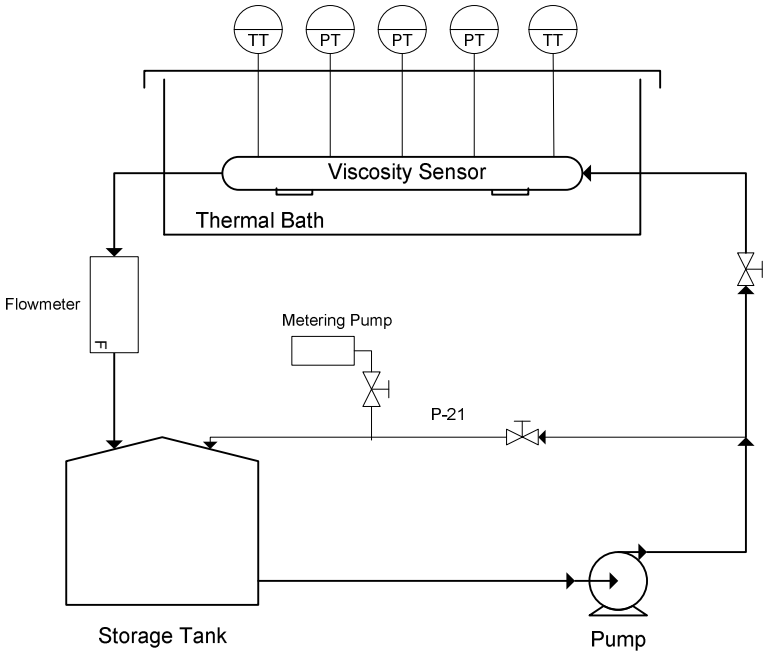

Fig. 4.3—Schematic of the closed flow loop.

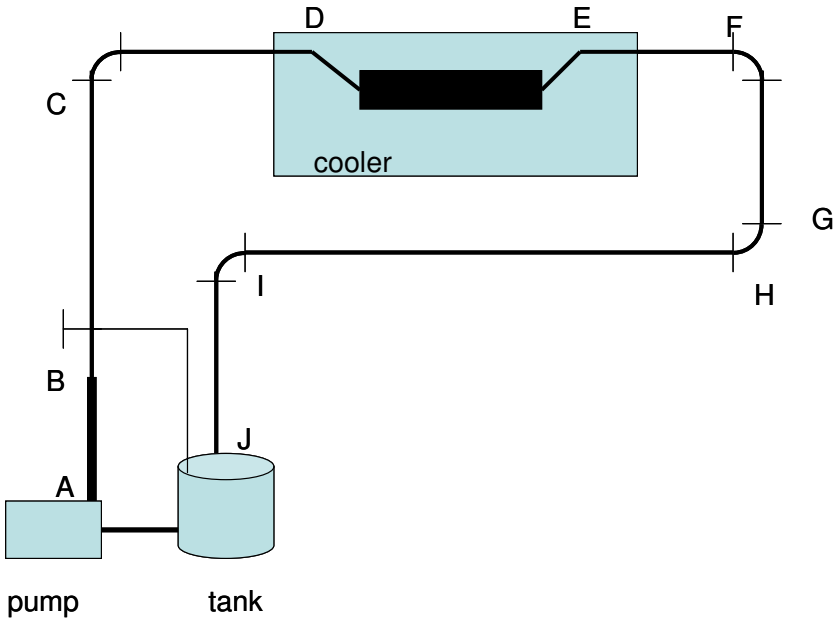

Fig. 4.4—Diagram of the closed flow loop.

The dimensions of the pipes in this new loop are shown in **Table 4.1**

Table 4.1— Specifications of flow loop pipes.

section	Length (in)	Internal Diameter (in)
A-B	22	2.75
B-C	33	0.5
C-D	15	0.5
D-E	14	0.5
E-F	10	0.5
F-G	15	0.5
G-H	10	0.5
H-I	58	0.5
I-J	22	0.5
Tank	6 gallons	

Considering the dimensions of the pipelines in the flow loop, the volume of the flowing system was calculated to be 0.7 gallons.

Additional refinements were made to the experimental setup. The scale of the pressure differential transducer was rescaled to 0-15 psia. Insulation in the pipelines was added to reduce heat losses and the plastic cooler was substituted by a thermal bath. The experiments indicated a maximum temperature of 180°F to be reached using water as heating fluid in the thermal baths. The generalized flow loop is shown in **Fig.4.5** to **4.7**

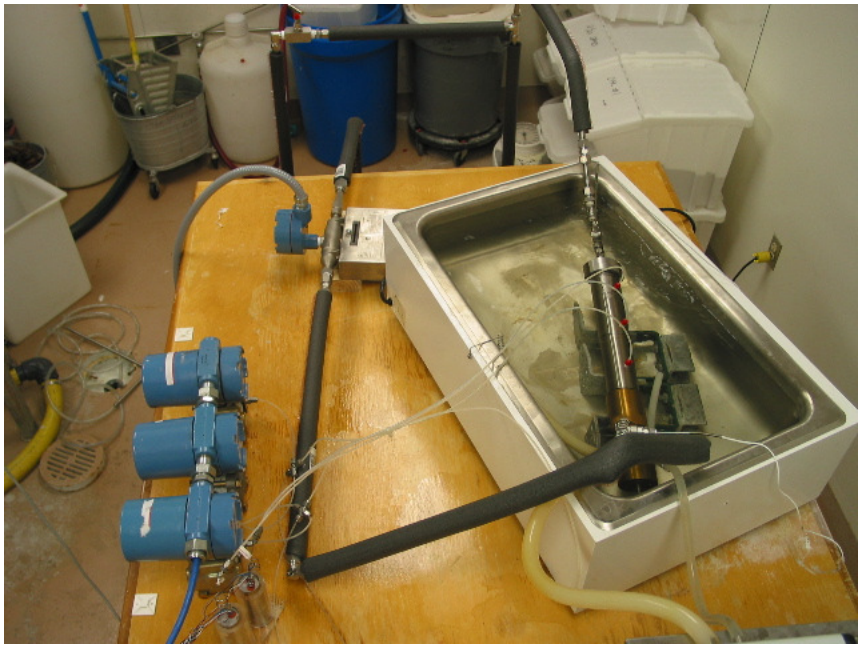

Fig. 4.5—Experimental flow loop. Final version.

Fig. 4.6—Flowmeter attached to the experimental flow loop.

Fig. 4.7—Storage tank and pump connected to the experimental flow loop.

The Precision thermal bath is capable of heating up to 190°F. To speed the heating process, it is necessary to add hot water to the thermal bath. For this purpose, we use an extra thermal bath is capable of 212°F. Due to heat losses; we were able to reach a maximum temperature of 180°F in the system It was not possible to heat the bath to a higher temperature. It took 6 hours to heat the system, from room temperature to 180°F.

Once the bath is heated and held at the desired temperature, the fluid sample is pumped in the flow loop. The measurement of differential pressure starts as soon as the

temperature of the fluid in the sensor stabilizes. We considered a variation of ±1°F to be reasonable criteria for temperature stability. Once the temperature has stabilized we considered that we had reached steady state. We allowed at least 10 minutes for temperature stabilization before taking measurements.

4.1.2 Experimental procedure

The following sequential procedure describes the operation of the flow loop with the viscosity sensor:

1. Install and test all the pipeline connections and electrical wiring system.
2. Charge fluid sample into storage tank.
3. Connect viscosity sensor in the flow loop
4. Attach pressure transducers and thermocouples to the sensor casing
5. Fill thermal bath with water.
6. Set the operating flow rate and temperature. Wait until stabilization
7. Take measurements.
8. Clean the system.

Detailed procedure and comments, on each step are provided as follows

Operation of the flow loop

The storage tank is filled with at a volume of least ¾ gallon of the fluid of interest. This volume is necessary to prevent the pump from drawing air into the loop. The fluid is poured inside the tank using the Isco syringe pump. The temperature of the fluid is

adjusted using the thermal bath controls. Given the time required to reach temperature stabilization, sometimes in excess of one hour, a second thermal bath is used to speed the heating or cooling to reach a particular temperature. The thermal regulator can be set for temperatures ranging between -20 and 300°F; however, testing only occurred at temperatures between 60 and 160 °F.

The viscosity sensor is assembled, connected to the flow loop and submerged in water inside the thermal bath. The pressure and temperature sensors are connected to the viscosity sensor.

Once the temperature is set and the storage tank is filled with fluid, the pump is turned on and the fluid is propelled into the viscosity sensor at full rate. Once the desired temperature is achieved and stable, the flow rate can be manually adjusted. Measurements are taken at least 5 approximately evenly spaced flow rates for each temperature. Each flow rate is held constant for at least two minutes. Data was recorded every 30 seconds, so at least four data points were recorded for each flow rate. The data recorded for each test is temperature, flow rate and pressure differential in the sensor.

Because of the extra heat generated by the pump, it is necessary to continuously monitor the temperature in the thermal baths to stabilize the temperature. For every change in flow rate it is necessary to adjust the thermal bath controls to reach the desired temperature.

Cleaning

The viscometer must be thoroughly cleaned after each test. To clean the system after testing oils, kerosene is used as the cleaning fluid to clean the viscometer and the flow loop. For water soluble fluids, such as glycerin and xhantan gum solutions, pure water is used as the cleaning fluid. Fluids are drained from the storage tank and pipes. The cleaning fluid is pumped through the flow loop and drained several times until the flow loop is clean.

Cross validation

The viscosity measurements obtained with the sensor were validated using a Brookfield DV-III+ rheometer. This rheometer can operate at temperatures in the range of: -100 to 300°C (-148 to 572°F), and features a speed range of 0.01-250 RPM, and a viscosity accuracy of ± 1.0% of full scale range. The operation of the Brookfield Rheometer is described in Appendix A.

4.2 Experimental Results

Characterization Fluids

The prototype sensor was characterized for fluid viscosities ranging from 1 to 28 cp. The viscosities of the fluids have been measured on a Brookfield viscometer at discrete temperatures from 68 to 150°F (20 to 65°C). The maximum flow rates in the sensor are expected to be approximately 1.0 gal/min. However, for the most viscous fluids, the flow rate was of less than 0.3 gal/min. Higher flow rates were achieved for water. Non-linear effects were observed at rates above 0.6 gal/min; suggesting the onset of turbulent flow. For the purposes of analysis and comparison, only those data at rates below 0.45 gal/min are presented. In order to span a range of viscosities, data have been acquired using water, a water-glycerin solution 50% weight, and motor oil 10W-30.

Fluid was pumped at a known rate from a temperature controlled reservoir through the sensor. The pressure and temperature at the inlet and outlet of the sensor are recorded with a data acquisition system. The flow rate and differential pressure ΔP are measured.

Temperature control was the main operational difficulty in this experiment. In order to get a stable temperature reading it was necessary to wait until the heat provided by the pump was offset by the thermal bath. For glycerin and motor oil, given the viscosity of these fluids, the pump started to overheat the fluid, making difficult to obtain a stable

reading at the desired value of temperature and rates. Once the flow rate was changed, the temperature fluctuated and we had to wait until it stabilized again. This limited the amount of data available to make the plots at certain temperatures.

The relationship between the differential pressure drop across the sensor, and flow rate can be described, using **Eq. 4.1**

$$\Delta P = f\,\mu Q\,, \quad \text{..... (4.1)}$$

The parameter f can be calculated theoretically using the geometry and rheology of the fluid or it can be determined experimentally by measuring the response of pressure drop as a function of the flow rate for a fluid of known viscosity. For simplicity, we use water at 68°F as calibration fluid since its properties are well known and it is readily available.

The data for water at an average temperature of 68°F is presented in **Fig. 4.8**. Since the viscosity of water as a function of temperature is known we can calculate the ratio $\Delta P/\mu$. This is plotted as a function of flow rate Q for differential pressures measured from the inlet to outlet of the sensor. The average value of water viscosity during the test is estimated as 1.01 cp. The observed linear behavior suggests that the pressure-flow rate relationship is described by the laminar flow model at the range of flow rates. The slope of the straight line adjusted to the data points represents the f factor shown in Eq. 4.1.

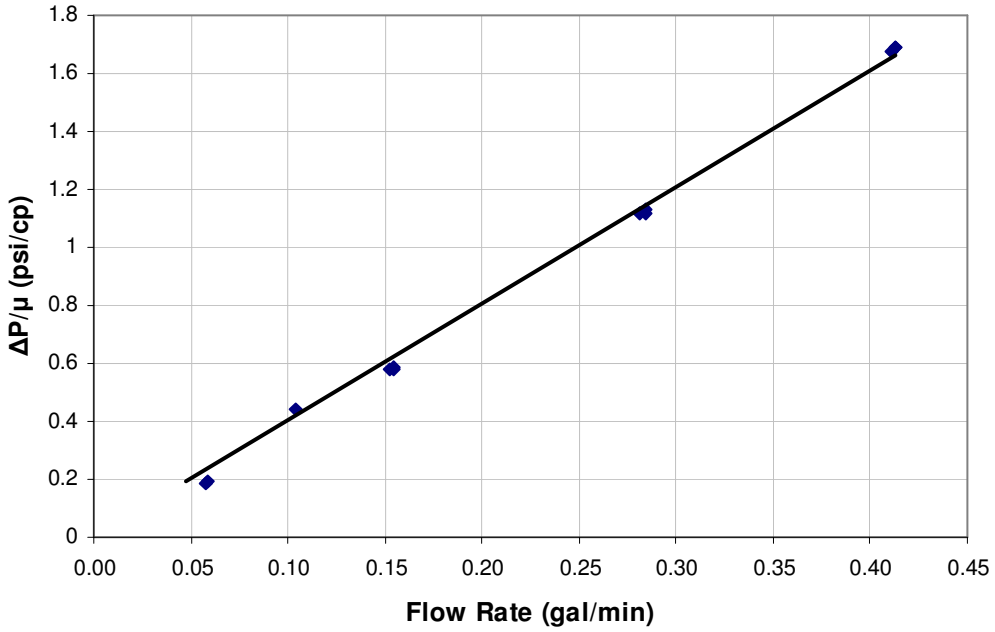

Fig. 4.8—ΔP/μ response as a function of flow rate for water, μ=1.01 cp at 68ºF.

Using the least squares method, we can fit the data shown in Fig. 4.8 to a straight line that crosses the origin of the coordinate system. The slope was calculated using the least squares method. The parameters of the regression are shown in **Table 4.2.**

Table 4.2—Regression statistics for water at 68 ºF.

				slope CI		
Slope	**Standard Error**	**t Stat**	**P-value**	**Lower 95%**	**Upper 95%**	**R^2**
4.018684	0.034871	115.2436	2.63×10^{-18}	3.941933	4.095435	0.999172

ANOVA	**F**	**Significance F**
Regression	13281.09	5.94×10^{-17}

The regression statistics indicate that the 99.9% of the variation in the pressure drop is explained by the model proposed in Eq. 4.1. The *t* test and the ANOVA analysis show that the calculated slope is statistically significant and that the model in Eq. 4.1 has a significant explanatory power to explain the relationship between the variables.

The value of the slope *f* is estimated as:

$$f = 4.02 \pm 0.08 \frac{\text{psi}}{\text{gal/min cp}}, \quad \text{..... (4.2)}$$

Similarly, we obtained additional tests at other temperatures for water. The results can be seen in Appendix C.

Fig. 4.9 shows the results of the experiment with water at an average temperature of 140°F. At this temperature the viscosity of the water is 0.46 cp and we observed higher flow rates through the device. We can see that we no longer obtain the same straight line relationship between the pressure drop and flow rate as shown in Eq. 4.1. Instead we obtain a power law trend. This may be caused by the onset of turbulence due to an increase in the Reynolds number, due to high flow velocities inside the device and the reduction of viscosity. Given this we restricted the tests to flow rates that produced linear results.

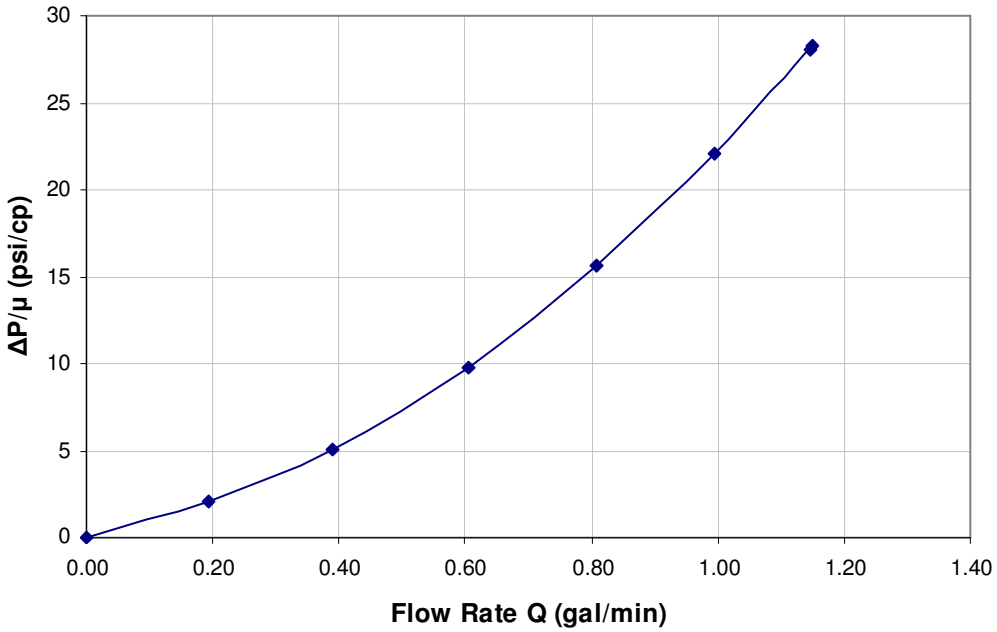

Fig. 4.9—ΔP/μ response as a function of flow rate for water, μ= 0.40 cp at 140 ºF

In order to cover a wider range of viscosity, we performed experiments with fluids with higher viscosity values. We prepared a viscous solution of water and glycerin in order to continue the tests at higher values of viscosity.

Glycerin is a chemical compound with the formula $C_3H_5(OH)_3$. It is commercially available and it has multiple applications in medicine, cosmetics and the pharmaceutical industry. We used glycerin 99.7% USP. Its properties as declared by the manufacturer are shown in **Table 4.3**:

Table 4.3— Properties of glycerin.

Property	
Appearance	Colorless Viscous Liquid
Boiling point (760 mm)	290°C
Chemical name	Glycerol
Density, 25°C	1.25802 g/cm^3
Empirical formula	$C_3H_8O_3$
Molecular weight	92.09 g/mol
Viscosity, Cp, 20°C	1410

The viscosity of water-glycerin solutions can be found in the literature. **Table C.1** in Appendix C shows the values of viscosity as a function of temperature and glycerin content. A solution of water and glycerin at 50% weight was selected since it spans a desirable range of viscosity for the range of temperatures in the experiments. The viscosity data for glycerin water solution at 50% weight is show in **Table 4.4**.

Table 4.4—Viscosity as a function of temperature for a solution of water and glycerin at 50% weight, measured values in Brookfield rheometer.

Temperature (°C)	Viscosity (cp)
20	6.00
30	4.20
40	3.12
50	2.30
60	1.90
70	1.48

The experimental data for a 50% glycerin solution at a range of temperatures 74-140°F is presented in **Fig 4.10**. The pressure ΔP is plotted as a function of flow rate Q (gal/min) for differential pressures measured from the inlet to outlet of the sensor. The slope of the

line represents the *f* factor multiplied by the viscosity of the fluid. In this plot we can see the pressure response of the sensor with fluids with different viscosity. For example, at 0.5 gal/min, the measured pressure drop of a 5.5 cp fluids is approximately 12 psi while a 1.9 cp fluid only causes a pressure drop of slightly less than 4 psi.

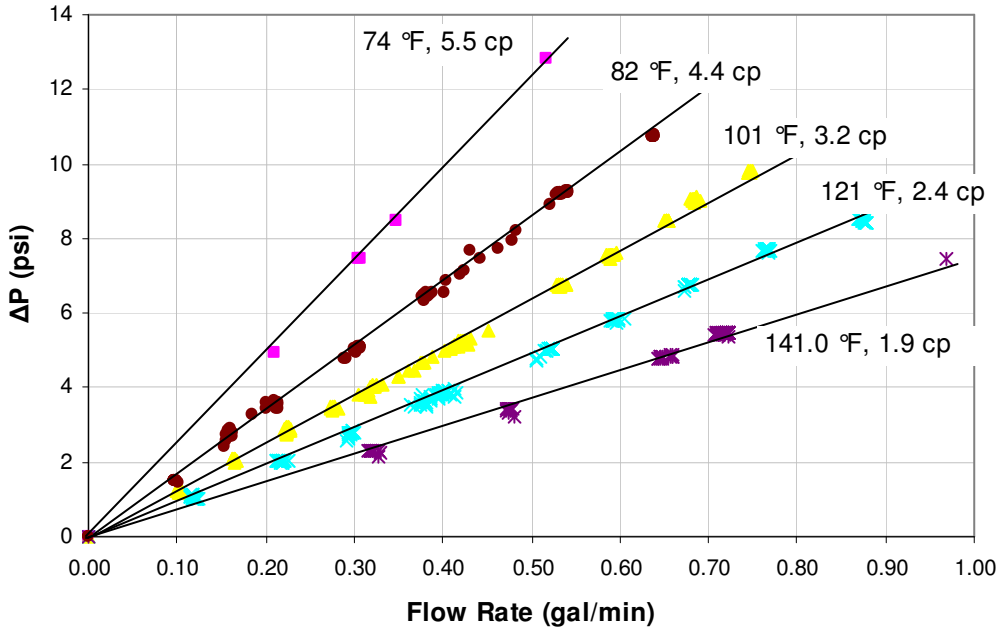

Fig. 4.10—Pressure drop in the sensor as a function of flow rate for a solution of glycerin and water at 50% weight at different average temperatures.

To test at even higher values of viscosities, we used motor oil 10W30. Valvoline 10W30 is widely available lubricant for motor vehicles. Some of the properties of the oil declared by the manufacturer are presented in **Table 4.5**.

Table 4.5—Viscosity and density declared by manufacturer for motor oil Valvoline® 10W-30.

Density @ 60 °F (kg/m^3)	Temperature (°C)	Dynamic Viscosity (cSt)	Kinematic Viscosity (cp)
879	40	70.8	62.23
	100	10.5	9.23

We used the Brookfield viscometer to measure the viscosity of 10W30 oil for a range of temperatures. The experimental data is presented in **Table. 4.6**

Table 4.6—Measured viscosity motor oil 10W-30, Brookfield rheometer.

Temperature (°C)	Viscosity (cp)
20	170.5
30	98.1
40	60.9
50	40.2
60	28.2
65	24.0

We can see that the viscosity of this fluid at low temperatures is significantly higher than any of the fluids previously used. The experimental equipment available was not capable of pumping the fluid at temperatures lower than 140°F. This limited our data sampling to 140 and 150°F. Even with this limitation, the viscosity of the motor oil at these temperatures is significantly higher than for the glycerin solutions used previously. The measured pressure response of the sensor in use with this viscous fluid is shown in **Fig. 4.11.**

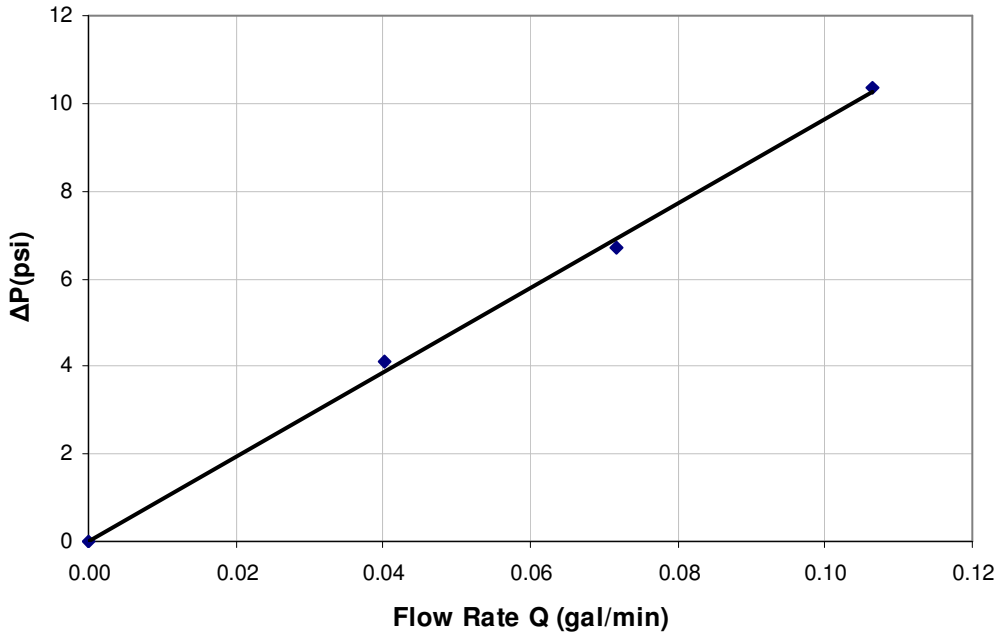

Fig. 4.11—Pressure drop in the sensor as a function of flow rate for motor oil 10W30 at an average temperature of 150°F.

In a similar way as with water, we are interested to see if there are any effects of the higher temperature on the *f* factor or slope. Since the sensor is made of materials that may experience thermal expansion or contraction due to changes in temperature there could be effect of temperature on the sensor response. For motor oil, the relationship $\Delta P/\mu$ as function of flow rate Q is shown in **Fig. 4.12.** The estimated *f* factor at this temperature is calculate using least squares regression and the parameters of the calculation are shown in **Table 4.7** and **Eq. 4.3**

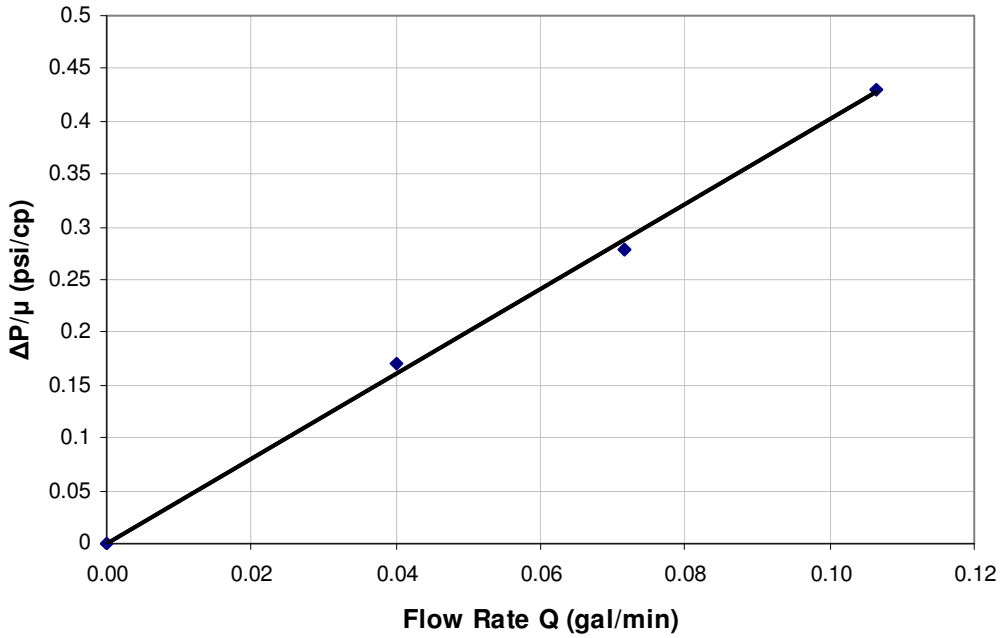

Fig. 4.12—ΔP/μ response as a function of flow rate for motor oil 10W30. Viscosity 24.0 cp at an average temperature of 150 ºF.

Table 4.7—Regression statistics for motor oil at 150 ºF.

				slope CI		
Slope	Standard Error	t Stat	P-value	Lower 95%	Upper 95%	R^2
4.02213	0.070782	56.82391	0.00031	3.717578	4.326681	0.999381

ANOVA	F	Significance F
Regression	3228.957	0.011202

$$f = 4.02 \pm 0.3 \frac{\text{psi}}{\text{gal/min cp}}, \quad \text{..... (4.3)}$$

Even though the confidence level of the slope coefficient is wider, since we could not collect as many points as with water or glycerin, still the results are within the range of

the water result. The question is, whether there is an effect of temperature in the *f* factor for the range of temperatures used in our experiments. To answer this question, since we know the independent experimental values of viscosity as a function of temperature for the fluids used in the experiments, we calculated the slope coefficients for each of the experimental runs with water, glycerin and motor oil. The calculated factors are shown in **Table 4.8**.

Table 4.8—Slope coefficients *f* for different experiments.

Fluid	Average temperature (°F)	Average Viscosity (cp)	*f* (psi min /gal cp)	±Δ*f* (psi min /gal cp)
Water	60	1.15	4.11	0.05
Water	65	1.06	4.16	0.06
Water	68	1.01	4.02	0.08
Glycerin	82	4.40	3.88	0.02
Glycerin	101	3.20	4.03	0.01
Glycerin	121	2.40	4.09	0.01
Glycerin	141	1.90	4.08	0.02
10W30	150	24.0	4.02	0.30

To investigate if there is a relationship between the temperature and the *f* factor, we calculated a linear regression between these two variables. The results are shown in **Table 4.9.**

Table 4.9—Regression statistics *f* factor and viscosity.

					slope CI		
	Coefficients	Standard Error	t Stat	P-value	Lower 95%	Upper 95%	R^2
Intercept	4.066219	0.104335	38.97268	1.91×10^{-8}	3.81092	4.321518	
slope	-0.00018	0.001021	-0.17589	0.866167	0.00268	0.002319	-0.1606

We can see that according to the very low coefficient R^2 there seems to be no correlation between the temperature and the *f* factor for the data set available. Similarly, the *P* value of the slope coefficient is higher than the accepted *P* level of 0.05, so we can reject the

relationship between temperature and f for the temperature range used in the experiments. It is possible that a device constructed with other materials could experience a larger thermal expansion that provokes a measureable difference in pressure drop as a function of temperature; however, for the temperature range of our experiments, this effect was not seen with our experimental equipment.

The next question is then, what is the value of f for this particular sensor configuration. One possible approach is just to calculate an average of f factor values presented in Table 4.8. Therefore:

$$f = 4.07 \pm 0.3 \frac{\text{psi}}{\text{gal/min cp}}, \quad \text{..... (4.4)}$$

for $60 \geq T \geq 160$, with T in °F

Another possibility, which is more practical, is to simply use the value of f obtained for a widely available fluid with known viscosity and use it as a calibration factor. We can select water at the calibration fluid and use f obtained for water at 68°F to calculate viscosities for other fluids and other temperatures.

$$f = 4.02 \pm 0.08 \frac{\text{psi}}{\text{gal/min cp}}, \quad \text{..... (4.5)}$$

for $60 \geq T \geq 160$, with T in °F

While it is true that the materials of the prototype expand and contract as a function of temperature, we did not observe any significant evidence that such

expansion/contraction is influencing the results more than the experimental error in our measurements for the range of temperatures in our experiments.

We believe that obtaining the *f* factor using water at room temperature as a calibration fluid is a practical approach to obtain reasonable accurate value of viscosity for the range of temperatures of our experiments.

The viscosity from the sensor is calculated from **Eq 4.6:**

$$\mu_{\text{sensor}} = \frac{\Delta P}{fQ}, \quad \text{..... (4.6)}$$

and the relative error using as reference the viscosity values obtained independently from the Brookfield viscometer is:

$$\%\ \text{Error} = \frac{\left|\mu_{\text{sensor}} - \mu_{\text{brookfield}}\right|}{\mu_{\text{brookfield}}} 100. \quad \text{..... (4.7)}$$

Where

Q : Flow rate (gal/min)

ΔP : Measured pressure difference in the sensor, (psi)

f : Coefficient from Eq. 4.5

$\mu_{\text{brookfield}}$ :: viscosity measured in the Brookfield rheometer, (cp)

In this case, using the value of *f* for water at 68°F, the average viscosity calculated from the sensor is show in **Table 4.10.** A cross-plot of the viscosity obtained from the senor and the Brookfield rheometer is shown in **Fig. 4.13.**

Table 4.10—Calculated viscosity from the sensor and measured from Brookfield.

fluid	Temperature (°F)	Viscosity from Brookfield (cp)	Viscosity from sensor (cp)	Relative Error (%)
water	60	1.15	1.17	2.16
water	65	1.06	1.08	2.16
Glycerin 50%	74	5.60	6.00	8.79
Glycerin 50%	82	4.40	4.18	4.96
Glycerin 50%	101	3.20	3.16	1.34
Glycerin 50%	121	2.40	2.37	1.44
Glycerin 50%	141	1.90	1.84	2.96
Velocite 6	60	4.10	4.40	8.08
10W30	150	24.00	24.16	0.67
10W30	140	28.2	26.80	5.14

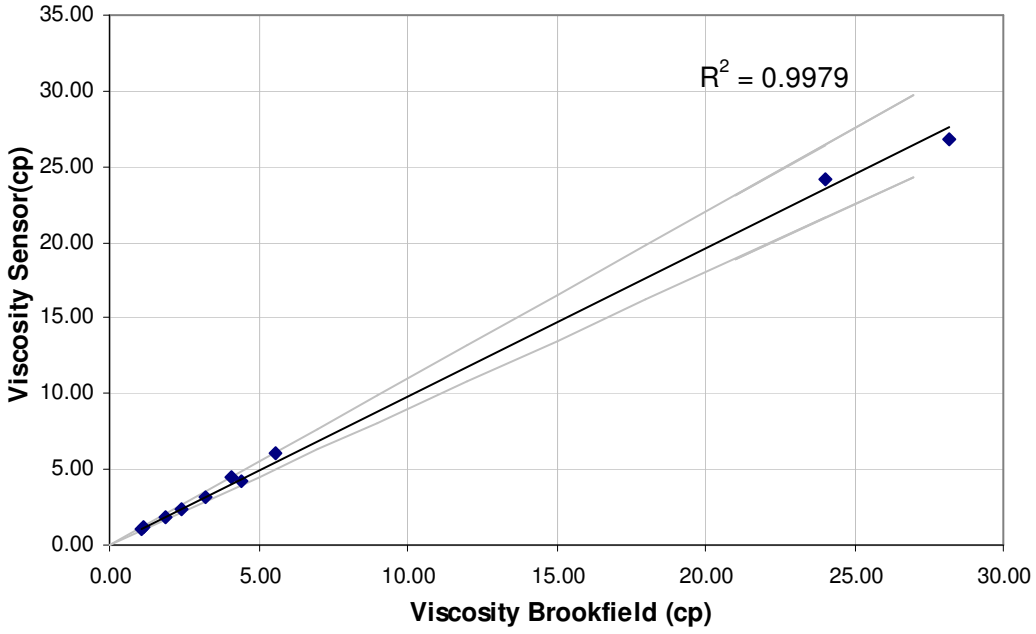

Fig. 4.13—Crossplot of viscosity measured in the Brookfield rheometer and viscosity calculated from the device response.

We can see that the viscosity calculated from the sensor is in good agreement with the values obtained from the Brookfield viscometer. The extra lines are the 10% error lines around the expected value of viscosity and the data points lie within the lines. The high value of R^2 appears to validate that statement. However, given that most of the measurements are clustered at viscosities lower than 5 cp and only two data points are at higher viscosity, this can create an artificially high R^2. To verify this, we plot the same crossplot, but we zoomed in the area with viscosities lower than 5 cp. This is shown in **Fig. 4.14.** In this plot we can see that at lower viscosities, the linear tendency is well defined and that the calculated viscosity from the sensor is s within 10% of the values obtained independently from the Brookfield viscometer.

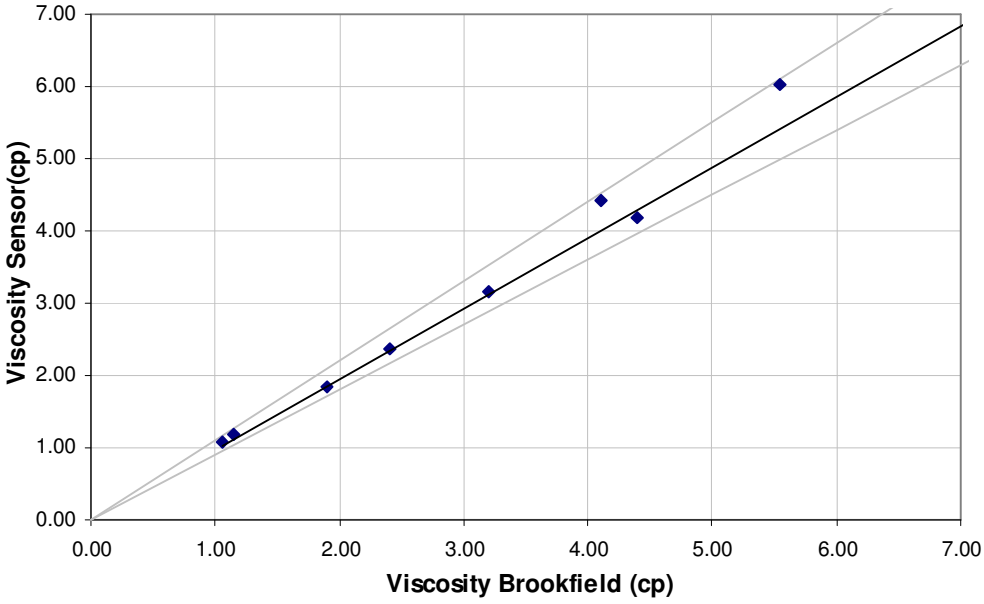

Fig. 4.14—Crossplot of viscosity measurements in the Brookfield rheometer and viscosity calculated from the sensor.

Uncertainties Associated with the Spring Assembly: Effect of the Spring Mechanism over Sensor Response

During the course of the experiments described previously, with water and solutions of glycerin, the sensor remained assembled in one piece since it was not necessary to clean it. We had observed good repeatability between tests. However, when we started to test with hydrocarbon oils we needed to remove and disassemble the sensor regularly for cleanup. When we compared the results, we noticed that the pressure differential – flow rate response had changed. The slope or geometry factor f changed and we could not obtain repeatable measurements reliably.

Due to the significant differences in the measured factor f from experiment to experiment we suspected a mechanical failure or jam in the flow loop was responsible of the discrepancies. We set out to troubleshoot the flow loop, trying to isolate any possible point in the experimental setup that could affect the measurements. Initially we investigated the possibility of solids blocking the sensor, therefore raising the pressure differential. No such blockages were found. Another possibility investigated was that the pressure transducers were not working properly but they were verified to be working correctly as well. We then examined the effect of the spring position in the geometry as a possible cause of changes in the measured response.

Experimental method

The viscosity sensor was cleaned and assembled. However, this time, the screw in the spring mechanism was fully rotated in a clockwise sense, to exert on the spring the maximum compression possible. The device was then connected to the flow loop.

A volume of six gallons of 10W30 oil was injected in the storage tank and pumped continuously through the viscosity sensor. With the support of the available thermal baths, the system was heated. The temperature of the system was monitored until it became stable at 150 °F.

Once the temperature became stable, we took measurements of differential pressure inside the sensor and flow rate every 30 seconds for 4 minutes. Once this was done, we loosened the screw in the spring mechanism a full turn on a counterclockwise sense, and measured another set of differential pressure and flow rate.

The screw in the spring contraption is designed to rotate a full turn at least 9 times until there is no more compression being exerted on the spring. We continued taking measurement of flow rate and differential pressure, as we rotated the screw on a counterclockwise sense. Once the screw was no longer compressing the spring mechanism, we stopped and considered this point to be the end of the experiment. Using the values of differential pressure and flow rate, we calculated the f factor for each position of the screw using Eq. 4.1.

Once this was done, we did the reverse experiment. We measured the pressure differential and flow rates, as we tightened the screw one full turn at a time on a clockwise sense. This was done until the spring could no longer be compressed. Once again, maximum compression was observed at nine full turns. As before, we calculated the *f* factor for each full rotation of the screw.

The results of this experiment are shown in **Fig 4.15** through **4.17**.

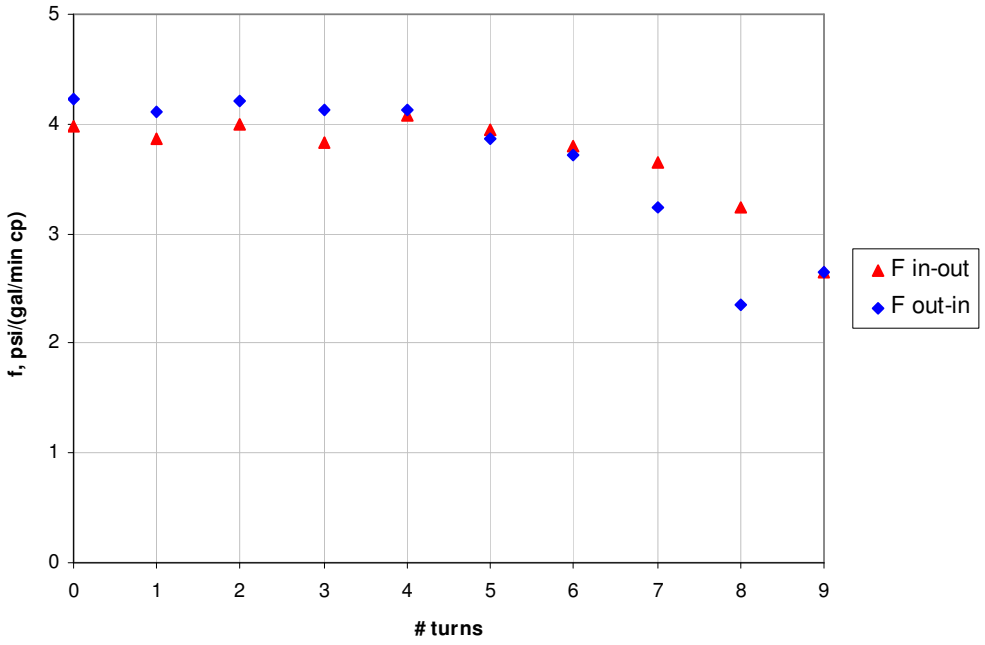

Fig. 4.15—*f* factor as a function of the number of turns in the screw of the spring mechanism. Total differential pressure 4 psia.

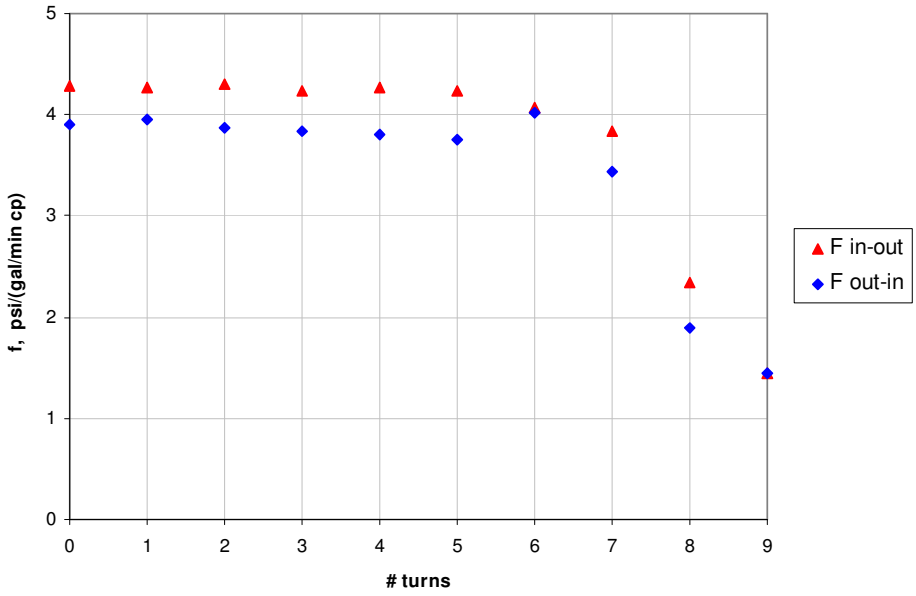

Fig. 4.16—*f* factor as a function of the number of turns in the screw of the spring mechanism. Total differential pressure 7 psia.

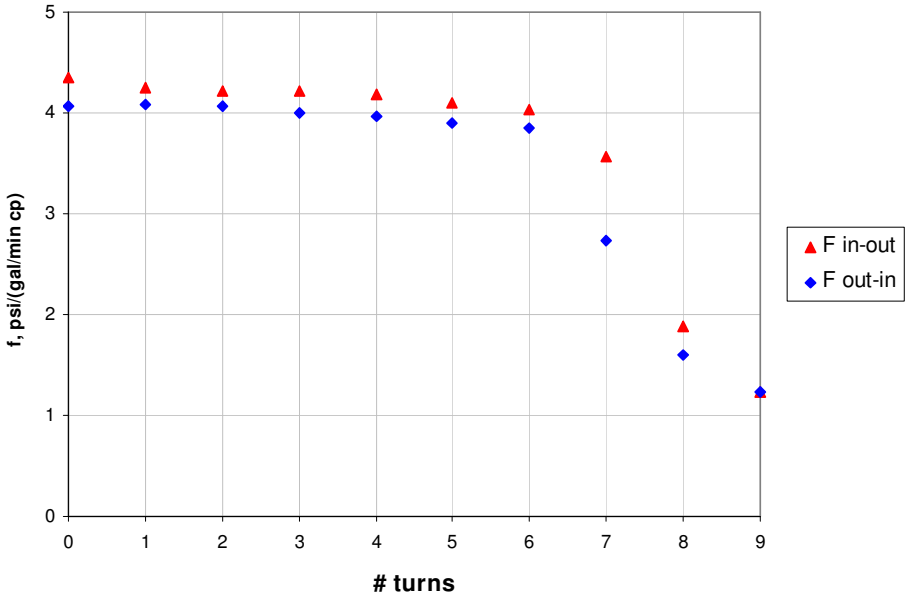

Fig. 4.17—*f* factor as a function of the number of turns in the screw of the spring mechanism. Total differential pressure 10 psia.

From Figs. 4.15, 4.16 and 4.17 we can see the effect on the calibration of the sensor by the position of the spring. The average value of *f* is approximately 4.00 in average. This value remains approximately constant as long as the screw is at least six full turns inside the spring mechanism. The plots suggest that past six turns of the screw, the spring is no longer offering a force to oppose the fluid and the inner pin of the sensor is displaced and the geometry of the sensor changes. This modification in the internal geometry drops the value of *f* as low as 1.00, which occurs when the screw is essentially loose from the spring. As we tightened the screw back in position, we restored the geometry up to some extent of its original configuration as we can see that the *f* factors obtained in both travel directions of the screw are not the exactly the same. This result stresses the importance of properly assembling the equipment and making sure that there are no changes in the calibration of the sensor once the sensor is in operation.

Evaluation of Viscosity of Oil Mixtures

To allow us to see the sensibility of the device to changes in viscosity in the fluid, we decided to test the device with a more viscous fluid, and inject a lighter fluid and measuring the changes in differential pressure response. In order to add and mix different oils in the system, we installed an Isco metering pump to inject the oils to mix.

1. Description of the Fluids for the Dilution Test

We used two oil samples for the dilution tests. The heavier oil, which we will refer to as Oil A, has a density of 7.538 lb/gal at 75°F. The lighter oil; Oil B, has a density of 7.037 lb/gal at 75°F as indicated in **Table 4.11**. These fluids were provided by Halliburton. We were not given any other information about the properties of the oils.

Table 4.11—Measured density of oil A and B at 75°F.

Fluid	Density (lb/gal) @ 75°F
Oil A	7.538
Oil B	7.037

Using a Brookfield DV III viscometer, we measured the viscosity of oils A and B. Using this equipment, we were able to measure the viscosity of Oil A. The measured viscosity as a function of temperature is shown in **Table 4.12.**

We measured the viscosity of Oil B with the similar equipment but its viscosity was too low to be measured reliably. The values of viscosity changed erratically with the speed of the spindle, suggesting the problem was a limitation of the spindle set used in the viscometer. We decided to use a cone and plate attachment in the Brookfield viscometer which is considered adequate for low viscosity fluids. We still observed some erratic measurements and had overall difficulty obtaining repeatable measurements of the viscosity of this oil. This may have been caused by the observed high volatility of this fluid. Nevertheless the results are shown in **Table 4.13**.

Table 4.12—Viscosity oil A, measured with Brookfield rheometer.

T(°F)	Viscosity (cp)
70	67.8
74	56.0
84	43.8
88	41.3
102	30.2
114	23.0
124	19.6
136	16.4
150	13.5
166	11.2

Table 4.13— Viscosity Oil B, measured with Brookfield rheometer.

T(°F)	Viscosity (cp)
100.4	4.57
140.0	3.00
161.0	2.23

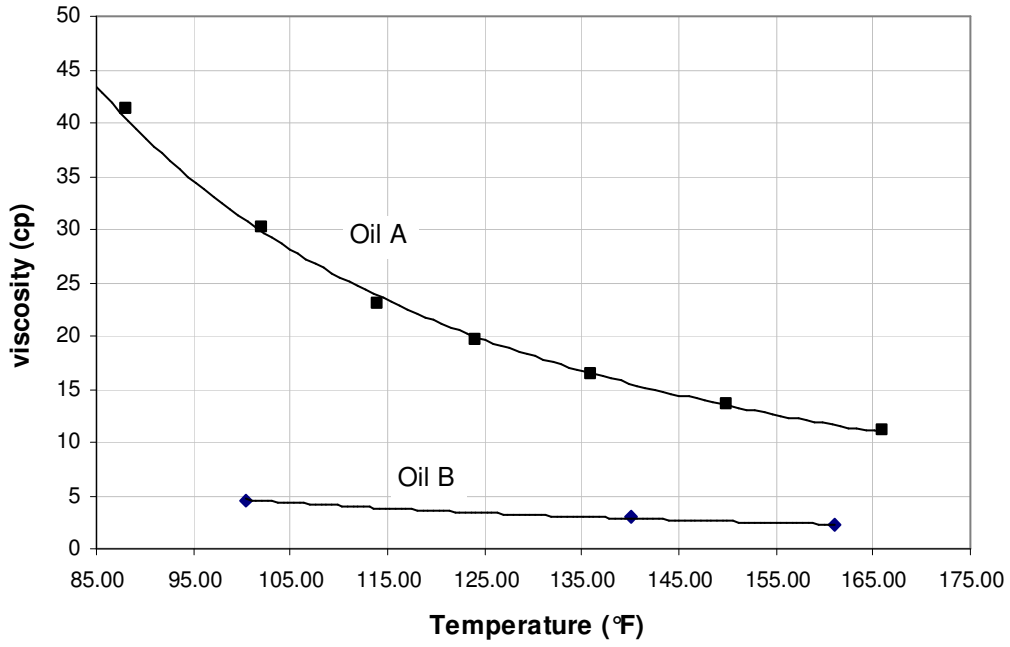

Fig. 4.18—Measured viscosity oil A and oil B from Brookfield rheometer.

Fig. 4.18 shows the measured viscosity of oil A and B in the Brookfield rheometer as a function of temperature. The dilution tests will start from oil A, and injecting fixed volumes of oil B, reducing the viscosity.

2. Dilution Tests

The procedure for testing is as follows:

1) Pre-heat the system at the desired temperature
2) Load the tank with oil A
3) Run test at the desired temperature.

4) With the metering pump, add new oil B.

5) Close valve 1, leave valve 2 open, and use the pump to mix the oils.

6) Open valve 1 and perform tests.

Oil A and B were used in the experiments in the flow loop with temperatures varying from 100 to 160°F. Several tests were done by mixing the heavy (Oil A) and light (Oil B) and measuring the pressure drop and rate changes with temperature.

We modified the initial flow loop setup to be able to inject oil directly in the heater tank. The Isco Metering pump was used to inject 300cm^3 of sample per load. The modification is illustrated in **Figs. 4.19-21**.

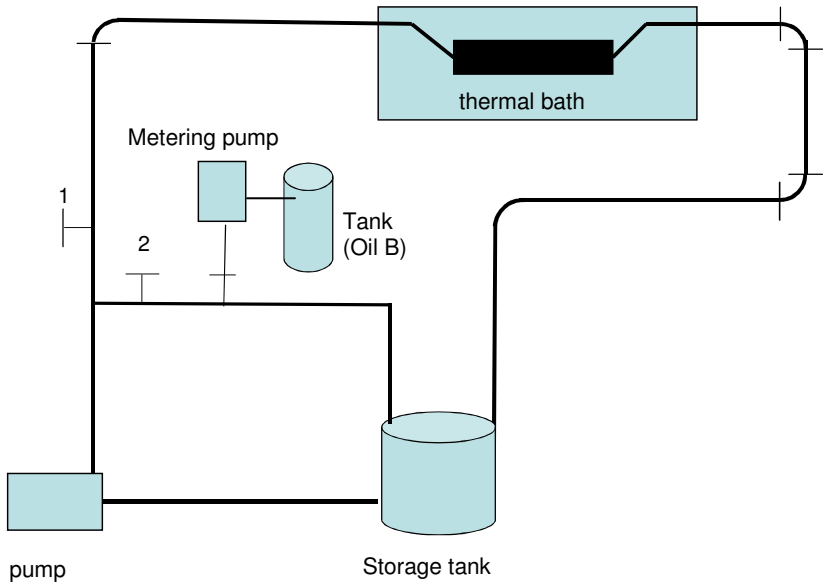

Fig. 4.19—Modified flow loop with a metering pump connected to the tank.

Fig. 4.20—Metering pump connected to the storage tank.

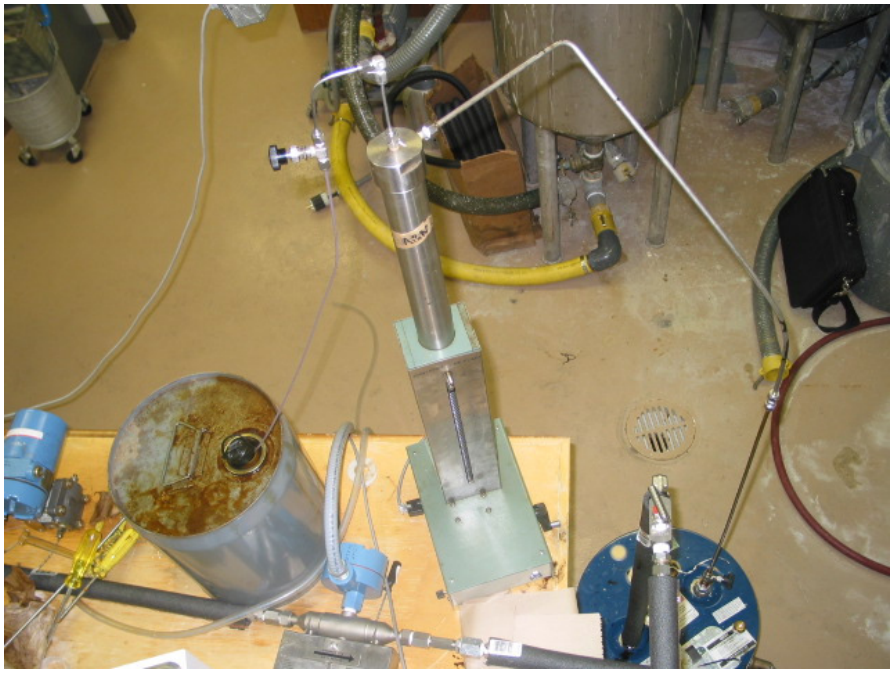

Fig. 4.21—Metering pump connected to tank B and storage tank

For the dilution tests we decided to dilute first the more viscous Oil A with the less viscous Oil B. We added a fixed mass of oil B into oil A in the storage tank and measured flow rates and pressures within the sensor at a range of temperatures. For this tests, the pressure transducers were recalibrated to display a pressure response in the range of 0-20 psia.

Initially we added 5306 grams of heavy oil A in the storage tank and measured the pressure drop and flow rate at the following temperatures: 100, 110, 120, 130, 140, 150 and 160°F. This range of temperatures was chosen because at temperatures lower than 100°F the flow rate was low and readings were unstable. At temperatures over 160°F, the heavy oil started to emit fumes.

Figs. 4.22 and **4.23** show a typical time-temperature curve and indicate the period of time where the temperature was stable to measure the pressure drop. We show the example for the pure oil A. The rest of the data is presented in Appendix. The fluctuations are caused when the flow rate is changed. After a period of time, the temperature stabilizes reasonably within 2 to 5 degrees Fahrenheit of the target desired temperature. In these dilution tests, it was sometimes difficult to stabilize temperature for temperatures lower than 120°F. The heat provided by the pump caused this problem. At higher temperatures it was easier stabilize the temperature. For the analysis, the

pressure and rate data was filtered in Excel, to only plot those points that correspond to the temperature desired.

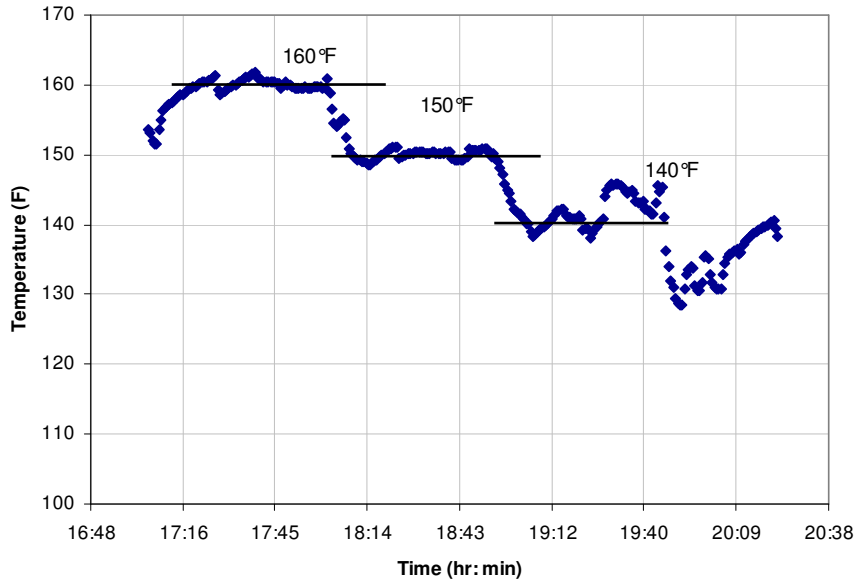

Fig. 4.22—Temperature in the viscosity sensor as a function of time for oil A, from 160°F to 140°F

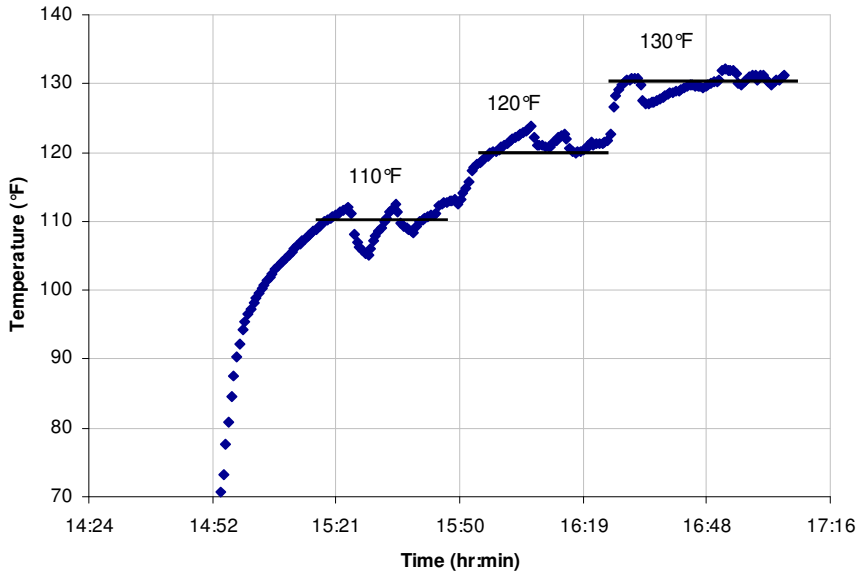

Fig. 4.23— Temperature in the viscosity sensor as a function of time for oil A, from 110°F to 130°F

The first test is pure Oil A. The observed sensor response as a function of flow rate and temperature is shown in **Fig. 4.24**

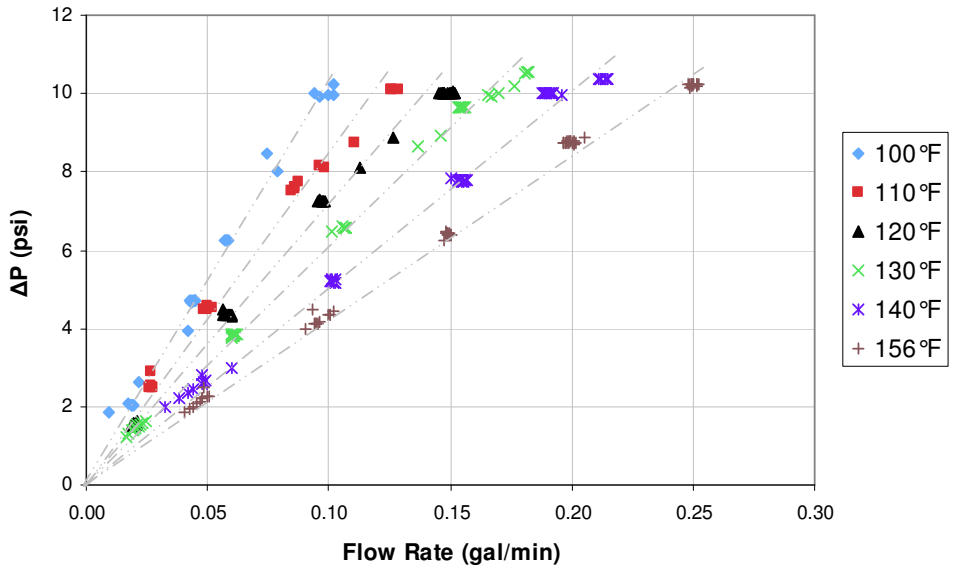

Fig. 4.24—Differential pressure vs. flow rate for oil A.

We can see the changes in slope as temperature increases. This is caused by the reduction of viscosity of the fluid. At temperatures higher than 140°F, the viscosity change is smaller and the curves appear to overlap together.

Since we determined an experimental independent value for the viscosity of Oil A using the Brookfield rheometer, we made a plot of $\Delta P/\mu$ as function of flow rate Q just like we did in previous experiments with other fluids. This was done to verify that the f factor remained the same as in previous experiments and that the internal geometry in the

sensor had not changed. However, for this experiment, the average f factor was estimated at 3.32 at these temperatures. (**Eq 4.8**)

$$f = 3.32 \pm 0.05 \frac{\text{psi}}{\text{gal/min cp}}. \quad \text{..... (4.8)}$$

This suggests that after cleaning and setting up the equipment from the previous experiment using water and glycerin, the spring screw was not fully tightened at the end of the sensor and therefore the calibrated f factor in Eq. 4.5 was no longer applicable. Since we had limited availability of Oil A, it was considered imperative to avoid losing sample as much as possible. We decided to continue the experiment, considering the first run with only Oil A as a calibration run, and, and since the subsequent injections of oil B in the system are done without disassembling the sensor or modifying the spring attachment, the geometry will remain constant and the f factor indicated in Eq. 4.8 should not change.

Once we did the initial test with Oil A, we injected Oil B into the heater tank in the volumes described in **Table 4.14**. Before measuring pressure drop and rate, we let the fluids mix in the inner loop for 15 minutes.

Table 4.14—Dilution tests. Mass and volume of oil B injected in oil A.

	Injected Volume, Oil B (cm^3)	Cumulative Voume Oil B (cm^3)	Cumulative Mass Oil B (g)	% Oil B (mass)
Test 1	300	300	252.96	4.55
Test 2	300	600	505.92	8.70
Test 3	300	900	758.88	12.51
Test 4	300	1200	1011.84	16.02
Test 5	300	1500	1264.8	19.25
Test 6	300	1800	1517.76	22.24
Test 7	600	2400	2023.68	27.61
Test 8	1200	3600	3035.52	36.39
Test 9	1200	4800	4047.36	43.27

After test 9 was performed, in order to economize the sample of oil B, we removed a portion of the mixture in the tank to continue to dilute samples at higher proportions of the light oil B. The initial mixture was at 43% oil B. We removed 6500 cm^3 of the mixture in the tank. After test 11, we removed 3500 cm^3 from the tank to prepare Test 12. **Table 4.15** shows the rest of the dilution tests and the volumes injected in the system.

Table 4.15—Continuation of dilution tests. Mass and volume of oil B injected in oil A.

	Injected Volume, Oil B (cm^3)	Cumulative Voume Oil B (cm^3)	Cumulative Mass Oil B (g)	Mass Oil A (g)	% Oil B (mass)
Test 10	1200	3077.19	2594.68	2075.08	55.26
Test 11	2400	5477.19	4618.36	2075.08	69.00
Test 12	2400	5298.96	4468.08	1098.29	80.27
Test 13	2400	7698.96	6491.76	1098.29	85.83

The differential pressure and flow rate data for each test is presented in appendix II. We then proceeded to calculate the expected values of viscosity for each of the oil mixtures

by using Eq. 4.6 and the value of *f* shown in Eq. 4.8. **Tables 4.16 and 4.17** show the calculated viscosity from the sensor for each mixture, as a function of both temperature and mass percentage of oil B in the mixture. The experimental data is located in Appendix C.

Table 4.16—Calculated viscosity for mixtures of oil A and B from device.

	(%) mass Oil B in mixture									
	0.00 %	**4.55%**	**8.70%**	**12.51%**	**16.02%**	**19.25%**	**22.24%**	**27.61%**	**36.39%**	**43.27%**
T (°F)	**μ (cp)**	**μ (cp)**	**μ (cp)**	**μ (cp)**	**μ (cp)**	**μ (cp)**	**μ (cp)**	**μ (cp)**	**μ (cp)**	**μ (cp)**
100	31.09	29.23	26.38	25.45	23.48	19.71	18.79	15.14	12.47	11.72
110	25.54	-	-	20.28	19.39	17.32	14.94	13.67	11.31	10.18
120	21.34	-	-	17.50	16.36	14.07	12.93	11.71	10.13	9.27
130	18.09	-	-	15.23	14.45	12.49	11.16	10.71	8.92	8.24
140	15.52	-	-	13.13	12.87	11.63	11.31	9.45	7.70	7.08
150	13.46	-	-	-	-	9.12	8.92	8.42	6.99	6.38
160	11.78	-	-	-	-	9.72	8.07	7.90	6.42	5.76

Table 4.16 —Continued.

	(%) mass Oil B in mixture			
	55.56 %	**69.0%**	**80.27%**	**85.53%**
T (°F)	**μ (cp)**	**μ (cp)**	**μ (cp)**	**μ (cp)**
100	7.01	-	4.67	-
110	5.28	-	-	-
120	21.34	3.69	3.69	-
130	-	-	-	3.07
140	4.37	3.47	2.88	2.81
150	-	-	-	-
160	3.51	2.82	2.41	2.35

Once the dilution tests were finished, we emptied the tank and cleaned the entire flow loop. We loaded the storage tank with pure Oil B. The sensor was reattached and carefully assembled, verifying that the spring screw was and installed correctly and that it was fully tightened. The measured viscosity for this oil from the viscosity sensor response, using the *f* factor is from Eq. 4.5 is presented in **Table 4.17**

Table 4.17—Measured Viscosity oil B measured from viscosity sensor.

T(°F)	Viscosity (cp)
100	3.53
120	2.56
130	2.28
140	2.07
160	1.75

The viscosity for Oil B from the Brookfield and the sensor are shown in **Fig. 4.25**

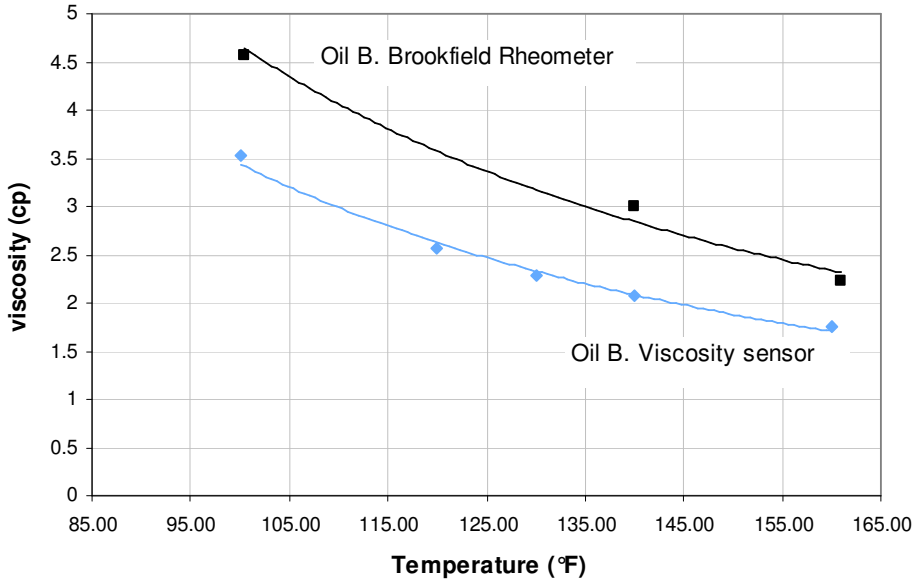

Fig. 4.25—Comparison of the viscosity of oil B measured from the Brookfield rheometer and the viscosity device.

The viscosity values obtained from the sensor for Oil B are lower than the readings taken from the Brookfield rheometer. We believe that while measuring with the Brookfield rheometer, part of the sample evaporated with the higher temperature due to a faulty seal in the cone and plate attachment, allowing some evaporation of the sample. Therefore, we will consider the values calculated from the viscosity sensor to be more representative of the sample of Oil B used in the dilution tests.

As expected, the viscosity of the mixtures of Oil A and B is bounded by the viscosity of the pure samples. As the temperature increases, the viscosity of the mixture decreased.

Also, as the mass of Oil B increases in the mixture the viscosity of the mixture also decreases. This is shown in **Figs. 4.26 and 4.27.**

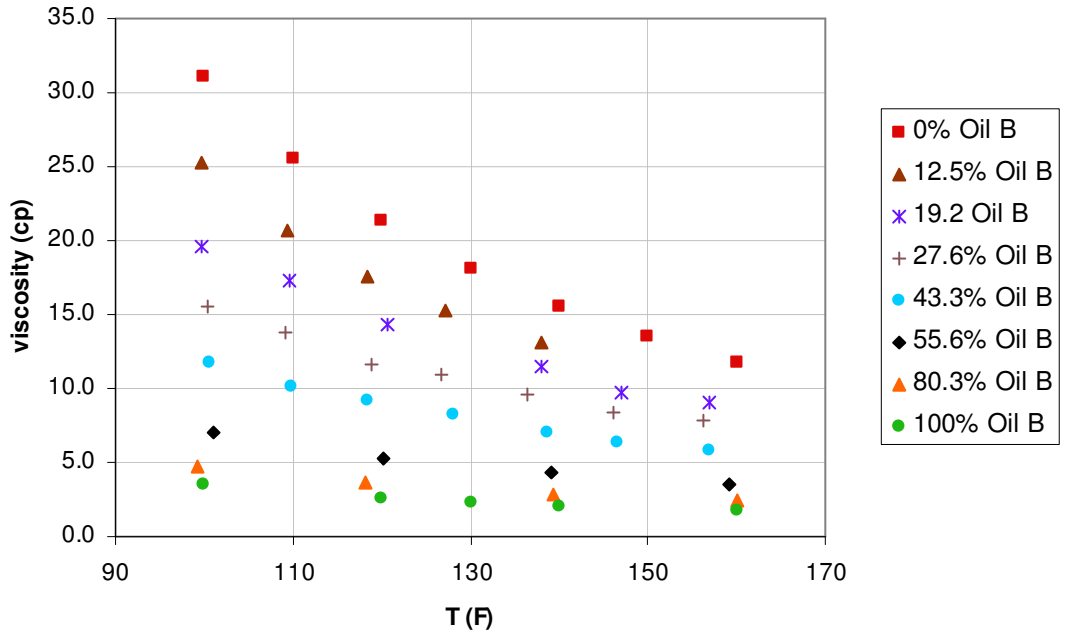

Fig. 4.26—Viscosity of mixture of oil A and B as a function of temperature, measured from the viscosity sensor.

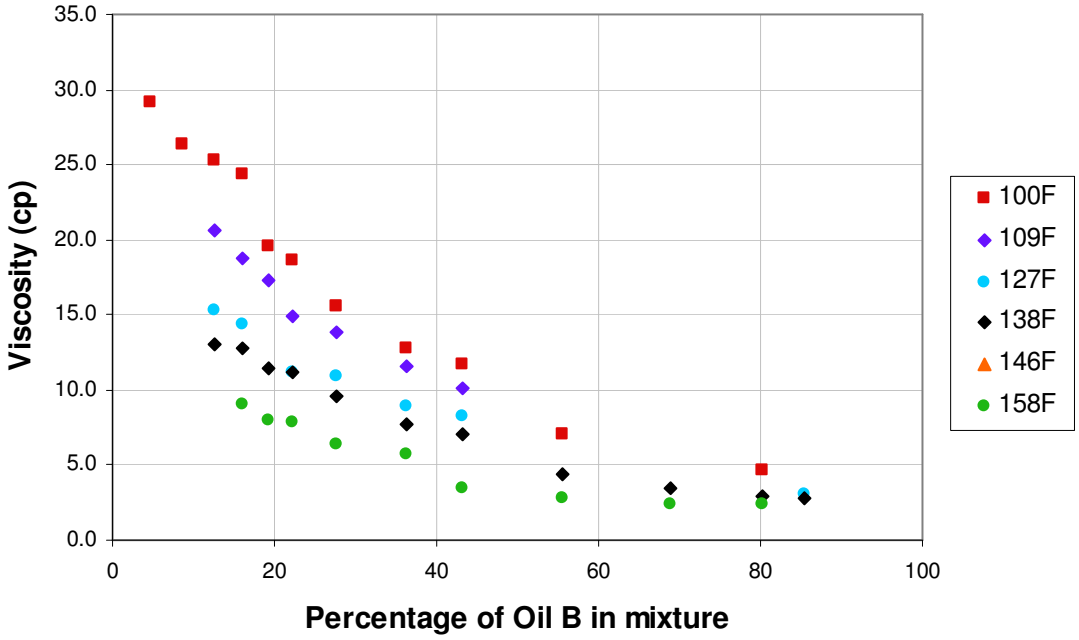

Fig. 4.27- Viscosity of mixture of oil A and B, as a function of composition of oil B, measured from viscosity sensor.

We believe it is important to emphasize that with our laboratory equipment, we were able to measure relatively small changes in pressure drop response and therefore small changes of viscosity in the more viscous Oil A in presence of small amounts of the lighter Oil B. This advocates the possibility of using the viscosity sensor as a continuous monitoring tool to detect the introduction of contaminants that affect the viscosity of the fluid.

With the calculated viscosity values from the sensor, we were requested to obtain mixing rules to characterize the viscosity of the mixture of Oil A and B as a function of

temperature and composition. In general a mixing rule is used to model the compositional effects on physical properties of mixtures. It consists on taking a weighted average of the physical properties of each pure component to obtain the physical property of the mixture. The underlying assumption to apply mixing rules is that the components of the mixture do not interact with each other. A typical equation of mixing rules for viscosity of a mixture is:

$$\mu_m{}^n = \sum_{i=1}^{Nc} (x_i \mu_i)^n \ , \quad \text{.....} \quad (4.9)$$

where μ_m is the viscosity of the mixture, and x is weight factor, which may be the mole fraction, volume fraction, or weight fraction of each component i. This rule is easy to adjust in a spreadsheet program. However this rule may not be flexible enough to model the viscosity of certain oil mixtures according to Mago[27]. A more flexible mixing rule is shown in **Eq.4.10:**

$$\mu_m = \prod_{i=1}^{Nc} \mu_i{}^{f(x_i)} \ , \quad \text{.....} \quad (4.10)$$

We adjusted the viscosity of the mixture using this mixing rule. Since we have two components- Oil A and B, we can expand Eq. 4.10 as:

$$\mu_m = \mu_A{}^{ax_A} \mu_B{}^{bx_B} \ , \quad \text{.....} \quad (4.11)$$

In order to include the temperature dependence, the viscosity of the pure oils A and B is modeled as a function of temperature by the following expression:

$$\mu_i = c\, e^{\frac{d}{T}} . \quad \text{..... (4.12)}$$

Where:

x_A and x_B are the percentage of components A and B on a molar fraction or weight basis.

T is the temperature in Kelvin.

μ_A and μ_B are the viscosity of pure component A and B at the temperature T

a, b, c, d are numerical constants.

For the mixture, we used the weight fraction and molar fraction as our choice of averaging factor. We adjusted the model to the experimental values using a fitting subroutine available in the Mathematica software package. Since we need the molecular weight of Oil A and Oil B to determine the mole fraction of each component in the mixture, the Katz-Firoozabadi method was used to determine an equivalent carbon number based on the density of each mixture at standard conditions. With this number, we estimated the molecular weight of Oil A and B. With this information we calculated the molar fraction of each component in the mixture. The estimated molecular weight for oil A and B are shown in **Table 4.18.**

Table 4.18—Estimated molecular weight of oil A and B from Katz-Firoozabadi correlation.

	Oil A	Oil B
Density (g/cm^3)	0.9032	0.8432
Molecular Weight	416	230

The adjusted coefficients for the viscosity of the pure Oil A and B are shown in are shown in **Table 4.19**. The adjusted mixing rules coefficients are presented in **Table 4.20**.

Table 4.19—Adjusted coefficients *c* and *d* for Eq.4.12.

	c	*d*
Oil A	0.00112	3178.487
Oil B	0.00157	2394.462

Table 4.20—Adjusted coefficients *a* and *b* for mixing rules in Eq.4.11.

	a	*b*	Average relative error (%)	R^2	Sum of squared residuals
Weight fraction basis	1.0206	0.7749	5.6	0.9917	20.355
Molar fraction basis	1.0522	1.2911	9.5	0.9784	56.63

Based on the statistical information obtained from the fitting routine, we consider the mixing rules on a weight fraction basis to describe the viscosity of the mixture as a function of composition and temperature more accurate than the model using the molar fraction basis. As an example, **Fig. 4.28** shows several experimental points and the model calculated with Eq. 4.11 on a weight fraction basis. The model loses accuracy as the amount of Oil B is increasing. The average relative error was calculated as 5.6%. Similar problems occurred with the model using the molar fraction basis. Overall the quality of the fit was poorer and this was reflected in the lower R^2 and the higher average relative error. A cross plot of predicted versus experimental viscosity is shown in **Fig.4.29.** We believe the predictions of the mixing rule can be improved by further

improving by selecting a different $f(x_i)$ function for Eq. 4.10. Nonetheless, for practical purposes, we think the model is reasonable.

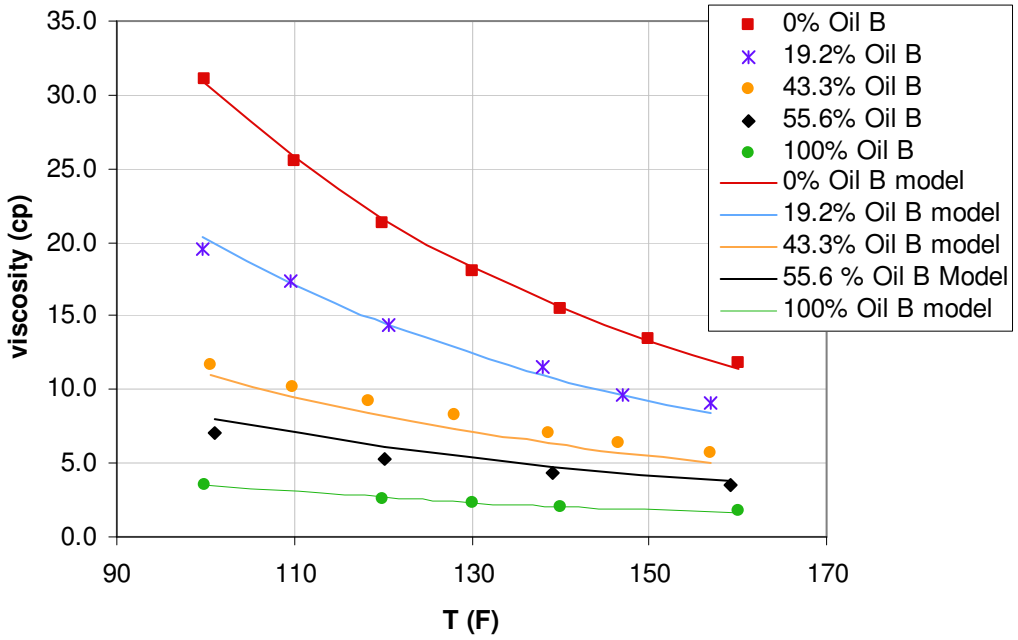

Fig. 4.28—Viscosity of mixture of Oil A and B, as a function of temperature and composition. Dots indicate the experimental values. Solid lines correspond to the mixing rule model shown in Eq. 4.11.

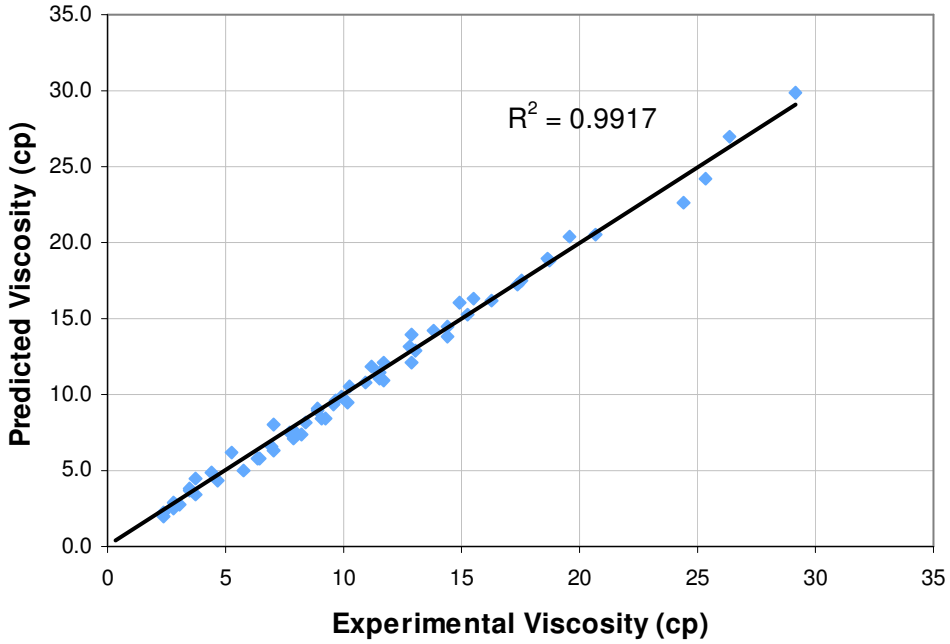

Fig. 4.29—Crossplot of viscosity of mixture of oil A and B. Predicted viscosity was calculated using Eq. 4.11.

Evaluation of a Non-Newtonian fluid

After we completed the characterization of the response of the device for Newtonian fluids, we explored the response of the device using a non-Newtonian fluid. Non-Newtonian fluids are typically found in petroleum engineering applications, specifically, in drilling and well stimulation operations.

Characterization Fluids

Xanthan gum is an extracellular polysaccharide used regularly as a rheology modifier in the food, cosmetic and petroleum industry applications. This substance is produced

by a process involving fermentation of glucose or sucrose by bacteria of the species *Xanthomonas campestris.*

The attractiveness of xanthan gum comes from its capability of producing a large increase in the viscosity of fluids by adding very small amounts of gum. In terms of rheology, solutions of xanthan gun at low concentrations exhibit high viscosity at low shear rates, and shear thinning or pseudoplastic behavior at high shear rates. These solutions are stable even when exposed to extreme temperatures, swings in pH and salt contamination, therefore making them ideal for numerous commercial applications. In the oil industry it is usually exploited as a thickener for drilling mud and as a viscosifier of hydraulic fracture fluids.

The fluids used in our tests were aqueous dispersions of 0.1% and 0.2% on a weight basis of xanthan gum. Xanthan gum was selected in order to observe the viscometer response to a shear thinning fluid. The dispersion was prepared by gradually dispersing the powder in the aqueous phase using mechanical agitation. The dispersion was allowed to fully hydrate and the sample was tested within 48 hours of preparation to reduce the risk of contamination or possible degradation.

The testing protocol was the same as for the Newtonian fluids. We cleaned and dried the complete flow loop, charged the xanthan gum mixture and measured the pressure drop response across the sensor geometry with changes in flow rate. In addition, we took a

small sample of the solution and we measured its rheological properties with the Brookfield rheometer after testing, to have as a reference.

We proceeded to run the tests, as before. However, the response of the equipment was different. At high flow rates we had no problem capturing information from the pressure transducers. However, testing at low rates was sometimes erratic and there was a lag in response. We believe this was caused by the sharp increase in viscosity at lower flow rates.

We tested dispersions at 0.1 and 0.2% on a weight basis. We considered a 0.5% solution. However, it was considered too viscous and it was not possible to use it in our flow loop due to pump limitations.

We conducted the test at a temperature of 60°F average. Due to the higher viscosity of the mixture, the pump produced extra heat when starting the test at low flow rates and we had to provide additional cooling in order to keep the temperature as stable as possible in the thermal bath. We reached flow rates up to 1 gallon/min.

The observed pressure drop – flow rate response observed in the device is shown in **Fig. 4.30.** The pressure drop response for pure water is shown as well as a reference. We can see the increase in the pressure drop as the concentration of xanthan gum increases.

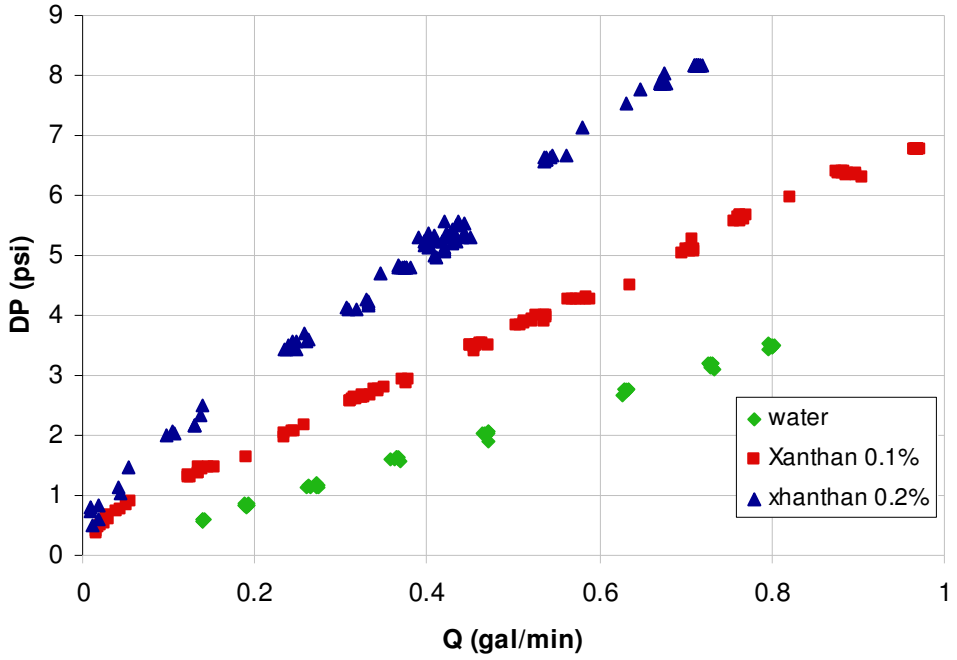

Fig. 4.30—Pressure drop as a function of flow rate for xanthan gum solutions and water.

Overall the pressure drop – flow rate response follows the same linear response expected from Newtonian fluids described in Eq. 4.1 at high flow rates. There was some scattering and instability in many of the collected data for the solution at 0.2% concentration.

It seems that the viscosity decrease due to shear thinning is no longer noticeable at flow rates in excess of 0.2 gallons per minute. However at lower flow rates, the shear rate is lower and the fluid should be thickening. At rates lower than 0.2 gal/min we can see that the trend appears not to be straight line and there is small changing slope towards the point of zero flow rate. This change in shape should be caused by the shear thinning

nature of the fluid. However, due to the characteristics of the geometry of the sensor, designed to maintain high shear rates, this effect seems confined to very low rates.

We can compare the rheology of the Xanthan gum fluid is presented in **Tables 4.21 and 4.22.**

The spindle used in the measurements did not allow for automatic calculation of the shear stress and shear rate data, for this we calculated the parameters manually using the expressions shown in Appendix A.

Table 4.21—Measured rheological properties for xhanthan gum solution at 0.1% using Brookfield viscometer.

RPM	xanthan 0.1% viscosity (cp)	% torque
250	18.1	76
220	18.4	67.5
200	18.6	62
180	18.9	56.7
150	20.2	50.3
120	22.7	45.3
90	26.5	39.7
60	33	33
30	48.6	24.3
20	60.6	20.1
10	85.2	14.2
6	108	10.7
3	140	7.2

Table 4.22—Measured rheological properties for xanthan gum solution at 0.2% using Brookfield rheometer.

xanthan 0.2%		
RPM	**viscosity (cp)**	**% torque**
20	273	91
15	338	84.6
10	457	76.1
6	661	66.3
3	1082	54.3

These values were obtained from the Brookfield rheometer and they indicate clearly the shear-thinning nature of the fluid. The apparent viscosity is reduced as the rotational speed is increased in the rheometer.

CHAPTER V

SIMULATION OF THE SENSOR RESPONSE

5.1 Introduction

In this chapter, we present the derivation of different mathematical expressions to describe the performance of the sensor. The main goal is to obtain an expression that allows us to model the pressure drop - flow rate response of the sensor. Such expressions will allow us to analyze the performance of the sensor and to optimize its physical dimensions based on the anticipated range of flow and type of fluid. Our specific objectives in this chapter are:

- Developing a fundamental model of the response of the sensor including geometrical variables.
- Generalizing this response to Newtonian and Non-Newtonian fluids, (power law fluids)

To develop a mathematical model of the sensor response, we started out by examining different approaches to model fluid flow under different geometries. There is abundance of literature on this particular topic, dealing with modeling of non-Newtonian flow under complex geometries and under a wide variety of conditions. We examined different approaches to attempt to solve this problem, from complex models to simplified approximations under different assumptions. Since we were given the geometric profile of the sensor prototype, we modeled the flow of Newtonian and power-law fluids under

this geometry using the following approaches: In particular, we examined the following techniques

- Modeling fluid flow by approximating the geometry of the device to simpler geometries for which analytical solutions for fluid flow have already been found in the literature.
- Modeling fluid flow by using a finite element technique to solve the equations of motion under certain assumptions

The derivation and application of each of these approaches is presented and discussed in this chapter.

5.2 Development of Approximate Solutions

Our objective is to model the flow of a power law fluid through the annular tapered space between two coaxial surfaces. Flow in tapered enclosures has a large number of applications in several industries. For example, in fuel injectors, die heads and extrusion press molds, fluid is forced to flow within the narrow gap formed between conical surfaces. **Fig. 5.1** shows three types of annular channels between conical surfaces with same axis. In (a), the annular space is formed between two cones with a common apex and different opening angle. In (b) the annular space is between cones without a common apex but equal opening angle. And finally in (c), the annular space is between cones without a common apex and with different opening angle. Form these figures it is t is clear that depending on the position of the apex of the cones and the opening angle, we can have an annular channel in which the gap increases (a), stays constant (b), or decreases (c), the further with the distance from the apex.

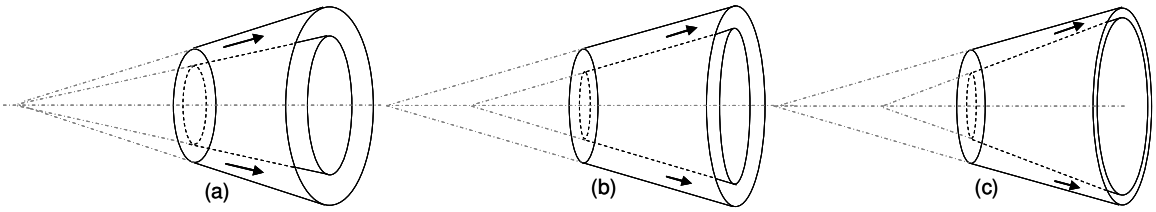

Fig. 5.1— Annular space between conical surfaces, (a) between cones with same apex, different opening angle, (b) between cones with different apex, same opening angle, (c) between cones without a common apex and different opening angle.

Depending on the direction of flow, the literature distinguishes the cases for divergent and convergent flow. Flow direction from the apex of the cone towards the base is referred to as divergent flow. Flow in the opposite direction is convergent flow.

There are a few analytical solutions proposed to model fluid flow in such tapered annular channels at low Reynolds number of fluids in the annular space between conical surfaces. For the cases shown in Fig.5.1 (a) and (b) Vatistas[18] and Ulev[19] developed analytical solutions; but to the best of our knowledge, there are no analytical solutions explicitly developed for the same type of geometry of our sensor. In our case of interest, the prototype geometry of our sensor is similar to case (c). The gap between cones becomes narrower furthest from the apex.

One alternative to model the flow inside a conical annular space is to divide the annulus into small segments and use the known solutions for flow in annular space between concentric cylinders, as shown in **Fig. 5.2**. We divide the annulus in several pieces of

length ΔL and calculate the pressure drop for each segment. The sum of all the pressure drops is the total pressure drop across the device.

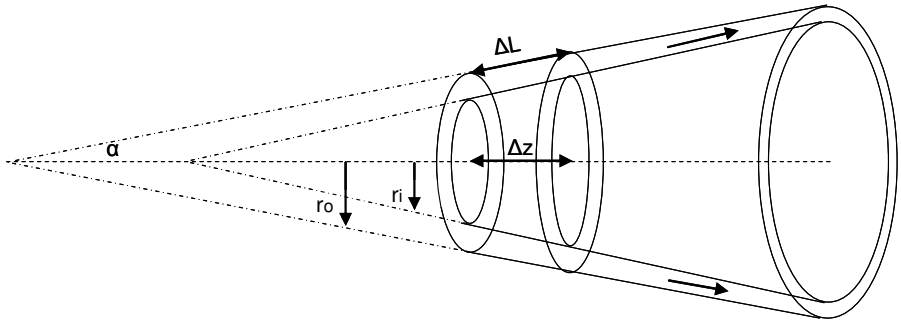

Fig. 5.2—Approximation of the annulus as series of concentric cylinders.

The basic annular flow model is discussed first and then applied to the particular geometrical configuration of the prototype device.

5.2.1 Analytical Solution

The problem of axial laminar flow of a power-law fluid in a concentric annular under an imposed pressure gradient with both cylinders stationary was first solved by Frederickson and Bird[12]. Here we present their solution.

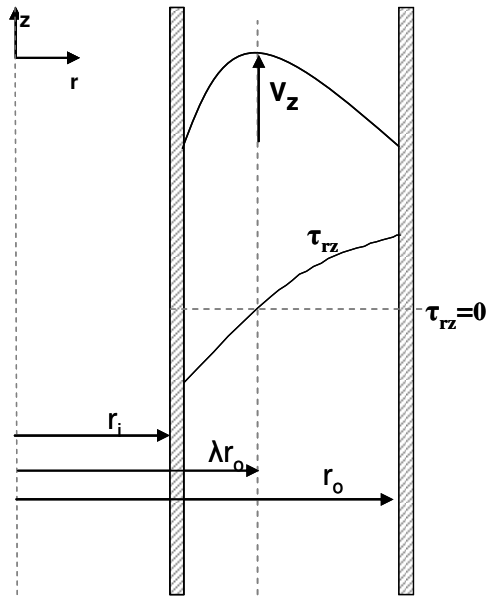

Fig. 5.3—Representation of axial flow in a concentric annulus. (from Frederickson[9])

Fig. 5.3 shows a schematic of pressure driven axial flow in a concentric annular channel. r_o and r_i are the outer and inner radius of the cylinders. The equations of motion and continuity can be written in cylindrical (r, θ, z) coordinate system. The system of equations can be simplified making the following assumptions:

- The fluid is incompressible.
- The flow is rotationally symmetric (no variation in the θ direction)
- The flow is in steady state.(time independent)
- The flow is laminar.
- The cylinders are long enough so that end effects can be neglected.
- The flow is isothermal (no change in temperature)

The shear stress distribution in the annulus can be described as:

$$\tau_{rz} = \frac{1}{2}\frac{\Delta P}{L}\left(r - \frac{(\lambda r_o)^2}{r} \right), \quad \text{..... (5.1)}$$

The axial distance $\lambda\, r_o$ represents the point in which $\tau_{rz} = 0$, and

$$\frac{\Delta P}{L} = \frac{p_0 - p_L}{L} + \rho g_z, \quad \text{..... (5.2)}$$

where p_0 and p_L are the static pressures at $z = 0$ and $z = L$, and L is the length of the annular, ρ is the mass density of the fluid and g_z is the component of gravitational acceleration in the direction of flow.

According to the power-law rheological model, the shear stress in this geometry is:

$$\tau_{rz} = -K\left|\frac{dv_z}{dr}\right|^{n-1}\left(\frac{dv_z}{dr}\right), \quad \text{..... (5.3)}$$

where K is the consistency index and n is the power-law index. Combining Eq. 5.1 and Eq. 5.3, the differential equation to solve is:

$$-\left|\frac{dv_z}{dr}\right|^{n-1}\left(\frac{dv_z}{dr}\right) = \frac{1}{2K}\frac{\Delta P}{L}\left(r - \frac{(\lambda r_o)^2}{r} \right). \quad \text{..... (5.4)}$$

Introducing a dimensionless variable $\xi = r / r_o$, the inner wall of the annular is then $\xi = r_i / r_o = \kappa$. The outer wall is $\xi = r_o / r_o = 1$. κ is also known as the aspect ratio of the annular channel. Changing variables, Eq. 5.4 is then:

$$-\left|\frac{dv_z}{d\xi}\right|^{n-1}\left(\frac{dv_z}{d\xi}\right) = r_o{}^n\,\frac{r_o}{2K}\frac{\Delta P}{L}\left(\xi - \frac{(\lambda)^2}{\xi} \right). \quad \text{..... (5.5)}$$

Integrating with the no slip wall boundary condition $v_z = 0$ at the walls of the cylinders at $\xi = \kappa$ and $\xi = 1$, the velocity profile is described by:

$$v_z = r_o\left(\frac{r_o}{2K}\Delta P\right)^s \int_{\kappa}^{\xi}\left(\frac{\lambda^2}{x} - x\right)^s dx \quad \kappa \le \xi \le \lambda, \quad \text{..... (5.6)}$$

$$v_z = r_o\left(\frac{r_o}{2K}\Delta P\right)^s \int_{\xi}^{1}\left(x - \frac{\lambda^2}{x}\right)^s dx \quad \lambda \le \xi \le 1, \quad \text{..... (5.7)}$$

where $s = 1/n$ and n is the power law index of the fluid.

At $\xi = \lambda$ both expressions **Eq. 5.6** and **Eq. 5.7** must give the same velocity, therefore the value of λ is found by solving the following equation:

$$\int_{\kappa}^{\lambda}\left(\frac{\lambda^2}{x} - x\right)^s dx - \int_{\lambda}^{1}\left(x - \frac{\lambda^2}{x}\right)^s dx = 0. \quad \text{..... (5.8)}$$

Eq. 5.8 can be solved numerically by an iterative procedure such as Newton's method. We solved Eq. 5.8, using the software Mathematica to obtain the values of λ as a function of the aspect ratio κ of the annular channel, and the reciprocal of the power-law index n. Convergence was obtained in a few iterations. For example, for an annular channel with an aspect ratio $\kappa = 0.1$, and a Newtonian fluid $n = 1$, the value of λ is obtained as follows in **Table 5.1**. The value of λ converges in nine iterations.

Table 5.1—Iterations to calculate the root of Eq. 5.8 for an aspect ratio κ=0.1 and power law index n=1.

Iteration	λ	Value of Eq. 5.8
1	0.10000	-0.47197
2	1.00000	1.80759
3	0.286342	-0.30621
4	0.580692	0.28144
5	0.439720	-0.04979
6	0.460910	-0.00584
7	0.463670	3.34×10^{-5}
8	0.463655	-9.9×10^{-8}
9	0.463655	8.8×10^{-10}

The solution of Eq. 5.8 for different values of s and κ is presented in **Fig. 5.4.** The value of λ is plotted as a function of s for annular geometries of aspect ratio κ.

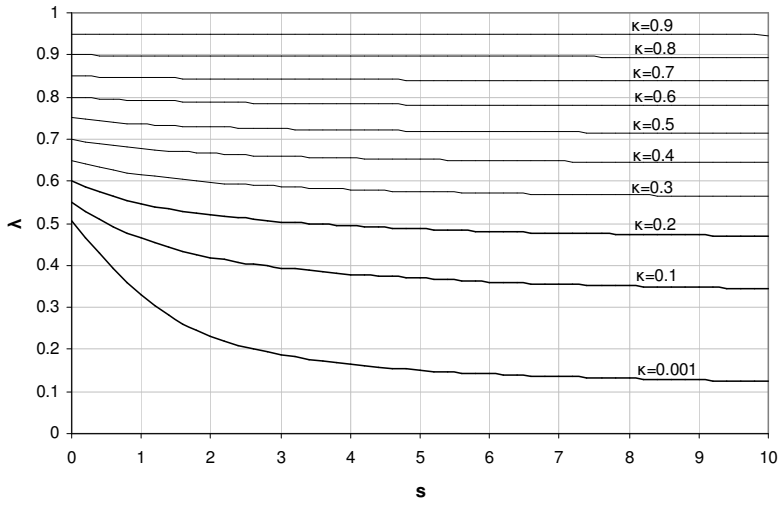

Fig. 5.4— λ calculated from solving Eq. 5.8 as function of aspect ratio κ and reciprocal of the power-law index n (s=1/n) for flow in concentric annular channel.

We can see that, λ has a greater variability for low values of κ. That is, for concentric annular channels with a large gap. As the gap between the cylinders is reduced, κ

increases and the value of λ becomes nearly constant for any value of *s* and its value is approximately the middle point between the inner and outer radius. This suggests that for annular geometries with narrow gaps, it is a good approximation to estimate the value of λ as $\lambda = \frac{\kappa + 1}{2}$.

This situation can be visualized better in **Fig. 5.5**. In this figure, λ is plotted as a function of the aspect ratio κ of the annular channel for three different values of *n*. We can see that as κ increases, the value of λ approach the line $\lambda = \frac{\kappa + 1}{2}$.

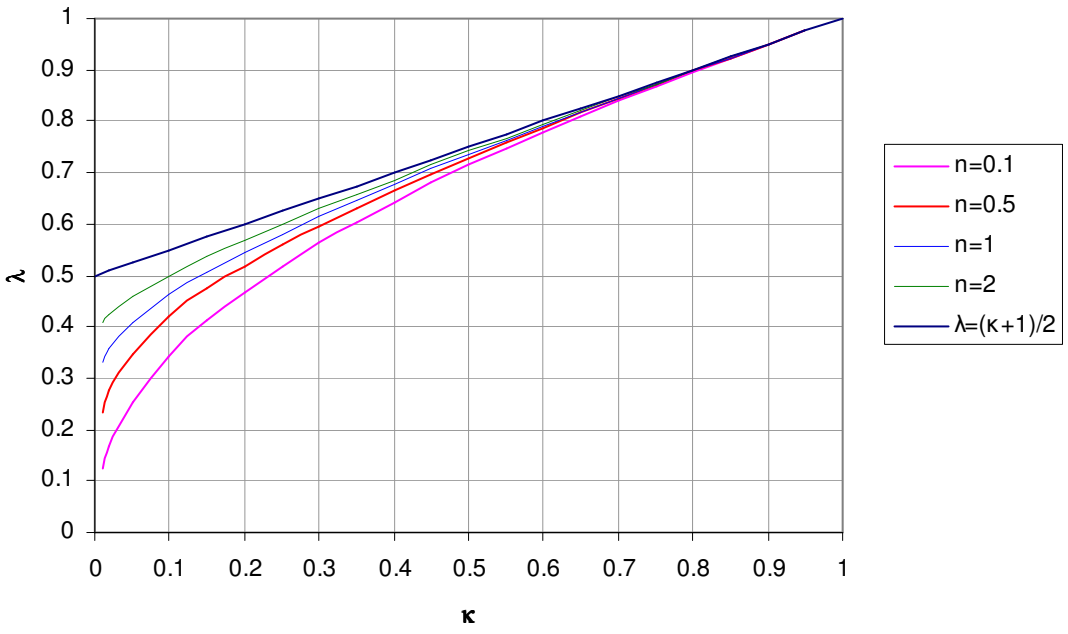

Fig. 5.5— λ calculated from Eq. 5.8 as a function of aspect ratio κ and power-law index n in concentric annular channel.

Eq. 5.6 and 5.7 can be expressed as:

$$v_z = r_o\left(\frac{r_o}{2K}\frac{\Delta P}{L}\right)^s v_{zD}, \quad \text{..... (5.9)}$$

where

$$v_{zD} = \begin{cases} \int_{\kappa}^{\xi}\left(\frac{\lambda^2}{x} - x\right)^s dx & \kappa \le \xi \le \lambda \\ \int_{\xi}^{1}\left(x - \frac{\lambda^2}{x}\right)^s dx & \lambda \le \xi \le 1 \end{cases} . \quad \text{..... (5.10)}$$

Once λ has been determined, the velocity profile can be calculated using **Eq. 5.9**. As an example, for a concentric annular with aspect ratio of $\kappa = 0.1$ the dimensionless velocity profile for different values of *s* is presented in **Fig. 5.6.**

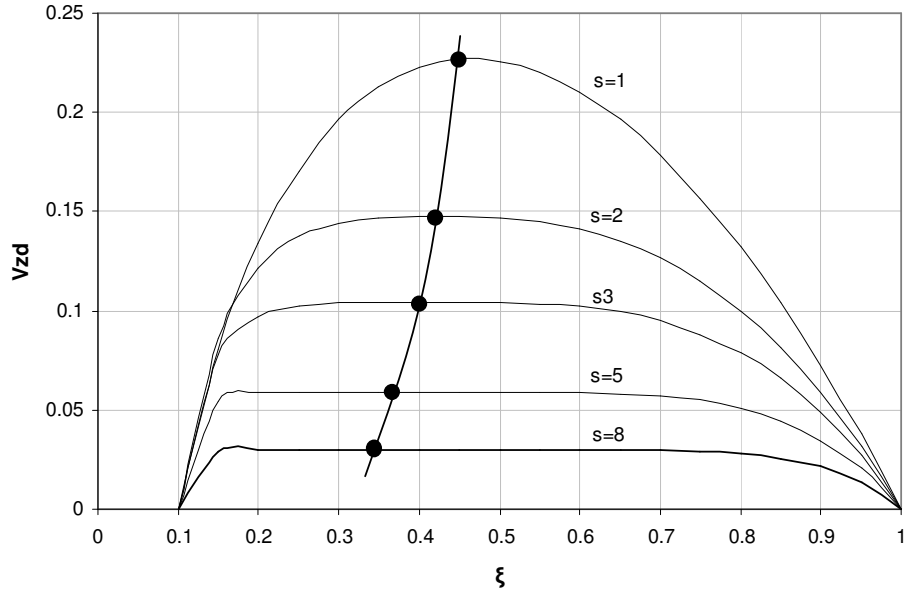

Fig. 5.6—Dimensionless velocity profile in concentric annular channel with aspect ratio κ=0.1. for for different values of the power-law index n, (s=1/n). The dots indicate the point where the dimensionless velocity Vzd reaches a maximum.

In Fig 5.6 the points $\xi = 0.1$ and $\xi = 1$ correspond to the inner and outer radius of the cylinders. As the value of *s* increases and therefore decreasing *n*, the velocity profile becomes flatter. The point where the velocity is at its maximum value, λ, is shown with dots. As we can see, for higher values of *s* (or lower n), the point where the velocity is at its maximum value is found closer to the inner cylinder wall. **Fig. 5.7** shows the dimensionless velocity profile for an annular geometry with a narrower gap, $\kappa = 0.5$. This annular channel is narrower and the profile is more symmetric. The point where the velocity v_{zD} reaches its maximum value shows less variation with the value of *s*. From $\lambda = 0.73$ at $s = 1$ to $\lambda = 0.71$ at $s = 5$.

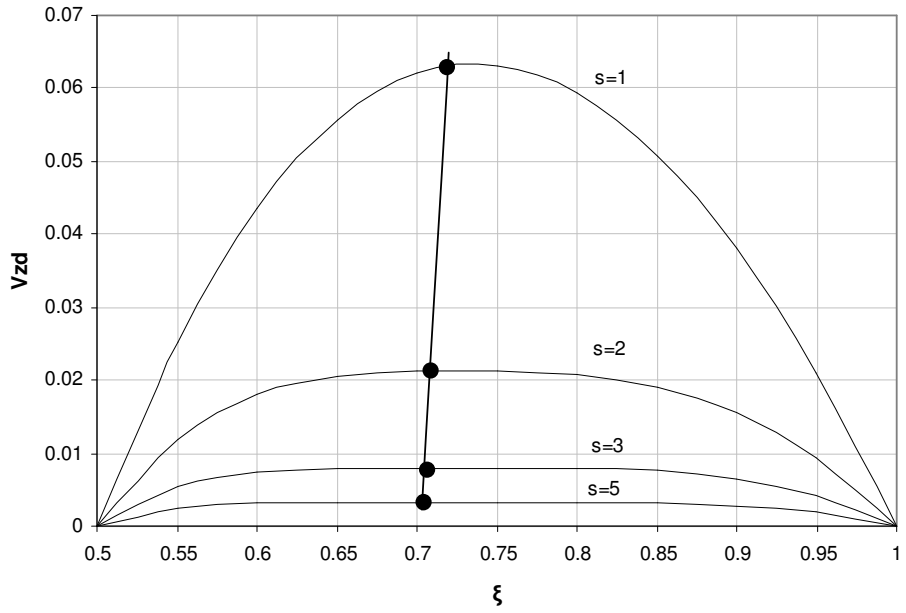

Fig. 5.7—Dimensionless velocity profile in concentric annular channel with aspect ratio κ=0.5 for different values of the power-law index n, (s=1/n). . The dots indicate the point where the dimensionless velocity Vzd reaches a maximum.

The volumetric flow rate Q is obtained integrating the velocity profile:

$$Q = 2\pi r_o^{\,2} \int_{\kappa}^{1} \xi v_z d\xi \,. \quad \text{..... (5.11)}$$

$$\frac{Q}{\pi r_o^{\,3}} = 2\left(\frac{r_o}{2K}\frac{\Delta P}{L}\right)^s \left[\begin{array}{l} \int_{\kappa}^{\lambda} \xi d\xi \int_{\kappa}^{\xi} \left(\frac{\lambda^2}{x} - x\right)^s dx \\ + \int_{\lambda}^{1} \xi d\xi \int_{\xi}^{1} \left(x - \frac{\lambda^2}{x}\right)^s dx \end{array}\right]. \quad \text{..... (5.12)}$$

Changing the order of integration

$$\frac{Q}{\pi r_o^{\,3}} = 2\left(\frac{r_o}{2K}\frac{\Delta P}{L}\right)^s \left[\int_{\kappa}^{\lambda} \left(\frac{\lambda^2}{x} - x\right)^s dx \int_{x}^{\lambda} \xi d\xi + \int_{\lambda}^{1} \left(x - \frac{\lambda^2}{x}\right)^s dx \int_{\lambda}^{x} \xi d\xi \right]. \quad \text{(5.13)}$$

$$\frac{Q}{\pi r_o^{\,3}} = \left(\frac{r_o}{2K}\frac{\Delta P}{L}\right)^s \left[\begin{array}{l} \int_{\kappa}^{\lambda} \left(\lambda^2 - x^2\right)\left(\frac{\lambda^2}{x} - x\right)^s dx + \\ \int_{\kappa}^{\lambda} \left(x^2 - \lambda^2\right)\left(x - \frac{\lambda^2}{x}\right)^s dx \end{array}\right]. \quad \text{..... (5.14)}$$

Rearranging:

$$Q = \pi r_o^{\,3} \left(\frac{r_o}{2K}\frac{\Delta P}{L}\right)^s \int_{\kappa}^{1} \left|\lambda^2 - x^2\right|^{s+1} x^{-s} dx \,. \quad \text{..... (5.15)}$$

The flow rate is then:

$$Q = \pi r_o^{\,3} \left(\frac{r_o}{2K}\frac{\Delta P}{L}\right)^s Q_D, \quad \text{..... (5.16)}$$

where

$$Q_D = \int_{\kappa}^{1} \left| \lambda^2 - x^2 \right|^{s+1} x^{-s} dx . \quad \text{..... (5.17)}$$

Frederickson and Bird[12] presented analytical expressions to calculate the value of the integral in Eq.5.17. However the expressions presented only work for integer values of *s*. To obtain the values of the dimensionless flow rate Q_d for *s* as an arbitrary real number it is necessary to interpolate from the curves provided in their paper. This is clearly a difficulty in the use of this method.

Hanks and Larsen[13] were able to overcome this limitation and further improve this previous work by solving analytically Eq. 5.16 in order to overcome the limitations for the calculation for any value of *s*. The details are reproduced in Appendix I.

With this result, we can calculate now flow rate as

$$Q = \pi \, r_o^{\,3} \left(\frac{r_o \Delta P}{2KL} \right)^s Q_D , \quad \text{..... (5.18)}$$

where

$$Q_D = \frac{1}{(3+s)} \left[-\left(\lambda^2 - \kappa^2 \right)^{1+s} \kappa^{1-s} + \left(1 - \lambda^2 \right)^{1+s} \right]. \quad \text{..... (5.19)}$$

Eq. 5.19 works for *s* as any arbitrary real number. **Fig. 5.8** presents the dimensionless flow rate Q_D calculated from Eq. 5.18 for different values of κ and *s*. The value of λ is calculated numerically solving Eq. 5.8 as shown previously.

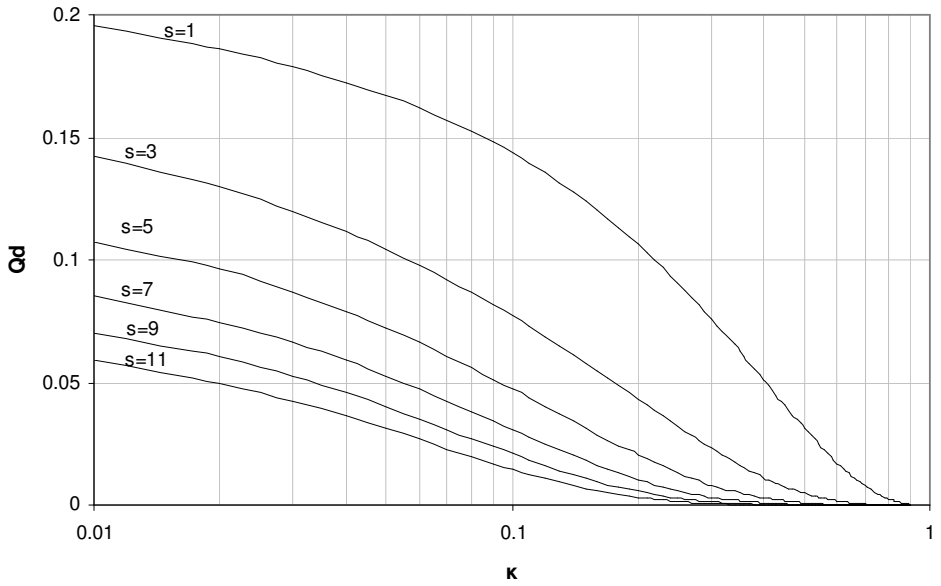

Fig. 5.8—Dimensionless flow rate Qd as a function of aspect ratio κ and power-law index n (s=1/n) for flow in concentric annular channels.

The pressure gradient is then

$$\frac{\Delta P}{L} = \frac{2K}{r_o}\left(\frac{(3n+1)Q}{n\pi r_o^{\,3} Y}\right)^n, \quad \text{..... (5.20)}$$

where

$$Y = \left[-\left(\lambda^2 - \kappa^2\right)^{1+1/n} \kappa^{1-1/n} + \left(1-\lambda^2\right)^{1+1/n}\right]. \quad \text{..... (5.21)}$$

Eq. 5.20 can be used to calculate the pressure drop for a given flow rate. λ is calculated numerically from Eq. 5.8.

For the case of a Newtonian fluid, n=1, we can compare the results from Eq 5.20 with the expression known from the literature for Newtonian fluid in concentric annular geometry.

For s=1 , λ is calculated as

$$\int_{\kappa}^{\lambda}\left(\frac{\lambda^2}{x}-x\right)dx-\int_{\lambda}^{1}\left(x-\frac{\lambda^2}{x}\right)dx=0, \quad \text{..... (5.22)}$$

$$\frac{1}{2}\left[-1+\kappa^2+2\lambda^2\left(-Ln(\lambda)+Ln\left(\frac{\lambda}{\kappa}\right)\right)\right]=0, \quad \text{..... (5.23)}$$

$$-1+\kappa^2-2Ln(\kappa)\lambda^2=0, \quad \text{..... (5.24)}$$

$$\lambda^2=\frac{\kappa^2-1}{2Ln(\kappa)}. \quad \text{..... (5.25)}$$

Introducing this into Eq. 5.19 and Eq. 5.18

$$Q_D=\frac{1}{4}\left[-\left(\lambda^2-\kappa^2\right)^2+\left(1-\lambda^2\right)^2\right]. \quad \text{..... (5.26)}$$

$$Q_D=\frac{1}{4}\left[1-\kappa^4+\frac{\left(\kappa^2-1\right)^2}{Ln(\kappa)}\right]. \quad \text{..... (5.27)}$$

$$Q=\frac{\pi r_o^{\,4}}{8\mu}\frac{\Delta P}{L}\left[1-\kappa^4+\frac{\left(\kappa^2-1\right)^2}{Ln(\kappa)}\right]. \quad \text{..... (5.28)}$$

since $\kappa=r_i/r_o$ and rearranging,

$$Q=\frac{\pi r_o^{\,4}}{8\mu}\frac{\Delta P}{L}\left[r_o^{\,4}-r_i^{\,4}+\frac{\left(r_i^{\,2}-r_o^{\,2}\right)^2}{Ln\left(r_i/r_o\right)}\right]. \quad \text{..... (5.29)}$$

Which is the same expression found in the literature for the flow rate as a function of the pressure drop for a Newtonian fluid in a concentric annular channel.

To use Eq. 5.20, we wish to express the variables in the following units

$\Delta P / L$: Pressure gradient in psi/in.

Q: flow rate, gal/min.

n: power law index, dimensionless.

K: consistency index, lbf s^n / ft^2.

r_o, r_i, outer and inner radii of the concentric cylinders, in.

$\kappa = r_i / r_o$, dimensionless.

λ, dimensionless.

Using dimensional analysis in Eq. 5.20 the units of the pressure gradient are

$$\text{units}\left[\Delta P / L\right] = \frac{\text{units}[K]}{\text{units}[r_o]}\left(\frac{\text{units}[Q]}{\text{units}[\text{r}_\text{o}^{\,3}]}\right)^n$$

$$\text{units}\left[\Delta P / L\right] = \frac{\text{lbf s}^n}{\text{ft}^2}\frac{1}{\text{in}}\left(\frac{\text{gal/min}}{\text{in}^3}\right)^n$$

Since we want the pressure gradient in psi/in, we apply the appropriate conversion factors

$$\text{units}\left[\Delta P / L\right] = \frac{\text{lbf}}{\text{ft}^2}\frac{\text{psi}}{144\dfrac{\text{lbf}}{\text{ft}^2}}\frac{\text{s}^n}{\text{in}}\left(\frac{\text{gal}}{\text{min}}\frac{231\,\text{in}^3}{\text{gal}}\frac{\text{min}}{60\text{s}}\frac{1}{\text{in}^3}\right)^n$$

$$\text{units}\left[\Delta P / L\right] = \frac{\text{psi}}{144}\frac{\text{s}^n}{\text{in}}\left(\frac{3.85}{\text{s}}\right)^n$$

$$\text{units}\left[\Delta P / L\right] = \frac{3.85^n}{144}\frac{\text{psi}}{\text{in}}$$

Since $\kappa = r_i / r_o$ and $s = 1/n$, then Eq. 5.20 can be written as:

$$\frac{\Delta P}{L} = \frac{K}{72}\left(\frac{3.85\left(1+3n\right)Q}{n\pi Y}\right)^n r_o^{\,-3n-1} \quad \text{..... (5.30)}$$

where

$$Y = \left[-\left(\lambda^2 - \kappa^2\right)^{1+1/n}\kappa^{1-1/n} + \left(1-\lambda^2\right)^{1+1/n}\right]. \quad \text{..... (5.31)}$$

and

$\Delta P / L$: Pressure gradient in psi/in.

Q: flow rate, gal/min.

n: power law index, dimensionless

K: consistency index, lbf s^n / ft^2.

r_o, r_i: outer and inner radius of the concentric cylinders, in.

λ: calculated from Eq. 5.8

Our objective is to apply this result to model the flow of power-law fluids in the prototype device. The geometry of this region can be described as similar to non-common apex tapered annular channels. Parnaby and Worth[28] propose a procedure in which they represent the tapered annular region as a series of parallel annular segments of increasing diameter. They calculate mean dimensions of each section and then

determine the individual pressure drop for each segment. The total pressure drop is calculated as the sum of the separate pressure drops. Shenoy[21] extended their solution and included the approximation solutions for power-law flow in non common apex tapered annular channels based on a lubrication approximation. The total pressure drop can be described as

$$\Delta P = \sum \Delta P_i \ . \quad \text{..... (5.32)}$$

Where ΔP_i is the pressure drop for segment *i*. The pressure gradient of each segment of length ΔL_i is

$$\frac{\Delta P_i}{\Delta L_i} = 2K\left(\frac{(3n+1)Q}{n\pi}\right)^n r_o^{-3n-1} Y^{-n} . \quad \text{..... (5.33)}$$

The length of each segment is taken along the length of the surface of the outer cone. This distance is approximately $\Delta L = \frac{\Delta z}{\cos\alpha}$. We can then write:

$$\frac{dP}{dz} = \frac{2K}{\cos(\alpha)}\left(\frac{(1+3n)Q}{n\pi}\right)^n r_o^{-3n-1} Y^{-n} . \quad \text{..... (5.34)}$$

Integrating over the length of the device:

$$\Delta P = \frac{2K}{\cos\alpha}\left(\frac{(3\mathrm{n}+1)Q}{\mathrm{n}\pi}\right)^n \int_0^L r_o^{-3n-1} Y^{-n} dz . \quad \text{..... (5.35)}$$

Rearranging

$$\Delta P = 2KQ^n \frac{}{\cos\alpha}\left(\frac{(3n+1)}{n\pi}\right)^n \int_0^L r_o^{-3n-1} Y^{-n} dz\,. \quad \text{..... (5.36)}$$

To calculate the pressure drop then using this approximation, it is necessary to calculate the integral in Eq.5.35

$$f = \int_0^L r_o^{-3n-1} Y^{-n} dz\,, \quad \text{..... (5.37)}$$

where

$$r_o(z) = z\tan(\alpha) + r_o(0),$$

$$r_i(z) = \sqrt{(z\tan(\alpha) + r_o(0))^2 - r_{fl}^{\,2}}\,,$$

$$Y = \left[-\left(\lambda^2 - \kappa^2\right)^{1+1/n} \kappa^{1-1/n} + \left(1-\lambda^2\right)^{1+1/n}\right],$$

$$\kappa = \frac{r_i(z)}{r_o(z)}.$$

λ is also a function of the aspect ratio κ so its value changes along the z axis. Given the need to calculate λ numerically from solving Eq. 5.8, The integral in Eq. 5.36 has to be integrated using a numerical method. We used a numerical integration subroutine in Mathematica to calculate this integral.

The outer and inner radii of the prototype also depend on design variables that are particularly tailored for a target application of the device. These variables are the opening angle α, the initial outer housing radius $r_o(0)$, and the radius of the flow line in which the device is attached to, r_{fl}. The aspect ratio profile of the prototype will change

depending on the particular values of these design parameters. We are interested in examining the effect of these parameters in the configuration of the flow region.

Fig.5.9 shows the inner and outer radii profile for a prototype device with $r_{fl} = 0.4$ in and $r_o(0) = 0.5$ in. The shaded area represents the flow region. In (a) the opening angle is set to $\alpha = 0°$ and in (b) the opening angle is set to $\alpha = 4°$. For $\alpha = 0°$ it is evident that the geometry is a concentric cylinder annulus. When the angle increases, the channel becomes narrower and steeper.

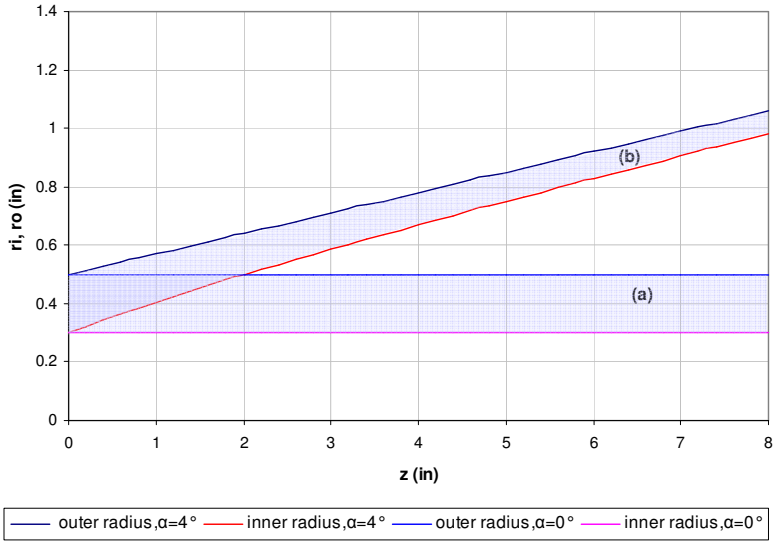

Fig. 5.9— Effect of angle α in the cross section profile. (a) inner and outer radii for α=0°, (b) inner and outer radii for α=4°. Both cases set to L= 8 in, $r_o(0)$ =0.5 in, r_{fl} = 0.4 in.

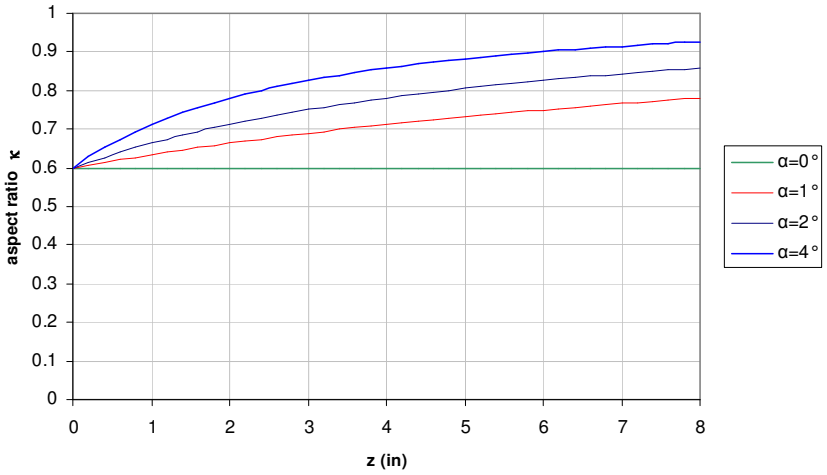

Fig. 5.10—Effect of angle α in the aspect ratio κ profile along the length of the device. L= 8 in, $r_o(0)$=0.5 in, r_{fl} = 0.4 in.

Fig. 5.10 shows the profile of the aspect ratio κ from the inlet to outlet of the sensor for different values of opening angle and $r_{fl} = 0.4$ in and $r_o(0) = 0.5$ in. For larger opening angles, the annulus becomes narrower and the aspect ratio κ increases along the profile of the device.

The initial outer housing radius $r_o(0)$, and the radius of the flow line in which the device is attached to, r_{fl} are variables that should be selected not only to achieve a target response in terms of pressure drop and flow rate, but also determine the size of the inner pin and outer casing and the fitting of the complete assembled tool in the process line. For example, the prototype we studied in the laboratory had its dimensions tailored to be compatible to those of the RDT.

At the inlet $z = 0$, the inner radius is

$$r_i(0) = \sqrt{r_o(0)^2 - r_{fl}^{\ 2}} .$$

It is clear that $r_o(0) \geq r_{fl}$. Therefore r_{fl} has to be no larger than the initial internal casing radius. For a fixed opening angle and initial outer casing radius, we can then see the effect of r_{fl} in the profile of the flow region. In **Fig. 5.11** and **Fig. 5.12** we plot the outer and inner radius profile for $\alpha = 4\circ$, $r_o(0) = 0.5$ in. and different ratios of $r_{fl} / r_o(0)$.

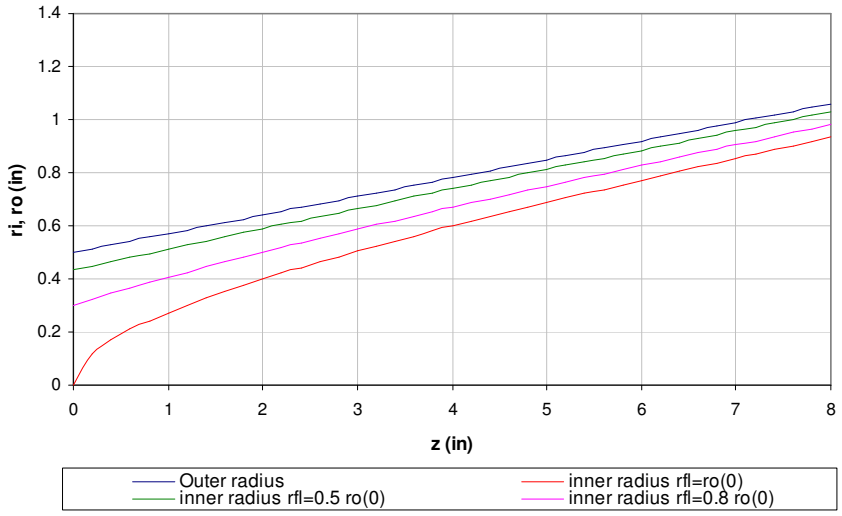

Fig. 5.11—Effect of r_{fl} in the r_i profile. L= 8 in, $r_o(0)$ =0.5 in, r_{fl} = 0.4 in, L-8 in.

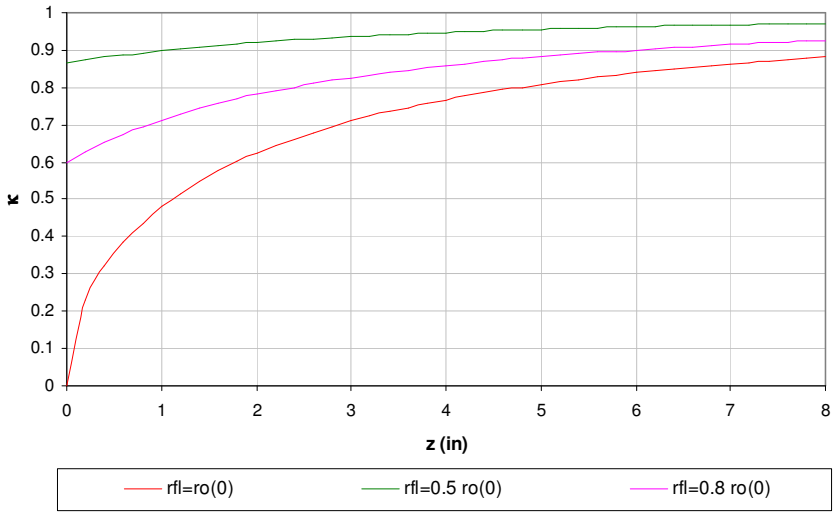

Fig. 5.12—Effect of r_{fl} in the aspect ratio κ profile along the length of the device. L= 8 in, $r_o(0)$=0.5 in, r_{fl} = 0.4 in.

Increasing the value of r_{fl} widens the gap in the flow region and the shape of the inner pin is more curved. When $r_{fl} = r_o(0)$, we obtain the maximum gap. Lower values of r_{fl} have the effect of narrowing the annular gap between the outer casing and inner pin surfaces and the overall shape of the inner pin profile is less curved and tends to approximate a straight line. This extreme case is not practical since the inner pin design requires an insert to attach the pin to the outer casing and there is an entry section before the section where the pressure is measured. Nevertheless, this is explored.

This suggests that when the inner pin has a shape that deviates from the conical shape, there may be entry effects that could affect the validity of the approximations to model

fluid flow for this geometry. Especially at the inlet of the device, where the curvature is more pronounced and the gap is the widest.

Figs. 5.13 and 5.14 show the values of λ along the profile of the sensor as a function of the for n=1 and n=0.5 respectively for different values of α with $r_{fl} = 0.11$ and $r_o(0) = 0.2183$. This plots indicate that, given the high aspect ratio, (narrow gap) the value of λ is not affected by the power-law index n.

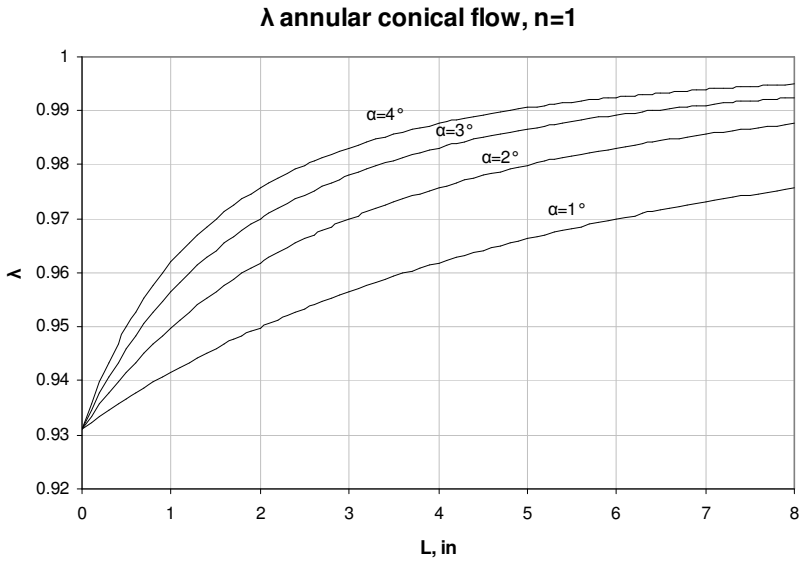

Fig. 5.13—λ for power law flow in annular conical flow along the length of the sensor, n=1, L=8 in.

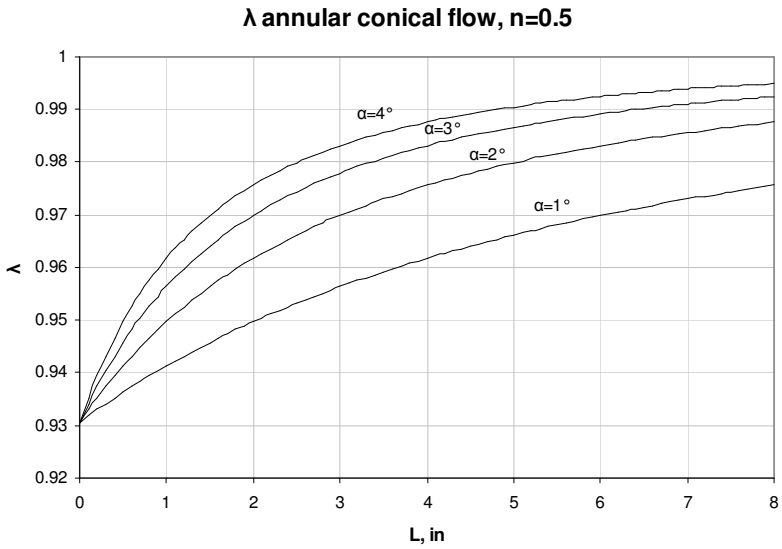

Fig. 5.14— λ for power law flow in annular conical flow along the length of the sensor, n=0.5 L=8 in.

In **Table 5.2** the first three columns show the values of λ as a function of the axial distance inside the device, for power law index of $n = 0.5$, $n = 1$ and $n = 1.5$ in a geometry with $\alpha = 3^\circ$ and $r_{fl} = 0.11$ and $r_o(0) = 0.2183$. The fourth column shows the value of the approximation $\lambda = (\kappa + 1)/2$. The last three columns show the relative error in a percentage basis, between the calculated value of λ and the approximation. The small error suggests that for these geometries, it is possible to assume that λ is located in the middle point between the inner and outer radii. This assumption would certainly simplify calculation of the pressure drop from Eq. 5.35.

Table 5.2— λ as a function of the axial distance inside the device, α=3°, $r_o(0)$=0.2183 in , r_{fl}=0.11 in.

L (inch)	n =0.5 λ	n =1 λ	n = 1.5 λ	λ=(κ+1)/2	Error (%) n=0.5	Error (%) n=1	Error (%) n=1.5
0.0	0.931	0.931	0.931	0.932	0.134	0.089	0.067
1	0.956	0.957	0.957	0.957	0.051	0.034	0.025
2	0.970	0.970	0.970	0.970	0.024	0.016	0.012
3	0.978	0.978	0.978	0.978	0.013	0.008	0.006
4	0.983	0.983	0.983	0.983	0.007	0.005	0.004
5	0.987	0.987	0.987	0.987	0.005	0.003	0.002
6	0.989	0.989	0.989	0.989	0.003	0.002	0.001
7	0.991	0.991	0.991	0.991	0.002	0.001	0.001
8	0.992	0.992	0.992	0.993	0.001	0.001	0.001

The *f* parameter for different values of angle α and power law index n is shown in **Fig. 5.15** for the device**.**

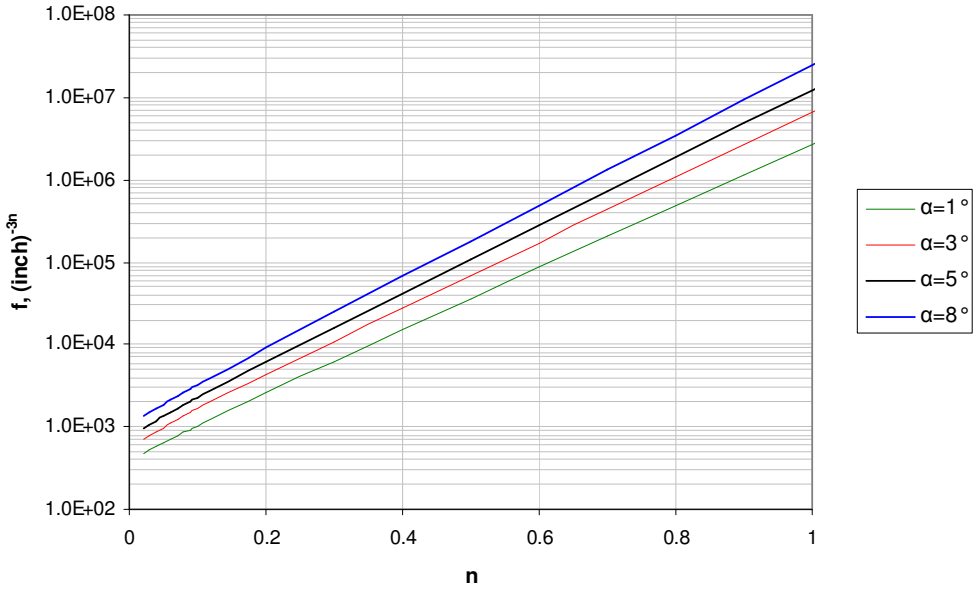

Fig. 5.15—*f* factor for annular conical flow in the device. L= 8in.

5.2.2 Slot Flow Approximation

Another approach to model the flow of a power law fluid in concentric cylinders annular channels is to assume that the annulus can be modeled as a narrow slot as indicated in **Fig. 5.16**.

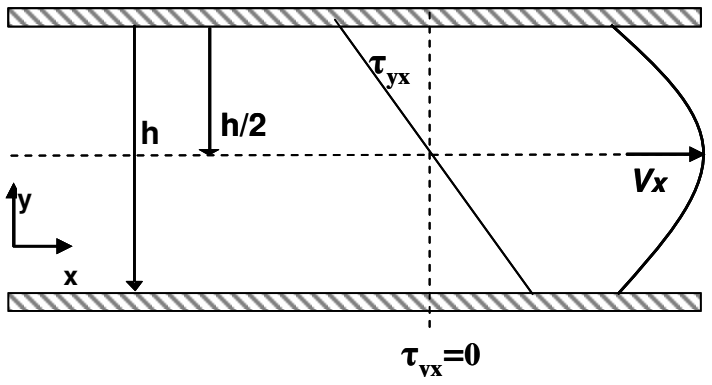

Fig. 5.16—Representation of axial flow in slot.

The equations of motion and continuity can be simplified making the following assumptions

- The fluid is incompressible
- The flow is in steady state
- The flow is laminar
- The cylinders are long enough so that end effects can be neglected.
- Isothermal flow

From the equation of motion

$$\frac{d\tau_{yx}}{dy} = \frac{\Delta p}{L} \quad , \quad \text{..... (5.38)}$$

$\frac{\Delta p}{L}$ represents the pressure gradient. For this case the gradient is constant and is defined as:

$$\frac{\Delta P}{L} = \frac{p_0 - p_L}{L} + \rho g \, , \quad \text{..... (5.39)}$$

where p_0 and p_L are the static pressures at the entry and exit of the annulus and L is the length of the annular

Assuming that shear stress changes linearly with distance $\frac{dp}{dx}$ in the slot, the shear stress must be zero at the distance $y = h/2$. Therefore, integrating Eq. 5.39:

$$\tau_{yx} = \frac{dP}{dL}\left(y - \frac{h}{2}\right) \quad \text{..... (5.40)}$$

The power law rheological model is:

$$\tau_{yx} = -K\left|\frac{dv_x}{dy}\right|^{n-1}\left(\frac{dv_x}{dy}\right) \quad \text{..... (5.41)}$$

The velocity gradient dv_x/dy is positive from $0 \le y \le h/2$ and negative in $h/2 \le y \le h$. Therefore the absolute value indicated in Eq. 5.41 does not have a continuous first derivative at $y = h/2$. We integrate Eq. 5.40 over half the slot

$$-K\left(\frac{dv_x}{dy}\right)^n = \frac{\Delta P}{L}\left(y - \frac{h}{2}\right) \quad \text{..... (5.42)}$$

$$\frac{dv_x}{dy} = \left(\frac{1}{K}\frac{\Delta P}{L}\right)^{1/n}\left(\frac{h}{2} - y\right)^{1/n} \quad \text{..... (5.43)}$$

Integrating Eq. 5.43 with the boundary condition $v_x = 0$ at $y = 0$, we obtain

$$v_x = \frac{1}{1+1/n}\left(\frac{1}{K}\frac{\Delta P}{L}\right)^{1/n}\left[\left(\frac{h}{2}\right)^{1+1/n} - \left(\frac{h}{2} - y\right)^{1+1/n}\right] \quad 0 \le y \le h/2 \quad \text{(5.44)}$$

The flow rate is obtained integrating Eq. 5.44.

$$Q = \pi\left(\frac{1}{K}\frac{\Delta P}{L}\right)^{1/n}\frac{\left(r_o^{\,2} - r_i^{\,2}\right)\left(r_o - r_i\right)^{1+1/n}}{2^{1/n}\left(4 + 2/n\right)}. \quad \text{..... (5.45)}$$

The pressure gradient is

$$\frac{\Delta P}{L} = K\left(\frac{2^{1/n}\left(4 + 2/n\right)Q}{\pi\left(r_o^{\,2} - r_i^{\,2}\right)\left(r_o - r_i\right)^{1+1/n}}\right)^n. \quad \text{..... (5.46)}$$

Rearranging:

$$\frac{\Delta P}{L} = 2K\left(\frac{(4n+2)Q}{n\pi}\right)^n\left(\frac{1}{\left(r_o^{\,2} - r_i^{\,2}\right)\left(r_o - r_i\right)^{1+1/n}}\right)^n. \quad \text{..... (5.47)}$$

Eq. 5.47 can be used to calculate the pressure drop for a given flow rate. To use this expression we wish to use the following units:

$\frac{\Delta P}{L}$: Pressure gradient in psi/in..

Q: flow rate, gal/min.

n: power law index, dimensionless

K: consistency index, lbf s^n / ft^2.

r_o, r_i, outer and inner radii of the annular space, in.

Using dimensional analysis in Eq. 5.47 the units of the pressure gradient are

$$\text{units}\left[\frac{\Delta P}{L}\right] = \text{units}[K]\left(\frac{\text{units}[Q]}{\text{units}[\text{r}_\text{o}^{\,2}]\text{units}[\text{r}_\text{o}]\text{units}[\text{r}_\text{o}^{\,1/n}]}\right)^n$$

$$\text{units}\left[\frac{\Delta P}{L}\right] = \frac{\text{lbf}\ \text{s}^n}{\text{ft}^2}\frac{1}{\text{in}}\left(\frac{\text{gal/min}}{\text{in}^3}\right)^n$$

Since we want the pressure gradient in psi/in we apply the appropriate conversion factors

$$\text{units}\left[\frac{\Delta P}{L}\right] = \frac{\text{lbf}}{\text{ft}^2}\frac{\text{psi}}{144\dfrac{\text{lbf}}{\text{ft}^2}}\frac{\text{s}^n}{\text{in}}\left(\frac{\text{gal}}{\text{min}}\frac{231\,\text{in}^3}{\text{gal}}\frac{\text{min}}{60\text{s}}\frac{1}{\text{in}^3}\right)^n$$

$$\text{units}\left[\frac{\Delta P}{L}\right] = \frac{\text{psi}}{144}\frac{\text{s}^n}{\text{in}}\left(\frac{3.85}{\text{s}}\right)^n$$

$$\text{units}\left[\frac{\Delta P}{L}\right] = \frac{3.85^n}{144}\frac{\text{psi}}{\text{in}}$$

Now we can write Eq. 5.47 as:

$$\frac{\Delta P}{L} = \frac{K}{72}\left(\frac{3.85(4n+2)Q}{n\pi}\right)^n\left(\frac{1}{\left(r_o^{\,2}-r_i^{\,2}\right)\left(r_o-r_i\right)^{1+1/n}}\right)^n . \quad \text{.....} \quad (5.48)$$

Integrating along the length of the sensor, in the same way as Eq. 5.35

$$\Delta P = 2KQ^n f_{slot} . \quad \text{.....} \quad (5.49)$$

where

$$f_{slot} = \frac{1}{\cos\alpha}\left(\frac{4n+2}{n\pi}\right)^{n}\int_{0}^{L}\left(\frac{1}{\left(r_o{}^{2}-r_i{}^{2}\right)\left(r_o-r_i\right)^{1+1/n}}\right)^{n} dz\,. \quad \text{.....} \quad (5.50)$$

As we have seen, the only difference between the analytical solution presented in Eq. 5.36 and the solution presented in Eq. 5.49 is the parameter f and f_{slot}.

Eq. 5.50 can be rearranged as:

$$f_{slot} = \frac{1}{Cos(\alpha)}\left(\frac{4n+2}{n\pi\, r_{fl}{}^{2}}\right)^{n}\int_{0}^{L}\left(r_o-r_i\right)^{-n-1} dz\,. \quad \text{.....} \quad (5.51)$$

$$f_{slot} = \frac{1}{Cos(\alpha)}\left(\frac{4n+2}{n\pi r_{fl}{}^{2}}\right)^{n} I\,. \quad \text{.....} \quad (5.52)$$

where

$$I = \int_{0}^{L}\left(r_o-r_i\right)^{-n-1} dz\,. \quad \text{.....} \quad (5.53)$$

Now, introducing the complete expressions for r_o and r_i:

$$I = \int_{0}^{L}\left(z\tan\alpha + r_o(0) - \sqrt{\left(z\tan\alpha + r_o(0)\right)^{2} - r_{fl}{}^{2}}\right)^{-(n+1)} dz\,. \quad \text{...} \quad (5.54)$$

The integral in Eq. 5.54 is of the form:

$$\int_{0}^{L}\left(az+b-\sqrt{(az+b)^{2}-c}\right)^{-(n+1)}, \quad \text{.....} \quad (5.55)$$

where $a = \tan\alpha$, $b = r_o(0)$ and $c = r_{fl}{}^{2}$. This indefinite integral can be integrated analytically using Mathematica. The solution is:

$$\frac{\left(az+b-\sqrt{(az+b)^2-c}\right)^{-n-1}\left(-b-az+(1+n)\sqrt{(az+b)^2-c}\right)}{an(2+n)}. \quad (5.56)$$

Using this information, we can express the solution of Eq. 5.52 as:

$$f_{slot}=\left(\frac{4n+2}{n\pi {r_{fl}}^2}\right)^n \frac{1}{\sin\alpha(n+2)n} I\ , \quad \text{..... (5.57)}$$

where

$$I = G - H\ . \quad \text{..... (5.58)}$$

$$G=\left(F-\sqrt{F^2-{r_{fl}}^2}\right)^{-n-1}\left(-F+(1+n)\sqrt{F^2-{r_{fl}}^2}\right). \quad \text{..... (5.59)}$$

$$F = L\tan\alpha + r_o(0). \quad \text{..... (5.60)}$$

$$H=\left(r_o(0)-\sqrt{r_o(0)^2-{r_{fl}}^2}\right)^{-n-1}\left(-r_o(0)+(1+n)\sqrt{r_o(0)^2-{r_{fl}}^2}\right). \quad (5.61)$$

This set of expressions can be used to calculate analytically the pressure drop for a selected sensor geometry.

The average shear rate $\dot{\gamma}$ is calculated as:

$$\dot{\gamma}(z,y)=\frac{2^{1/n}(4+2/n)Q}{\pi\left({r_o}^2-{r_i}^2\right)(r_o-r_i)^{1+1/n}}\left(\frac{(r_o-r_i)}{2}-y\right)^{1/n}. \quad \text{..... (5.62)}$$

To use this expression we wish to use the following units:

y: axial distance from inner wall, inches

$\dot{\gamma}$: shear rate 1/s.

Q: flow rate, gal/min.

n: power law index, dimensionless

K: consistency index, lbf s^n / ft^2.

r_o, r_i, outer and inner radii of the annular space, in.

Using dimensional analysis in Eq. 5.66 the units are

$$\text{units}[\dot{\gamma}] = \frac{\text{units}[Q]}{\text{units}[r]^2 \,\text{units}[r]^{1+1/n}} \text{units}[r]^{1/n}$$

$$\text{units}[\dot{\gamma}] = \frac{\text{gal/min}}{\text{in}^2 \text{in}^{1+1/n}} \text{in}^{1/n}$$

$$\text{units}[\dot{\gamma}] = \left(\frac{\text{gal}}{\text{min}} \frac{231\,\text{in}^3}{\text{gal}} \frac{\text{min}}{60\text{s}} \frac{1}{\text{in}^3} \right) \frac{\text{in}^{1/n}}{\text{in}^2 \text{in}^{1+1/n}}$$

$$\text{units}[\dot{\gamma}] = \frac{231\,\text{in}^3}{60\text{s}} \frac{\text{in}^{1/n}}{\text{in}^2 \text{in}^{1+1/n}}$$

$$\text{units}[\dot{\gamma}] = 3.85 \frac{1}{s}$$

At the wall, $y = 0$ the average shear rate $\dot{\gamma}_w$ is

$$\dot{\gamma}_w = 3.85 \frac{2^{1/n}(4 + 2/n)Q}{\pi r_{fl}{}^2 (r_o - r_i)^{1+1/n}} \left(\frac{(r_o - r_i)}{2} \right)^{1/n}, \quad \text{..... (5.63)}$$

or in the selected set of units:

$$\dot{\gamma}_w = 3.85 \frac{(4 + 2/n)Q}{\pi r_{fl}{}^2 (r_o - r_i)} \quad \text{..... (5.64)}$$

And an apparent viscosity η_{app} is then calculated as:

$$\eta_{app} = K \dot{\gamma}^{n-1} \quad \text{..... (5.65)}$$

This approximation simplifies the calculations significantly compared to the solution in Eq.5.35 since the point where the shear stress is zero; λ, is assumed to be $\lambda = \frac{\kappa + 1}{2}$. This greatly eases the speed of calculations. There is a concern of how valid is this approximation for the particular geometries of interest. This approximation is reported to be accurate for aspect ratios $\kappa_o > 0.3$[29]. As we already saw before, the narrow gap of the prototype devices ensures that the aspect ratio κ is larger than 0.3. This suggests that the slot flow approximation is sufficiently adequate to model the pressure drop - flow rate response because it is simpler to calculate and does not require a numerical method.

Characterization of a Fluid with the Device

In practice, the device is used to measure the pressure drop and flow rate. One could impose a pressure rate would be used to measure pressure drops for a series of flow rates, or to measure flow rates after imposing certain pressure differential. By using Eq. 5.69, we can estimate the rheological parameters, *K* and *n*. Taking the logarithm of From Eq.5.49

$$Ln\Delta P = Ln\left(\frac{K}{72}3.85^n Q^n f_{slot}\right) \quad \text{..... (5.66)}$$

$$Ln\Delta P = Ln\left(\frac{K}{72}3.85^n f_{slot}\right) + nLnQ \quad \text{..... (5.67)}$$

That is, the slope of the plot $Ln\Delta P$ vs LnQ can be used to determine *n,* if there is sufficient experimental data. . If the fluid behaves as a power-law material, plotting $Ln\Delta P$ vs LnQ, should produce a straight line. The value of *K* is obtained from the intersection with the vertical axis. In order to use Eq. 5.67 to isolate *K* we need to know the factor f_{slot}.

$$K = \frac{72b}{3.85^n f_{slot}} \quad \text{..... (5.68)}$$

where

K : consistency index, lbf s^n / ft^2

a : coefficient from least squares fit, psi $(min/gal)^n$

f_{slot} : factor in $1/(in^{3n})$

In summary, the procedure for this is:

1. Plot $Ln\Delta P$ vs LnQ
2. Adjust by least squares, to a straight line fit $y = ax + b$
3. a is the index n.
4. With the value of n, and the geometry of the device, use Eq. 5.51 to calculate f_{slot}. (or use Fig. 5.15)
5. Calculate K using Eq. 5.68

Example 1

A flow test of a solution of xanthan gum at produced the results shown in **Fig. 5.17**. The length of the sensor is 8 in, the angle $\alpha = 3^{\circ}$ and $r_{fl} = 0.11\,\text{in}$ and $r_o(0) = 0.2183$ in

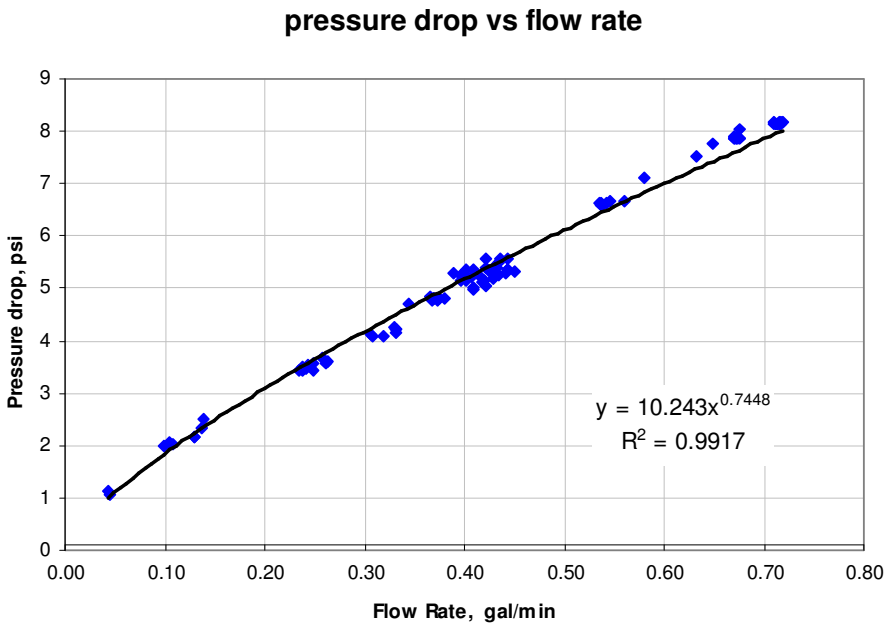

Fig.5.17—Pressure drop vs flow rate. Xhantan gum, 0.1 %.

A least squares fit of the data to a potential function produced the following results

$a = n = 0.7448$

$b = 10.243$

for $n = 0.7448$, and the geometry the device, $f_{slot} = 649801$

then:

$$K = \frac{72(10.243)}{3.85^{0.7448}649801} = 4.16\times10^{-4}\,\frac{\text{lbf}}{\text{ft}^2}\,s^{0.7448}$$

The rheological parameters for this fluid obtained from the sensor are

$n = 0.7448$

$K = 4.16 \times 10^{-4} \frac{\text{lbf}}{\text{ft}^2} s^{0.7448}$

A particular goal of this section is to represent the mathematical models that describe the device response in the form of type-curves. The expressions found for the slot flow model approximation can be expressed in a series of plots that allow quick estimations.

The expressions for pressure drop and shear rate for a selected geometry of the viscosity prototype is presented as curve types in **Figs. 5.18 and 5.19**

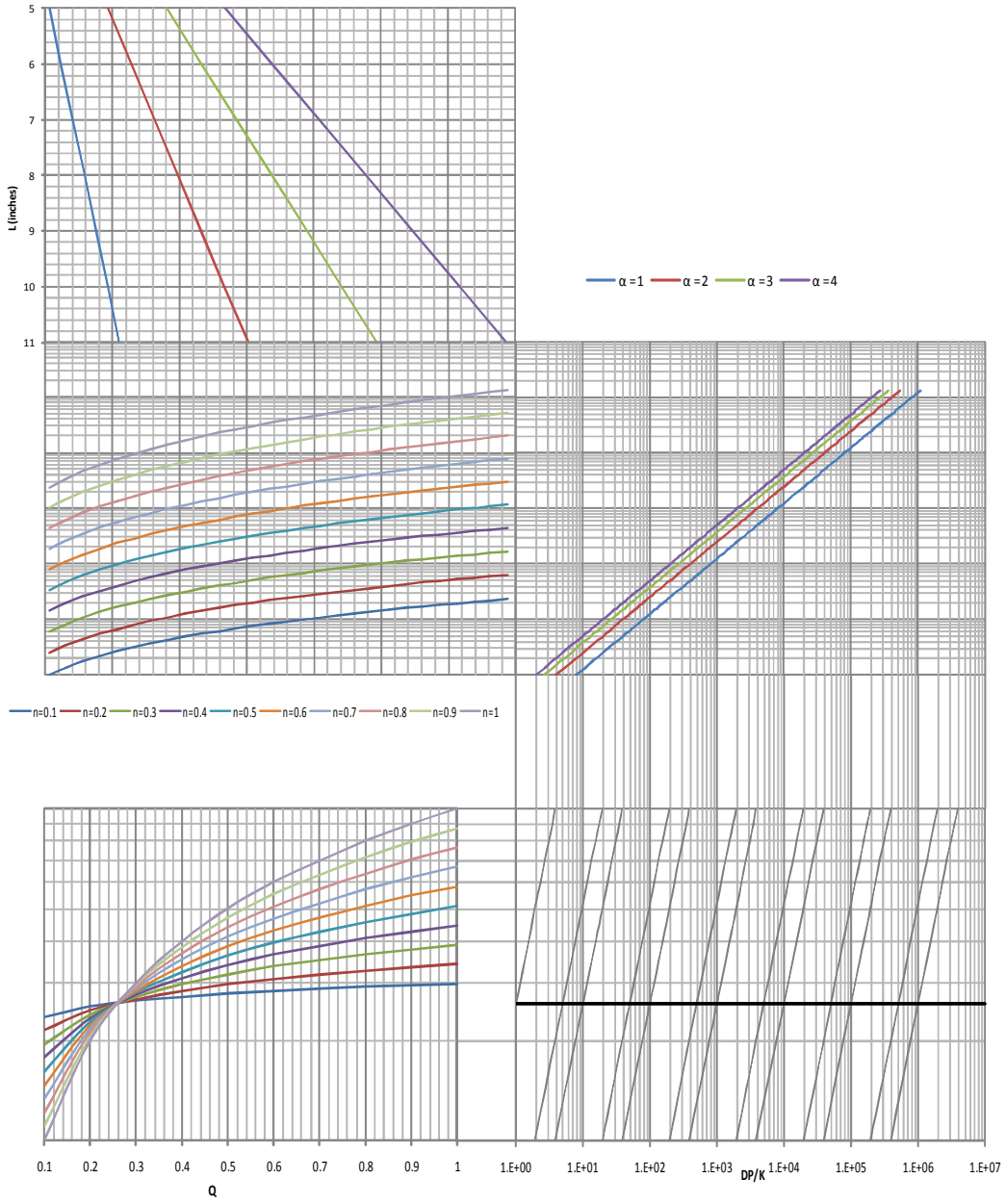

Fig. 5.18—Type curve to determine pressure drop for the device.

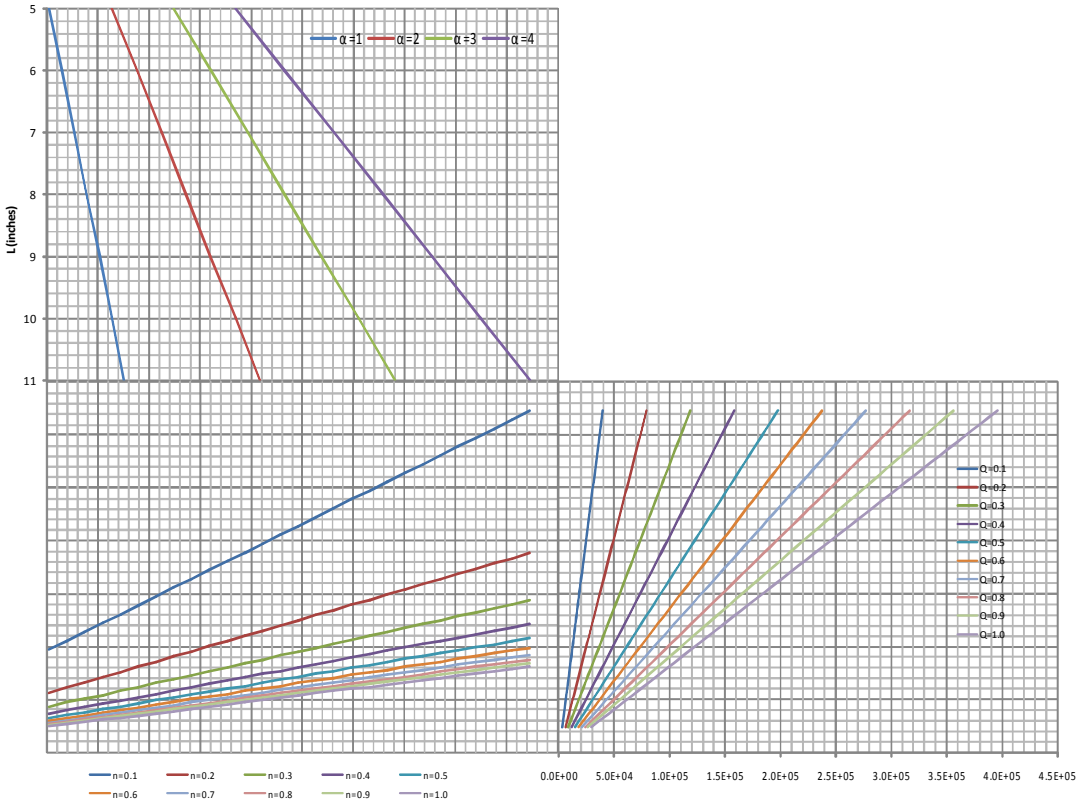

Fig. 5.19—Type curve to determine shear rate at outlet of the sensor.

Depending on the geometry of the device, sets of curves can be generated.

Laminar Flow Criteria

The development of these approximate solutions is based on a number of assumptions as mentioned previously. A key assumption in these models is that the flow is in laminar conditions. To obtain meaningful rheological data, the device must operate in the laminar flow regime.

Traditionally, it has been accepted as a general rule that flow of Newtonian fluids in laminar regime occurs if $N_{\mathrm{Re}} < 2100$, even if experimental studies have observed transition to turbulence at lower N_{Re} in certain conditions[10].

For non-newtonian fluids in concentric annuli several studies have proposed similar guidelines to estimate this transition. General guidelines for transition between laminar to turbulent flow have been proposed, for pipe and concentric annular flow. Viloria[29] reported a complete series of expressions to determine the Reynolds number for different rheological models in concentric annular flow. For power-law fluids in concentric cylindrical annular, the Reynolds number is calculated as

$$N_{\mathrm{Re}} = \frac{109 v^{2-n} \rho v}{K} \left(\frac{0.0208 (D_o - D_i)}{2 + 1/n} \right) \quad \text{..... (5.69)}$$

Where

D_o, D_i : outer and inner diameter of the annular space (in).

v :average fluid velocity, ft/s

ρ: fluid density, lb/gal

K: consistency index, Pa-s^n

A general guideline the critical value for laminar flow $N_{\mathrm{Re}c}$ is found with the expression:

$$N_{\mathrm{Re}c} = 3470 - 1370n, \quad \text{..... (5.70)}$$

which for the case of Newtonian fluids, yields the well known $N_{\mathrm{Re}c} = 2100$

Another alternative to calculate the transition from laminar flow to turbulence is presented by Gucuyener[30]. The author presented a modified Reynolds number developed for several rheological models under pipe and concentric annular geometries. Their expression to calculate the Reynolds number for a power-law fluid in a concentric annular is::

$$N_{\mathrm{Re}m} = \frac{D_e{}^n v_a{}^{2-n} \rho}{8^{n-1} K} \left(\frac{4n}{3n+1} \right)^n \quad \text{..... (5.71)}$$

where D_e is an equivalent diameter, calculated from:

$$D_e = D_o \phi^{\frac{n}{n+1}}, \quad \text{..... (5.72)}$$

$$\phi = \frac{1}{1-\kappa^2} \left(\frac{Y}{3+1/n} \right)^n, \quad \text{..... (5.73)}$$

And Y was defined previously as

$$Y = -\left(\lambda^2 - \kappa^2\right)^{1+1/n} \kappa^{1-1/n} + \left(1-\lambda^2\right)^{1+1/n}.$$

This calculation requires knowledge of λ, which can be obtained from solving numerically Eq.5.8

The critical values for this modified Reynolds number for different aspect ratio κ and power law index n are calculated in their paper.

$$N_{\mathrm{Re}\,C} = \frac{404}{\beta\varphi_i(\xi_c)\left(-\dfrac{d\varphi_o}{d\xi}\right)_{\xi_{co}}} \quad \text{..... (5.74)}$$

ξ_c, is found numerically from solving:

$$-\left(\frac{d\varphi_o}{d\xi}\right)^2\Bigg|_{\xi_{oc}} + \varphi_o(\xi_{oc}) - \left(\frac{d^2\varphi_o}{d\xi^2}\right)^2\Bigg|_{\xi_{oc}} = 0\,, \quad \text{..... (5.75)}$$

$$\varphi_o(\xi) = \int_{\xi}^{1} \left(\zeta^2 - \lambda^2\right)^{1/n} \zeta^{-1/n}\,, \quad \text{..... (5.76)}$$

$$\frac{d\varphi_o}{d\xi} = \left(\xi^2 - \lambda^2\right)^{1/n} \xi^{-1/n}. \quad \text{..... (5.77)}$$

We calculated the corresponding critical value modified Reynolds number using Mathematica. This is presented in **Fig. 5.20.** The value of the modified critical Reynolds number is presented as a function of the aspect ratio κ and the power law index *n*.

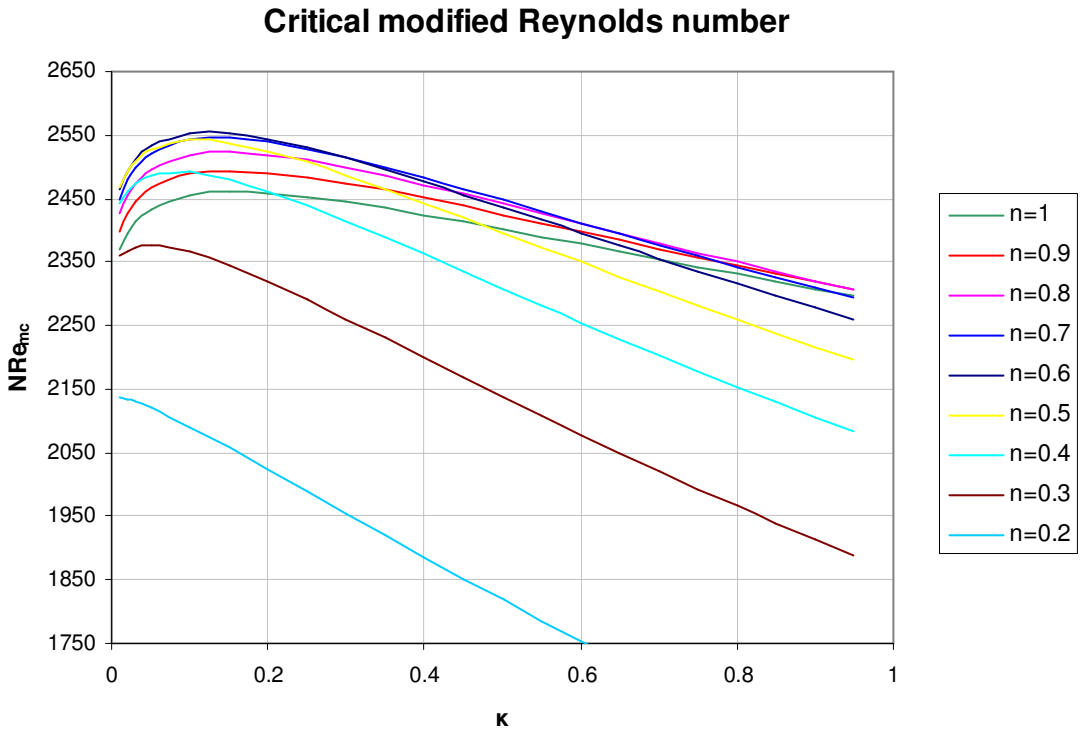

Fig. 5.20—Modified critical Reynolds number for flow in concentric annular as a function of aspect ratio κ and power-law index.

Example 2

For a device with the following dimensions L=8in, α= 3°, $r_{fl} = 0.11\,\text{in}$ and $r_o(0) = 0.2183\,\text{in}$ and a fluid with K=0.1 Pa.s^n, n=0.6, and a density of 0.996 g/cm^3 , calculate the predicted pressure drop for flow rate less than 1 gallon per minute.

First we calculate the Reynolds number profile along the length of the device. Since the highest rate is 1 gallon per minute, we calculate the Reynolds number N_{Re} and the Modified Reynolds number $N_{\mathrm{Re}m}$ at this flow rate.

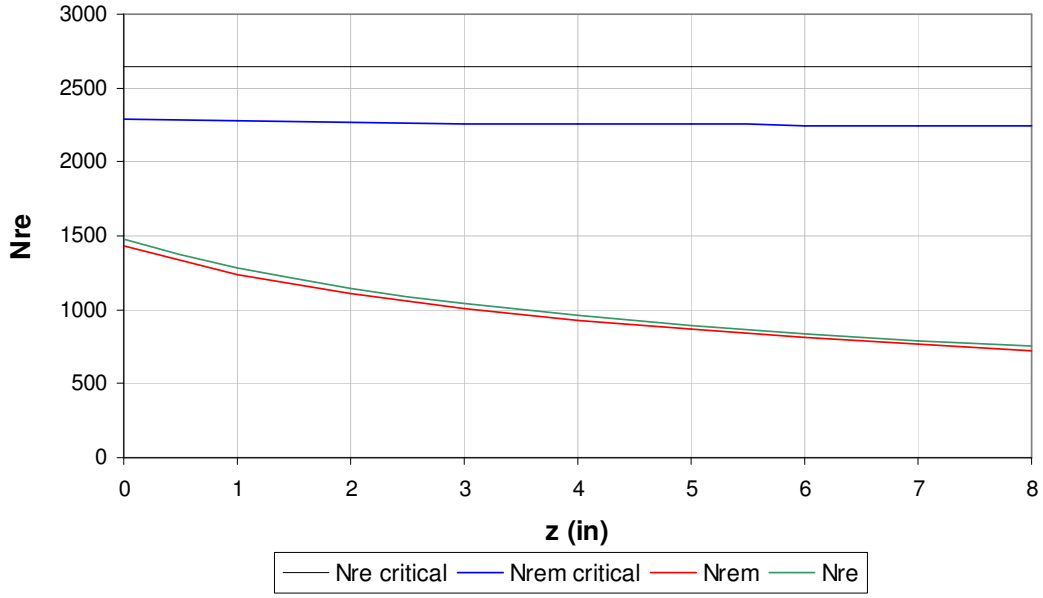

Fig. 5.21—Reynolds number profile. Q=1 gal/min, K=0.1 Pa. s^n n=0.6.

Fig. 5.21 shows the calculated Reynolds number profile using Eq. 5.68 and Eq. 5.70. The critical Reynolds numbers calculated from Eq.5.69 and Eq.5.73 are also shown for comparison. We can observe that the difference between N_{Re} and $N_{\mathrm{Re}m}$ at this particular flow rate, rheology and geometrical configuration is small.. In practical terms, it suggests that the Reynolds number N_{Re} calculated from the simpler expression Eq. 5.68 should be sufficient to check laminar flow conditions.

One interesting feature of this geometry is the reduction in Reynolds number. We can see that the Reynolds number is reduced along the profile of the device. Using Eq.5.45 the estimated pressure drop is shown in **Fig. 5.22**.

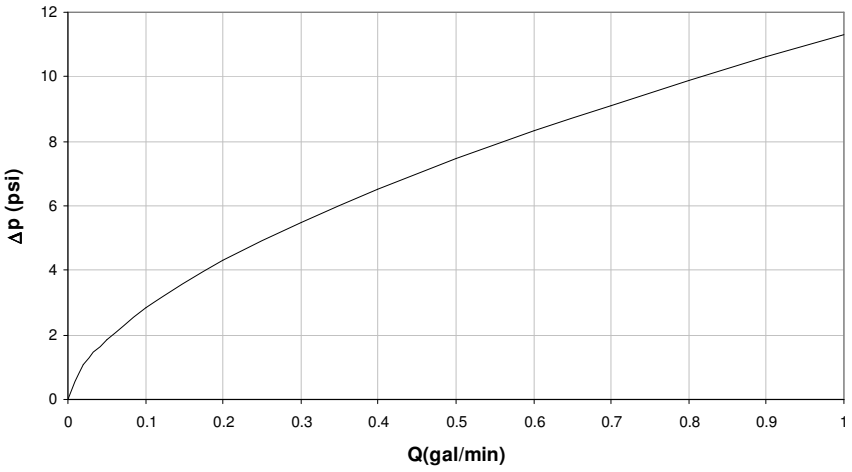

Fig. 5.22—Pressure drop vs. flow rate. K=0.1 Pa. s^n n=0.6.

Table 5.3—Pressure drop and apparent viscosity at wall. K=0.1 Pa. s^n, n=0.6.

Q(gal.min)	ΔP (psi)	η app wall (cp)
0.10	2.84	2.34
0.20	4.30	1.96
0.30	5.48	1.77
0.40	6.52	1.64
0.50	7.45	1.55
0.60	8.31	1.48
0.70	9.12	1.42
0.80	9.88	1.37
0.90	10.60	1.33
1.00	11.29	1.30

The average shear rate at the wall along the profile of the device is shown in **Fig. 5.23**:

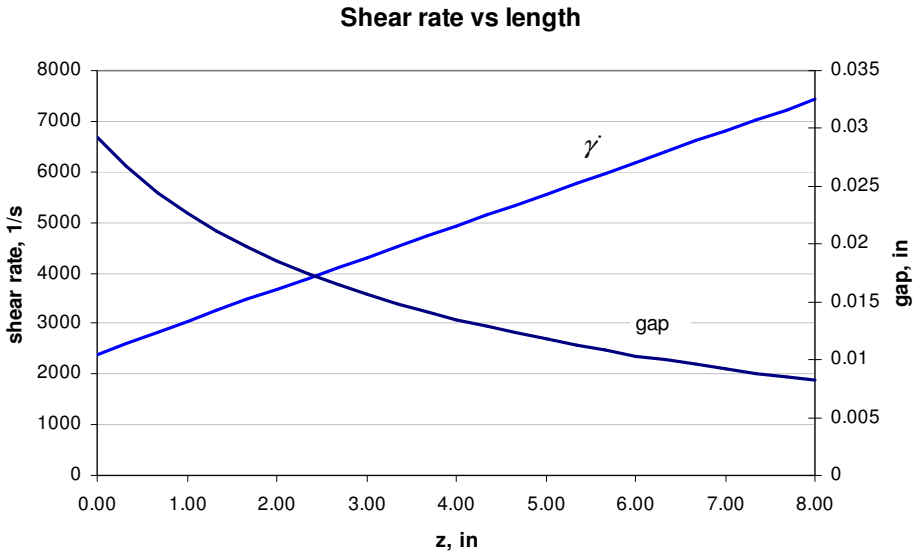

Fig. 5.23— Shear rate at wall vs length. Q=0.1 gal/min, L=8 in, n=0.6.

For different flow rates, we can observe how the shear rate changes. **Fig. 5.24** shows the average shear rate for different flow rates. We can observe the sharp increase in the shear rate with the increase in flow rate.

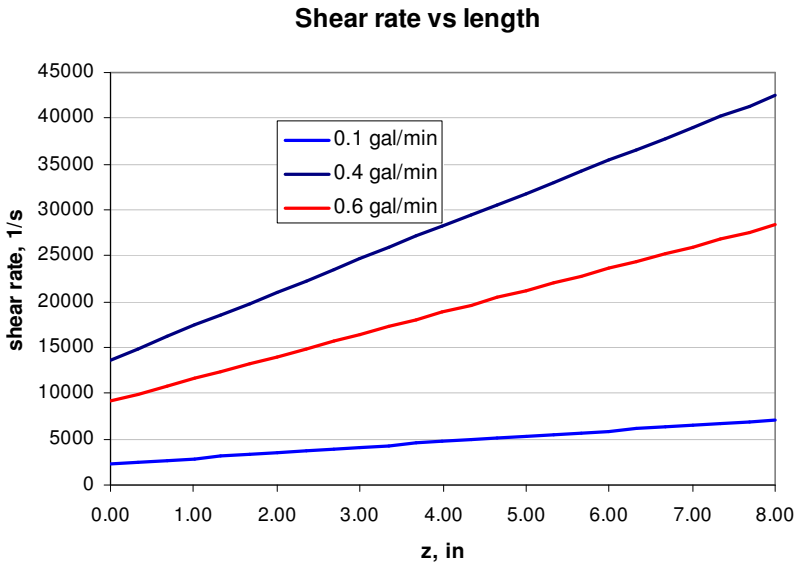

Fig. 5.24—Shear rate vs. length. L=8 in, α=3°.

We have shown so far, how to determine the rheological parameters (*K, n*) of a power law fluid, using the flow rate and pressure drop data obtained from a specified geometry. Now we would like to turn to the design aspect. Operators of the device are likely to be faced with questions such as: what physical dimensions are necessary to obtain a flow rate at an acceptable pressure drop across the device. Given a particular flow rate, what pressure drop what is the maximum expected pressure. These answers can be obtained, from Eq. 5.49:

$$\Delta P = \frac{K}{72}(3.85\,Q)^n f_{slot}\,.$$

And f_{slot} is calculated from Eq.5.50:

$$f_{slot} = \frac{1}{Cos(\alpha)}\left(\frac{4n+2}{n\pi\, r_{fl}{}^{2}}\right)^{n}\int_{0}^{L}(r_o - r_i)^{-n-1}\,dz$$

The difficulty this method lies in the determination of the factor f_{slot} for a given set of physical dimensions. We already have the full solution of this integral, but another simple approach is to approximate this complex function to a much simpler function

As we can see, this term is a function of both the geometry of the device, (opening angle and length) as well as a function of the power law index of the fluid. Any physical dimension change will require the computation of the geometry factor. The goal of this exercise is to transform this function into an expression that is easy to use and would not need anything more than a calculator, or that can be displayed as a chart.

Rearranging Eq 5.49, into a general form

$$\frac{\Delta P}{K} = \beta Q^{n}$$

Where $\beta(\alpha, n, L, r_{fl}, r_o(0))$ is a function of the geometry of the sensor and the power law index of the fluid.

We want to write a simpler function for β that reproduces the behavior of the factor f_{slot}, but without the need to evaluate the integral.. To explore the behavior of this multivariate function, we made a number of plots to see the behavior of the function as

the arguments change: The plot of this function, with *L* for different alphas is shown in **Figs. 5.25 and 5.26**.

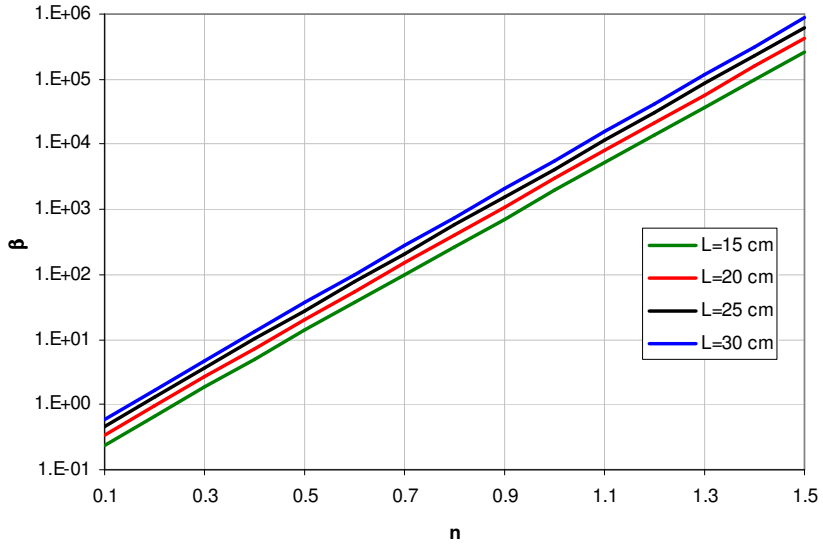

Fig. 5.25—β as function of power law index n and length of device. α = 1°.

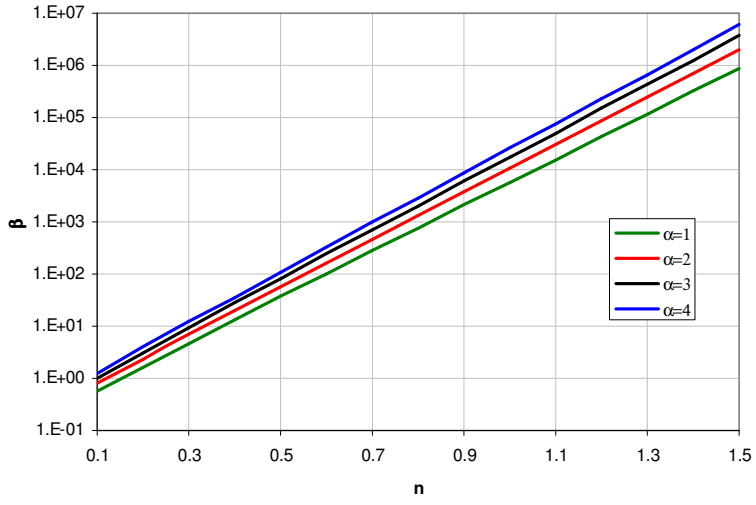

Fig. 5.26—β as function of power law index n and α. L=30 cm.

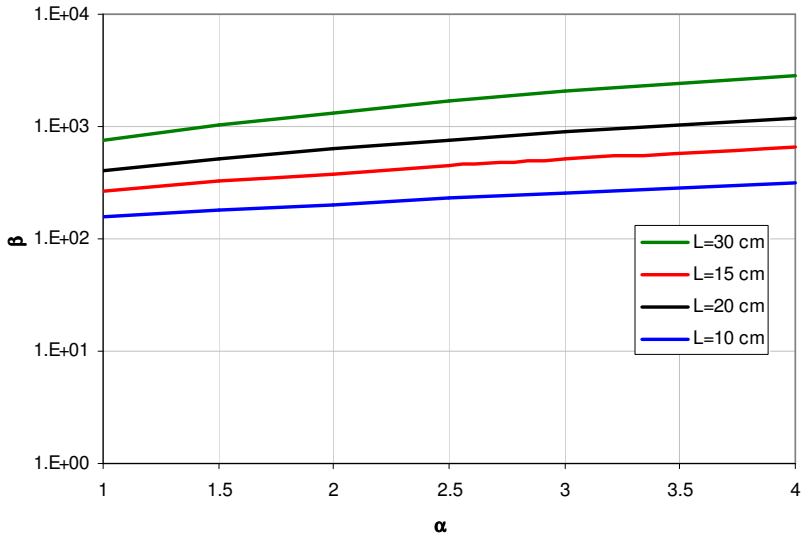

Fig. 5.27—β as function of α and length of device. n=0.8.

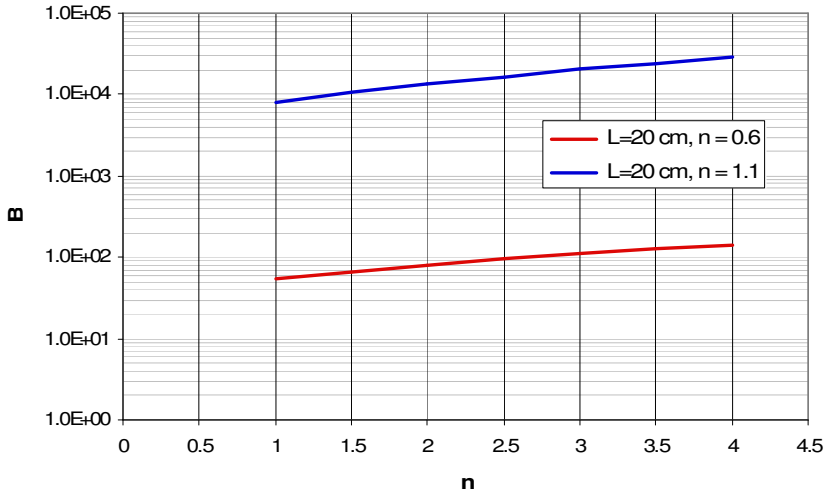

Fig. 5.28—β as function of α (n, L constant).

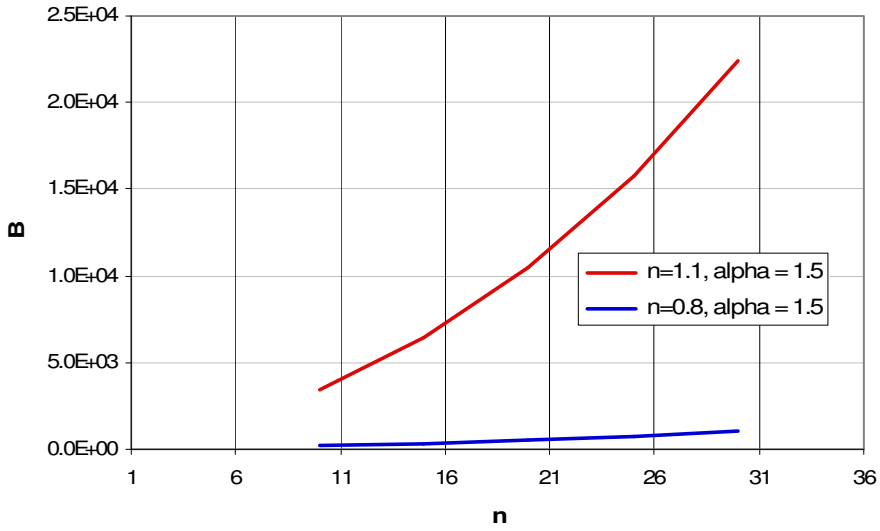

Fig. 5.29—β as function of L (n, α constant).

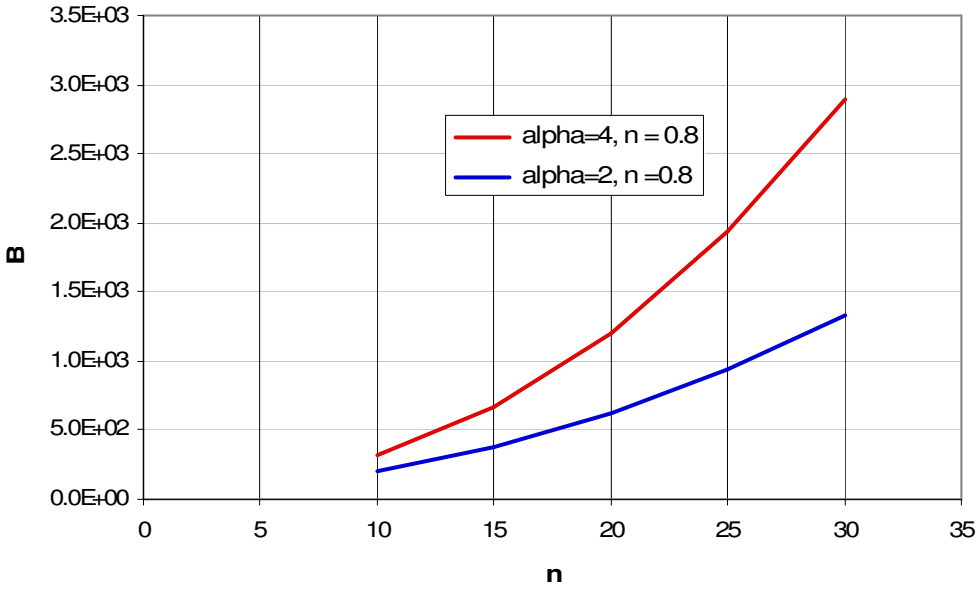

Fig. 5.30— β as function of L (n constant, α).

Based on observations from this plots, we can try to adjust the function to a simpler model. From **Fig. 5.25** and **Fig. 5.26**, we can see that the function shows an exponential trend, as a function of the power law index n.

: $\beta(\alpha,n,L)=A(\alpha,L)e^{Bn}$

From **Fig. 5.27** and **Fig. 5.28**, we can approximate $\beta(\alpha,n,L)=A(\alpha,L)e^{Bn}$ as a potential function of the angle α:

$$\beta(\alpha,n,L)=A(n,L)\alpha^{B}$$

And, from **Fig. 5.29** and **Fig. 5.30**, we can also see β behaves as a potential function of the length of the device L:

$$\beta(\alpha,n,L)=A(n,\alpha)L^{B}$$

Combining the three observations, we can use the following model for the function:

$$\beta(\alpha,n,L)=\left(A_0e^{A_1n}\right)(\alpha)^{A_2}(L)^{A_3} \quad \text{..... (5.78)}$$

This model can be linearized as:

$$Ln(\beta)=Ln(A_0)+A_1n+A_2Ln(\alpha)+A_3Ln(L)$$

To estimate the values of the coefficients we adjusted using least squares fit to a set of data points of β with α, n and L in the ranges shown in Table 5.4.

Table 5.4—Range of parameters.

parameter	range
n	0.1-1.5
α (°)	1-4
L (cm)	10-30
Q (gal/min)	0.1-1

To obtain better predictions, we separated the data for shear thinning and shear thickening fluids. The result of our correlation is:

$$\beta(\alpha, n, L) = A_0 \ \exp(A_1 n)\ \alpha^{A_2}\ \mathrm{L}^{A_3} \quad \text{..... (5.79)}$$

The coefficients were adjusted numerically using a linear fit subroutine in the software package SAS. The results are presented in **Tables 5.5 and 5.6:**

Table 5.5—Correlation coefficients n ≤ 1.

parameter	value
A_0	7.285046×10^{-4}
A_1	10.41027
A_2	1.66062
A_3	0.64733
R^2	0.99865

Table 5.6—Correlation coefficients n > 1.

parameter	value
A_0	2.11781×10^{-4}
A_1	10.27202
A_2	2.02256
A_3	1.00123
R^2	0.994787

To compare the results from the correlation, we can see the scatter plots in **Fig. 5.31** and **Fig. 5.32**.

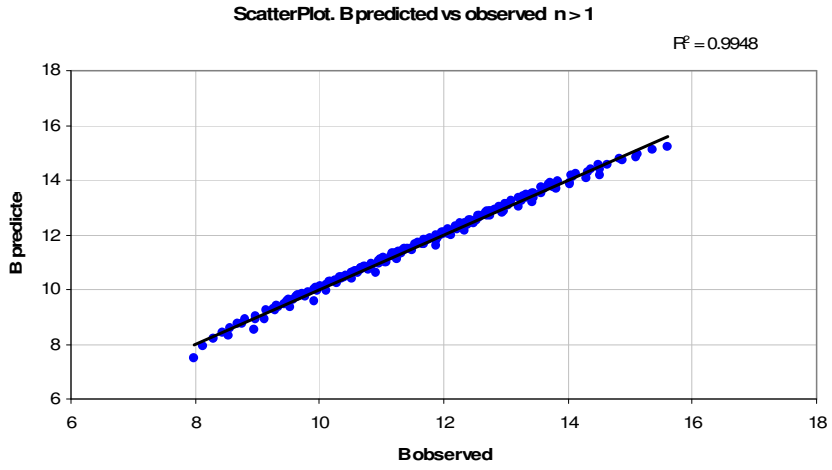

Fig. 5.31—Scatter plot, β predicted vs. observed for n>1.

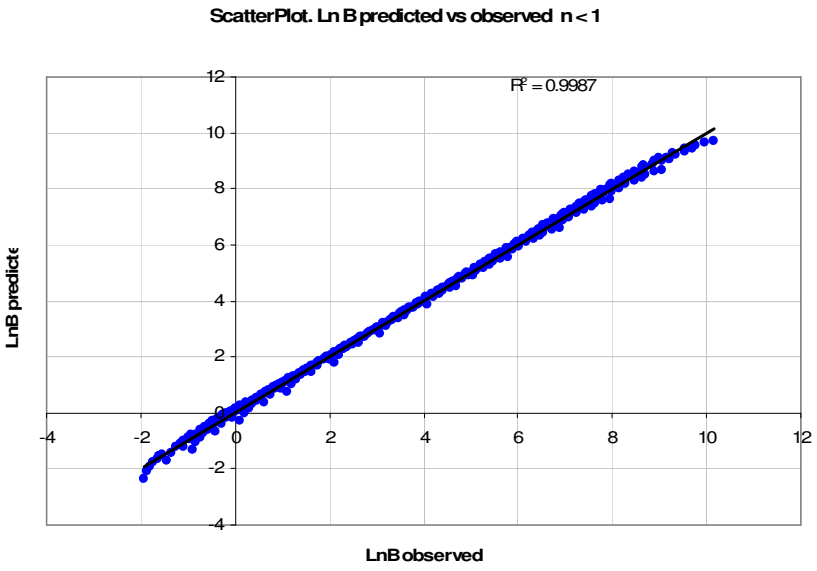

Fig.5. 32 —Scatter plot, Ln β predicted vs observed for n<1.

This correlation suffers from some large errors in the predicted β values for certain combinations of variables, especially for the upper and lower boundaries of the interval of the parameters. However, we consider that the results provided for are acceptable for very quick estimates when only a calculator is available.

Example 3

For a device with the following dimensions L=8in, α= 3°, $r_{fl} = 0.11\,\text{in}$ and $r_o(0) = 0.2183\,\text{in}$ and a fluid with *K*=0.1 Pa.s^n, n=0.6, and a density of 0.996 g/cm^3 , calculate the predicted pressure drop for flow rate less than 1 gallon per minute.

Using the model described in Eq. 5.79, with the coefficients shown in **Table 5.5**, we obtain the following: results, shown in **Table 5.7.** and plotted in **Fig. 5.33**.

Table 5.7—Pressure drop vs flow rate calculated using slot flow approximation and Eq.5.79 for example 3. K=0.1 Pa. s^n n=0.6.

Q(gal.min)	ΔP slot flow (psi)	ΔP Eq,5.79 (psi)	Relative error (%)
0.10	2.84	2.86	0.70
0.20	4.30	4.33	0.70
0.30	5.48	5.52	0.70
0.40	6.52	6.56	0.70
0.50	7.45	7.50	0.70
0.60	8.31	8.37	0.70
0.70	9.12	9.18	0.70
0.80	9.88	9.95	0.70
0.90	10.60	10.68	0.70
1.00	11.29	11.37	0.70

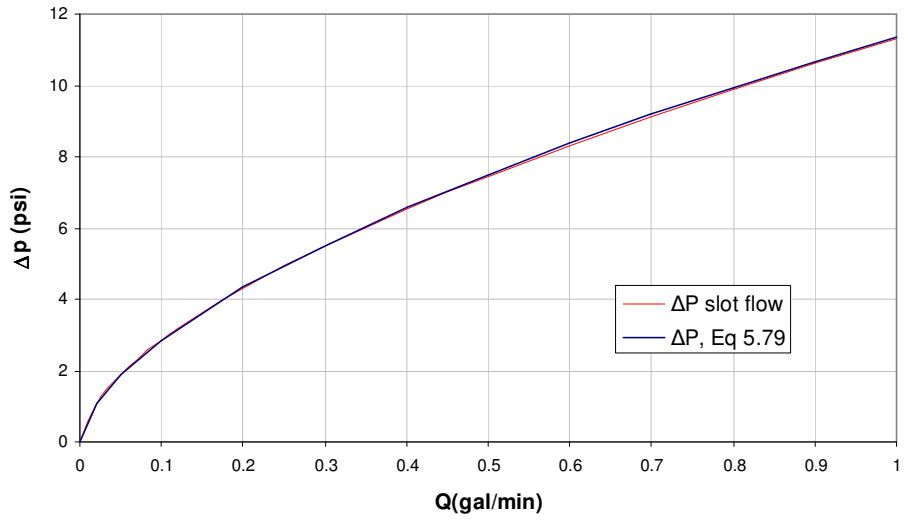

Fig. 5.33—Pressure drop vs flow rate. K=0.1 Pa. s^n n=0.6 for slow flow approximation and the model in Eq. 5.79.

5.3 Finite Element Simulation

In order to solve the motion equations for the exact geometry of the sensor, a program was used to calculate the pressure drop across the sensor using the finite element method.(FEM). The program solves the steady state power-law isothermal flow in axysimetric problems using 6 noded triangular elements. The Penalty method formulation is used with reduced integration. The procedure is described as follows

5.3.1 Governing Equations

For steady state laminar flow of an incompressible fluid in the geometry of the sensor, we can take advantage of the symmetry of the system and assume that all variables remain constant in the direction around the axis of symmetry. This assumption reduces the problem to a two-dimensional problem. Since we are interested in low Reynolds number flows, we can assume that the flow regime is dominated by the viscous term, therefore we will neglect the inertia term in the equation of motion Eq. 2.13. We expand the equations described in Chapter II in a cylindrical coordinate system:

The continuity equation:

$$\frac{\partial v_r}{\partial r} + \frac{v_r}{r} + \frac{\partial v_z}{\partial z} = 0 . \quad \text{..... (5.80)}$$

The equation of motion in the *r* and *z* directions:

$$\begin{aligned} &-\frac{\partial p}{\partial r}+\frac{\partial}{\partial r}\left(2\eta\frac{\partial v_r}{\partial r}\right)+\frac{2\eta}{r}\frac{\partial v_r}{\partial r}-\frac{2\eta}{r}\frac{v_r}{r}+\frac{\partial v_z}{\partial z}\left[\eta\left(\frac{\partial v_z}{\partial r}+\frac{\partial v_r}{\partial z}\right)\right]=0 \\ &-\frac{\partial p}{\partial z}+\frac{\partial}{\partial z}\left(2\eta\frac{\partial v_z}{\partial z}\right)+\frac{\eta}{r}\left(\frac{\partial v_z}{\partial r}+\frac{\partial v_r}{\partial z}\right)+\frac{\partial}{\partial r}\left[\eta\left(\frac{\partial v_z}{\partial r}+\frac{\partial v_r}{\partial z}\right)\right]=0 \end{aligned} \quad . \quad (5.81)$$

The rheological model for a power law fluid:

$$\eta = K(\dot{\gamma})^{n-1} . \quad \text{..... (5.82)}$$

And the shear rate is calculated as:

$$\dot{\gamma}=\sqrt{2\left(\frac{\partial v_r}{\partial r}\right)^2+2\left(\frac{v_r}{r}\right)^2+2\left(\frac{\partial v_z}{\partial z}\right)^2+\left(\frac{\partial v_z}{\partial r}+\frac{\partial v_r}{\partial z}\right)^2} . \quad \text{..... (5.83)}$$

These equations are solved using the penalty method, described in Chapter II.

5.3.2 Penalty method equations

The penalty method element stiffness equations for each element in the mesh in the cylindrical coordinate system is::

$$\begin{bmatrix} A_{ij}^{11} & A_{ij}^{12} \\ A_{ij}^{21} & A_{ij}^{22} \end{bmatrix}\begin{pmatrix} v_{rj} \\ v_{zj} \end{pmatrix}=\begin{pmatrix} B_j^1 \\ B_j^2 \end{pmatrix} \quad , \quad \text{..... (5.84)}$$

and each of the coefficients in the local stiffness matrix is calculated as:

$$A_{ij}^{11} = \int_e \left[\begin{aligned} &\lambda\left(\frac{\partial N_i}{\partial r}\frac{\partial N_j}{\partial r}+\frac{N_i}{r}\frac{N_j}{r}+\frac{N_i}{r}\frac{\partial N_j}{\partial r}+\frac{\partial N_i}{\partial r}\frac{N_j}{r}\right)+ \\ &+\eta\left(\frac{2N_i}{r}\frac{N_j}{r}+2\frac{\partial N_i}{\partial r}\frac{\partial N_j}{\partial r}+\frac{\partial N_i}{\partial z}\frac{\partial N_j}{\partial z}\right) \end{aligned}\right] rdrdz \quad , \quad \text{..... (5.85)}$$

$$A_{ij}^{12} = \int_e \left[\lambda \left(\frac{\partial N_i}{\partial r} \frac{\partial N_j}{\partial z} + \frac{N_i}{r} \frac{\partial N_j}{\partial z} \right) + \eta \frac{\partial N_i}{\partial z} \frac{\partial N_j}{\partial r} \right] r dr dz \quad , \ldots\ldots\ldots\ldots\ldots \quad (5.86)$$

$$A_{ij}^{21} = \int_e \left[\lambda \left(\frac{\partial N_i}{\partial z} \frac{\partial N_j}{\partial r} + \frac{N_j}{r} \frac{\partial N_i}{\partial z} \right) + \eta \frac{\partial N_i}{\partial r} \frac{\partial N_j}{\partial z} \right] r dr dz \quad , \ldots\ldots\ldots\ldots\ldots \quad (5.87)$$

$$A_{ij}^{21} = \int_e \left[\lambda \frac{\partial N_i}{\partial z} \frac{\partial N_j}{\partial z} + \eta \left(\frac{\partial N_i}{\partial r} \frac{\partial N_j}{\partial r} + 2 \frac{\partial N_i}{\partial z} \frac{\partial N_j}{\partial z} \right) \right] r dr dz \quad , \ldots\ldots\ldots\ldots \quad (5.88)$$

$$B_j^1 = \int_{\Gamma e} N_i \left[\left(\lambda \left(\frac{\partial v_r^{\,e}}{\partial r} + \frac{v_r^{\,e}}{r} + \frac{\partial v_z^{\,e}}{\partial z} \right) + 2\eta \frac{\partial v_r^{\,e}}{\partial z} \right) n_r + \eta \left(\frac{\partial v_r^{\,e}}{\partial z} + \frac{\partial v_z^{\,e}}{\partial r} \right) n_z \right] r \, d\Gamma_e \quad , (5.89)$$

and

$$B_j^2 = \int_{\Gamma e} N_i \left[\eta \left(\frac{\partial v_z^{\,e}}{\partial r} + \frac{\partial v_r^{\,e}}{\partial z} \right) n_r + \left(\lambda \left(\frac{\partial v_r^{\,e}}{\partial r} + \frac{v_r^{\,e}}{r} + \frac{\partial v_z^{\,e}}{\partial z} \right) + 2\eta \frac{\partial v_z^{\,e}}{\partial z} \right) n_z \right] r \, d\Gamma_e \quad (5.90)$$

N_i and N_j represent the shape functions for the element. In our case, for shape functions, we used six noded triangular elements. The shape functions for this element in the local coordinate system are:

$$
\begin{aligned}
N_1^e &= \eta(2\eta - 1) \\
N_2^e &= 4\eta(1 - \xi - \eta) \\
N_3^e &= (1 - \xi - \eta)(1 - 2\xi - 2\eta) \\
N_4^e &= 4\xi(1 - \xi - \eta) \\
N_5^e &= \xi(2\xi - 1) \\
N_6^e &= 4\eta\xi
\end{aligned}
\qquad \text{..... (5.91)}
$$

The system described is written for every element in the mesh. Then the full stiffness matrix of the grid is assembled and the system of equations is solved, obtaining the primary variables v_r and v_z for every node in the grid. The pressure is calculated once the velocity field has converged satisfactorily. The flow diagram for the code is presented in **Fig. 5.34**. It delineates the strategy and steps to calculate the solution of the fluid flow problem.

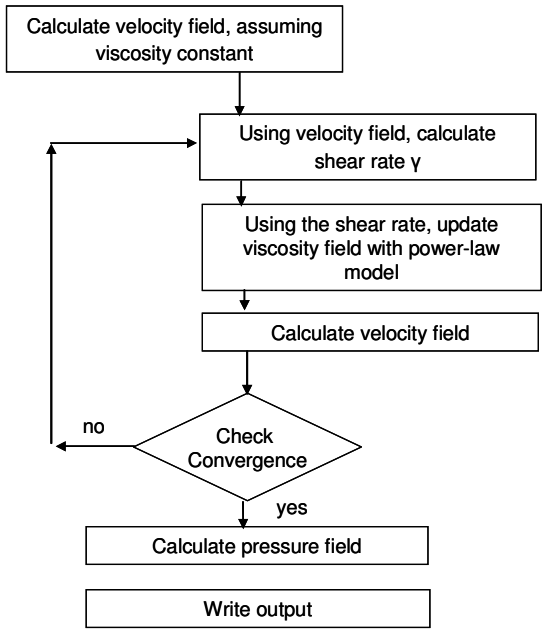

Fig. 5.34—Flow chart for finite element program.

In this iterative procedure, we start by solving the velocity field, assuming that the viscosity of the fluid is constant. Using this velocity field, we calculate the shear rate, and using the power law rheological model. we update the apparent viscosity at each node. With this new viscosity in each node, we calculate again the velocity field. The convergence criterion is to check the change in the velocity field from iteration to the next one. Once the change is smaller than a predetermined tolerance, we can then calculate the pressure field and write the output file for post-processing. The calculation is considered as converged when the velocity field satisfies **Eq. 5.92**:

$$\sqrt{\frac{\sum_{i=1}^{N}\left|X_i^{j+1}-X_i^{j}\right|^2}{\sum_{i=1}^{N}\left|X_i^{j+1}\right|^2}} \le \varepsilon \,. \quad \text{..... (5.92)}$$

r in this expression is the iteration number, N is the degrees of freedom and ε is the tolerance value.

.The boundary conditions for our problem are shown in **Fig 5.35**. At the inlet, the flow entering the domain is set as a parabolic profile of velocity in the entrance of the sensor. We imposed different flow rates in the entry by using the following relationship to adjust the parabolic profile depending on the flow rate:

$$q = 2\pi \int_{r_1}^{r_2} r v_z dr \,. \quad \text{..... (5.93)}$$

For the walls, we impose a no slip zero velocity condition. $v_z = 0$, $v_r = 0$ along the lines of the solid walls: The code also allows the possibility of using a slip in the walls.

This functionality is available, and is discussed in the Appendix in the explanation of the software code.

At the exit of the domain we imposed no boundary conditions. Usually if the fluid is fully developed, one can impose a particular velocity profile in the exit. However in this case, since we have the velocity as a function of both *r* and *z*, we do not know the shape of the profile at the exit.

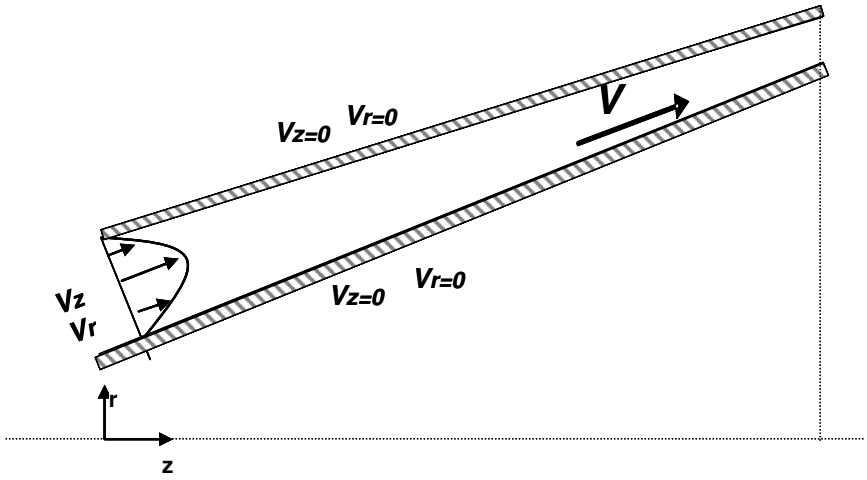

Fig. 5.35—Boundary conditions for the flow domain.

The program solves the flow equation using the penalty method. The proper value of the penalty parameter is usually between 10^7 and 10^9, depending on the word length of the computer. For the computer system used, the best accuracy was obtained when the penalty parameter was set to 10^8

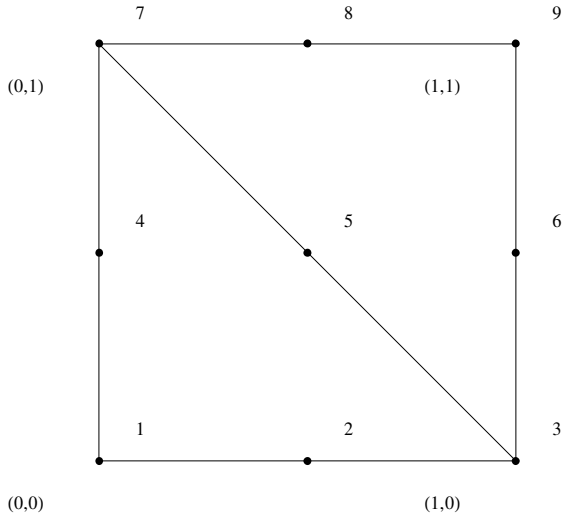

Fig. 5.36—Typical triangular element used in the simulation mesh showing the numbering scheme.

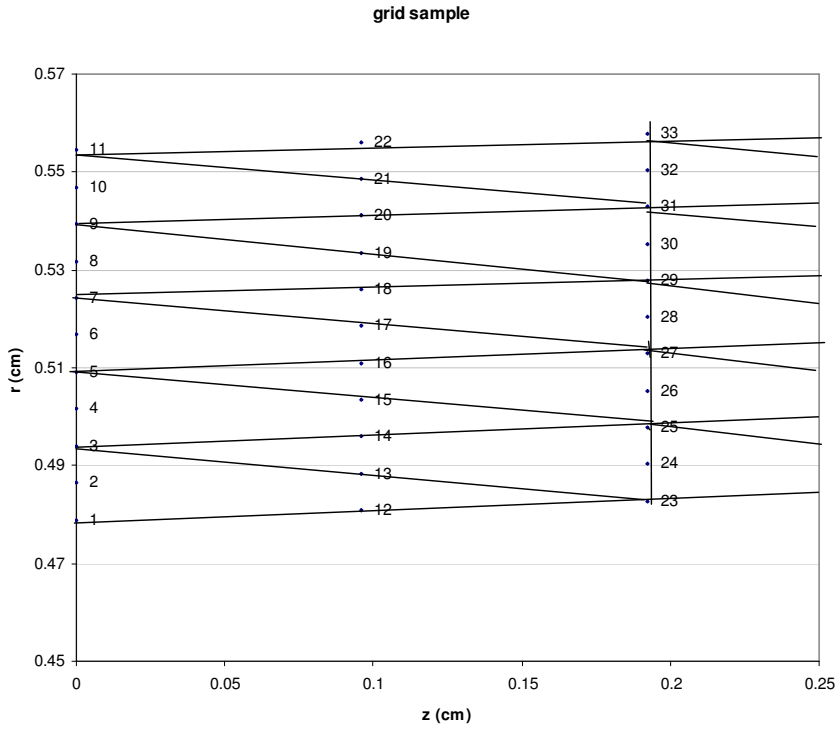

Fig. 5.37—Finite element mesh showing six noded triangular elements.

Preliminary verification of the code was accomplished by comparing numerical and analytical fully developed velocity profiles and pressure drop for axial flow in concentric cylinders. Numerical simulations assessed the entrance development length to achieve fully developed laminar flow for a range of different configurations of the sensor. The tests involved a number of different grid resolutions with the objective to determine the best resolution to obtain grid independent results. A grid 10x100 grid of triangular elements was found to be reasonable compromise between simulation time and accuracy. **Fig. 5.36** and **Fig. 5.37** show the shape of the elements used in the grid. We created a pre-processing code to generate the triangular mesh, using the same design parameters as the device, opening angle, length, inner and outer radius. The code creates the grid, assigns boundary conditions and feeds the data file to the main subroutine which then calculates the solution of the equations of motion using the finite element method.

Having this method to solve the equations in the general geometry without resorting to the approximating to cylinders could be used to determine the ranges of validity of the approximations described earlier in this chapter. It would be preferable to validate the approximations and modeling using experimental data, but since we only were provided with one prototype, it was not possible to do this. We can now compare the solution of the Frederickson & Bird, the slot flow approximation, to the finite element solution. This will allow us to determine the ranges in which these approximations are valid and workable.

The parameters that govern the response of the device are the rheological parameters, K and n and in terms of geometry, the opening angle α, initial outer radius $r_o(0)$ and radius of the flow line r_{fl}. Using this program we can compare the predicted pressure drop for the geometry of the prototype.

For an angle of zero degrees, $\alpha = 0^\circ$, the sensor geometry coincides with a concentric annular geometry. We can compare the pressure drop obtained from the fully analytical solution from Eq.5.18 with the pressure drop from the slot flow approximation provided by Eq.5.80 and the pressure drop calculated from the finite element method code. **Table 5.8** shows these results as well. The agreement of the results from the three methods is evident.

Table 5.8—Pressure drop as a function of power-law index. α=0°, K=0.1 Pa-s^n, L=8 in, Q=0.5 gal/min.

n	ΔP Frederickson & Bird (psia)	ΔP slot flow approximation (psia)	ΔP FEM (psia)
1.2	471.503	471.672	469.490
1.1	193.929	193.998	193.240
1.0	79.691	79.720	79.470
0.9	32.711	32.723	32.640
0.8	13.408	13.413	13.390
0.7	5.486	5.487	5.480
0.6	2.239	2.239	2.240
0.5	0.910	0.911	0.910
0.4	0.368	0.368	0.370
0.3	0.148	0.148	0.150
0.2	0.059	0.059	0.057
0.1	0.023	0.023	0.023

We are interested in comparing the results of the simulation and finding when the approximate solutions start to diverge. In terms of geometry, we are interested in finding the cases where we diverge from the cylindrical geometry. These cases appear to be, when the opening angle is large and the conical shape is pronounced and when the aspect ratio κ is low. Large aspect ratio occurs when the gap between the inner pin and outer case is very narrow. This is the case for the geometry of the prototype.

To compare the approximation of the flow by Eq.5.30 with the pressure drops obtained from the finite element program we changed the geometry of the sensor. In **Tables 5.9**. **5.10, 5.11 and 5.12**, and **Figs. 5.38, 5.39, 5.40 and 5.41** we present the results for α=1° and α=6°. The radius of the flow line and the initial outer radii remain the same in these examples.

Table 5.9—Pressure drop vs. power law index. α=1°, K=0.1 Pa. s^n, L=8 in, Q=0.5 gal/min.

n	ΔP slot flow (psia)	ΔP FEM (psia)	Absolute Error
1.2	876.516	839.8	36.716
1.1	348.8	359.8	0.11
1	138.7	135.3	3.4
0.9	55.1	54.2	0.9
0.8	21.8	21.6	0.2
0.7	8.6	8.	0.6
0.6	3.4	3.4	0
0.5	1.3	1.37	0.07
0.4	0.5	0.53	0.03
0.3	0.2	0.20	0
0.2	0.08	0.08	0
0.1	0.03	0.02	0.01

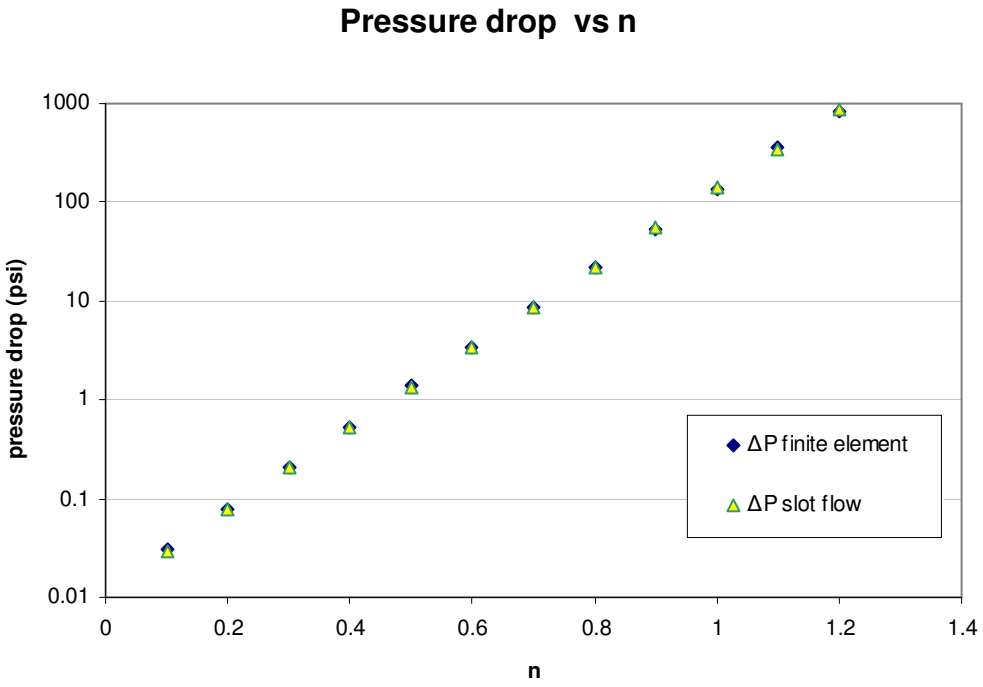

Fig. 5.38—Pressure drop vs. power law index. α=1°, K=0.1 Pa. s^n, L=8 in , Q=0.5 gal/min.

Table 5.10—Pressure drop vs. flow rate. α=1°, K=0.1 Pa. s^n, n=0.665, L=8 in.

Q (gal/min)	ΔP slot flow (psia)	ΔP FEM (psia)	Absolute Error
0.1	2.14906	2.14317	0.00589
0.2	3.40748	3.39816	0.00932
0.3	4.46205	4.44985	0.01220
0.4	5.40280	5.38801	0.01479
0.5	6.26706	6.24991	0.01715
0.6	7.07488	7.05553	0.01935
0.7	7.83861	7.81715	0.02146
0.8	8.56650	8.54305	0.02345
0.9	9.26446	9.23910	0.02536
1	9.93685	9.90965	0.02720

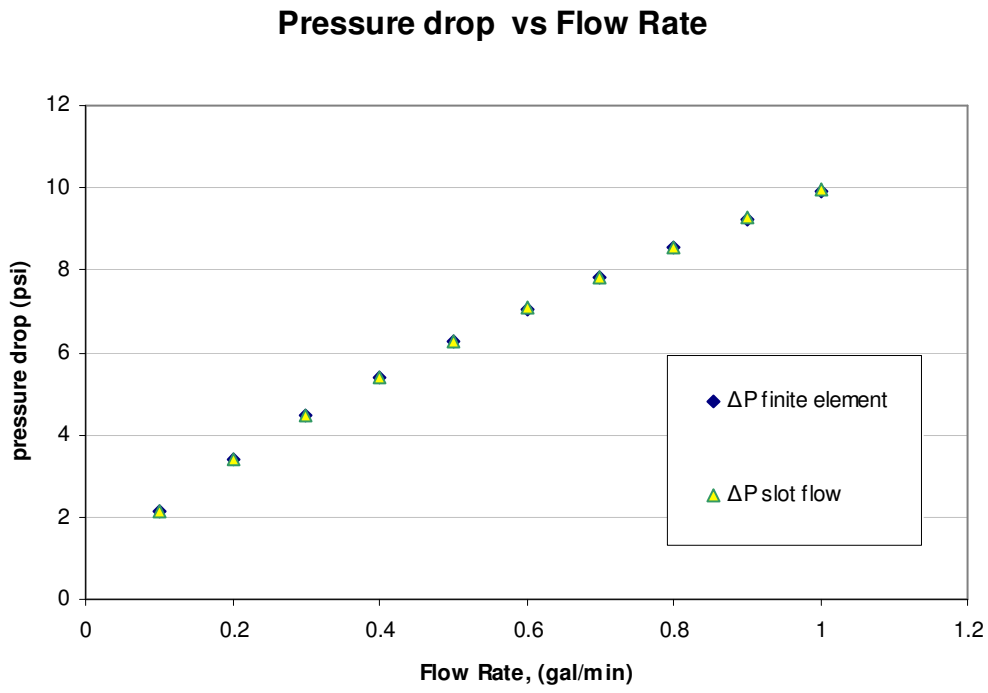

Fig. 5.39—Pressure drop vs. flow rate. α=1°, K=0.1 Pa. s^n, n=0.665, L=8 in.

Table 5.11—Pressure drop vs. power law index. α=6°, K=0.1 Pa. s^n, L=8 in, Q=0.5 gal/min.

n	ΔP slot flow (psia)	ΔP FEM (psia)	Absolute Error
1.2	6029.38	5879.46	149.92
1.1	2177.16	2146.62	30.54
1	786.14	782.25	3.89
0.9	283.79	284.53	0.74
0.8	102.36	103.29	0.93
0.7	36.91	37.42	0.51
0.6	13.28	13.52	0.24
0.5	4.77	4.87	0.1
0.4	1.70	1.74	0.04
0.3	0.60	0.59	0.01
0.2	0.21	0.22	0.01
0.1	0.07	0.07	0

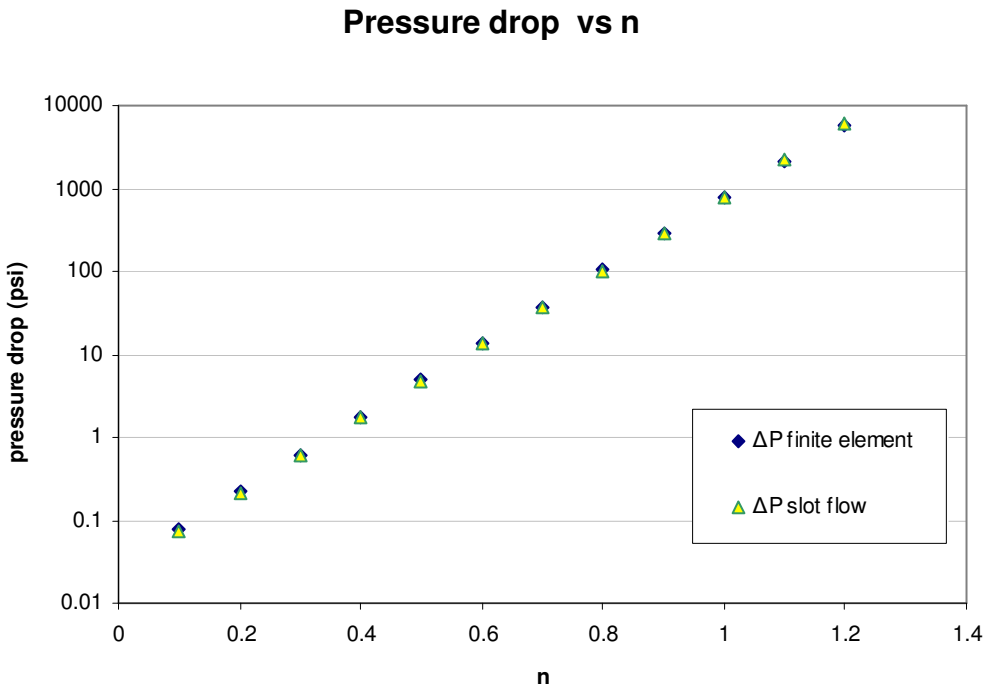

Fig. 5.40—Pressure drop vs. consistency index. α=6°, K=0.1 Pa. s^n, L=8 in, Q=0.5 gal/min.

Table 5.12—Pressure drop vs. flow rate. α=6°, K=0.1 Pa. s^n, n=0.665, L=8 in.

Q (gal/min)	ΔP slot flow (psia)	ΔP FEM (psia)	Absolute Error
0.1	8.86	8.98	0.12
0.2	14.03	14.25	0.22
0.3	18.38	18.66	0.28
0.4	22.26	22.59	0.33
0.5	25.82	26.21	0.39
0.6	29.14	29.59	0.45
0.7	32.29	32.78	0.49
0.8	35.29	35.82	0.53
0.9	38.20	38.74	0.54
1	40.94	41.56	0.62

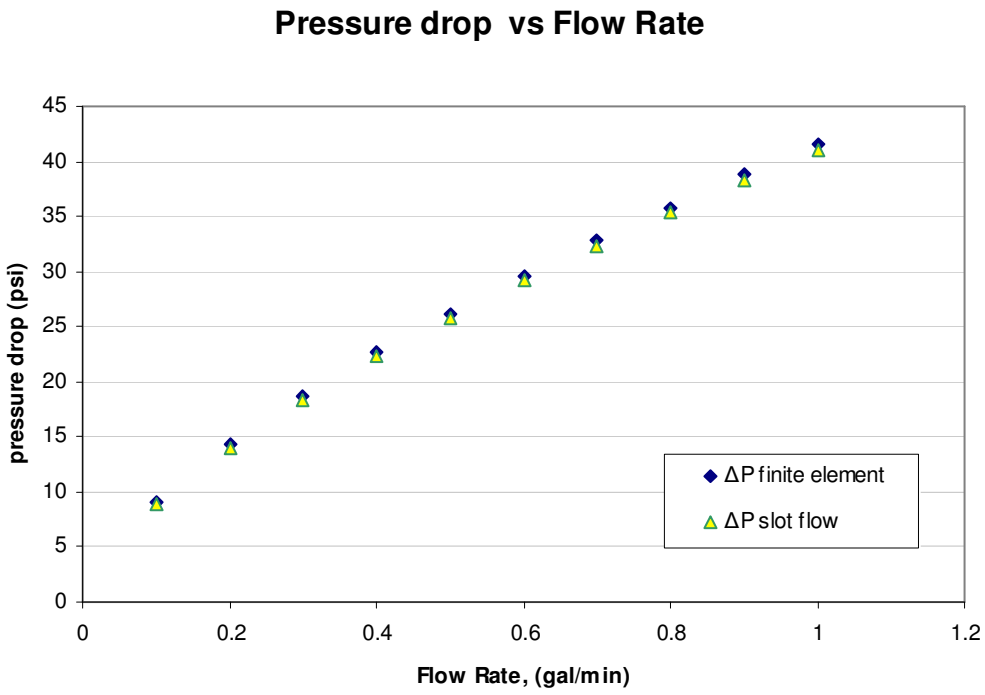

Fig. 5.41—Pressure drop vs. flow rate. α=6°, K=0.1 Pa. s^n, n=0.665, L=8 in.

As we can see, the Slot Flow approximation follows very closely the results of the Finite Element modeling. However we are interested in knowing the limits in which we can use this approximation with reasonable accuracy. To determine the point where the slot flow approximation and the FEM code start to diverge, we calculated the pressure drop as a function of the angle for both methods. The results are shown in **Table 5.13**: and **Table 5.14**.

Table 5.13—Pressure drop vs. angle. K=0.1 Pa. s^n, n=0.665, L=8 in, Q = 0.6 gal/min.

Angle (º)	ΔP slot flow (psia)	ΔP FEM (psia)
0	4.28	4.38
1	7.07	7.24
3	14.32	14.6
6	29.14	29.59
9	48.76	48.76
12	73.70	72.39
15	104.95	100.52
20	175.37	159.9
25	278.90	225.07
30	435.18	297.1
35	679.38	362.6
40	1077.21	408.8
45	1758.52	429.8

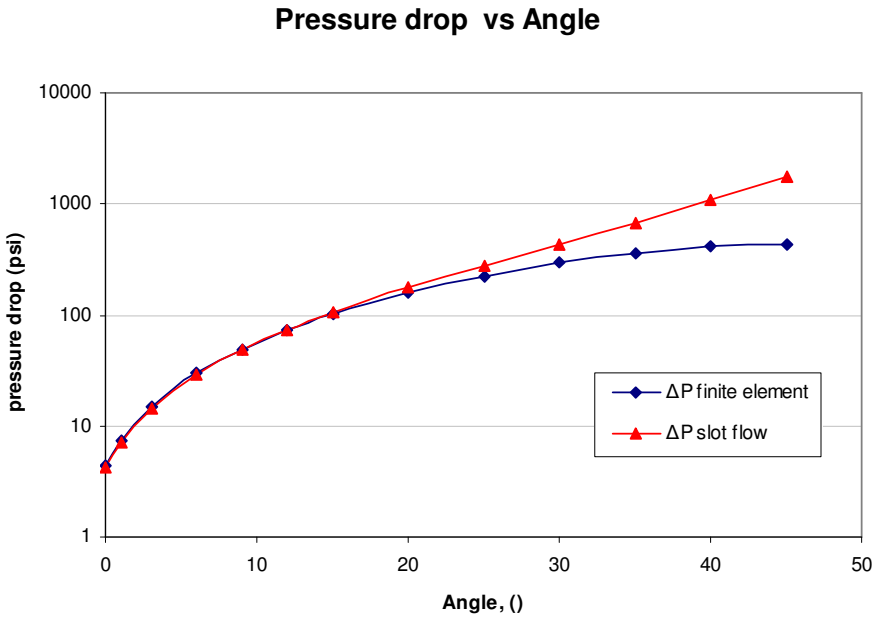

Fig. 5.42—Pressure drop vs. angle for finite element model and slot flow approximation model. K=0.1 Pa. s^n, n=0.665, L=8 in , Q = 0.5 gal/min.

Table 5.14—Pressure drop vs angle. K=0.1 Pa. s^n, n=1 , L=8 in, Q = 0.5 gal/min.

Angle α (°)	ΔP slot flow	ΔP FEM
0	79.7	79.5
3	369.7	367.2
6	892.5	871.3
9	1664.3	1567.7
12	2711.4	2416.2
15	4070.8	3411.9
20	7181.8	5257.0
30	18153.0	8782.2

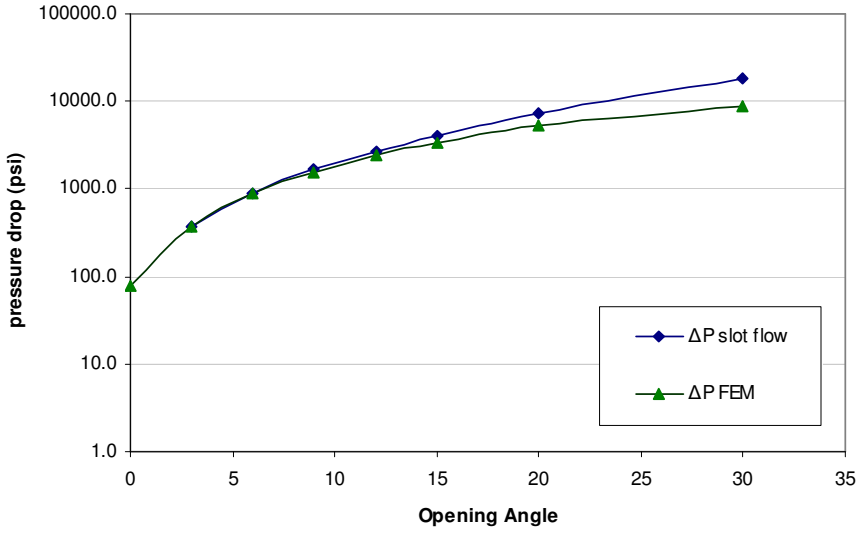

Fig. 5.43—Pressure drop vs. angle for finite element model and slot flow approximation model. K=0.1 Pa. s^n, n=1, L=8 in , Q = 0.5 gal/min.

From **Fig. 5.42** and **Fig. 5.43** it becomes apparent that the region where the slot flow approximation starts to lose validity is for angles greater than 12º. This result has been reported by Vlachopoulos[29]

The reason for this discrepancy is because the pressure is a function of both *r* and *z*. for small values of the opening angle, the contribution of *r* to the total pressure drop is very small. The slot flow approximation assumes that there is no pressure change in *r* direction, so both methods give similar results. For $\alpha \geq 12^{\circ}$, the contribution of *r* to the total pressure drop becomes larger and can no longer be neglected.

These results suggest that the slot flow approximation, Eq. 5.49 is an appropriate expression to describe the flow in the sensor, for $\alpha \geq 12^{\circ}$. These experiments verify that, for the typical desired geometries, the slot flow approximation is a valid approximation for our range of interest.

CHAPTER VI

DISCUSSION OF RESULTS

6.1 Objectives

In chapter IV, we described the experimental results obtained when using the sensor with Newtonian and non Newtonian fluids. We found a simplified expression to describe the sensor pressure drop response due to changes in flow rate by obtaining experimentally a proportionality constant *f*, which represents the geometrical features of the sensor geometry. We also investigated the response of the sensor for a shear-thinning fluid.

In chapter V, we presented several models to describe mathematically the sensor performance, by describing the sensor geometry as a series of concentric cylinders. We compared this solution to the solution obtained a finite element method. The results suggest that for the range of geometrical parameters, the simplified slot flow approximation is sufficiently accurate for prediction the pressure drop-flow rate response of the sensor for Newtonian and for power law fluids.

The aim of this chapter is to analyze the results obtained experimentally and the results obtained from the simulation models in light of the experimental results.

Newtonian Fluid

In Chapter III and IV, the performance of the sensor was described by a simplified model describe the following expression:

$$\Delta P = f\,\mu Q\,, \quad \text{..... (6.1)}$$

The parameter *f* can be calculated theoretically using the geometry and rheology of the fluid or it can be determined experimentally by measuring the response of pressure drop as a function of the flow rate for a fluid of known viscosity. Using several fluids, we determined experimentally that an average value for this parameter is

$$f = 4.02 \frac{\text{psi}}{\text{gal/min cp}}\,, \quad \text{..... (6.2)}$$

We wanted to compare this number with the equivalent number obtained from the analytical methods illustrated in Chapter V. We were provided the measured dimensions of the prototype device. The information consists of the tapered dimensions of the device, for the inner and outer conical pin. The expressions for the inner and outer radius have been presented as

$$r_o(z) = z\tan(\alpha) + r_o(0)\,, \quad \text{..... (6.3)}$$

$$r_i(z) = \sqrt{(z\tan(\alpha) + r_o(0))^2 - r_{fl}{}^2}\,, \quad \text{..... (6.4)}$$

and we can define the gap as

$$gap(z) = r_o(z) - r_i(z), \quad \text{..... (6.5)}$$

The theoretical and the measured profile of the device and the gap is shown in **Fig. 6.1**

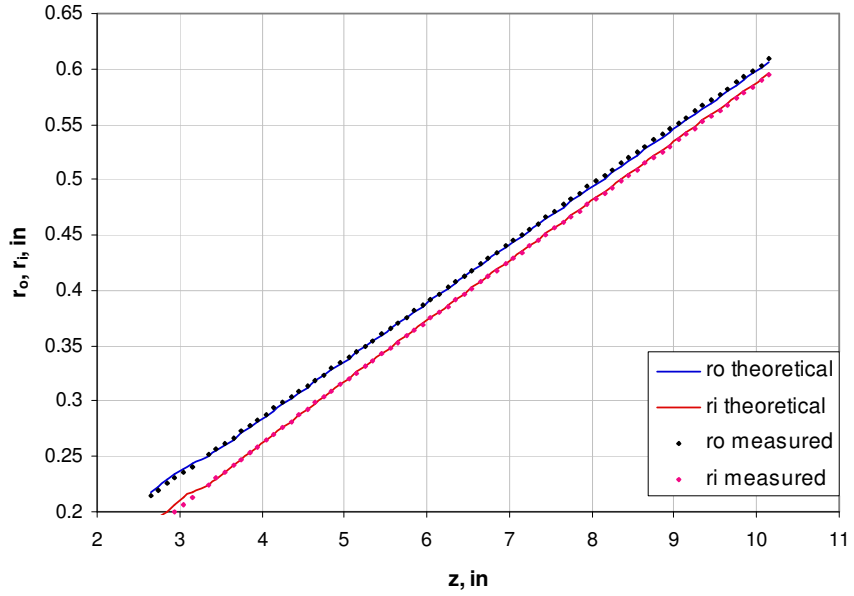

Fig. 6.1—Inner and outer radius for the prototype device.

We discretised the annular space in N number of segments and we calculated the pressure drop for each individual segment, as explained in Chapter V

$$\Delta p_i = \frac{K}{72}\left(\frac{3.85(4n+2)Q}{n\pi}\right)^n \left(\frac{1}{(r_o^{\,2} - r_i^{\,2})(r_o - r_i)^{1+1/n}}\right)\Delta L. \quad \text{..... (6.6)}$$

The total pressure drop is then calculated as:

$$\Delta P = \Delta p_1 + \Delta p_2 + ... + \Delta p_N \quad \text{..... (6.7)}$$

With the calculated pressure drop and flow rate, we can then estimate

$$f = \frac{\Delta P}{2KQ^n}, \quad \text{..... (6.8)}$$

Using the dimensions provided of the profile of the inner pin and outer casing as indicated in the Appendix E, we obtain:

$$f = 3.97 \frac{\text{psi}}{\text{gal/min cp}}, \quad \text{..... (6.9)}$$

The result is very close to the experimental value determined from the experiments with newtonian fluids, described in Chapter IV.

Non -Newtonian Fluid

As discussed in Chapter V, we can analyze the behavior of a power-law fluid in the device with the following expression:

$$Ln\Delta P = Ln\left(2Kf_{slot}\right) + nLnQ \quad \text{..... (6.10)}$$

That is, the slope of the plot $Ln\Delta P$ vs LnQ can be used to determine *n,* if there is sufficient experimental data. If the fluid behaves as a power-law material, plotting

$Ln\Delta P$ vs LnQ , should produce a straight line. **Fig. 6.2** shows the results for a Xanthan gum solutions tested in the device.

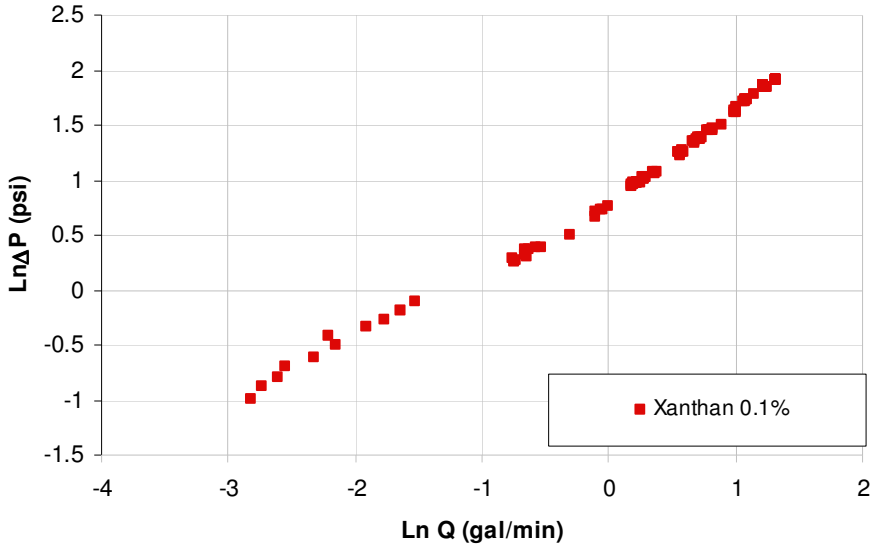

Fig. 6.2—Log-log plot of pressure drop vs. flow rate for xanthan gum solution 0.1% weight.

In this plot we observe there are two slopes, one at low flow rates and another at larger flow rates.. Since the fluid is shear thinning, we measure its properties with the Brookfield viscometer. These are indicated in **Table 6.1** and **Table 6.2**

Table 6.1—Rheology of xanthan gum solution 0. 1% obtained from Brookfield DV-III

RPM	viscosity (cp)	% torque	Torque (dyn*cm)	Shear Stress (dyn/cm^2)	Shear Rate (1/s)
250	18.1	76	512.01	12.253	67.697
220	18.4	67.5	454.75	10.883	59.146
200	18.6	62	417.69	9.996	53.742
180	18.9	56.7	381.99	9.142	48.368
150	20.2	50.3	338.87	8.110	40.147
120	22.7	45.3	305.19	7.304	32.174
90	26.5	39.7	267.46	6.401	24.154
60	33	33	222.32	5.320	16.123
30	48.6	24.3	163.71	3.918	8.061
20	60.6	20.1	135.41	3.241	5.348
10	85.2	14.2	95.67	2.289	2.687
6	108	10.7	72.09	1.725	1.597
3	140	7.2	48.51	1.161	0.829

Table 6.2—Rheology of xanthan gum solution 0.2% obtained from Brookfield DV-III

RPM	viscosity (cp)	% torque	Torque (dyn*cm)	Shear Stress (dyn/cm^2)	Shear Rate (1/s)
20	273	91	613.067	14.672	5.374
15	338	84.6	569.950	13.640	4.035
10	457	76.1	512.686	12.269	2.685
6	661	66.3	446.663	10.689	1.617
3	1082	54.3	365.819	8.755	0.809
1	2304	38.3	258.027	6.175	0.268
0.5	3593	29.5	198.742	4.756	0.132
0.1	8878	14.7	99.034	2.370	0.027

The power law coefficients were determined and are shown in **Table 6.3**. These parameters are in agreement with published values for xanthan gum dispersions at the same concentration.[32-33]

Table 6.3—Power law coefficients for xanthan gum solutions obtained from Brookfield DV-III

Concentration 0.1%	
K (mPa-s^n)	0.120
n	0.535
Concentration 0.2%	
K (mPa-s^n)	0.899
n	0.303

We can now use the slot flow model and calculate the pressure drop in the actual profile of the prototype. The comparison between the experimental and model for Xanthan gum at 0.1% is shown in **Fig. 6.3.** For low shear rates the power law model fits the experimental data. At larger flow rates and shear rates, the experimental data shows higher pressure drops than predicted. This could have been caused by a transition from laminar flow to turbulence as we increased the flow rate and the fluid became less viscous. The Reynolds number was calculated using the rheological information in Table 6.3. The maximum Reynolds number occurs at the entry of the sensor. It was observed that for flow rates higher than 0.6 gal/min, the Reynolds number approaches the critical value.

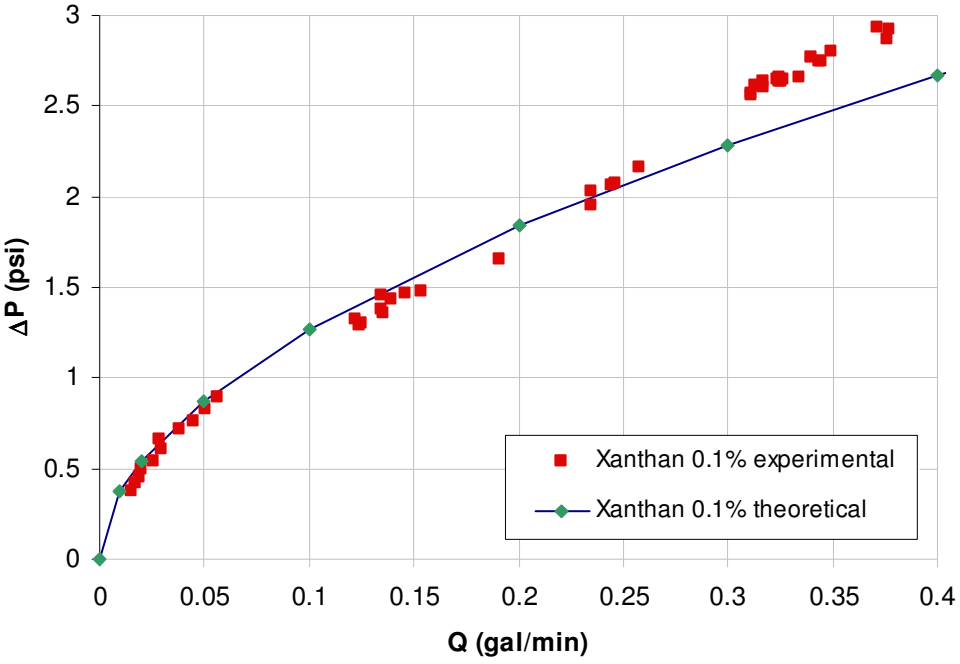

Fig. 6.3— Presure drop vs. flow rate for xanthan gum solution 0.1% weight.

CHAPTER VII

CONCLUSIONS AND RECOMMENDATIONS

7.1 Conclusions

The performance of the prototype sensor for Newtonian fluids tested in the laboratory (water, glycerin and hydrocarbon oils) with viscosities from 1 to 28 cp, proves the feasibility of the design for use as a viscosity monitoring tool. The linearity of the differential pressure response as a function of flow rate suggests that the flow regime is laminar over the range of flow rates shown.

The assembly and operation of the device is straightforward. The operator must be aware of the potential problems with the self cleaning mechanism or the design should be altered to prevent operation unless the inner pin and outer casing fit correctly in the exact location to avoid changes in the annular geometry.

Sensor accuracy and resolution of the device are dependent on those of the flow rate and differential pressure measuring devices, and on the accuracy with which the parameter f is determined.

To summarize, in this research we presented the following products:

- Complete description of sensor performance for Newtonian and non-Newtonian fluids (power law)
- Development of a simple model to determine the rheological parameters for Newtonian and Power Law fluids in the sensor.
- Generation of curve types, simplified models for quick estimation of the response of the sensor
- Software to model analytically and numerically the response of the sensor, using several approximations.

We provided three different ways to estimate the pressure drop – flow rate response of the device as a function of the rheology of the fluid as well as the geometrical variables of the device: 1) A finite element code to model power law flow in the tapered annular and 2) approximate solutions based on analytical models derived for power-law flow in concentric annuli. We believe the solution using the slot flow approximation to be a good compromise between accuracy and practicality. Furthermore, we developed simplified expressions to calculate the pressure drop and curve types to use this approximation.

7.2 Recommendations

In a practical application, the factor f should be determined experimentally. This is accomplished by immersing the sensor in a bath whose temperature is the same as that of

the calibration fluid being pumped through the sensor. Measurements of the differential pressure across the device as a function of known flow rate, viscosity and fluid temperature may then obtained. Applying a linear fit to a plot of $\Delta P/\mu$ versus Q produces a line whose slope is the factor f at this temperature.

Design of a commercial tool should consider the optimization of the dimensions based on the expected range of flow rate and viscosity. Feasibility and sensor geometry for any application may be easily calculated using the tools and algorithms developed in this study. Given the anticipated flow rates, and fluid densities and viscosities, optimal geometries and performance estimates may be calculated.

Possible future research work on this device includes field testing of the sensor in oilfield applications, to study the impact of solids and other contaminants in the measurements. The theoretical work presented in this study could be expanded to propose modifications to the geometry of the device and addition of attachments to expand the range of measurement and to address the operational issues.

NOMENCLATURE

Latin

m = mass (lb)

t = time (s)

p = pressure (psia)

v = velocity (ft/s)

Q = flow rate (gal/min)

D = diameter (in)

r = radial distance(in)

r_i, r_o = internal and external radius (in)

$r_o(0)$ = initial external radius (in)

L = length (in)

z = axial distance (in)

T = temperature (°F)

x = distance (in)

y = distance (in)

K = consistency index (lbf s^n/ft^2)

n = power law index, dimensionless

N_{Re} = Reynolds number, dimensionless

N_{Rem} = modified Reynolds number, dimensionless

N_{ReC} = critical Reynolds number, dimensionless

Greek

τ = shear stress (lbf/ft^2)

τ_w = wall shear stress (lbf/ft^2)

$\dot{\gamma}$ = shear rate (1/s)

$\dot{\gamma}_w$ = wall shear rate (1/s)

μ = Newtonian viscosity (cp)

η = apparent viscosity (cp)

ρ = density (lb/gal)

Δp = pressure drop (psia)

λ = dimensionless parameter

ξ = dimensionless parameter

κ = aspect ratio, dimensionless

ε = tolerance value, dimensionless

REFERENCES

1. Maglione, R., Robotti, G. and Romagnoli, R. 2000. In-Situ Rheological Characterization of Drilling Mud. *SPEJ* **5**(4): 377-386.SPE-66285-PA.
2. Maglione, R., Robotti, G. and Romagnoli, R. 1996. A Drilling Well as Viscometer: Studying the Effects of Well Pressure and Temperature on the Rheology of the Drilling Fluids. Paper SPE 36885 presented at the European Petroleum Conference, Milan, Italy, 22-24 October.
3. Chen, Z., et al. 2005. Rheology and Hydraulics of Polymer (HEC) Based Drilling Foams at Ambient Temperature Conditions. Paper SPE 94273 presented at the SPE Production and Operations Symposium, Oklahoma City, Oklahoma, 16-19 April..
4. Chen, Z., et al 2005. Rheology of Aqueous Drilling Foam Using a Flow-Through Rotational Viscometer. Paper SPE 93431 presented at the SPE International Symposium on Oilfield Chemistry, Houston, Texas, 2-4 February.
5. Kalotay, P. 1994. On-line Viscosity Measurement using Coriolis Mass Flowmeters. *Flow Meas. Instrum.* **5**(4): 303-308.
6. Dealy, J.M. 1990. Challenges in Process Rheometry. *Rheologica Acta* **29**: 519-522.
7. Tucker, G.S. 1993. Novel Techniques for Characterizing the Flow of Solids and Liquids. *Trends in Food Science & Technology* **4**: 243-246.

8. O'Connor, W. 1995. In-line Viscometry in the Dairy Processing Industry. *Journal of the Society of Dairy Technology* **48**(2): 44-49.

9. Zimmer, L., Haley, T., and Campanella O. 2001. A Comparative Study of the Performance of Selected In-Line Viscometers on Newtonian and Shear-thinning Fluids. *Journal of Texture Studies* **32**: 75-103.

10. Steffe, J.F. 1992. *Rheological Methods in Food Process Engineering*. East Lansing, Michigan: Freeman Press.

11. Enzendorfer, C., et al. 1995. Pipe Viscometry of Foams. *Journal of Rheology*. **39**(2): 345-358.

12. Fredrickson, A.G. and Bird, R.B. 1958. Non-Newtonian Flow in Annuli. *Industrial and Engineering Chemistry* **50**(3): 347-352.

13. Hanks, R.W. and Larsen K.M. 1979. The Flow of Power-Law Non-Newtonian Fluids in Concentric Annuli. *Ind. Eng. Chem. Fundam.* **18**(1): 33-35.

14. Prasanth, N. and Shenoy U.V. 1992. Poiseuille Flow of a Power-Law Fluid between Coaxial Cylinders. *Journal of Applied Polymer Science* **46**(7): 1189-1194.

15. Tuoc, T.K. and J.M. McGiven. 1994. Laminar Flow of Non-Newtonian Fluids in Annuli. *Trans. IChemE* **72**(A5): p. 669-676.

16. Escudier, M.P., et al. 2002. Fully Developed Laminar Flow of Non-Newtonian Liquids through Annuli: Comparison of Numerical Calculations with Experiments. *Experiments in Fluids* **33**(1): 101-110.

17. Escudier, M.P., Oliveira, P.J. and Pinho, F.T. 2002. Fully Developed Laminar flow of Purely Viscous Non-Newtonian Liquids through Annuli, Including the Effects of Eccentricity and Inner-cylinder Rotation. *International Journal of Heat and Fluid Flow* **23**(1): 52-73.

18. Vatistas, G.H. and Ghaly, W.S. 1999. Converging and Diverging Flow in Narrow Conical Passages. *Acta Mechanica* **136**(3-4): 209-222.

19. Ulev, L.M. 1998. Slow Flows between Coaxial Conical Surfaces. *Journal of Engineering Physics and Thermophysics* **71**(6): p. 1056-1063.

20. Ulev, L.M. 2001. Laminar Heat Transfer in Diffuser Flow in a Coaxial Conical Channel in the Case of Boundary Conditions of the First Kind. *Journal of Engineering Physics and Thermophysics* **74**(1): 26-34.

21. Shenoy, U.V. 1996. Flow of Power-Law Flids Between Coaxial Cylinders. In *Handbook of Applied Polymer Processing Technology*, ed. N. Cheremisinoff and B Cheremisinoff, Chap 3, 72-75. New York: Marcel Dekker.

22. Nassehi, V. 2002. *Practical Aspects of Finite Element Modelling of Polymer Processing*. New York: Wiley.

23. Huang, H.C. 1999. *Finite Element Analysis of Non-Newtonian Flow*. London: Springer.

24. Heinrich, J.C. and Pepper, D. W. 1999. *Intermediate Finite Element Method, Fluid Flow and Heat Transfer Applications*. Philadelphia: Taylor & Francis.

25. Macosko, C.W. 1994. *Rheology. Principles, Measurements and Applications*. Poughkeepsie, New York: Wiley-VCH.

26. Proett, M. et al. 2004. Method and Apparatus for Determining Fluid Viscosity. 2004, US Patent 6,755,079.

27. Mago, A. 2006. Adequate Description of Heavy Oil Viscosities and a Method to Assess Optimal Steam Cyclic Periods for Thermal Reservoir Simulation. MS thesis. Texas A&M University, College Station.

28. Parnaby, J. and Worth, R.A. 1974. Variator Mandrel Forces in Blow Moulded Parison Control Systems-—Computer-Aided Design. *Proc. Instn. Mech. Eng*. **188**(25): 357-364.

29. Viloria, M. 2006. Analysis of Drilling Fluid Rheology and Tool Joint Effect to Reduce Errors in Hydraulics Calculations, Ph.D. dissertation, Texas A&M University, College Station.

30. Gucuyener I. and Mehmetoglu, T. 1996. Characterization of Flow Regime in Concentric Annuli and Pipes for Yield-pseudoplastic Fluids. *Journal of Petroleum Science and Engineering* **16**(1-3): 45-60.

31. Vlachopoulos, J. and Scott, P.1985. Pressure Drop for Molten Polymer Flow. *Advances in Polymer Technology*. **5**(2): 81-86.

32. Ahmed, J. and Ramaswamy, H. 2005. Rheology of Xanthan Gum: Effect of Concentration, Temperature and High Pressure. *Journal of Food Science Technology* **42**(4): 355-358.

33. Speers, R.A. and Tung, M.A. 1986. Concentration and Temperature Dependence of Flow Behavior of Xanthan Gum Dispersions. *Journal of Food Science* **51**(1): 96-99.

APPENDIX A

Brookfield DV-III+ operation

The rotating viscometer measures fluid parameters of shear stress and viscosity at given shear rates. The viscometer has a cylindrical spindle which is driven through a calibrated spring. The viscous drag of the fluid against the cylindrical spindle is measured by the spring deflection. Then a rotary transducer measures the spring deflection. The range of the viscosity (in centipoises) is determined by the rotational speed of the spindle, the size and shape of the spindle, the container the cone spindle is rotating in, and the full-scale torque of the calibrated spring.

The temperature of the spindle is controlled by using a circulating temperature water bath. The tests are conducted at ambient pressure. For highly viscous fluids, the spindle must be introduced in the sample very slowly in order to keep the sample free of air bubbles during the rotation.

The procedure to operate the Brookfield rheometer is

1. Assemble and level the rheometer in the operating table.
2. Remove any spindle attached to the rheometer, and press the Autozero function in the screen.

3. Select the appropriate spindle. The type of spindle will depend on the volume of the sample of the fluid and the expected viscosity. The selection is done following the guidelines indicated in the rheometer manual.
4. Attach the spindle it to the rheometer. Enter its number in the control unit
5. Introduce the spindle into the sample and attach the spindle to the coupling nut.
6. Adjust the thermal bath control until the desired temperature is reached.
7. Enter the speed of rotation using the number pad.
8. Record torque and viscosity.

The DV-III+ Rheometer is turned on, leveled and autozeroed. The level is adjusted using the knobs located in the base and confirmed using the bubble on the top of the head. The rheometer is set to autozero prior to each measurement. The sample of fluid is poured into a 600 ml low form Griffin beaker. This container is submerged in the thermal bath. Special care must be taken to avoid evaporation of the fluid at high temperatures.

The choice of spindle will depend on the expected viscosity of the fluid. For the fluids tested in the flow loop, the cylindrical spindle LV1 was selected. For lower viscosities, the cone and plate spindle was used.

The Shear rate is calculated as

$$\dot{\gamma} = \frac{2\omega r_c^{\,2} r_b^{\,2}}{x\left(r_c^{\,2} - r_b^{\,2}\right)}, \quad \text{..... (A.1)}$$

The shear stress in dyn/cm^2 is

$$\tau = \frac{M\,2\omega r_c^{\,2} r_b^{\,2}}{2x r_b^{\,2} L}, \quad \text{..... (A.2)}$$

The viscosity in poise is

$$\eta = \frac{\tau}{\dot{\gamma}}, \quad \text{..... (A.3)}$$

where

ω: angular velocity of the spindle (rad/s) $\omega = \frac{2\pi}{60}\text{RPM}$

r_c: radius of container (cm)

r_c: radius of spindle (cm)

x: radius at which shear rate is being calculated

M: torque input by instrument (dyn-cm)

L: effective length of spindle (cm)

For the experiment, we used the spindle LV #61. Its dimensions are:

Table A.1— Brookfield DVIII coefficients.

Coefficient (cm)	
L	7.493
Rb	0.9421
Rc	4.125

APPENDIX B

Data Acquisition

The data acquisition system and software was provided by Halliburton and modified to adapt it to our experimental set up successfully. The hardware-software solution we used consisted of the following

1- HP Agilent box, which receives analog signals from the flow meter and the Rosemount pressure transducers.

2- Digital display, brand Paroscientific "Digiquartz pressure computer" which receives the signal from the Paroscientific pressure transducers.

3- Generic data acquisition box, which receives the signal from Paroscientific pressure transducers.

These are connected to a personal computer running LabView via serial port. The subroutines in Labview read the signals coming from the boxes and write them to a Microsoft Excel file. A diagram with the data acquisition layout is shown on **Fig. B.1**

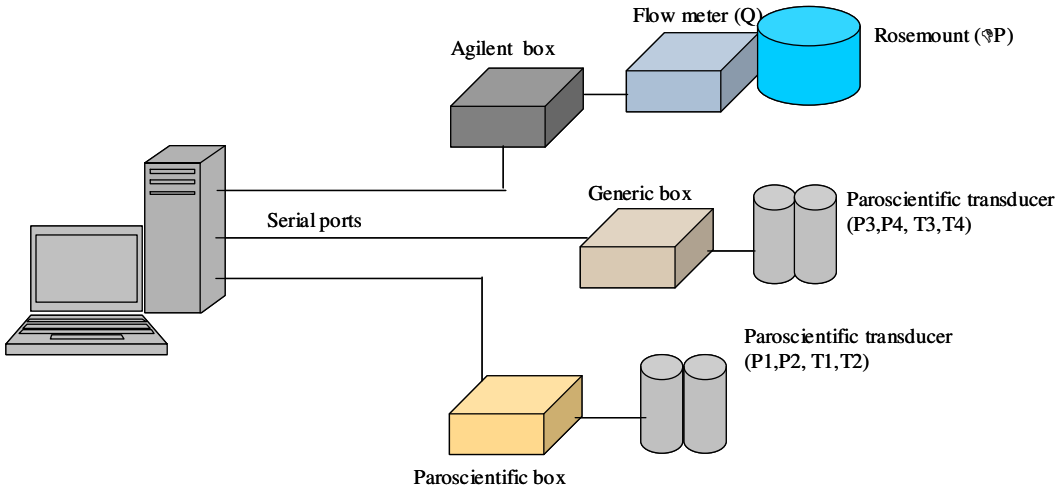

Fig. B.1— Data Acquisition setup.

The Labview control interface is shown in **Fig. B.2**.

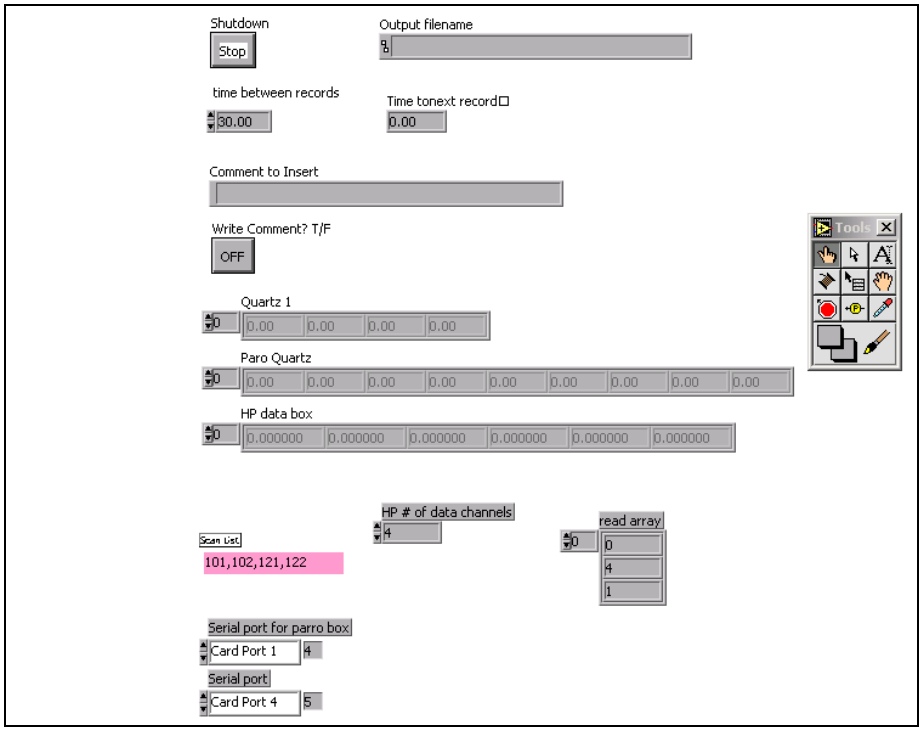

Fig. B.2—LabView data acquisition interface.

In the interface, we specify the name of the output file. The output is generated as a Microsoft Excel file. The Labview routine scans the HP Agilent box readings in channels 101 and 102 for temperature and the 121 and 122 for the analog signals coming from the flow meter and the Rosemount transducer.

The Paroscientific pressure transducers also have a built in temperature sensor. This is also recorded a temperature reading along with the pressure by default. However, this temperature is measured at the transducer and not in the viscosity sensor, therefore it is not used for calculations. We measured the temperature at the inlet and outlet of the sensor with dedicated temperature sensors. These were installed inside the thermal bath

and connected to the Agilent box. inports 102 and 107. The temperature readings are written in the Excel file along with the other pressure data.

The Paroscientific pressure transducers were calibrated following the instructions provided by the manufacturer.

We changed the scale of the differential pressure transducer. The former range was 0-100 psia. The new range was set to 0-15 psia. The documentation of transducer specified an accuracy of ±0.25% of the upper range limit. We also checked the specifications of the flowmeter, and the maximum temperature it supports is 177 °C, or 350.6°F; well above the temperatures of use in the experiments.

APPENDIX C

Experimental data

Table C1—Experimental Pressure Drop – Flow rate water Temperature Average 65°F

T (°F)	Q (gal/min)	ΔP (psia)
65.549	0.469	2.005
65.510	0.466	2.030
65.501	0.471	2.039
65.487	0.469	2.048
65.512	0.464	2.048
65.518	0.471	2.053
65.542	0.470	2.053
65.145	0.368	1.571
65.123	0.367	1.604
65.083	0.361	1.611
65.106	0.358	1.611
65.065	0.365	1.618
65.090	0.365	1.629
65.128	0.364	1.639
65.136	0.368	1.638
65.147	0.365	1.639
65.169	0.366	1.639
64.700	0.271	1.125
64.616	0.273	1.148
64.570	0.273	1.166
64.564	0.271	1.175
64.547	0.271	1.181
64.562	0.271	1.184
64.583	0.271	1.189
64.566	0.263	1.153
64.536	0.259	1.150
64.579	0.264	1.145
64.107	0.189	0.804
63.977	0.189	0.819
63.890	0.188	0.833
63.888	0.189	0.840
63.889	0.191	0.846
63.935	0.193	0.850
63.907	0.188	0.853

T (°F)	Q (gal/min)	ΔP (psia)
63.957	0.192	0.851
63.983	0.192	0.850
64.057	0.190	0.850
63.749	0.141	0.598
63.487	0.138	0.583
63.397	0.140	0.583
63.378	0.138	0.581
63.355	0.140	0.588
63.323	0.139	0.590
63.444	0.139	0.588
63.430	0.141	0.584

Table C2—Experimental Pressure Drop – Flow rate water Temperature Average =60°F

T (°F)	Q (gal/min)	ΔP (psia)
60.782	0.456	2.108
60.385	0.462	2.169
60.269	0.467	2.190
60.134	0.462	2.196
60.170	0.464	2.185
60.068	0.460	2.188
59.186	0.314	1.378
59.053	0.306	1.408
59.146	0.306	1.424
59.144	0.300	1.429
59.155	0.307	1.423
58.768	0.177	0.918
58.270	0.180	0.834
58.223	0.180	0.850
58.185	0.174	0.858
58.100	0.176	0.853

Table C3—Experimental Pressure Drop – Flow rate water Temperature Average =68°F

T (°F)	Q (gal/min)	ΔP (psia)
68.920	0.413	1.689
68.100	0.411	1.675
68.455	0.284	1.120
68.005	0.281	1.118
68.650	0.154	0.583
68.123	0.152	0.578
68.585	0.057	0.189
68.144	0.104	0.439
68.856	0.059	0.191

T (°F)	Q (gal/min)	ΔP (psia)
68.748	0.154	0.582
68.638	0.284	1.128
68.185	0.413	1.687

Table C4—Experimental Pressure Drop – Flow rate water Temperature Average =140°F

T (°F)	Q (gal/min)	ΔP (psia)
139.923	1.148	11.230
140.127	1.148	11.287
139.974	0.996	8.830
139.867	0.808	6.265
139.979	0.605	3.902
139.747	0.388	2.014
140.184	0.193	0.812

Table C5—Experimental Pressure Drop – Flow rate water Temperature Average =100°F

T (°F)	Q (gal/min)	ΔP (psia)
104.485	1.116	11.174
101.216	1.107	11.201
100.185	0.382	2.523
100.609	0.299	1.901
99.973	0.190	1.177

Glycerin data

Table C6—Experimental Pressure Drop – Flow rate Glycerin Temperature Average =100°F

T (°F)	Q (gal/min)	ΔP (psia)
100.599	0.746	9.774
100.592	0.746	9.776
100.591	0.746	9.783
100.591	0.745	9.780
100.591	0.745	9.779
100.594	0.747	9.780
100.593	0.747	9.780
100.602	0.745	9.783
100.600	0.745	9.780
100.590	0.747	9.786
100.597	0.745	9.785
100.604	0.747	9.790
100.607	0.746	9.788

T (°F)	Q (gal/min)	ΔP (psia)
100.617	0.749	9.798
100.617	0.745	9.794
99.682	0.684	8.951
99.367	0.684	9.028
99.334	0.683	9.053
99.338	0.683	9.071
99.361	0.683	9.079
99.395	0.680	9.085
99.415	0.685	9.081
99.459	0.683	9.079
99.515	0.685	9.091
99.568	0.684	9.090
99.612	0.687	9.100
99.679	0.686	9.091
99.731	0.686	9.088
99.818	0.684	9.063
99.872	0.684	9.053
99.954	0.682	9.038
100.031	0.685	9.034
100.130	0.683	9.026
100.189	0.685	9.035
100.300	0.687	9.026
100.386	0.689	9.026
100.494	0.686	9.023
100.569	0.688	9.021
100.662	0.686	9.018
100.738	0.689	9.006
100.813	0.690	9.005
100.781	0.652	8.481
100.774	0.651	8.449
100.802	0.651	8.454
100.853	0.654	8.464
100.904	0.653	8.471
100.942	0.654	8.475
100.978	0.652	8.471
101.032	0.651	8.458
101.095	0.653	8.454
101.160	0.654	8.459
101.162	0.653	8.453
101.208	0.656	8.456
101.291	0.653	8.454
101.331	0.656	8.455
101.360	0.653	8.450
101.282	0.588	7.458
101.278	0.586	7.521
101.258	0.586	7.550

T (°F)	Q (gal/min)	ΔP (psia)
101.235	0.585	7.570
101.291	0.588	7.583
101.303	0.591	7.589
101.343	0.592	7.581
101.360	0.587	7.576
101.424	0.589	7.581
101.451	0.591	7.585
101.500	0.589	7.589
101.529	0.596	7.591
101.590	0.591	7.585
101.623	0.589	7.576
101.694	0.594	7.578
101.729	0.591	7.576
101.752	0.591	7.570
101.779	0.541	6.785
101.751	0.530	6.681
101.782	0.533	6.705
101.827	0.531	6.739
101.881	0.533	6.748
101.912	0.533	6.765
101.930	0.532	6.766
101.966	0.530	6.773
101.992	0.539	6.765
102.048	0.531	6.768
102.114	0.530	6.770
102.146	0.530	6.766
102.174	0.536	6.761
102.213	0.533	6.766
102.251	0.529	6.763
102.294	0.533	6.764
102.352	0.532	6.763
102.397	0.535	6.756
102.429	0.531	6.755
102.430	0.532	6.754
102.440	0.535	6.755
102.482	0.536	6.753
102.487	0.532	6.756
102.353	0.430	5.171
102.366	0.452	5.544
102.157	0.410	5.026
102.128	0.410	5.103
102.129	0.411	5.076
102.149	0.431	5.291
102.207	0.421	5.240
102.232	0.424	5.266
102.238	0.424	5.216

T (°F)	Q (gal/min)	ΔP (psia)
102.274	0.418	5.234
102.234	0.417	5.108
102.262	0.425	5.279
102.260	0.424	5.263
102.244	0.421	5.233
102.266	0.413	5.115
102.299	0.423	5.218
102.299	0.420	5.226
102.331	0.427	5.275
102.316	0.408	5.048
102.291	0.414	5.126
102.274	0.424	5.219
102.241	0.401	4.993
102.232	0.410	5.058
102.211	0.388	4.850
102.202	0.422	5.199
102.101	0.367	4.430
102.057	0.380	4.666
102.040	0.377	4.658
101.987	0.376	4.643
101.943	0.350	4.310
101.847	0.349	4.271
101.930	0.362	4.466
101.981	0.377	4.678
102.020	0.377	4.684
101.997	0.374	4.684
101.850	0.317	3.749
101.624	0.314	3.816
101.556	0.312	3.821
101.486	0.316	3.916
101.457	0.322	4.008
101.459	0.325	4.058
101.343	0.304	3.814
101.375	0.318	3.996
101.348	0.320	4.003
101.327	0.322	4.040
101.301	0.320	4.046
101.281	0.320	4.059
101.323	0.321	4.033
101.288	0.331	4.098
101.016	0.275	3.400
101.140	0.281	3.451
101.173	0.278	3.466
101.123	0.275	3.465
101.113	0.272	3.455
101.082	0.277	3.489

T (°F)	Q (gal/min)	ΔP (psia)
101.059	0.274	3.490
100.798	0.223	2.764
100.669	0.224	2.740
100.616	0.223	2.788
100.548	0.223	2.800
100.516	0.225	2.825
100.507	0.229	2.829
100.471	0.223	2.834
100.466	0.224	2.834
100.473	0.224	2.928
100.648	0.227	2.924
100.659	0.225	2.910
100.628	0.225	2.901
100.593	0.224	2.894
100.598	0.227	2.903
100.575	0.221	2.871
100.577	0.227	2.884
100.586	0.227	2.898
100.540	0.224	2.883
100.420	0.224	2.899
100.142	0.165	1.964
99.767	0.164	2.094
99.613	0.163	2.088
99.507	0.164	2.085
99.466	0.166	2.080
99.407	0.166	2.075
99.367	0.166	2.071
99.335	0.166	2.064
99.329	0.164	2.076
99.351	0.166	2.068
99.314	0.166	2.045
98.625	0.103	1.196
98.313	0.102	1.195
98.151	0.103	1.229
98.070	0.103	1.258
97.921	0.105	1.279
97.997	0.104	1.276
97.954	0.103	1.269
97.913	0.100	1.253
97.921	0.104	1.245
97.904	0.102	1.239
97.981	0.101	1.234
97.967	0.100	1.230
97.996	0.100	1.225
98.046	0.100	1.219

Table C7—Experimental Pressure Drop – Flow rate Glycerin Temperature Average 121°F

T (°F)	Q (gal/min)	ΔP (psia)
121.985	0.878	8.416
121.855	0.879	8.423
121.758	0.879	8.428
121.646	0.878	8.431
121.537	0.875	8.435
121.425	0.878	8.445
121.328	0.877	8.454
121.208	0.874	8.463
121.121	0.874	8.474
121.024	0.876	8.484
120.954	0.874	8.491
120.865	0.873	8.499
120.798	0.873	8.505
120.744	0.871	8.509
120.681	0.870	8.515
120.609	0.872	8.519
120.558	0.874	8.525
120.509	0.873	8.530
120.484	0.872	8.535
120.469	0.873	8.539
120.454	0.871	8.543
120.457	0.870	8.544
120.435	0.872	8.546
119.147	0.767	7.603
119.014	0.767	7.650
118.985	0.764	7.675
118.981	0.764	7.681
118.990	0.762	7.686
119.015	0.765	7.693
119.057	0.768	7.699
119.107	0.766	7.701
119.145	0.767	7.705
119.203	0.763	7.705
119.278	0.766	7.705
119.316	0.766	7.704
119.417	0.766	7.703
119.508	0.766	7.699
119.583	0.767	7.696
119.678	0.767	7.693
119.797	0.770	7.691
119.858	0.760	7.669
119.877	0.674	6.615

T (°F)	Q (gal/min)	ΔP (psia)
119.953	0.674	6.679
120.055	0.674	6.714
120.132	0.677	6.735
120.224	0.678	6.746
120.331	0.678	6.754
120.425	0.680	6.756
120.474	0.677	6.760
120.526	0.676	6.759
120.549	0.678	6.760
120.592	0.679	6.755
120.638	0.678	6.751
120.681	0.678	6.750
120.689	0.679	6.748
120.741	0.679	6.745
120.771	0.678	6.746
120.812	0.680	6.744
120.830	0.681	6.744
120.877	0.679	6.741
120.906	0.679	6.740
120.936	0.678	6.741
120.970	0.678	6.739
120.981	0.677	6.739
121.011	0.678	6.740
121.033	0.676	6.741
121.068	0.679	6.739
121.092	0.679	6.738
121.121	0.679	6.735
121.086	0.604	5.829
121.073	0.596	5.758
121.086	0.597	5.793
121.119	0.592	5.809
121.166	0.594	5.824
121.206	0.594	5.831
121.222	0.594	5.838
121.235	0.592	5.833
121.258	0.591	5.826
121.285	0.593	5.821
121.291	0.594	5.816
121.297	0.592	5.818
121.324	0.594	5.813
121.309	0.592	5.809
121.341	0.590	5.808
121.365	0.590	5.806
121.366	0.592	5.809
121.405	0.593	5.811
121.427	0.597	5.836

T (°F)	Q (gal/min)	ΔP (psia)
121.405	0.595	5.853
121.372	0.595	5.856
121.374	0.598	5.853
121.384	0.598	5.850
121.386	0.597	5.854
121.229	0.505	4.703
121.208	0.506	4.779
121.195	0.510	4.850
121.179	0.514	4.965
121.216	0.516	4.994
121.231	0.518	5.014
121.240	0.518	5.030
121.250	0.521	5.043
121.252	0.524	5.050
121.256	0.519	5.058
121.237	0.522	5.060
121.255	0.523	5.065
121.238	0.521	5.065
121.281	0.521	5.069
121.307	0.525	5.066
121.314	0.520	5.066
121.314	0.522	5.069
121.319	0.522	5.068
121.308	0.520	5.068
121.343	0.523	5.066
121.356	0.522	5.065
121.370	0.523	5.065
121.371	0.524	5.064
121.398	0.522	5.065
121.404	0.523	5.064
121.388	0.522	5.065
121.406	0.525	5.064
121.398	0.524	5.060
121.403	0.523	5.060
121.439	0.521	5.060
121.469	0.524	5.059
121.472	0.523	5.058
121.471	0.522	5.055
121.451	0.521	5.055
121.445	0.522	5.059
121.451	0.524	5.058
121.422	0.522	5.060
121.425	0.522	5.058
121.458	0.523	5.058
121.498	0.522	5.060
121.342	0.414	3.750

T (°F)	Q (gal/min)	ΔP (psia)
121.273	0.415	3.849
121.161	0.381	3.485
121.127	0.374	3.515
121.061	0.378	3.603
121.084	0.381	3.601
121.107	0.381	3.561
121.138	0.369	3.498
121.226	0.376	3.664
121.236	0.375	3.706
121.271	0.387	3.736
121.302	0.376	3.619
121.349	0.386	3.664
121.354	0.363	3.518
121.407	0.377	3.671
121.437	0.378	3.643
121.471	0.380	3.635
121.525	0.394	3.815
121.577	0.395	3.868
121.589	0.396	3.870
121.620	0.400	3.906
121.634	0.407	3.905
121.635	0.407	3.924
121.686	0.414	3.963
121.718	0.400	3.919
121.743	0.402	3.910
121.774	0.399	3.843
121.811	0.400	3.879
121.847	0.408	3.813
121.852	0.397	3.823
121.892	0.392	3.788
121.938	0.396	3.785
121.962	0.398	3.883
121.984	0.376	3.784
121.996	0.395	3.709
122.030	0.385	3.726
122.018	0.385	3.699
122.048	0.394	3.743
122.098	0.400	3.800
122.104	0.394	3.776
122.148	0.402	3.841
122.160	0.402	3.849
122.189	0.401	3.843
122.195	0.400	3.813
122.198	0.399	3.838
122.009	0.292	2.564
121.932	0.293	2.653

T (°F)	Q (gal/min)	ΔP (psia)
121.943	0.294	2.681
121.997	0.295	2.720
122.028	0.294	2.740
122.051	0.294	2.768
122.034	0.296	2.764
121.994	0.294	2.768
121.948	0.296	2.774
121.952	0.297	2.786
121.933	0.296	2.791
121.925	0.298	2.795
121.897	0.296	2.798
121.902	0.296	2.798
121.908	0.297	2.798
121.899	0.299	2.801
121.875	0.297	2.804
121.874	0.298	2.816
121.872	0.298	2.818
121.678	0.219	1.994
121.541	0.218	1.984
121.493	0.217	1.994
121.467	0.217	2.005
121.376	0.220	2.016
121.423	0.225	2.023
121.438	0.220	2.026
121.392	0.221	2.033
121.372	0.218	2.041
121.372	0.219	2.046
121.382	0.225	2.051
121.382	0.212	2.035
121.402	0.220	2.026
121.461	0.217	2.050
121.462	0.216	2.060
121.438	0.214	2.045
121.454	0.212	2.029
121.453	0.213	2.024
121.442	0.213	2.024
121.443	0.213	2.016
121.434	0.218	2.006
121.483	0.215	2.029
121.452	0.215	2.034
121.490	0.220	2.045
121.496	0.222	2.051
121.546	0.218	2.063
121.485	0.220	2.063
121.481	0.218	2.063
121.072	0.118	1.100

T (°F)	Q (gal/min)	ΔP (psia)
120.826	0.116	1.093
120.697	0.117	1.118
120.653	0.115	1.115
120.599	0.117	1.100
120.580	0.117	1.088
120.550	0.117	1.079
120.553	0.117	1.070
120.569	0.117	1.064
120.582	0.116	1.060
120.577	0.118	1.055
120.589	0.116	1.051
120.582	0.118	1.045
120.590	0.119	1.043
120.605	0.118	1.040
120.592	0.120	1.036
120.608	0.118	1.035
120.624	0.119	1.033
120.574	0.119	1.031
120.601	0.118	1.029
120.642	0.119	1.028
120.724	0.120	1.026
120.717	0.121	1.023
120.703	0.121	1.021
120.584	0.123	1.019
120.593	0.121	1.018
120.605	0.121	1.015
120.591	0.122	1.013
120.596	0.122	1.010
120.595	0.121	1.008
120.597	0.121	1.005
120.641	0.123	1.006
120.652	0.121	1.008
120.659	0.122	1.008
120.708	0.122	1.013
120.747	0.122	1.014
120.718	0.122	1.014
120.616	0.122	1.014
120.608	0.120	1.013
120.613	0.120	1.010
120.652	0.121	1.010
120.655	0.123	1.010

Table C8—Experimental Pressure Drop – Flow rate Glycerin Temperature Average 141°F

T (°F)	Q (gal/min)	ΔP (psia)
141.219	0.722	5.379
141.280	0.719	5.439
141.345	0.720	5.460
141.428	0.720	5.474
141.509	0.718	5.481
141.626	0.721	5.485
141.644	0.720	5.488
141.643	0.722	5.489
141.676	0.719	5.488
141.669	0.719	5.488
141.688	0.722	5.486
141.705	0.720	5.485
141.715	0.720	5.484
141.738	0.721	5.484
141.736	0.721	5.484
141.760	0.720	5.484
141.769	0.722	5.484
141.782	0.717	5.484
141.801	0.718	5.485
141.832	0.722	5.485
141.839	0.722	5.485
141.836	0.721	5.485
141.854	0.723	5.485
141.857	0.721	5.485
141.860	0.723	5.485
141.865	0.722	5.485
141.900	0.720	5.484
141.908	0.720	5.481
141.912	0.719	5.479
141.943	0.723	5.476
141.939	0.715	5.475
141.948	0.713	5.476
141.935	0.711	5.470
141.913	0.709	5.460
141.948	0.709	5.456
141.956	0.710	5.451
141.970	0.712	5.446
141.998	0.710	5.443
141.993	0.707	5.441
142.015	0.709	5.440
142.006	0.710	5.440
142.008	0.712	5.441
142.022	0.711	5.443
142.061	0.711	5.444

T (°F)	Q (gal/min)	ΔP (psia)
142.013	0.643	4.789
141.996	0.646	4.783
142.002	0.644	4.791
142.025	0.648	4.798
142.044	0.646	4.801
142.053	0.646	4.806
142.061	0.646	4.808
142.065	0.646	4.811
142.066	0.648	4.813
142.068	0.647	4.813
142.089	0.657	4.811
142.116	0.659	4.826
142.111	0.659	4.845
142.139	0.657	4.866
142.164	0.659	4.873
141.889	0.480	3.234
141.704	0.474	3.320
141.538	0.476	3.368
141.417	0.477	3.389
141.237	0.472	3.401
141.125	0.476	3.408
141.043	0.476	3.415
141.025	0.473	3.418
141.030	0.476	3.419
141.026	0.472	3.420
141.070	0.474	3.420
141.085	0.479	3.418
141.112	0.473	3.421
141.108	0.474	3.423
141.054	0.477	3.426
141.079	0.475	3.429
141.076	0.477	3.429
140.856	0.327	2.164
140.681	0.329	2.255
140.480	0.328	2.288
140.342	0.322	2.298
140.208	0.321	2.295
140.020	0.327	2.290
139.874	0.318	2.296
139.723	0.318	2.296
139.624	0.316	2.298
139.513	0.318	2.294
139.382	0.318	2.295
139.238	0.318	2.299
139.118	0.318	2.299
139.010	0.317	2.299

T (°F)	Q (gal/min)	ΔP (psia)
138.914	0.319	2.300
138.818	0.317	2.301
138.743	0.321	2.301
138.696	0.320	2.303
141.023	0.968	7.478

Table C9—Experimental Pressure Drop – Flow rate Glycerin Temperature Average 82°F

T (°F)	Q (gal/min)	ΔP (psia)
83.650	0.542	9.221
83.389	0.542	9.248
83.180	0.540	9.291
83.058	0.541	9.284
82.950	0.535	9.164
82.908	0.528	9.185
82.883	0.537	9.208
82.876	0.533	9.236
82.900	0.532	9.198
82.926	0.533	9.208
82.967	0.534	9.251
82.988	0.530	9.234
83.049	0.540	9.235
83.035	0.533	9.164
83.075	0.532	9.195
83.090	0.522	8.910
82.911	0.462	7.733
83.003	0.478	7.924
83.031	0.482	8.211
82.825	0.442	7.439
82.609	0.431	7.648
82.619	0.387	6.480
82.621	0.404	6.878
82.744	0.420	7.014
83.045	0.425	7.118
82.823	0.377	6.444
82.734	0.379	6.323
82.760	0.383	6.424
82.805	0.380	6.473
82.820	0.381	6.496
82.851	0.388	6.523
82.865	0.380	6.493
82.910	0.381	6.531
82.955	0.402	6.548
82.603	0.303	4.928
82.517	0.300	4.983

T (°F)	Q (gal/min)	ΔP (psia)
82.432	0.291	4.794
82.399	0.289	4.773
82.465	0.306	5.055
82.510	0.301	5.061
82.569	0.302	5.065
82.616	0.304	5.080
82.631	0.305	5.064
82.658	0.306	5.070
82.716	0.306	5.081
82.714	0.302	5.069
82.736	0.308	5.088
82.737	0.304	5.079
82.033	0.215	3.413
81.846	0.212	3.416
81.768	0.212	3.526
81.765	0.214	3.565
81.739	0.213	3.579
81.696	0.210	3.548
81.776	0.213	3.604
81.511	0.185	3.275
81.659	0.202	3.443
81.545	0.201	3.570
81.778	0.210	3.671
81.412	0.154	2.409
81.181	0.156	2.560
81.221	0.160	2.684
81.156	0.158	2.668
81.107	0.161	2.666
81.148	0.160	2.678
81.177	0.159	2.729
81.194	0.159	2.844
81.266	0.161	2.878
81.278	0.159	2.830
81.264	0.161	2.803
81.269	0.157	2.734
81.207	0.160	2.750
81.259	0.160	2.769
81.464	0.162	2.775
81.528	0.161	2.773
81.536	0.162	2.770
80.294	0.101	1.475
79.628	0.100	1.500
79.454	0.099	1.515
79.391	0.097	1.506
79.344	0.097	1.499
79.295	0.097	1.504
79.328	0.097	1.495

Table C10—Experimental Pressure Drop – Flow rate Glycerin Temperature Average 101°F

T (°F)	Q (gal/min)	ΔP (psia)
100.599	0.746	9.774
100.592	0.746	9.776
100.591	0.746	9.783
100.591	0.745	9.780
100.591	0.745	9.779
100.594	0.747	9.780
100.593	0.747	9.780
100.602	0.745	9.783
100.600	0.745	9.780
100.590	0.747	9.786
100.597	0.745	9.785
100.604	0.747	9.790
100.607	0.746	9.788
100.617	0.749	9.798
100.617	0.745	9.794
99.682	0.684	8.951
99.367	0.684	9.028
99.334	0.683	9.053
99.338	0.683	9.071
99.361	0.683	9.079
99.395	0.680	9.085
99.415	0.685	9.081
99.459	0.683	9.079
99.515	0.685	9.091
99.568	0.684	9.090
99.612	0.687	9.100
99.679	0.686	9.091
99.731	0.686	9.088
99.818	0.684	9.063
99.872	0.684	9.053
99.954	0.682	9.038
100.031	0.685	9.034
100.130	0.683	9.026
100.189	0.685	9.035
100.300	0.687	9.026
100.386	0.689	9.026
100.494	0.686	9.023
100.569	0.688	9.021
100.662	0.686	9.018
100.738	0.689	9.006
100.813	0.690	9.005
100.781	0.652	8.481

T (°F)	Q (gal/min)	ΔP (psia)
100.774	0.651	8.449
100.802	0.651	8.454
100.853	0.654	8.464
100.904	0.653	8.471
100.942	0.654	8.475
100.978	0.652	8.471
101.032	0.651	8.458
101.095	0.653	8.454
101.160	0.654	8.459
101.162	0.653	8.453
101.208	0.656	8.456
101.291	0.653	8.454
101.331	0.656	8.455
101.360	0.653	8.450
101.282	0.588	7.458
101.278	0.586	7.521
101.258	0.586	7.550
101.235	0.585	7.570
101.291	0.588	7.583
101.303	0.591	7.589
101.343	0.592	7.581
101.360	0.587	7.576
101.424	0.589	7.581
101.451	0.591	7.585
101.500	0.589	7.589
101.529	0.596	7.591
101.590	0.591	7.585
101.623	0.589	7.576
101.694	0.594	7.578
101.729	0.591	7.576
101.752	0.591	7.570
101.779	0.541	6.785
101.751	0.530	6.681
101.782	0.533	6.705
101.827	0.531	6.739
101.881	0.533	6.748
101.912	0.533	6.765
101.930	0.532	6.766
101.966	0.530	6.773
101.992	0.539	6.765
102.048	0.531	6.768
102.114	0.530	6.770
102.146	0.530	6.766
102.174	0.536	6.761
102.213	0.533	6.766
102.251	0.529	6.763

T (°F)	Q (gal/min)	ΔP (psia)
102.294	0.533	6.764
102.352	0.532	6.763
102.397	0.535	6.756
102.429	0.531	6.755
102.430	0.532	6.754
102.440	0.535	6.755
102.482	0.536	6.753
102.487	0.532	6.756
102.353	0.430	5.171
102.366	0.452	5.544
102.157	0.410	5.026
102.128	0.410	5.103
102.129	0.411	5.076
102.149	0.431	5.291
102.207	0.421	5.240
102.232	0.424	5.266
102.238	0.424	5.216
102.274	0.418	5.234
102.234	0.417	5.108
102.262	0.425	5.279
102.260	0.424	5.263
102.244	0.421	5.233
102.266	0.413	5.115
102.299	0.423	5.218
102.299	0.420	5.226
102.331	0.427	5.275
102.316	0.408	5.048
102.291	0.414	5.126
102.274	0.424	5.219
102.241	0.401	4.993
102.232	0.410	5.058
102.211	0.388	4.850
102.202	0.422	5.199
102.101	0.367	4.430
102.057	0.380	4.666
102.040	0.377	4.658
101.987	0.376	4.643
101.943	0.350	4.310
101.847	0.349	4.271
101.930	0.362	4.466
101.981	0.377	4.678
102.020	0.377	4.684
101.997	0.374	4.684
101.850	0.317	3.749
101.624	0.314	3.816
101.556	0.312	3.821

T (°F)	Q (gal/min)	ΔP (psia)
101.486	0.316	3.916
101.457	0.322	4.008
101.459	0.325	4.058
101.343	0.304	3.814
101.375	0.318	3.996
101.348	0.320	4.003
101.327	0.322	4.040
101.301	0.320	4.046
101.281	0.320	4.059
101.323	0.321	4.033
101.288	0.331	4.098
101.016	0.275	3.400
101.140	0.281	3.451
101.173	0.278	3.466
101.123	0.275	3.465
101.113	0.272	3.455
101.082	0.277	3.489
101.059	0.274	3.490
100.798	0.223	2.764
100.669	0.224	2.740
100.616	0.223	2.788
100.548	0.223	2.800
100.516	0.225	2.825
100.507	0.229	2.829
100.471	0.223	2.834
100.466	0.224	2.834
100.473	0.224	2.928
100.648	0.227	2.924
100.659	0.225	2.910
100.628	0.225	2.901
100.593	0.224	2.894
100.598	0.227	2.903
100.575	0.221	2.871
100.577	0.227	2.884
100.586	0.227	2.898
100.540	0.224	2.883
100.420	0.224	2.899
100.142	0.165	1.964
99.767	0.164	2.094
99.613	0.163	2.088
99.507	0.164	2.085
99.466	0.166	2.080
99.407	0.166	2.075
99.367	0.166	2.071
99.335	0.166	2.064
99.329	0.164	2.076

T (°F)	Q (gal/min)	ΔP (psia)
99.351	0.166	2.068
99.314	0.166	2.045
98.625	0.103	1.196
98.313	0.102	1.195
98.151	0.103	1.229
98.070	0.103	1.258
97.921	0.105	1.279
97.997	0.104	1.276
97.954	0.103	1.269
97.913	0.100	1.253
97.921	0.104	1.245
97.904	0.102	1.239
97.981	0.101	1.234
97.967	0.100	1.230
97.996	0.100	1.225
98.046	0.100	1.219

Motor Oil 10W30

Table C11—Experimental Pressure Drop – Flow rate Motor Oil 10W30 Temperature Average 150°F

T (°F)	Q (gal/min)	ΔP (psia)
150.5	0.040	4.094
150.3	0.072	6.696
150	0.106	10.336

Oil A

Table C12— Experimental Pressure Drop – Flow rate Oil A Temperature Average 100°F

Q (gal/min)	ΔP (psia)
0.096	9.935
0.075	8.459
0.094	9.995
0.100	9.973
0.102	9.944
0.079	7.996
0.057	6.240
0.058	6.254
0.058	6.254
0.058	6.265
0.021	2.634
0.043	4.723
0.044	4.693
0.044	4.699
0.045	4.699
0.045	4.709
0.045	4.706
0.043	4.671
0.043	4.686
0.009	1.875
0.042	3.920
0.018	2.085
0.019	2.060
0.019	2.033
0.019	2.029
0.102	10.256

Table C13 —Experimental Pressure Drop – Flow rate Oil A Temperature Average 110°F

Q (gal/min)	ΔP (psia)
0.126	10.109
0.125	10.096
0.129	10.116
0.096	8.171
0.111	8.731
0.098	8.115
0.087	7.745

Q (gal/min)	ΔP (psia)
0.085	7.509
0.086	7.584
0.086	7.598
0.086	7.605
0.050	4.569
0.050	4.478
0.049	4.505
0.052	4.524
0.027	2.915
0.027	2.519
0.027	2.511
0.027	2.511
0.027	2.509
0.026	2.499
0.028	2.485

Table C14—Experimental Pressure Drop – Flow rate Oil A Temperature Average 120°F

Q (gal/min)	ΔP (psia)
0.145	10.009
0.146	10.011
0.147	10.016
0.147	10.018
0.148	10.024
0.147	10.021
0.148	10.018
0.147	10.024
0.149	10.026
0.150	10.019
0.150	10.023
0.150	10.023
0.151	10.028
0.152	10.020
0.152	10.028
0.127	8.885
0.113	8.128
0.098	7.245
0.097	7.261
0.096	7.274
0.095	7.261
0.097	7.251
0.098	7.255
0.056	4.463
0.057	4.328

Q (gal/min)	ΔP (psia)
0.057	4.331
0.057	4.331
0.058	4.330
0.059	4.331
0.057	4.340
0.058	4.346
0.059	4.345
0.060	4.344
0.059	4.336
0.059	4.336
0.060	4.329
0.060	4.318
0.020	1.551
0.021	1.615
0.020	1.573
0.021	1.546
0.019	1.526
0.019	1.496
0.151	10.039

Table C15—Experimental Pressure Drop – Flow rate Oil A Temperature Average 130°F

Q (gal/min)	ΔP (psia)
0.165	9.941
0.167	9.938
0.170	9.986
0.176	10.211
0.181	10.503
0.181	10.535
0.182	10.553
0.182	10.543
0.146	8.903
0.153	9.628
0.154	9.638
0.154	9.630
0.155	9.636
0.156	9.645
0.155	9.639
0.137	8.670
0.101	6.490
0.106	6.580
0.106	6.591
0.106	6.584
0.107	6.578

Q (gal/min)	ΔP (psia)
0.107	6.579
0.061	3.820
0.061	3.865
0.060	3.865
0.061	3.841
0.060	3.834
0.061	3.834
0.062	3.835
0.060	3.825
0.061	3.803
0.060	3.771
0.060	3.781
0.017	1.308
0.016	1.205
0.024	1.616
0.023	1.573
0.021	1.553
0.023	1.530
0.022	1.511
0.020	1.485
0.020	1.428
0.020	1.389
0.019	1.383

Table C16—Experimental Pressure Drop – Flow rate Oil A Temperature Average 140°F

Q (gal/min)	ΔP (psia)
0.215	10.366
0.215	10.366
0.214	10.356
0.212	10.379
0.211	10.378
0.212	10.375
0.196	9.963
0.192	9.991
0.192	10.013
0.192	10.025
0.189	10.015
0.188	10.023
0.189	10.011
0.190	10.006
0.191	9.999
0.190	9.998
0.151	7.838

Q (gal/min)	ΔP (psia)
0.154	7.806
0.153	7.774
0.154	7.764
0.156	7.784
0.156	7.769
0.154	7.774
0.154	7.759
0.156	7.763
0.154	7.770
0.157	7.769
0.154	7.771
0.154	7.770
0.155	7.774
0.155	7.775
0.155	7.776
0.101	5.240
0.101	5.266
0.103	5.256
0.101	5.204
0.101	5.193
0.102	5.173
0.102	5.141
0.060	2.989
0.048	2.806
0.049	2.680
0.048	2.615
0.048	2.585
0.044	2.453
0.042	2.355
0.038	2.204
0.033	1.973

Table C17—Experimental Pressure Drop – Flow rate Oil A Temperature Average 150°F

Q (gal/min)	ΔP (psia)
0.241	10.219
0.242	10.235
0.240	10.233
0.240	10.251
0.239	10.255
0.238	10.259
0.234	10.231
0.235	10.234
0.235	10.249

0.236	10.270
0.235	10.288
0.235	10.279
0.235	10.288
0.235	10.276
0.235	10.269
0.234	10.266
0.234	10.261
0.236	10.271
0.236	10.273
0.237	10.288
0.235	10.286
0.195	8.801
0.201	9.381
0.198	9.365
0.198	9.361
0.198	9.364
0.199	9.361
0.197	9.360
0.198	9.349
0.198	9.346
0.198	9.344
0.186	8.986
0.180	8.579
0.184	8.743
0.125	6.233
0.149	7.206
0.149	7.143
0.148	7.106
0.149	7.106
0.148	7.100
0.149	7.095
0.149	7.099
0.149	7.103
0.149	7.094
0.148	7.085
0.116	5.943
0.104	5.019
0.104	5.024
0.104	5.016
0.104	5.009
0.103	5.010
0.104	5.013
0.103	4.999
0.038	2.341
0.036	1.976
0.035	1.836

0.048	2.243
0.047	2.499
0.047	2.404
0.045	2.364
0.045	2.328
0.045	2.298
0.044	2.229
0.042	2.174

Table C18—Experimental Pressure Drop – Flow rate Oil A Temperature Average 156°F

Q (gal/min)	ΔP (psia)
0.249	10.223
0.248	10.215
0.249	10.201
0.249	10.218
0.250	10.225
0.250	10.233
0.249	10.219
0.250	10.216
0.251	10.229
0.252	10.231
0.252	10.231
0.252	10.208
0.205	8.861
0.199	8.771
0.197	8.761
0.197	8.758
0.197	8.755
0.198	8.769
0.199	8.769
0.198	8.753
0.199	8.745
0.200	8.765
0.201	8.760
0.200	8.751
0.201	8.769
0.202	8.756
0.201	8.690
0.148	6.264
0.150	6.404
0.148	6.453
0.148	6.458
0.148	6.439
0.149	6.433

0.149	6.424
0.149	6.418
0.149	6.416
0.149	6.393
0.149	6.385
0.150	6.400
0.150	6.398
0.094	4.489
0.102	4.421
0.100	4.364
0.100	4.348
0.100	4.338
0.095	4.131
0.094	4.116
0.096	4.145
0.095	4.139
0.095	4.136
0.091	3.963
0.049	2.498
0.048	2.221
0.050	2.251
0.050	2.244
0.048	2.200
0.047	2.115
0.045	2.094
0.044	2.009
0.043	1.960
0.041	1.876
0.248	10.161

Dilution Tests Oil A + Oil B

Test 1

Table C19—Experimental Pressure Drop – Flow rate Mixture Test 1 Temperature Average 99°F

Q (gal/min)	ΔP (psia)
0.098	9.538
0.099	9.531
0.100	9.534
0.098	9.534
0.100	9.524
0.099	9.525
0.101	9.525

Q (gal/min)	ΔP (psia)
0.101	9.530
0.093	9.073
0.082	7.920
0.082	7.931
0.080	7.938
0.081	7.941
0.082	7.935
0.082	7.946
0.082	7.950
0.082	7.945
0.044	4.278
0.053	5.135
0.052	5.174
0.053	5.189
0.054	5.203
0.053	5.211
0.053	5.213
0.053	5.216
0.054	5.220
0.054	5.226
0.054	5.235
0.054	5.240
0.054	5.250
0.011	1.431
0.011	1.421
0.012	1.421
0.011	1.374
0.011	1.336
0.012	1.304
0.058	5.718
0.059	5.716
0.060	5.721

Test 2

Table C20—Experimental Pressure Drop – Flow rate Mixture Test 2 Temperature Average 98°F

Q (gal/min)	ΔP (psia)
0.01634	2.10250
0.01690	2.13375
0.01727	2.10000
0.01803	2.06875
0.01803	2.05500
0.01821	2.07250

Q (gal/min)	ΔP (psia)
0.01859	2.13000
0.01896	2.09875
0.01934	2.14125
0.01972	2.05875
0.05107	5.38750
0.05239	5.37625
0.05258	5.38375
0.05333	5.34500
0.07192	6.87500
0.07210	6.87750
0.07229	6.88875
0.07248	6.88125
0.07285	6.87125
0.07285	6.87750
0.07398	6.92000
0.08281	8.18500
0.08356	8.19250
0.08375	8.19500
0.08375	8.18625
0.08412	8.04250
0.08506	8.19750
0.08525	8.17750
0.08544	8.19750
0.08600	8.19625
0.08637	8.19375
0.08769	8.14125
0.08806	8.56125
0.08938	8.31750
0.08957	8.32750
0.09501	8.97250

Table C21—Experimental Pressure Drop – Flow rate Mixture Test 3 Temperature Average 99°F

Q (gal/min)	ΔP (psia)
0.115	9.828
0.115	9.829
0.115	9.830
0.115	9.833
0.116	9.818
0.115	9.814
0.116	9.821
0.115	9.820
0.116	9.825
0.116	9.818

Q (gal/min)	ΔP (psia)
0.117	9.813
0.117	9.820
0.116	9.830
0.115	9.840
0.115	9.833
0.116	9.834
0.117	9.820
0.116	9.831
0.117	9.848
0.117	9.873
0.117	9.863
0.116	9.843
0.118	9.835
0.117	9.850
0.093	7.958
0.101	8.405
0.106	8.639
0.106	8.630
0.106	8.634
0.106	8.639
0.106	8.631
0.104	8.634
0.103	8.633
0.103	8.625
0.106	8.626
0.103	8.631
0.105	8.639
0.105	8.638
0.106	8.640
0.106	8.655
0.104	8.648
0.104	8.659
0.104	8.658
0.104	8.644
0.105	8.661
0.104	8.645
0.099	8.211
0.085	7.150
0.079	6.804
0.079	6.819
0.080	6.833
0.080	6.835
0.079	6.831
0.080	6.831
0.080	6.828
0.080	6.829

Q (gal/min)	ΔP (psia)
0.080	6.831
0.079	6.820
0.079	6.825
0.080	6.820
0.080	6.823
0.081	6.824
0.080	6.828
0.081	6.828
0.081	6.829
0.080	6.819
0.081	6.828
0.081	6.828
0.080	6.816
0.052	4.611
0.050	4.633
0.051	4.655
0.052	4.668

Table C22—Experimental Pressure Drop – Flow rate Mixture Test 3 Temperature Average 109°F

Q (gal/min)	ΔP (psia)
0.124	8.414
0.123	8.483
0.122	8.476
0.123	8.478
0.123	8.481
0.124	8.473
0.124	8.470
0.124	8.468
0.124	8.479
0.124	8.478
0.125	8.474
0.124	8.483
0.125	8.470
0.125	8.466
0.125	8.465
0.126	8.468
0.126	8.499
0.125	8.490
0.127	8.569
0.129	8.579
0.122	8.233
0.121	8.211
0.122	8.114

Q (gal/min)	ΔP (psia)
0.115	7.919
0.109	7.371
0.101	6.933
0.102	6.933
0.101	6.929
0.102	6.935
0.103	6.940
0.102	6.934
0.102	6.935
0.102	6.949
0.103	6.948
0.101	6.940
0.102	6.945
0.102	6.948
0.101	6.946
0.102	6.949
0.102	6.953
0.101	6.955
0.101	6.968
0.100	6.961
0.101	6.970
0.101	6.969
0.101	6.975
0.102	6.983
0.101	6.981
0.100	6.979
0.103	6.983
0.102	6.993
0.103	6.988
0.101	6.993
0.102	6.975
0.103	6.984
0.101	6.989
0.102	7.001
0.102	7.000
0.101	7.005
0.100	7.006
0.102	7.000
0.101	7.010
0.100	7.008
0.100	7.013
0.101	7.019
0.080	5.728
0.077	5.729
0.080	5.724
0.080	5.726

Q (gal/min)	ΔP (psia)
0.080	5.719
0.081	5.718
0.079	5.719
0.057	4.093
0.054	4.081
0.054	4.089
0.054	4.089
0.052	4.098

Table C23—Experimental Pressure Drop – Flow rate Mixture Test 3 Temperature Average 118°F

Q (gal/min)	ΔP (psia)
0.191	10.476
0.189	10.466
0.190	10.470
0.188	10.466
0.189	10.486
0.189	10.495
0.188	10.488
0.148	8.933
0.149	8.946
0.149	8.948
0.149	8.959
0.150	8.948
0.149	8.939
0.151	8.941
0.150	8.943
0.150	8.945
0.152	8.941
0.149	8.874
0.109	6.525
0.110	6.610
0.110	6.614
0.111	6.606
0.111	6.609
0.112	6.600
0.112	6.604
0.111	6.605
0.111	6.615
0.111	6.616
0.110	6.568
0.109	6.568
0.110	6.571
0.110	6.578
0.110	6.575

0.077	4.754
0.077	4.763
0.076	4.776
0.076	4.734
0.076	4.741
0.077	4.748
0.075	4.721
0.075	4.738

Table C24—Experimental Pressure Drop – Flow rate Mixture Test 3 Temperature Average 127°F

Q (gal/min)	ΔP (psia)
0.214	10.384
0.213	10.379
0.213	10.369
0.213	10.381
0.213	10.383
0.212	10.373
0.213	10.383
0.213	10.388
0.213	10.380
0.215	10.390
0.216	10.380
0.178	9.026
0.172	9.020
0.170	8.968
0.172	9.053
0.171	9.045
0.173	9.014
0.174	9.025
0.175	9.026
0.175	9.030
0.176	9.033
0.178	9.074
0.176	9.049
0.177	9.053
0.178	9.023
0.177	9.030
0.177	9.041
0.177	9.020
0.179	9.074
0.178	9.035
0.177	9.005
0.177	8.999
0.178	8.995

0.179	9.034
0.177	9.044
0.177	9.063
0.177	9.005
0.176	9.025
0.171	8.800
0.148	7.635
0.149	7.736
0.149	7.740
0.148	7.725
0.148	7.708
0.147	7.696
0.149	7.693
0.148	7.694
0.149	7.701
0.149	7.710
0.150	7.715
0.150	7.715
0.150	7.709
0.151	7.704
0.151	7.713
0.152	7.719
0.143	7.566
0.110	5.706
0.110	5.688
0.110	5.686
0.110	5.675
0.110	5.664
0.110	5.660
0.111	5.729
0.112	5.726
0.092	4.768
0.089	4.616
0.088	4.606
0.089	4.581
0.090	4.579
0.088	4.571
0.089	4.569
0.090	4.571
0.089	4.565
0.088	4.561
0.088	4.531
0.086	4.496
0.085	4.479
0.085	4.475
0.085	4.473
0.085	4.470
0.085	4.454

0.079	4.139
0.081	4.188
0.080	4.184
0.079	4.171

Table C25—Experimental Pressure Drop – Flow rate Mixture Test 3 Temperature Average 138°F

Q (gal/min)	ΔP (psia)
0.243	10.314
0.242	10.311
0.245	10.319
0.244	10.320
0.244	10.305
0.242	10.311
0.244	10.305
0.244	10.318
0.245	10.320
0.245	10.313
0.245	10.294
0.244	10.278
0.245	10.264
0.245	10.280
0.246	10.264
0.246	10.261
0.247	10.288
0.246	10.293
0.232	9.883
0.211	9.385
0.203	9.415
0.205	9.373
0.207	9.365
0.207	9.371
0.207	9.360
0.206	9.348
0.207	9.361
0.209	9.368
0.209	9.366
0.210	9.366
0.211	9.364
0.210	9.354
0.212	9.360
0.197	8.959
0.190	8.490
0.190	8.423
0.189	8.408

0.190	8.404
0.190	8.401
0.189	8.408
0.191	8.414
0.189	8.421
0.191	8.426
0.191	8.413
0.191	8.411
0.190	8.394
0.160	7.065
0.157	6.990
0.158	7.001
0.158	6.993
0.158	6.995
0.159	6.991
0.158	6.986
0.158	6.985
0.159	6.975
0.159	6.965
0.159	6.970
0.160	6.959
0.160	6.969
0.127	5.200
0.128	5.656
0.128	5.649
0.128	5.645
0.129	5.635
0.129	5.648
0.128	5.626
0.129	5.613
0.128	5.611
0.128	5.606
0.128	5.606
0.128	5.605
0.127	5.601
0.128	5.595
0.070	2.896
0.097	4.301
0.097	4.304
0.099	4.370
0.099	4.385
0.099	4.386
0.100	4.391
0.099	4.383
0.099	4.355
0.098	4.314
0.100	4.350
0.099	4.351

0.099	4.345
0.099	4.330
0.099	4.328
0.097	4.323
0.098	4.311
0.098	4.309
0.098	4.290
0.098	4.288
0.098	4.253
0.097	4.234
0.097	4.228
0.098	4.224
0.097	4.224
0.098	4.226
0.096	4.196
0.098	4.194
0.097	4.186
0.098	4.183
0.097	4.163
0.096	4.173
0.097	4.160
0.097	4.179
0.094	4.034
0.094	4.018
0.072	3.113
0.070	3.084
0.071	3.084
0.071	3.049
0.069	3.039
0.070	3.036
0.069	3.023
0.069	3.026
0.069	2.991
0.069	2.986
0.068	2.965
0.066	2.904
0.064	2.839
0.065	2.835
0.065	2.829
0.063	2.771
0.061	2.710
0.062	2.703
0.062	2.690
0.060	2.663
0.061	2.668
0.061	2.668
0.040	1.909

0.038	1.731
0.037	1.719
0.037	1.683
0.037	1.673
0.037	1.650
0.034	1.613
0.032	1.564
0.033	1.544
0.030	1.484
0.031	1.453
0.018	1.021
0.020	1.006
0.019	0.981
0.022	0.984
0.020	0.956
0.020	0.974
0.018	0.964
0.020	0.954
0.020	0.916
0.016	0.834
0.014	0.744
0.013	0.681
0.014	0.655
0.014	0.640
0.013	0.633
0.014	0.630
0.010	0.608
0.012	0.570
0.008	0.538
0.010	0.508
0.009	0.494
0.007	0.408

Test 4

Table C26—Experimental Pressure Drop – Flow rate Mixture Test 4 Temperature Average 98°F

Q (gal/min)	ΔP (psia)
0.100	8.348
0.101	8.370
0.101	8.349
0.102	8.345
0.103	8.343
0.102	8.315
0.103	8.315
0.102	8.306
0.104	8.316
0.103	8.321
0.104	8.323
0.099	7.915
0.079	6.481
0.081	6.493
0.080	6.496
0.080	6.500
0.082	6.503
0.080	6.506
0.082	6.509
0.081	6.514
0.059	4.796
0.059	4.826
0.062	4.888
0.062	4.891
0.063	4.890
0.062	4.906
0.063	4.903
0.062	4.913
0.063	4.921
0.063	4.923
0.063	4.925
0.063	4.933
0.063	4.935
0.062	4.941
0.041	3.481
0.043	3.534
0.041	3.549
0.041	3.560
0.041	3.563
0.041	3.555
0.041	3.555

Q (gal/min)	ΔP (psia)
0.041	3.551
0.043	3.546
0.040	3.500
0.041	3.501
0.042	3.504
0.043	3.495
0.042	3.493
0.042	3.491
0.041	3.501
0.041	3.501
0.042	3.504
0.041	3.489
0.042	3.476
0.042	3.464
0.017	1.624

Table C27—Experimental Pressure Drop – Flow rate Mixture Test 4 Temperature Average =109°F

Q (gal/min)	ΔP (psia)
0.163	9.731
0.162	9.733
0.163	9.735
0.163	9.728
0.164	9.730
0.164	9.739
0.165	9.740
0.165	9.733
0.165	9.739
0.165	9.734
0.165	9.724
0.165	9.723
0.164	9.721
0.165	9.731
0.167	9.741
0.166	9.734
0.167	9.736
0.166	9.713
0.167	9.714
0.165	9.724
0.165	9.739
0.165	9.731
0.166	9.749
0.165	9.751
0.165	9.744

Q (gal/min)	ΔP (psia)
0.165	9.754
0.165	9.739
0.165	9.741
0.164	9.744
0.164	9.738
0.164	9.735
0.148	9.131
0.135	8.646
0.129	8.676
0.131	8.695
0.132	8.679
0.132	8.681
0.133	8.678
0.133	8.691
0.133	8.698
0.134	8.693
0.134	8.683
0.135	8.681
0.135	8.695
0.136	8.691
0.136	8.695
0.135	8.689
0.135	8.679
0.135	8.679
0.136	8.690
0.137	8.696
0.137	8.711
0.135	8.709
0.130	8.483
0.127	8.126
0.124	7.989
0.122	7.878
0.120	7.683
0.118	7.704
0.119	7.691
0.119	7.706
0.120	7.696
0.120	7.699
0.119	7.705
0.120	7.701
0.120	7.698
0.121	7.696
0.120	7.696
0.120	7.688
0.122	7.693
0.122	7.698

Q (gal/min)	ΔP (psia)
0.122	7.695
0.124	7.688
0.100	6.324
0.099	6.283
0.100	6.294
0.099	6.295
0.100	6.296
0.100	6.303
0.100	6.300
0.099	6.305
0.099	6.309
0.099	6.315
0.100	6.321
0.101	6.320
0.102	6.331
0.099	6.325
0.101	6.325
0.100	6.326
0.100	6.326
0.100	6.329
0.100	6.339
0.099	6.335
0.099	6.343
0.100	6.350
0.100	6.353
0.099	6.361
0.099	6.360
0.098	6.363
0.099	6.373
0.099	6.381
0.098	6.378
0.098	6.376
0.100	6.381
0.099	6.381
0.097	6.386
0.100	6.388
0.100	6.406
0.100	6.399
0.099	6.415
0.098	6.416
0.079	5.279
0.078	5.226
0.078	5.234
0.079	5.250
0.077	5.241
0.080	5.256

Q (gal/min)	ΔP (psia)
0.080	5.264
0.080	5.259
0.078	5.261
0.079	5.269
0.078	5.265
0.079	5.264
0.079	5.260
0.079	5.255
0.081	5.240
0.078	5.243
0.080	5.216
0.080	5.218
0.061	4.168
0.060	4.059
0.060	4.059
0.061	4.059
0.061	4.056
0.060	4.060
0.061	4.058
0.060	4.063
0.060	4.064
0.060	4.069
0.060	4.070
0.060	4.078
0.061	4.084
0.060	4.093
0.061	4.095
0.062	4.098
0.061	4.089
0.061	4.093
0.061	4.094
0.059	4.098
0.062	4.106
0.061	4.110

Table C28—Experimental Pressure Drop – Flow rate Mixture Test 4 Temperature Average 112°F

Q (gal/min)	ΔP (psia)
0.198	10.341
0.198	10.334
0.199	10.350
0.198	10.339
0.199	10.314
0.201	10.331
0.199	10.346

Q (gal/min)	ΔP (psia)
0.201	10.321
0.200	10.334
0.201	10.330
0.179	9.458
0.174	9.585
0.172	9.595
0.172	9.600
0.172	9.606
0.172	9.604
0.173	9.598
0.158	8.799
0.158	8.801
0.157	8.774
0.144	7.911
0.143	7.901
0.144	7.909
0.143	7.909
0.143	7.898
0.123	7.216
0.098	5.573
0.100	5.571
0.096	5.448
0.097	5.471
0.097	5.486
0.097	5.493
0.099	5.593
0.099	5.579
0.099	5.564
0.099	5.554
0.100	5.558
0.100	5.556
0.099	5.550
0.094	5.419
0.079	4.459
0.080	4.451
0.080	4.450
0.080	4.449
0.080	4.453
0.079	4.454
0.080	4.458
0.079	4.460
0.080	4.456
0.080	4.459
0.078	4.328
0.077	4.328
0.075	4.338

Q (gal/min)	ΔP (psia)
0.077	4.338
0.077	4.340
0.076	4.349
0.040	2.418
0.038	2.430

Table C29—Experimental Pressure Drop – Flow rate Mixture Test 4 Temperature Average 130°F

Q (gal/min)	ΔP (psia)
0.219	10.236
0.221	10.238
0.221	10.241
0.221	10.240
0.223	10.241
0.222	10.223
0.183	8.674
0.178	8.696
0.174	8.718
0.174	8.718
0.176	8.725
0.176	8.700
0.177	8.704
0.177	8.686
0.177	8.686
0.177	8.689
0.122	5.991
0.121	5.991
0.122	5.979
0.122	5.963
0.122	5.969
0.123	5.973
0.123	5.961
0.123	5.944
0.081	4.063
0.081	3.985
0.082	3.976
0.082	3.979
0.082	3.970
0.081	3.899
0.044	2.231
0.037	1.908
0.036	1.888
0.036	1.875
0.037	1.869

Q (gal/min)	ΔP (psia)
0.038	1.865
0.175	8.183

Table C30—Experimental Pressure Drop – Flow rate Mixture Test 4 Temperature Average 137°F

Q (gal/min)	ΔP (psia)
0.245	10.111
0.239	10.163
0.247	10.234
0.249	10.279
0.250	10.275
0.228	9.806
0.204	8.789
0.199	8.754
0.199	8.741
0.199	8.740
0.200	8.746
0.200	8.745
0.201	8.736
0.151	6.560
0.152	6.566
0.152	6.561
0.152	6.558
0.100	4.496
0.099	4.341
0.101	4.341
0.099	4.336
0.099	4.335
0.045	2.146
0.045	2.033
0.044	2.025
0.045	2.019
0.045	2.015
0.045	2.008
0.194	7.948

Test 5

Table C31—Experimental Pressure Drop – Flow rate Mixture Test 5 Temperature Average 99°F

Q (gal/min)	ΔP (psia)
0.158	9.643
0.158	9.646
0.157	9.645
0.158	9.649
0.158	9.656
0.158	9.661
0.157	9.666
0.157	9.659
0.157	9.666
0.156	9.676
0.156	9.673
0.156	9.668
0.155	9.669
0.133	8.620
0.124	8.250
0.123	8.250
0.124	8.250
0.124	8.249
0.124	8.249
0.126	8.236
0.125	8.214
0.126	8.220
0.126	8.221
0.123	8.050
0.123	8.060
0.125	8.078
0.115	7.540
0.102	6.584
0.102	6.604
0.100	6.624
0.101	6.620
0.100	6.626
0.101	6.631
0.100	6.635
0.102	6.636
0.101	6.641
0.101	6.640
0.101	6.638
0.101	6.634
0.102	6.639
0.102	6.640
0.101	6.640

Q (gal/min)	ΔP (psia)
0.102	6.638
0.103	6.650
0.101	6.656
0.102	6.664
0.103	6.674
0.101	6.668
0.100	6.668
0.101	6.665
0.101	6.661
0.102	6.664
0.102	6.670
0.101	6.671
0.103	6.685
0.102	6.686
0.101	6.699
0.103	6.693
0.103	6.700
0.102	6.708
0.102	6.714
0.101	6.708
0.102	6.713
0.104	6.713
0.103	6.714
0.101	6.714
0.101	6.706
0.102	6.711
0.101	6.714
0.101	6.709
0.102	6.718
0.101	6.725
0.102	6.724
0.102	6.728
0.102	6.735
0.101	6.723
0.100	6.728
0.078	5.309
0.078	5.319
0.079	5.321
0.080	5.313
0.078	5.309
0.078	5.305
0.078	5.254
0.078	5.260
0.078	5.296
0.079	5.294
0.079	5.294

Q (gal/min)	ΔP (psia)
0.078	5.294
0.078	5.298
0.079	5.298
0.079	5.303
0.079	5.301
0.080	5.305
0.080	5.310
0.079	5.314
0.078	5.290
0.079	5.328
0.078	5.330
0.079	5.329
0.079	5.343
0.078	5.318
0.078	5.315
0.064	4.650
0.054	3.870
0.054	3.896
0.053	3.914
0.053	3.923
0.054	3.880
0.052	3.868
0.054	3.861
0.052	3.851
0.053	3.840
0.053	3.830
0.026	2.129
0.025	2.073
0.025	2.075
0.024	2.080
0.026	2.065
0.025	2.063
0.023	2.055
0.025	2.035
0.022	2.003
0.025	1.988
0.022	1.963
0.023	1.974
0.024	1.960
0.022	1.956
0.025	1.940
0.023	1.920
0.023	1.925
0.024	1.921

Table C32. —Experimental Pressure Drop – Flow rate Mixture Test 5 Temperature Average =110°F

Q (gal/min)	ΔP (psia)
0.161	9.608
0.162	9.595
0.164	9.596
0.164	9.598
0.164	9.595
0.181	10.205
0.181	10.211
0.183	10.211
0.181	10.205
0.182	10.200
0.182	10.205
0.183	10.195
0.181	10.196
0.182	10.176
0.182	10.154
0.182	10.143
0.184	10.155
0.157	8.908
0.118	7.115
0.118	7.113
0.119	7.114
0.120	7.110
0.119	7.109
0.120	7.109
0.121	7.115
0.121	7.111
0.121	7.110
0.121	7.134
0.121	7.125
0.122	7.130
0.122	7.129
0.124	7.136
0.123	7.146
0.123	7.164
0.123	7.163
0.124	7.164
0.124	7.154
0.123	7.154
0.123	7.158
0.100	5.819

Q (gal/min)	ΔP (psia)
0.100	5.819
0.100	5.824
0.099	5.825
0.101	5.831
0.100	5.828
0.100	5.825
0.077	4.546
0.077	4.554
0.078	4.558
0.078	4.563
0.078	4.566
0.079	4.564
0.076	4.519
0.077	4.495
0.077	4.504
0.077	4.500
0.052	3.278
0.052	3.169
0.052	3.169
0.052	3.176
0.052	3.175
0.052	3.180
0.052	3.181
0.053	3.175
0.034	2.216
0.034	2.089
0.033	2.080
0.032	2.073
0.032	2.074
0.033	2.070
0.033	2.066
0.032	2.061
0.033	2.059
0.031	2.035
0.019	1.239
0.019	1.223
0.006	0.481

Table C33—Experimental Pressure Drop – Flow rate Mixture Test 5 Temperature Average 120°F

Q (gal/min)	ΔP (psia)
0.183	9.045
0.184	9.036

Q (gal/min)	ΔP (psia)
0.185	9.050
0.184	9.033
0.186	9.051
0.186	9.046
0.186	9.041
0.186	9.045
0.189	9.055
0.188	9.055
0.188	9.044
0.188	9.039
0.187	9.025
0.187	9.018
0.188	9.031
0.188	9.029
0.189	9.024
0.189	9.034
0.190	9.040
0.190	9.034
0.191	9.041
0.190	9.044
0.189	9.048
0.190	9.033
0.191	9.048
0.190	9.051
0.189	9.043
0.191	9.038
0.190	9.038
0.191	9.038
0.192	9.041
0.189	9.036
0.190	9.035
0.191	9.018
0.190	9.006
0.190	9.014
0.191	9.026
0.192	9.013
0.192	9.024
0.192	9.029
0.191	9.021
0.190	9.019
0.191	9.019
0.190	9.020
0.191	9.025
0.191	9.025
0.189	9.035

Q (gal/min)	ΔP (psia)
0.190	9.046
0.191	9.036
0.191	9.031
0.183	8.645
0.181	8.629
0.180	8.606
0.163	7.804
0.161	7.694
0.160	7.695
0.162	7.695
0.162	7.708
0.161	7.705
0.160	7.701
0.161	7.701
0.162	7.711
0.161	7.708
0.163	7.706
0.161	7.710
0.161	7.701
0.162	7.709
0.161	7.708
0.160	7.708
0.162	7.718
0.161	7.706
0.162	7.718
0.161	7.706
0.162	7.708
0.161	7.704
0.163	7.703
0.161	7.699
0.161	7.708
0.164	7.704
0.163	7.700
0.162	7.680
0.163	7.676
0.137	6.491
0.136	6.483
0.137	6.478
0.136	6.473
0.136	6.481
0.137	6.474
0.136	6.471
0.094	4.554
0.119	5.630
0.091	4.715

Q (gal/min)	ΔP (psia)
0.090	4.353
0.089	4.358
0.090	4.348
0.089	4.344
0.089	4.330
0.090	4.319
0.071	3.446
0.069	3.445
0.070	3.433
0.071	3.441
0.069	3.438
0.069	3.438
0.069	3.439
0.070	3.435
0.070	3.435
0.070	3.429
0.070	3.429
0.071	3.433
0.070	3.433
0.071	3.426
0.071	3.424
0.070	3.416
0.070	3.414
0.070	3.418
0.070	3.411
0.069	3.411
0.069	3.409
0.068	3.338
0.068	3.338
0.067	3.334
0.069	3.361
0.068	3.353
0.069	3.349
0.069	3.326
0.067	3.324
0.066	3.325
0.065	3.294
0.066	3.296
0.066	3.295
0.033	1.878
0.034	1.831
0.034	1.838
0.035	1.845
0.033	1.843

Table C34—Experimental Pressure Drop – Flow rate Mixture Test 5 Temperature Average 130°F

Q (gal/min)	ΔP (psia)
0.244	10.105
0.245	10.118
0.238	10.134
0.250	10.154
0.250	10.196
0.248	10.205
0.250	10.200
0.251	10.195
0.250	10.199
0.252	10.200
0.250	10.199
0.251	10.199
0.253	10.198
0.254	10.238
0.253	10.230
0.254	10.235
0.252	10.223
0.253	10.216
0.251	10.195
0.253	10.201
0.254	10.190
0.254	10.303
0.253	10.310
0.254	10.305
0.254	10.296
0.254	10.286
0.252	10.286
0.253	10.261
0.254	10.250
0.251	10.246
0.252	10.241
0.251	10.249
0.251	10.233
0.250	10.244
0.250	10.243
0.250	10.250
0.249	10.221
0.250	10.211
0.251	10.219
0.251	10.241
0.250	10.248
0.250	10.249

Q (gal/min)	ΔP (psia)
0.249	10.250
0.250	10.250
0.248	10.246
0.250	10.250
0.248	10.253
0.249	10.258
0.248	10.249
0.248	10.255
0.248	10.246
0.246	10.254
0.249	10.261
0.249	10.260
0.249	10.259
0.248	10.259
0.249	10.256
0.248	10.259
0.249	10.236
0.249	10.230
0.250	10.235
0.251	10.238
0.250	10.255
0.250	10.265
0.250	10.276
0.250	10.279
0.249	10.275
0.249	10.273
0.251	10.278
0.249	10.289
0.249	10.281
0.251	10.296
0.250	10.289
0.249	10.288
0.249	10.285
0.250	10.273
0.219	9.268
0.208	9.094
0.208	9.080
0.207	9.069
0.208	9.073
0.208	9.073
0.202	8.800
0.241	10.358
0.205	8.781
0.204	8.798
0.205	8.794

Q (gal/min)	ΔP (psia)
0.204	8.798
0.205	8.801
0.179	7.551
0.179	7.553
0.178	7.568
0.180	7.556
0.178	7.561
0.177	7.555
0.178	7.551
0.177	7.543
0.177	7.546
0.177	7.546
0.178	7.578
0.178	7.569
0.177	7.571
0.164	7.351
0.160	6.900
0.160	6.895
0.162	6.896
0.161	6.893
0.162	6.889
0.162	6.900
0.161	6.901
0.162	6.906
0.160	6.906
0.161	6.911
0.161	6.910
0.162	6.911
0.136	5.904
0.135	5.791
0.135	5.781
0.135	5.780
0.134	5.776
0.134	5.776
0.134	5.769
0.135	5.754
0.093	4.059
0.094	4.100
0.093	4.089
0.094	4.088
0.094	4.080
0.094	4.080
0.091	4.063
0.091	3.970
0.090	3.954

Q (gal/min)	ΔP (psia)
0.090	3.941
0.090	3.929
0.090	3.916
0.090	3.879
0.090	3.904
0.089	3.894
0.089	3.856
0.089	3.854
0.088	3.813
0.068	3.029
0.069	3.028
0.068	3.018
0.068	3.013
0.068	3.001
0.027	1.366
0.028	1.355
0.013	0.925
0.014	0.713
0.248	10.124

Table C35—Experimental Pressure Drop – Flow rate Mixture Test 5 Temperature Average 140°F

Q (gal/min)	ΔP (psia)
0.268	10.168
0.268	10.165
0.270	10.168
0.268	10.163
0.270	10.155
0.270	10.163
0.272	10.171
0.272	10.163
0.275	10.161
0.273	10.156
0.274	10.155
0.273	10.165
0.273	10.161
0.272	10.165
0.272	10.165
0.272	10.173
0.272	10.169
0.271	10.160
0.271	10.171
0.262	9.999

Q (gal/min)	ΔP (psia)
0.240	9.436
0.240	9.435
0.240	9.443
0.240	9.435
0.242	9.420
0.242	9.419
0.242	9.414
0.242	9.409
0.242	9.416
0.243	9.419
0.226	8.745
0.225	8.738
0.225	8.724
0.226	8.725
0.225	8.713
0.224	8.711
0.225	8.718
0.224	8.733
0.224	8.730
0.225	8.735
0.224	8.735
0.206	8.005
0.207	8.019
0.206	8.011
0.207	8.006
0.209	8.006
0.207	7.990
0.208	7.994
0.183	6.981
0.182	6.981
0.182	6.984
0.159	6.039
0.157	6.033
0.158	6.025
0.133	5.296
0.134	5.063
0.132	5.053
0.133	5.048
0.133	5.044
0.133	5.040
0.133	5.039
0.134	5.048
0.115	4.411
0.116	4.416
0.113	4.416
0.114	4.415

Q (gal/min)	ΔP (psia)
0.085	3.269
0.084	3.260
0.084	3.236
0.083	3.225
0.083	3.214
0.082	3.193
0.081	3.175
0.083	3.168
0.083	3.161
0.082	3.154
0.051	2.078
0.049	1.969
0.049	1.948
0.048	1.919
0.048	1.913
0.048	1.906
0.047	1.885
0.046	1.880
0.047	1.866
0.045	1.828
0.045	1.838
0.075	2.868
0.075	2.865
0.062	2.425
0.061	2.425
0.063	2.416
0.063	2.409
0.025	1.109
0.026	1.085
0.024	1.035
0.022	0.994
0.021	0.944
0.021	0.905
0.020	0.876
0.020	0.856
0.018	0.840
0.020	0.826
0.018	0.818
0.018	0.796

Table C36—Experimental Pressure Drop – Flow rate Mixture Test 5 Temperature Average 150°F

Q (gal/min)	ΔP (psia)
0.320	9.899
0.319	9.900
0.319	9.914
0.316	9.906
0.316	9.923
0.318	9.933
0.316	9.939
0.315	9.948
0.314	9.939
0.314	9.926
0.311	9.964
0.311	9.973
0.312	9.973
0.312	9.983
0.312	9.978
0.312	9.986
0.312	9.983
0.312	9.969
0.311	9.970
0.311	9.960
0.311	9.969
0.310	9.971
0.311	9.964
0.311	9.978
0.310	9.983
0.312	9.973
0.312	9.990
0.312	9.976
0.310	9.971
0.311	9.973
0.312	9.970
0.312	9.971
0.313	9.973
0.311	9.978
0.313	9.984
0.312	9.979
0.312	9.973
0.312	9.966
0.282	9.370
0.281	9.368
0.284	9.375
0.282	9.361
0.284	9.355

Q (gal/min)	ΔP (psia)
0.283	9.360
0.285	9.355
0.285	9.356
0.286	9.348
0.266	8.676
0.267	8.676
0.266	8.686
0.267	8.684
0.268	8.685
0.269	8.670
0.269	8.673
0.269	8.679
0.264	8.513
0.249	7.994
0.247	7.984
0.249	7.986
0.247	7.970
0.248	7.988
0.247	7.985
0.248	7.976
0.247	7.986
0.247	7.981
0.246	7.969
0.228	7.549
0.222	7.186
0.220	7.185
0.204	6.649
0.180	5.883
0.180	5.854
0.182	5.865
0.180	5.860
0.181	5.850
0.159	5.434
0.163	5.279
0.161	5.274
0.145	4.786
0.143	4.701
0.143	4.694
0.143	4.691
0.143	4.684
0.143	4.686
0.142	4.681
0.114	3.770
0.115	3.773
0.113	3.765

Q (gal/min)	ΔP (psia)
0.113	3.746
0.113	3.733
0.090	3.225
0.082	2.769
0.083	2.763
0.081	2.746
0.082	2.738
0.081	2.726
0.081	2.703
0.080	2.693
0.080	2.659
0.080	2.649
0.078	2.604
0.078	2.586
0.077	2.579
0.029	1.378
0.042	1.418
0.041	1.411
0.041	1.403
0.016	0.658
0.015	0.573
0.014	0.551
0.014	0.531

Table C37—Experimental Pressure Drop – Flow rate Mixture Test 5 Temperature Average 160°F

Q (gal/min)	ΔP (psia)
0.324	9.916
0.323	9.923
0.323	9.890
0.325	9.870
0.328	9.866
0.328	9.863
0.330	9.856
0.330	9.869
0.330	9.870
0.329	9.873
0.330	9.871
0.331	9.881
0.287	8.883
0.288	8.891
0.289	8.894

Q (gal/min)	ΔP (psia)
0.289	8.878
0.290	8.885
0.279	8.550
0.279	8.520
0.278	8.503
0.281	8.514
0.280	8.494
0.256	7.775
0.255	7.696
0.256	7.713
0.256	7.713
0.256	7.688
0.256	7.715
0.256	7.699
0.255	7.691
0.256	7.690
0.255	7.685
0.255	7.690
0.255	7.675
0.256	7.684
0.254	7.685
0.236	7.098
0.235	7.063
0.235	7.056
0.235	7.090
0.235	7.095
0.236	7.095
0.236	7.101
0.235	7.095
0.236	7.088
0.236	7.091
0.235	7.084
0.235	7.085
0.237	7.079
0.236	7.078
0.236	7.073
0.236	7.073
0.237	7.071
0.237	7.073
0.237	7.069
0.238	7.055
0.216	6.430
0.217	6.419
0.215	6.408
0.216	6.409

Q (gal/min)	ΔP (psia)
0.216	6.404
0.216	6.405
0.216	6.404
0.216	6.403
0.192	5.714
0.193	5.718
0.193	5.715
0.191	5.648
0.191	5.643
0.192	5.640
0.191	5.631
0.192	5.618
0.190	5.541
0.174	5.191
0.176	5.050
0.174	5.059
0.174	5.060
0.174	5.056
0.173	5.064
0.172	5.139
0.152	4.590
0.152	4.541
0.151	4.551
0.151	4.553
0.152	4.570
0.150	4.563
0.116	3.606
0.118	3.610
0.117	3.608
0.116	3.556
0.116	3.551
0.115	3.539
0.116	3.538
0.115	3.523
0.115	3.520
0.115	3.514
0.116	3.506
0.115	3.498
0.116	3.490
0.331	9.779
0.285	8.329
0.156	4.649
0.155	4.649
0.156	4.649
0.156	4.650

Q (gal/min)	ΔP (psia)
0.154	4.649
0.156	4.651
0.156	4.648
0.154	4.648
0.155	4.640
0.154	4.634
0.155	4.628
0.154	4.625
0.153	4.634
0.155	4.638
0.154	4.635
0.153	4.603
0.154	4.654
0.155	4.644
0.156	4.651
0.153	4.650
0.154	4.630
0.152	4.600
0.153	4.605
0.152	4.585
0.152	4.599
0.153	4.601
0.152	4.594
0.152	4.595
0.152	4.596
0.151	4.591
0.152	4.596
0.152	4.595
0.152	4.595
0.152	4.598
0.152	4.593
0.152	4.590
0.152	4.588
0.151	4.568
0.122	3.698
0.120	3.683
0.120	3.678
0.120	3.676
0.120	3.676
0.120	3.674
0.121	3.675
0.120	3.673
0.086	2.666
0.084	2.598
0.081	2.508

Q (gal/min)	ΔP (psia)
0.079	2.491
0.074	2.356
0.070	2.204
0.067	2.123
0.067	2.103
0.067	2.110
0.064	2.043
0.064	2.005
0.060	1.901
0.053	1.720
0.030	1.114
0.029	0.958
0.208	6.045
0.330	9.836

Test 6

Table C38 —Experimental Pressure Drop – Flow rate Mixture Test 6 Temperature Average 100°F

Q (gal/min)	ΔP(psia)
0.143	9.125
0.144	9.145
0.143	9.146
0.145	9.150
0.145	9.149
0.144	9.133
0.166	10.154
0.170	10.311
0.150	9.134
0.147	9.144
0.142	8.969
0.131	8.286
0.130	8.189
0.131	8.206
0.131	8.211
0.132	8.215
0.131	8.214
0.131	8.216
0.126	7.813
0.109	6.805
0.110	6.815
0.110	6.811

Q (gal/min)	ΔP(psia)
0.109	6.795
0.110	6.799
0.111	6.791
0.111	6.789
0.110	6.783
0.112	6.785
0.112	6.784
0.111	6.788
0.111	6.785
0.112	6.791
0.105	6.546
0.091	5.613
0.091	5.635
0.092	5.641
0.092	5.650
0.093	5.654
0.092	5.650
0.091	5.653
0.092	5.650
0.092	5.651
0.091	5.655
0.091	5.644
0.092	5.644
0.092	5.644
0.092	5.653
0.093	5.654
0.094	5.658
0.093	5.669
0.092	5.670
0.092	5.670
0.066	4.100
0.065	4.121
0.065	4.114
0.064	4.115
0.065	4.121
0.038	2.799
0.036	2.525

Table C39—Experimental Pressure Drop – Flow rate Mixture Test 6 Temperature Average 110°F

Q (gal/min)	ΔP (psia)
0.220	10.380
0.220	10.391

Q (gal/min)	ΔP (psia)
0.220	10.401
0.219	10.408
0.174	8.869
0.174	8.874
0.162	8.431
0.152	7.763
0.152	7.755
0.154	7.765
0.153	7.744
0.155	7.751
0.123	6.238
0.122	6.219
0.097	5.228
0.071	3.756
0.070	3.684
0.070	3.671
0.062	3.464
0.047	2.473
0.024	1.451
0.023	1.293
0.255	10.226
0.253	10.234
0.251	10.243
0.251	10.250
0.248	10.268
0.250	10.264
0.249	10.231
0.204	9.103
0.203	9.105
0.205	9.115
0.205	9.105
0.206	9.103
0.207	9.106
0.205	9.098
0.183	8.064
0.183	8.060
0.149	6.700
0.148	6.655
0.149	6.636
0.149	6.628
0.149	6.623
0.110	4.990
0.110	4.974
0.110	4.971
0.110	4.966

0.110	4.960
0.111	4.963
0.110	4.958
0.081	3.911
0.081	3.678
0.080	3.655
0.042	2.211
0.061	2.711
0.061	2.710
0.059	2.710
0.060	2.713
0.062	2.714
0.061	2.719
0.061	2.721
0.060	2.724
0.062	2.728
0.061	2.733
0.061	2.738
0.061	2.743
0.062	2.746
0.027	1.275
0.028	1.263
0.236	9.983
0.246	10.214

Table C40—Experimental Pressure Drop – Flow rate Mixture Test 6 Temperature Average 120°F

Q (gal/min)	ΔP (psia)
0.285	10.073
0.285	10.076
0.284	10.086
0.284	10.099
0.284	10.098
0.241	8.994
0.235	9.011
0.235	9.006
0.234	9.014
0.234	9.024
0.234	9.020
0.236	9.031
0.234	9.023
0.235	9.018
0.237	9.021
0.237	9.028

Q (gal/min)	ΔP (psia)
0.237	9.033
0.237	9.029
0.237	9.025
0.237	9.026
0.229	8.735
0.227	8.651
0.228	8.643
0.186	7.369
0.184	7.044
0.183	7.035
0.161	6.165
0.161	6.159
0.130	5.099
0.130	4.993
0.129	4.991
0.129	4.990
0.106	4.240
0.106	4.121
0.106	4.121
0.106	4.120
0.072	3.126
0.071	2.875
0.073	2.853
0.072	2.844
0.073	2.841
0.072	2.836
0.073	2.830
0.073	2.826
0.073	2.821
0.035	1.489
0.032	1.214
0.034	1.211
0.033	1.214
0.032	1.208
0.269	9.889
0.279	10.070
0.282	10.070
0.280	10.085
0.281	10.105
0.279	10.096
0.280	10.104

Table C41. Experimental Pressure Drop – Flow rate Mixture Test 6 Temperature Average 130°F

Q (gal/min)	ΔP (psia)
0.272	10.285
0.271	10.285
0.271	10.275
0.275	10.261
0.212	8.149
0.214	8.135
0.212	8.111
0.214	8.109
0.214	8.108
0.214	8.096
0.216	8.088
0.216	8.066
0.216	8.068
0.215	8.069
0.217	8.060
0.216	8.054
0.217	8.053
0.216	8.049
0.218	8.043
0.211	7.908
0.184	6.813
0.183	6.773
0.180	6.769
0.182	6.765
0.153	5.778
0.155	5.718
0.155	5.715
0.155	5.713
0.155	5.703
0.154	5.705
0.155	5.711
0.156	5.705
0.155	5.689
0.123	4.515
0.124	4.505
0.124	4.500
0.123	4.459
0.093	3.366
0.093	3.365
0.063	2.388
0.063	2.315

Q (gal/min)	ΔP (psia)
0.063	2.266
0.060	2.236
0.060	2.199
0.060	2.164
0.060	2.134
0.060	2.105
0.059	2.083
0.059	2.060
0.058	2.023
0.057	1.965
0.056	1.904
0.053	1.868
0.056	1.861
0.035	1.219
0.033	1.199
0.035	1.181
0.033	1.163
0.032	1.118
0.030	1.099
0.031	1.078
0.030	1.065
0.031	1.051
0.029	1.034
0.029	1.024
0.029	1.014
0.028	1.000
0.027	0.990
0.028	0.978
0.027	0.966
0.027	0.955

Table C42—Experimental Pressure Drop – Flow rate Mixture Test 6 Temperature Average =140°F

Q (gal/min)	ΔP (psia)
0.352	9.775
0.351	9.771
0.351	9.786
0.348	9.785
0.347	9.793
0.345	9.786
0.344	9.780

Q (gal/min)	ΔP (psia)
0.344	9.806
0.343	9.814
0.341	9.816
0.299	9.190
0.299	9.194
0.299	9.186
0.300	9.180
0.299	9.169
0.299	9.166
0.299	9.168
0.301	9.171
0.300	9.164
0.300	9.168
0.300	9.166
0.301	9.155
0.302	9.159
0.302	9.156
0.303	9.164
0.281	8.536
0.282	8.545
0.282	8.543
0.280	8.444
0.253	7.644
0.253	7.638
0.253	7.630
0.243	7.425
0.225	6.805
0.225	6.805
0.227	6.871
0.183	5.534
0.183	5.531
0.183	5.536
0.182	5.526
0.157	5.231
0.155	4.723
0.156	4.718
0.155	4.708
0.155	4.705
0.122	3.754
0.122	3.740
0.121	3.739
0.122	3.736
0.122	3.731
0.121	3.728
0.094	2.886

Q (gal/min)	ΔP (psia)
0.094	2.875
0.093	2.870
0.093	2.859
0.092	2.851
0.093	2.844
0.037	1.321
0.036	1.168
0.036	1.159
0.035	1.148
0.035	1.130
0.034	1.110
0.039	0.969
0.039	1.210
0.038	1.183
0.037	1.169
0.336	9.809
0.341	9.810
0.341	9.793
0.342	9.795
0.341	9.800
0.340	9.785

Table C43. Experimental Pressure Drop – Flow rate Mixture Test 6 Temperature Average 150°F

Q (gal/min)	ΔP (psia)
0.358	9.726
0.358	9.738
0.359	9.741
0.360	9.746
0.361	9.750
0.359	9.725
0.359	9.725
0.358	9.701
0.360	9.715
0.360	9.699
0.360	9.706
0.359	9.709
0.359	9.703
0.361	9.701
0.358	9.689
0.361	9.704
0.361	9.705
0.362	9.703

0.360	9.701
0.361	9.709
0.361	9.689
0.361	9.700
0.362	9.705
0.361	9.691
0.362	9.708
0.363	9.710
0.362	9.710
0.364	9.691
0.363	9.678
0.365	9.683
0.363	9.664
0.362	9.651
0.363	9.660
0.363	9.663
0.364	9.664
0.366	9.668
0.364	9.655
0.364	9.651
0.365	9.665
0.365	9.670
0.366	9.666
0.367	9.665
0.366	9.659
0.366	9.674
0.366	9.661
0.365	9.660
0.366	9.655
0.366	9.658
0.367	9.661
0.365	9.656
0.367	9.649
0.367	9.651
0.368	9.653
0.368	9.646
0.367	9.640
0.369	9.656
0.368	9.653
0.369	9.658
0.367	9.656
0.368	9.643
0.369	9.648
0.369	9.644
0.369	9.644
0.368	9.629

0.370	9.639
0.369	9.631
0.370	9.633
0.370	9.640
0.369	9.641
0.369	9.634
0.369	9.636
0.369	9.639
0.369	9.628
0.368	9.623
0.370	9.634
0.370	9.626
0.369	9.616
0.371	9.633
0.371	9.635
0.370	9.633
0.373	9.644
0.370	9.619
0.369	9.628
0.371	9.640
0.372	9.651
0.370	9.645
0.370	9.641
0.370	9.644
0.370	9.663
0.370	9.666
0.370	9.669
0.365	9.656
0.368	9.671
0.369	9.668
0.369	9.663
0.369	9.663
0.369	9.645
0.369	9.664
0.368	9.660
0.369	9.668
0.369	9.654
0.370	9.656
0.369	9.664
0.370	9.664
0.369	9.660
0.369	9.653
0.369	9.655
0.369	9.655
0.368	9.655
0.369	9.670

0.371	9.675
0.370	9.681
0.370	9.668
0.370	9.665
0.370	9.658
0.369	9.658
0.370	9.670
0.370	9.670
0.370	9.669
0.370	9.670
0.369	9.658
0.369	9.663
0.368	9.663
0.369	9.656
0.369	9.664
0.370	9.666
0.346	9.286
0.339	9.308
0.339	9.298
0.340	9.316
0.341	9.318
0.341	9.313
0.342	9.314
0.340	9.300
0.340	9.294
0.342	9.290
0.341	9.310
0.343	9.301
0.318	8.724
0.318	8.736
0.318	8.723
0.316	8.723
0.316	8.716
0.315	8.694
0.306	8.400
0.304	8.381
0.304	8.378
0.305	8.381
0.306	8.384
0.305	8.378
0.306	8.373
0.308	8.393
0.306	8.369
0.307	8.356
0.306	8.366
0.308	8.370

0.306	8.356
0.308	8.370
0.306	8.369
0.308	8.390
0.306	8.378
0.306	8.388
0.305	8.393
0.304	8.381
0.305	8.384
0.305	8.395
0.270	7.410
0.270	7.388
0.270	7.388
0.272	7.390
0.272	7.383
0.273	7.375
0.272	7.368
0.273	7.366
0.274	7.361
0.275	7.375
0.275	7.363
0.274	7.358
0.276	7.369
0.276	7.363
0.275	7.354
0.257	6.865
0.257	6.868
0.257	6.868
0.257	6.878
0.258	6.878
0.257	6.884
0.256	6.880
0.257	6.884
0.256	6.884
0.256	6.903
0.255	6.900
0.256	6.899
0.256	6.888
0.254	6.881
0.256	6.884
0.255	6.885
0.255	6.886
0.256	6.884
0.247	6.704
0.233	6.311
0.234	6.318

0.217	5.864
0.216	5.864
0.217	5.859
0.191	5.214
0.192	5.201
0.191	5.205
0.192	5.204
0.174	4.725
0.173	4.724
0.151	4.140
0.151	4.134
0.152	4.133
0.151	4.079
0.151	4.075
0.150	4.069
0.151	4.063
0.151	4.056
0.150	4.044
0.151	4.036
0.150	4.024
0.150	4.011
0.151	4.013
0.121	3.238
0.121	3.226
0.121	3.221
0.121	3.213
0.121	3.218
0.120	3.218
0.121	3.220
0.121	3.223
0.120	3.231
0.120	3.268
0.119	3.259
0.117	3.208
0.120	3.248
0.119	3.241
0.120	3.238
0.120	3.233
0.120	3.224
0.087	2.594
0.086	2.345
0.086	2.338
0.087	2.335
0.085	2.333
0.086	2.331
0.086	2.333

0.045	1.286
0.046	1.283
0.045	1.276
0.046	1.271
0.046	1.261
0.046	1.259
0.046	1.251
0.045	1.236
0.046	1.231
0.045	1.209
0.043	1.206
0.044	1.201
0.043	1.199
0.044	1.195
0.042	1.154
0.042	1.154
0.041	1.148
0.041	1.146
0.042	1.146
0.041	1.140
0.013	0.406
0.012	0.396
0.011	0.380
0.010	0.373
0.011	0.364
0.011	0.349
0.009	0.336
0.010	0.319
0.010	0.311
0.009	0.300

Test 7

Table C44—Experimental Pressure Drop – Flow rate Mixture Test 7 Temperature Average 100°F

Q (gal/min)	ΔP (psia)
0.206	10.198
0.165	8.660
0.166	8.639
0.166	8.640
0.167	8.643
0.166	8.605
0.168	8.638
0.169	8.628

Q (gal/min)	ΔP (psia)
0.169	8.631
0.170	8.646
0.168	8.616
0.150	7.749
0.150	7.731
0.152	7.744
0.151	7.725
0.152	7.743
0.128	6.920
0.127	6.500
0.127	6.504
0.127	6.510
0.127	6.523
0.128	6.508
0.126	6.498
0.127	6.496
0.101	5.296
0.102	5.246
0.102	5.264
0.100	5.261
0.101	5.258
0.103	5.245
0.101	5.229
0.102	5.241
0.102	5.230
0.103	5.223
0.103	5.219
0.103	5.220
0.104	5.220
0.103	5.230
0.105	5.219
0.065	3.359
0.065	3.395
0.063	3.410
0.064	3.413
0.065	3.409
0.064	3.413
0.064	3.430
0.065	3.435
0.065	3.405
0.065	3.416
0.064	3.415
0.064	3.423
0.065	3.420
0.065	3.420

Q (gal/min)	ΔP (psia)
0.063	3.335
0.063	3.344
0.063	3.343
0.064	3.400
0.064	3.391
0.066	3.391
0.065	3.394
0.065	3.391
0.064	3.399
0.064	3.399
0.064	3.405
0.064	3.408
0.065	3.409
0.065	3.415
0.065	3.425
0.065	3.420
0.065	3.408
0.065	3.404
0.065	3.386
0.063	3.385
0.064	3.384
0.064	3.384
0.063	3.388
0.065	3.391
0.064	3.395
0.064	3.395
0.063	3.388
0.064	3.385
0.062	3.386
0.063	3.394
0.064	3.388
0.063	3.383
0.032	1.864
0.031	1.885

Table C45—Experimental Pressure Drop – Flow rate Mixture Test 7 Temperature Average 110°F

Q (gal/min)	ΔP (psia)
0.196	8.810
0.192	8.815
0.192	8.803
0.191	8.808
0.193	8.794

Q (gal/min)	ΔP (psia)
0.194	8.809
0.193	8.809
0.193	8.814
0.193	8.808
0.194	8.810
0.194	8.806
0.192	8.811
0.161	7.343
0.161	7.351
0.161	7.355
0.160	7.360
0.161	7.368
0.159	7.366
0.161	7.364
0.162	7.368
0.161	7.365
0.161	7.366
0.162	7.361
0.160	7.353
0.144	6.558
0.142	6.559
0.143	6.560
0.143	6.558
0.143	6.551
0.143	6.550
0.143	6.553
0.143	6.554
0.143	6.553
0.144	6.550
0.143	6.551
0.142	6.549
0.143	6.549
0.144	6.549
0.140	6.545
0.144	6.551
0.144	6.540
0.145	6.546
0.143	6.541
0.144	6.543
0.143	6.540
0.144	6.535
0.143	6.531
0.144	6.528
0.143	6.528
0.143	6.530

Q (gal/min)	ΔP (psia)
0.143	6.526
0.144	6.526
0.144	6.521
0.144	6.524
0.144	6.524
0.107	4.958
0.108	4.970
0.107	4.968
0.107	4.970
0.108	4.971
0.055	2.706
0.056	2.723
0.055	2.726
0.055	2.734
0.055	2.731
0.055	2.706
0.054	2.689
0.054	2.683
0.054	2.679
0.055	2.675
0.054	2.674
0.054	2.669
0.054	2.646
0.052	2.628
0.053	2.625
0.053	2.626
0.054	2.630
0.054	2.630
0.054	2.634
0.054	2.633
0.055	2.701
0.055	2.699
0.054	2.685
0.054	2.726

Table C46. Experimental Pressure Drop – Flow rate Mixture Test 7 Temperature Average =120°F

Q (gal/min)	ΔP (psia)
0.275	10.121
0.275	10.126
0.275	10.128
0.273	10.104
0.228	9.045
0.227	9.011
0.226	9.013
0.228	9.020
0.227	9.026
0.228	9.025
0.228	9.031
0.212	8.369
0.213	8.366
0.212	8.356
0.213	8.358
0.213	8.349
0.197	7.795
0.196	7.729
0.197	7.728
0.197	7.731
0.197	7.724
0.197	7.729
0.197	7.720
0.168	6.641
0.168	6.655
0.169	6.654
0.167	6.656
0.169	6.656
0.131	5.251
0.131	5.233
0.131	5.231
0.132	5.231
0.130	5.228
0.131	5.220
0.098	4.025
0.098	3.989
0.098	3.988
0.099	3.979
0.099	3.974
0.058	2.383
0.057	2.388

Q (gal/min)	ΔP (psia)
0.032	1.686
0.032	1.405
0.029	1.381
0.030	1.381
0.031	1.385
0.254	9.886
0.270	10.093
0.274	10.094

Table C47—Experimental Pressure Drop – Flow rate Mixture Test 7 Temperature Average 130°F

Q (gal/min)	ΔP (psia)
0.265	9.383
0.254	9.430
0.254	9.426
0.255	9.418
0.255	9.418
0.257	9.423
0.256	9.421
0.256	9.414
0.257	9.411
0.258	9.418
0.258	9.406
0.259	9.401
0.259	9.390
0.238	8.659
0.240	8.670
0.223	8.085
0.223	8.061
0.223	8.070
0.223	8.058
0.224	8.073
0.224	8.064
0.223	8.063
0.223	8.068
0.225	8.064
0.223	8.060
0.198	7.170
0.198	7.151
0.197	7.149
0.198	7.153

Q (gal/min)	ΔP (psia)
0.169	6.121
0.167	6.119
0.168	6.133
0.168	6.134
0.168	6.125
0.168	6.125
0.167	6.120
0.167	6.119
0.169	6.123
0.169	6.116
0.168	6.116
0.117	4.405
0.117	4.294
0.116	4.290
0.118	4.288
0.117	4.281
0.060	2.314
0.061	2.288
0.060	2.283
0.060	2.253
0.058	2.226
0.057	2.183
0.057	2.128
0.057	2.118
0.057	2.120
0.055	2.125
0.055	2.116
0.056	2.126
0.056	2.124
0.057	2.124
0.057	2.113
0.056	2.113
0.017	0.686
0.015	0.666
0.286	10.003

Table C48—Experimental Pressure Drop – Flow rate Mixture Test 7 Temperature Average 140°F

Q (gal/min)	ΔP (psia)
0.278	8.895
0.278	8.890
0.278	8.888

Q (gal/min)	ΔP (psia)
0.278	8.888
0.279	8.891
0.278	8.880
0.278	8.881
0.278	8.888
0.270	8.558
0.270	8.564
0.270	8.559
0.272	8.568
0.271	8.556
0.270	8.558
0.254	8.071
0.252	8.021
0.252	8.013
0.252	8.025
0.234	7.444
0.233	7.445
0.234	7.448
0.234	7.451
0.210	6.719
0.210	6.719
0.209	6.731
0.210	6.728
0.210	6.718
0.210	6.711
0.210	6.705
0.191	6.204
0.191	6.091
0.190	6.085
0.172	5.510
0.174	5.503
0.172	5.494
0.173	5.490
0.172	5.499
0.173	5.501
0.172	5.503
0.143	4.576
0.144	4.575
0.143	4.576
0.143	4.579
0.111	3.691
0.111	3.641
0.111	3.644
0.111	3.641
0.054	1.933

Q (gal/min)	ΔP (psia)
0.054	1.831
0.052	1.783
0.013	0.538

Table C49—Experimental Pressure Drop – Flow rate Mixture Test 7 Temperature Average 150°F

Q (gal/min)	ΔP (psia)
0.345	9.501
0.345	9.499
0.346	9.504
0.345	9.505
0.343	9.506
0.345	9.519
0.343	9.516
0.343	9.510
0.344	9.520
0.299	8.425
0.297	8.418
0.298	8.416
0.298	8.430
0.300	8.424
0.299	8.403
0.297	8.400
0.299	8.419
0.299	8.416
0.299	8.411
0.299	8.416
0.299	8.416
0.274	7.735
0.273	7.738
0.246	6.926
0.245	6.921
0.244	6.908
0.245	6.910
0.246	6.904
0.245	6.918
0.241	6.790
0.212	5.936
0.210	5.933
0.210	5.925
0.210	5.924
0.210	5.921

Q (gal/min)	ΔP (psia)
0.209	5.918
0.209	5.924
0.209	5.924
0.208	5.924
0.210	5.930
0.180	5.195
0.179	5.088
0.177	5.090
0.178	5.085
0.178	5.093
0.178	5.096
0.178	5.095
0.178	5.093
0.177	5.076
0.177	5.068
0.177	5.060
0.176	5.024
0.176	5.010
0.176	5.008
0.137	3.969
0.091	2.663
0.090	2.629
0.089	2.618
0.089	2.609
0.068	1.974
0.068	1.973
0.066	1.968
0.066	1.956
0.065	1.943
0.026	0.849
0.026	0.835
0.024	0.821
0.352	9.735
0.360	9.723
0.358	9.716
0.359	9.713
0.359	9.724
0.356	9.719

Table C50—Experimental Pressure Drop – Flow rate Mixture Test 7 Temperature Average =160°F

Q (gal/min)	ΔP (psia)
0.356	9.720

Q (gal/min)	ΔP (psia)
0.361	9.708
0.363	9.716
0.363	9.705
0.364	9.698
0.318	8.641
0.363	9.698
0.364	9.690
0.367	9.685
0.368	9.661
0.368	9.658
0.370	9.650
0.373	9.674
0.371	9.658
0.374	9.654
0.344	9.105
0.343	9.090
0.342	9.088
0.344	9.073
0.343	9.075
0.343	9.075
0.345	9.075
0.343	9.081
0.346	9.060
0.347	9.064
0.347	9.060
0.348	9.049
0.347	9.044
0.348	9.048
0.349	9.050
0.350	9.051
0.321	8.333
0.321	8.343
0.321	8.329
0.321	8.314
0.324	8.320
0.278	7.170
0.280	7.178
0.277	7.170
0.279	7.179
0.245	6.309
0.245	6.306
0.243	6.306
0.243	6.304
0.244	6.300
0.216	5.631

Q (gal/min)	ΔP (psia)
0.217	5.626
0.216	5.603
0.215	5.600
0.216	5.600
0.216	5.598
0.215	5.593
0.214	5.588
0.215	5.581
0.216	5.575
0.216	5.573
0.179	4.866
0.177	4.590
0.149	3.899
0.139	3.638
0.113	3.020
0.114	2.958
0.112	2.941
0.112	2.935
0.111	2.926
0.111	2.916
0.112	2.911
0.070	1.854
0.070	1.843
0.069	1.820
0.063	1.686
0.061	1.636
0.058	1.611
0.022	0.678
0.023	0.640
0.019	0.594
0.018	0.564
0.017	0.536
0.016	0.509
0.017	0.486
0.369	9.565

Table C51—Experimental Pressure Drop – Flow rate Mixture Test 8 Temperature Average 100°F

Q (gal/min)	ΔP (psia)
0.210	9.126
0.210	9.125
0.211	9.123
0.211	9.121

Q (gal/min)	ΔP (psia)
0.211	9.114
0.213	9.126
0.215	9.126
0.214	9.113
0.213	9.113
0.216	9.138
0.188	7.914
0.188	7.876
0.187	7.894
0.188	7.883
0.187	7.881
0.166	6.980
0.165	6.979
0.164	6.970
0.164	6.974
0.165	6.979
0.164	6.969
0.163	6.966
0.162	6.966
0.163	6.958
0.164	6.953
0.165	6.949
0.166	6.963
0.167	6.949
0.165	6.946
0.166	6.951
0.167	6.941
0.165	6.935
0.166	6.923
0.165	6.920
0.167	6.925
0.167	6.920
0.132	5.519
0.134	5.523
0.132	5.520
0.132	5.518
0.133	5.520
0.134	5.520
0.132	5.514
0.132	5.519
0.132	5.516
0.131	5.518
0.132	5.526
0.134	5.526
0.133	5.523

Q (gal/min)	ΔP (psia)
0.132	5.525
0.131	5.526
0.134	5.530
0.133	5.536
0.133	5.530
0.133	5.530
0.131	5.534
0.134	5.529
0.132	5.538
0.132	5.540
0.133	5.539
0.134	5.541
0.134	5.540
0.107	4.811
0.108	4.615
0.109	4.625
0.107	4.624
0.108	4.629
0.109	4.634
0.107	4.633
0.107	4.636
0.108	4.633
0.108	4.634
0.109	4.636
0.108	4.635
0.108	4.635
0.106	4.636
0.109	4.624
0.107	4.616
0.107	4.610
0.109	4.601
0.107	4.593
0.107	4.585
0.076	3.385
0.077	3.374
0.076	3.368
0.078	3.358
0.074	3.354
0.077	3.341
0.078	3.340
0.078	3.334
0.076	3.328
0.078	3.321
0.078	3.325
0.077	3.325

Q (gal/min)	ΔP (psia)
0.077	3.326
0.078	3.323
0.075	3.321
0.075	3.318
0.077	3.314
0.077	3.310
0.077	3.314
0.078	3.318
0.076	3.339
0.075	3.350
0.075	3.325
0.074	3.321
0.076	3.324
0.075	3.315
0.075	3.286
0.073	3.264
0.073	3.266
0.072	3.258
0.071	3.258
0.072	3.259

Table C52—Experimental Pressure Drop – Flow rate Mixture Test 8 Temperature Average 110°F

Q (gal/min)	ΔP (psia)
0.274	10.168
0.274	10.151
0.275	10.154
0.276	10.148
0.274	10.128
0.261	9.874
0.254	9.896
0.255	9.908
0.254	9.901
0.255	9.895
0.256	9.889
0.256	9.895
0.256	9.904
0.257	9.896
0.258	9.880
0.260	9.888
0.260	9.884
0.226	8.718
0.227	8.721

Q (gal/min)	ΔP (psia)
0.227	8.719
0.228	8.706
0.227	8.700
0.226	8.695
0.228	8.704
0.214	8.388
0.212	8.076
0.213	8.076
0.211	8.091
0.212	8.085
0.210	8.074
0.210	8.073
0.177	6.859
0.176	6.861
0.177	6.860
0.176	6.866
0.177	6.866
0.142	5.503
0.141	5.529
0.140	5.526
0.141	5.528
0.141	5.519
0.141	5.518
0.143	5.506
0.139	5.494
0.141	5.486
0.140	5.478
0.142	5.469
0.141	5.450
0.142	5.439
0.143	5.431
0.107	4.108
0.104	4.095
0.106	4.089
0.106	4.085
0.106	4.079
0.107	4.073
0.105	4.064
0.106	4.056
0.103	4.054
0.104	4.054
0.105	4.056
0.107	4.054
0.104	4.028
0.102	4.020

Q (gal/min)	ΔP (psia)
0.103	4.023
0.103	3.989
0.104	3.991
0.104	3.991
0.102	3.989
0.102	3.993
0.106	4.010
0.103	4.009
0.104	4.025
0.105	4.023
0.045	2.140
0.087	3.365
0.086	3.354
0.084	3.345
0.037	1.669

Table C53—Experimental Pressure Drop – Flow rate Mixture Test 8 Temperature Average 120°F

Q (gal/min)	ΔP (psia)
0.294	10.078
0.294	10.068
0.294	10.061
0.295	10.043
0.294	10.053
0.291	10.044
0.294	10.048
0.294	10.049
0.296	10.049
0.296	10.034
0.296	10.046
0.296	10.040
0.295	10.055
0.293	10.046
0.295	10.063
0.295	10.055
0.296	10.058
0.270	8.928
0.271	8.926
0.271	8.935
0.269	8.928
0.269	8.920
0.269	8.930
0.265	8.550

0.264	8.533
0.261	8.546
0.260	8.549
0.261	8.565
0.262	8.566
0.261	8.583
0.262	8.584
0.260	8.570
0.259	8.581
0.258	8.589
0.259	8.589
0.258	8.585
0.258	8.584
0.258	8.590
0.257	8.605
0.257	8.604
0.256	8.605
0.255	8.595
0.258	8.584
0.258	8.599
0.258	8.605
0.259	8.604
0.258	8.609
0.259	8.585
0.259	8.594
0.260	8.595
0.259	8.598
0.262	8.618
0.261	8.605
0.260	8.593
0.243	8.043
0.242	8.029
0.242	8.038
0.242	8.028
0.226	7.548
0.228	7.540
0.228	7.543
0.228	7.535
0.227	7.534
0.228	7.541
0.227	7.540
0.227	7.535
0.227	7.525
0.228	7.520
0.227	7.514
0.227	7.503

0.227	7.504
0.227	7.488
0.230	7.499
0.227	7.509
0.228	7.508
0.228	7.513
0.229	7.508
0.229	7.500
0.229	7.501
0.229	7.501
0.228	7.506
0.229	7.500
0.229	7.511
0.229	7.505
0.227	7.496
0.228	7.504
0.228	7.503
0.228	7.490
0.228	7.496
0.229	7.490
0.230	7.488
0.229	7.498
0.228	7.485
0.229	7.480
0.228	7.483
0.228	7.480
0.228	7.474
0.228	7.481
0.228	7.484
0.228	7.489
0.229	7.484
0.227	7.476
0.228	7.479
0.228	7.476
0.229	7.485
0.229	7.470
0.228	7.483
0.229	7.469
0.228	7.474
0.229	7.475
0.229	7.469
0.230	7.476
0.230	7.474
0.229	7.464
0.229	7.483
0.228	7.468

0.229	7.460
0.230	7.458
0.230	7.461
0.229	7.458
0.229	7.460
0.228	7.455
0.229	7.450
0.227	7.446
0.229	7.453
0.229	7.449
0.230	7.443
0.230	7.446
0.228	7.444
0.231	7.441
0.229	7.443
0.230	7.436
0.228	7.436
0.230	7.450
0.230	7.444
0.231	7.453
0.228	7.439
0.230	7.438
0.229	7.438
0.229	7.436
0.228	7.446
0.231	7.443
0.230	7.445
0.231	7.440
0.229	7.429
0.231	7.429
0.229	7.421
0.228	7.426
0.228	7.428
0.228	7.424
0.227	7.423
0.229	7.424
0.227	7.420
0.231	7.419
0.231	7.421
0.229	7.419
0.230	7.419
0.229	7.411
0.229	7.406
0.230	7.410
0.230	7.413
0.231	7.411

0.231	7.416
0.230	7.411
0.232	7.409
0.206	6.873
0.207	6.719
0.207	6.723
0.207	6.725
0.205	6.720
0.205	6.734
0.206	6.724
0.205	6.719
0.209	6.730
0.207	6.719
0.206	6.738
0.206	6.733
0.207	6.746
0.206	6.741
0.206	6.741
0.206	6.736
0.204	6.739
0.206	6.746
0.205	6.744
0.205	6.750
0.203	6.745
0.206	6.746
0.204	6.746
0.205	6.754
0.166	5.701
0.164	5.526
0.165	5.533
0.165	5.524
0.166	5.516
0.164	5.505
0.164	5.506
0.166	5.506
0.165	5.508
0.163	5.505
0.164	5.511
0.166	5.501
0.115	3.989
0.117	3.996
0.116	3.989
0.116	3.998
0.116	3.993
0.116	3.986
0.116	3.978

0.116	3.978
0.116	3.983
0.116	3.986
0.117	3.989
0.116	3.980
0.116	3.974
0.116	3.980
0.117	3.980
0.118	3.978
0.113	3.911
0.113	3.888
0.112	3.865
0.112	3.849
0.073	2.605
0.071	2.561
0.069	2.520
0.067	2.464

Table C54—Experimental Pressure Drop – Flow rate Mixture Test 8 Temperature Average 130°F

Q (gal/min)	ΔP (psia)
0.332	9.825
0.333	9.823
0.335	9.813
0.334	9.811
0.334	9.793
0.336	9.804
0.333	9.805
0.334	9.803
0.336	9.801
0.335	9.806
0.336	9.811
0.335	9.800
0.304	8.963
0.295	8.995
0.298	9.003
0.298	9.001
0.299	9.003
0.299	9.011
0.300	9.011
0.300	9.018
0.301	9.014
0.301	9.015
0.301	9.005

Q (gal/min)	ΔP (psia)
0.302	9.011
0.302	8.993
0.302	9.009
0.302	8.993
0.304	9.005
0.302	8.991
0.304	8.986
0.304	8.983
0.303	8.975
0.303	8.984
0.303	8.993
0.305	8.994
0.305	8.978
0.305	8.986
0.285	8.480
0.285	8.460
0.286	8.461
0.286	8.470
0.286	8.449
0.287	8.465
0.286	8.453
0.289	8.453
0.287	8.455
0.287	8.445
0.287	8.458
0.287	8.443
0.287	8.440
0.287	8.440
0.286	8.444
0.287	8.441
0.287	8.450
0.289	8.448
0.288	8.441
0.288	8.448
0.288	8.448
0.288	8.451
0.287	8.429
0.289	8.451
0.288	8.439
0.288	8.438
0.288	8.441
0.289	8.436
0.288	8.435
0.290	8.425
0.290	8.421

Q (gal/min)	ΔP (psia)
0.288	8.399
0.288	8.401
0.288	8.398
0.289	8.395
0.290	8.394
0.289	8.404
0.289	8.413
0.290	8.420
0.290	8.419
0.289	8.423
0.291	8.433
0.292	8.431
0.292	8.431
0.292	8.421
0.290	8.420
0.290	8.435
0.291	8.415
0.291	8.439
0.288	8.441
0.289	8.441
0.287	8.429
0.287	8.425
0.286	8.430
0.286	8.448
0.287	8.444
0.285	8.448
0.263	7.843
0.262	7.859
0.263	7.860
0.263	7.844
0.263	7.843
0.262	7.839
0.262	7.820
0.264	7.828
0.264	7.829
0.265	7.824
0.263	7.814
0.266	7.820
0.266	7.836
0.264	7.815
0.265	7.813
0.265	7.815
0.266	7.819
0.266	7.811
0.268	7.814

Q (gal/min)	ΔP (psia)
0.243	7.325
0.244	7.181
0.244	7.178
0.243	7.169
0.242	7.161
0.243	7.168
0.244	7.169
0.243	7.171
0.244	7.166
0.220	6.483
0.219	6.484
0.220	6.478
0.219	6.468
0.220	6.473
0.222	6.476
0.220	6.474
0.221	6.470
0.220	6.466
0.220	6.461
0.220	6.461
0.220	6.454
0.168	5.025
0.168	5.031
0.168	5.024
0.167	5.028
0.169	5.020
0.170	5.013
0.169	5.003
0.169	5.006
0.168	4.999
0.169	5.001
0.169	4.996
0.146	4.343
0.147	4.341
0.146	4.338
0.144	4.338
0.145	4.324
0.144	4.318
0.141	4.261
0.144	4.245
0.144	4.295
0.146	4.288
0.144	4.286
0.144	4.281
0.144	4.276

Q (gal/min)	ΔP (psia)
0.145	4.271
0.144	4.269
0.145	4.260
0.145	4.260
0.144	4.250
0.145	4.244
0.101	3.084
0.101	3.075
0.102	3.073
0.100	3.064
0.101	3.063
0.102	3.041
0.099	3.031
0.102	3.030
0.078	2.149
0.023	0.748

Table C55—Experimental Pressure Drop – Flow rate Mixture Test 8 Temperature Average 140°F

Q (gal/min)	ΔP (psia)
0.373	9.620
0.373	9.620
0.374	9.624
0.373	9.608
0.375	9.623
0.374	9.605
0.375	9.594
0.375	9.595
0.376	9.576
0.376	9.593
0.376	9.588
0.377	9.589
0.375	9.570
0.327	8.669
0.332	8.670
0.329	8.666
0.332	8.681
0.333	8.666
0.332	8.661
0.332	8.665
0.333	8.668
0.333	8.655
0.335	8.671

Q (gal/min)	ΔP (psia)
0.336	8.661
0.333	8.643
0.334	8.649
0.337	8.631
0.334	8.639
0.333	8.636
0.337	8.635
0.336	8.634
0.336	8.629
0.336	8.608
0.339	8.605
0.338	8.604
0.340	8.630
0.340	8.623
0.338	8.629
0.339	8.618
0.339	8.618
0.341	8.620
0.341	8.630
0.339	8.620
0.339	8.624
0.339	8.629
0.338	8.621
0.339	8.615
0.340	8.608
0.340	8.619
0.340	8.605
0.340	8.601
0.340	8.610
0.341	8.606
0.324	8.239
0.305	7.733
0.304	7.726
0.305	7.745
0.305	7.745
0.304	7.735
0.303	7.729
0.305	7.721
0.306	7.740
0.306	7.744
0.306	7.736
0.281	7.143
0.282	7.175
0.283	7.179
0.283	7.163

Q (gal/min)	ΔP (psia)
0.281	7.160
0.282	7.163
0.282	7.178
0.280	7.160
0.281	7.154
0.278	7.151
0.281	7.158
0.282	7.159
0.280	7.159
0.279	7.149
0.281	7.148
0.280	7.153
0.280	7.164
0.281	7.155
0.281	7.155
0.279	7.155
0.280	7.144
0.279	7.151
0.281	7.151
0.280	7.155
0.257	6.561
0.256	6.551
0.258	6.564
0.256	6.556
0.256	6.553
0.257	6.548
0.255	6.534
0.257	6.534
0.256	6.534
0.256	6.535
0.257	6.535
0.257	6.538
0.257	6.536
0.256	6.533
0.257	6.544
0.257	6.535
0.256	6.543
0.256	6.539
0.258	6.544
0.257	6.540
0.254	6.541
0.258	6.541
0.257	6.534
0.256	6.523
0.256	6.533

Q (gal/min)	ΔP (psia)
0.258	6.531
0.257	6.535
0.256	6.539
0.257	6.533
0.258	6.544
0.254	6.529
0.256	6.528
0.256	6.528
0.257	6.514
0.256	6.523
0.256	6.521
0.256	6.541
0.257	6.533
0.256	6.535
0.256	6.528
0.256	6.523
0.257	6.526
0.257	6.533
0.256	6.535
0.256	6.533
0.257	6.525
0.256	6.525
0.255	6.520
0.255	6.518
0.254	6.515
0.255	6.510
0.257	6.523
0.256	6.520
0.257	6.515
0.257	6.511
0.256	6.509
0.258	6.508
0.256	6.490
0.257	6.490
0.259	6.489
0.223	5.621
0.223	5.625
0.222	5.625
0.222	5.641
0.222	5.625
0.222	5.618
0.223	5.623
0.222	5.628
0.223	5.629
0.195	4.933

Q (gal/min)	ΔP (psia)
0.193	4.928
0.194	4.921
0.194	4.920
0.194	4.929
0.195	4.926
0.168	4.283
0.169	4.283
0.167	4.280
0.168	4.269
0.167	4.268
0.167	4.260
0.167	4.246
0.166	4.239
0.167	4.236
0.165	4.228
0.166	4.226
0.165	4.219
0.167	4.224
0.167	4.220
0.140	3.813
0.139	3.584
0.139	3.525
0.137	3.521
0.138	3.520
0.138	3.530
0.138	3.528
0.138	3.526
0.140	3.555
0.137	3.528
0.138	3.533
0.139	3.560
0.140	3.554
0.139	3.541
0.140	3.544
0.139	3.556
0.102	2.648
0.101	2.623
0.101	2.618
0.102	2.610
0.100	2.611
0.100	2.586
0.099	2.578
0.099	2.558
0.098	2.551
0.098	2.538

Q (gal/min)	ΔP (psia)
0.098	2.524
0.098	2.514
0.097	2.505
0.096	2.503
0.097	2.503
0.097	2.503
0.096	2.500
0.098	2.499
0.097	2.493
0.097	2.495
0.096	2.496
0.097	2.496
0.097	2.493
0.098	2.493
0.052	1.394
0.051	1.365
0.051	1.359
0.049	1.350
0.050	1.344
0.050	1.335
0.048	1.333
0.047	1.310
0.048	1.301
0.047	1.274
0.046	1.265
0.046	1.255
0.047	1.246
0.045	1.240
0.046	1.235
0.045	1.220
0.045	1.210
0.046	1.209
0.008	0.323
0.010	0.308
0.008	0.296

Table C56—Experimental Pressure Drop – Flow rate Mixture Test 8 Temperature Average 150F

Q (gal/min)	ΔP (psia)
0.404	9.393
0.406	9.394
0.406	9.368
0.408	9.375

Q (gal/min)	ΔP (psia)
0.407	9.384
0.410	9.413
0.411	9.416
0.407	9.389
0.409	9.403
0.408	9.400
0.411	9.404
0.409	9.391
0.408	9.376
0.408	9.404
0.408	9.399
0.410	9.404
0.411	9.405
0.409	9.398
0.409	9.403
0.409	9.403
0.409	9.405
0.408	9.399
0.410	9.416
0.409	9.413
0.383	8.824
0.376	8.853
0.374	8.851
0.376	8.850
0.376	8.846
0.377	8.853
0.378	8.843
0.377	8.836
0.377	8.828
0.378	8.824
0.379	8.821
0.350	8.279
0.349	8.171
0.349	8.170
0.350	8.173
0.348	8.158
0.350	8.164
0.325	7.625
0.317	7.409
0.317	7.379
0.316	7.389
0.316	7.388
0.316	7.399
0.307	7.158
0.305	7.100

Q (gal/min)	ΔP (psia)
0.304	7.089
0.275	6.410
0.277	6.400
0.275	6.400
0.275	6.403
0.276	6.405
0.241	5.606
0.241	5.610
0.240	5.609
0.242	5.614
0.242	5.605
0.240	5.594
0.206	4.830
0.207	4.820
0.206	4.810
0.206	4.804
0.224	5.233
0.224	5.229
0.188	4.505
0.187	4.378
0.187	4.371
0.188	4.371
0.188	4.368
0.188	4.364
0.188	4.368
0.155	3.634
0.155	3.623
0.155	3.623
0.156	3.625
0.116	2.775
0.116	2.754
0.115	2.740
0.115	2.738
0.116	2.738
0.115	2.731
0.115	2.728
0.115	2.716
0.114	2.704
0.089	2.093
0.088	2.080
0.087	2.068
0.086	2.055
0.085	2.049
0.086	2.036
0.087	2.028

Q (gal/min)	ΔP (psia)
0.087	2.023
0.084	1.970
0.082	1.955
0.083	1.941
0.082	1.939
0.082	1.925
0.052	1.379
0.051	1.233
0.051	1.228
0.051	1.219
0.050	1.213
0.050	1.198
0.049	1.203
0.050	1.215
0.049	1.199
0.020	0.540
0.019	0.521
0.017	0.485
0.017	0.460

Table C57—Experimental Pressure Drop – Flow rate Mixture Test 8 Temperature Average =160°F

Q (gal/min)	ΔP (psia)
0.437	9.250
0.438	9.248
0.438	9.246
0.436	9.243
0.440	9.253
0.440	9.256
0.440	9.239
0.441	9.226
0.414	8.805
0.413	8.804
0.413	8.795
0.414	8.801
0.415	8.808
0.376	8.024
0.339	7.160
0.341	7.176
0.339	7.181
0.339	7.176
0.339	7.161
0.337	7.174

Q (gal/min)	ΔP (psia)
0.321	6.809
0.321	6.805
0.285	6.066
0.283	6.050
0.283	6.051
0.249	5.313
0.256	5.451
0.255	5.451
0.256	5.460
0.256	5.456
0.257	5.459
0.257	5.463
0.254	5.466
0.226	4.861
0.228	4.874
0.226	4.869
0.226	4.863
0.227	4.858
0.227	4.853
0.227	4.854
0.226	4.855
0.225	4.854
0.225	4.861
0.226	4.854
0.204	4.353
0.203	4.354
0.202	4.350
0.201	4.329
0.194	4.186
0.178	3.858
0.155	3.411
0.143	3.084
0.142	3.079
0.143	3.081
0.142	3.084
0.129	2.930
0.107	2.370
0.108	2.370
0.107	2.358
0.106	2.353
0.106	2.353
0.105	2.360
0.107	2.358
0.105	2.358
0.107	2.356

Q (gal/min)	ΔP (psia)
0.105	2.356
0.107	2.354
0.107	2.343
0.106	2.333
0.107	2.330
0.104	2.328
0.088	1.983
0.075	1.720
0.075	1.715
0.076	1.715
0.078	1.700
0.052	1.345
0.052	1.176
0.050	1.173
0.051	1.173
0.050	1.171
0.048	1.169
0.035	0.868
0.037	0.861

Test 9

Table C58—Experimental Pressure Drop – Flow rate Mixture Test 9 Temperature Average 99°F

Q (gal/min)	ΔP (psia)
0.265	10.199
0.266	10.186
0.264	10.199
0.267	10.201
0.265	10.203
0.266	10.189
0.269	10.201
0.234	9.044
0.229	9.083
0.227	9.103
0.226	9.056
0.227	9.070
0.227	9.090
0.229	9.089
0.230	9.071
0.229	9.061
0.229	9.065

Q (gal/min)	ΔP (psia)
0.231	9.060
0.229	9.058
0.229	9.056
0.231	9.048
0.232	9.048
0.205	8.059
0.204	8.091
0.206	8.089
0.207	8.093
0.206	8.068
0.206	8.058
0.207	8.053
0.206	8.036
0.207	8.026
0.207	8.029
0.206	8.021
0.208	8.023
0.208	8.019
0.210	8.016
0.209	8.026
0.210	8.023
0.208	8.009
0.210	8.016
0.177	6.730
0.177	6.733
0.176	6.734
0.156	6.004
0.155	6.016
0.156	6.021
0.156	6.023
0.156	6.025
0.155	6.028
0.158	6.031
0.155	6.030
0.156	6.033
0.156	6.026
0.155	6.028
0.155	6.025
0.159	6.020
0.120	4.714
0.121	4.725
0.120	4.719
0.120	4.713
0.091	3.638
0.092	3.641

Q (gal/min)	ΔP (psia)
0.089	3.644
0.091	3.624
0.008	0.385
0.009	0.375

Table C59—Experimental Pressure Drop – Flow rate Mixture Test 9 Temperature Average =110°F

Q (gal/min)	ΔP (psia)
0.304	10.000
0.303	9.979
0.305	9.990
0.306	9.954
0.306	9.963
0.304	9.951
0.305	9.964
0.256	8.951
0.258	8.964
0.259	8.953
0.261	8.955
0.259	8.950
0.266	8.943
0.267	8.934
0.266	8.938
0.266	8.941
0.265	8.938
0.266	8.939
0.240	8.083
0.238	8.054
0.237	8.061
0.236	8.063
0.236	8.083
0.237	8.096
0.239	8.086
0.237	8.075
0.239	8.065
0.239	8.056
0.240	8.061
0.238	8.055
0.201	7.063
0.205	6.763
0.200	6.765
0.202	6.785
0.202	6.661

Q (gal/min)	ΔP (psia)
0.173	5.870
0.175	5.874
0.173	5.865
0.174	5.869
0.172	5.876
0.171	5.880
0.173	5.881
0.173	5.888
0.175	5.900
0.172	5.901
0.173	5.910
0.173	5.896
0.173	5.908
0.171	5.904
0.173	5.914
0.171	5.908
0.172	5.919
0.174	5.924
0.173	5.919
0.171	5.915
0.173	5.911
0.128	4.466
0.128	4.489
0.129	4.490
0.128	4.488
0.129	4.483
0.130	4.484
0.128	4.471
0.127	4.469
0.130	4.459
0.128	4.453
0.128	4.446
0.129	4.445
0.129	4.431
0.079	2.754

Table C60—Experimental Pressure Drop – Flow rate Mixture Test 9 Temperature Average =120°F

Q (gal/min)	ΔP (psia)
0.325	9.881
0.328	9.901
0.326	9.874
0.327	9.865

Q (gal/min)	ΔP (psia)
0.326	9.846
0.328	9.849
0.285	8.880
0.279	8.884
0.282	8.859
0.284	8.879
0.279	8.496
0.280	8.499
0.279	8.513
0.279	8.505
0.279	8.499
0.279	8.476
0.278	8.495
0.278	8.496
0.277	8.501
0.279	8.503
0.278	8.516
0.278	8.500
0.277	8.495
0.277	8.486
0.275	8.506
0.277	8.508
0.276	8.500
0.277	8.509
0.277	8.513
0.276	8.528
0.277	8.529
0.276	8.494
0.278	8.485
0.277	8.510
0.276	8.511
0.277	8.505
0.278	8.520
0.276	8.516
0.276	8.523
0.275	8.498
0.277	8.508
0.277	8.510
0.277	8.520
0.277	8.519
0.276	8.525
0.279	8.539
0.277	8.529
0.278	8.515
0.277	8.506

Q (gal/min)	ΔP (psia)
0.277	8.515
0.278	8.506
0.277	8.515
0.278	8.515
0.276	8.514
0.277	8.525
0.277	8.508
0.276	8.523
0.277	8.504
0.277	8.526
0.277	8.511
0.278	8.526
0.277	8.529
0.277	8.525
0.278	8.533
0.279	8.534
0.278	8.535
0.279	8.520
0.278	8.520
0.278	8.516
0.279	8.516
0.278	8.531
0.276	8.513
0.277	8.525
0.277	8.514
0.276	8.503
0.278	8.518
0.277	8.504
0.277	8.515
0.278	8.511
0.278	8.515
0.277	8.509
0.278	8.544
0.279	8.526
0.275	8.504
0.279	8.511
0.278	8.515
0.277	8.514
0.279	8.514
0.278	8.521
0.279	8.540
0.279	8.525
0.278	8.520
0.276	8.526
0.281	8.530

Q (gal/min)	ΔP (psia)
0.277	8.524
0.278	8.488
0.277	8.500
0.276	8.514
0.278	8.525
0.277	8.521
0.278	8.509
0.277	8.501
0.278	8.515
0.278	8.519
0.278	8.521
0.278	8.501
0.278	8.508
0.277	8.510
0.277	8.529
0.277	8.518
0.277	8.494
0.277	8.499
0.279	8.536
0.276	8.528
0.277	8.495
0.278	8.494
0.278	8.486
0.277	8.526
0.277	8.498
0.278	8.515
0.278	8.510
0.278	8.534
0.277	8.525
0.277	8.510
0.278	8.501
0.277	8.529
0.277	8.518
0.275	8.506
0.277	8.511
0.277	8.506
0.279	8.529
0.275	8.525
0.277	8.519
0.277	8.505
0.276	8.491
0.277	8.505
0.278	8.511
0.276	8.516
0.278	8.550

Q (gal/min)	ΔP (psia)
0.280	8.541
0.278	8.543
0.275	8.530
0.277	8.516
0.277	8.513
0.277	8.524
0.277	8.524
0.275	8.526
0.277	8.533
0.278	8.535
0.277	8.538
0.276	8.526
0.278	8.539
0.277	8.538
0.276	8.546
0.278	8.550
0.276	8.513
0.276	8.519
0.275	8.513
0.275	8.495
0.275	8.508
0.275	8.489
0.276	8.496
0.276	8.514
0.252	7.830
0.251	7.815
0.250	7.835
0.253	7.839
0.253	7.835
0.253	7.838
0.252	7.829
0.230	7.083
0.229	7.155
0.230	7.139
0.231	7.130
0.231	7.130
0.232	7.123
0.232	7.128
0.232	7.120
0.231	7.124
0.232	7.110
0.233	7.096
0.232	7.091
0.233	7.094
0.184	5.651

Q (gal/min)	ΔP (psia)
0.184	5.660
0.184	5.660
0.184	5.660
0.184	5.661
0.186	5.649
0.186	5.644
0.186	5.648
0.184	5.645
0.186	5.651
0.187	5.648
0.186	5.628
0.171	5.368
0.148	4.545
0.150	4.539
0.149	4.531
0.149	4.531
0.148	4.526
0.147	4.523
0.147	4.534
0.148	4.533
0.148	4.543
0.147	4.540
0.149	4.543
0.150	4.549
0.146	4.546
0.149	4.546
0.149	4.550
0.149	4.554
0.148	4.551
0.147	4.553
0.146	4.553
0.148	4.551
0.147	4.551
0.096	3.194
0.097	3.055
0.099	3.065
0.096	3.024
0.096	3.020
0.098	3.018
0.097	3.009
0.097	3.004
0.097	3.000
0.095	2.993
0.097	2.971
0.096	2.975

Q (gal/min)	ΔP (psia)
0.097	2.985
0.096	2.983
0.097	2.978
0.097	2.971
0.096	2.969
0.034	1.143
0.034	1.143
0.033	1.143

Table C61—Experimental Pressure Drop – Flow rate Mixture Test 9 Temperature Average =130°F

Q (gal/min)	ΔP (psia)
0.323	8.760
0.323	8.750
0.324	8.754
0.307	8.368
0.308	8.373
0.273	7.429
0.272	7.428
0.239	6.475
0.238	6.490
0.215	5.881
0.216	5.871
0.214	5.854
0.175	4.826
0.153	4.559
0.151	4.150
0.088	2.655
0.116	3.228
0.115	3.219
0.115	3.214
0.077	2.218
0.076	2.184
0.034	1.138
0.032	0.998
0.031	0.988
0.032	0.978

Table C62—Experimental Pressure Drop – Flow rate Mixture Test 9 Temperature Average 140°F

Q (gal/min)	ΔP (psia)
0.365	8.545
0.365	8.549
0.365	8.556
0.319	7.494
0.318	7.488
0.319	7.491
0.320	7.493
0.285	6.641
0.284	6.646
0.284	6.645
0.256	6.000
0.256	5.995
0.205	4.844
0.205	4.824
0.205	4.819
0.159	3.751
0.157	3.764
0.158	3.768
0.110	2.664
0.109	2.663
0.109	2.661
0.051	1.356

Table C63—Experimental Pressure Drop – Flow rate Mixture Test 9 Temperature Average =150°F

Q (gal/min)	ΔP (psia)
0.449	9.176
0.449	9.194
0.406	8.470
0.398	8.541
0.397	8.516
0.397	8.513
0.397	8.501
0.398	8.508
0.399	8.515
0.378	8.045
0.378	8.028
0.344	7.329
0.342	7.305
0.316	6.729

Q (gal/min)	ΔP (psia)
0.316	6.723
0.316	6.726
0.278	5.951
0.280	5.945
0.279	5.935
0.280	5.940
0.256	5.485
0.256	5.486
0.257	5.490
0.256	5.478
0.256	5.466
0.210	4.476
0.209	4.488
0.176	3.785
0.177	3.779
0.143	3.465
0.140	3.005
0.139	3.003
0.090	1.955
0.087	1.940
0.036	0.950
0.036	0.859
0.036	0.854
0.438	9.208
0.443	9.199
0.445	9.220

Table C64—Experimental Pressure Drop – Flow rate Mixture Test 9 Temperature Average =150°F

Q (gal/min)	ΔP (psia)
0.016	0.366
0.456	8.991
0.478	8.995
0.478	9.010
0.476	9.001
0.478	9.021
0.477	9.010
0.476	9.023
0.474	9.001
0.475	9.023
0.475	9.024
0.474	9.033

0.476	9.026
0.475	9.015
0.474	9.031
0.472	9.019
0.474	9.020
0.474	9.011
0.472	9.008
0.474	9.050
0.473	9.029
0.473	9.031
0.474	9.010
0.473	9.001
0.473	9.000
0.437	8.360
0.432	8.394
0.429	8.378
0.430	8.363
0.431	8.395
0.433	8.396
0.414	8.000
0.416	8.024
0.415	8.039
0.367	7.049
0.367	7.058
0.369	7.059
0.367	7.056
0.368	7.046
0.366	7.049
0.364	6.996
0.343	6.629
0.342	6.644
0.342	6.643
0.342	6.643
0.344	6.641
0.343	6.630
0.345	6.629
0.325	6.224
0.324	6.198
0.324	6.185
0.322	6.184
0.324	6.194
0.323	6.195
0.323	6.186
0.322	6.190
0.322	6.189
0.322	6.199

0.324	6.203
0.326	6.204
0.325	6.205
0.324	6.196
0.325	6.199
0.300	5.740
0.301	5.739
0.299	5.739
0.299	5.750
0.301	5.744
0.299	5.741
0.298	5.749
0.298	5.758
0.267	5.165
0.268	5.164
0.268	5.154
0.269	5.149
0.267	5.159
0.268	5.151
0.269	5.150
0.270	5.144
0.237	4.571
0.238	4.554
0.239	4.558
0.237	4.563
0.238	4.555
0.238	4.543
0.239	4.541
0.237	4.550
0.238	4.559
0.236	4.540
0.206	3.951
0.178	3.446
0.179	3.433
0.177	3.421
0.153	2.968
0.152	2.961
0.125	2.470
0.124	2.399
0.090	1.814
0.089	1.791
0.090	1.793
0.093	1.813
0.039	0.880
0.038	0.813
0.040	0.810

0.037	0.808
0.037	0.800
0.469	8.980
0.484	8.966

Test 10

Table C65—Experimental Pressure Drop – Flow rate Mixture Test 10 Temperature Average 160°F

Q (gal/min)	ΔP (psia)
0.406	9.410
0.406	9.413
0.404	9.424
0.404	9.420
0.401	9.414
0.402	9.418
0.403	9.420
0.403	9.421
0.402	9.424
0.400	9.429
0.401	9.444
0.399	9.453
0.398	9.440
0.398	9.443
0.399	9.439
0.399	9.433
0.399	9.445
0.397	9.443
0.398	9.453
0.397	9.440
0.394	9.450
0.299	7.314
0.355	8.733
0.305	6.964
0.309	6.831
0.262	6.491
0.283	6.589
0.270	6.139
0.266	6.281
0.257	5.980
0.271	6.440
0.346	8.615
0.276	6.239
0.294	6.575

Q (gal/min)	ΔP (psia)
0.359	8.155
0.265	6.263
0.350	8.208
0.375	8.884
0.372	8.884
0.301	6.988
0.337	7.518
0.370	8.675
0.375	8.805
0.377	8.808
0.381	8.894
0.379	8.825
0.238	5.299
0.232	5.433
0.256	5.428
0.258	5.880
0.260	5.875
0.211	5.280
0.272	5.891
0.223	5.473
0.257	5.351
0.262	5.916
0.257	5.820
0.254	5.660
0.260	5.775
0.252	5.479
0.249	5.658
0.208	4.691
0.214	4.585
0.202	4.784
0.225	4.878
0.190	4.139
0.141	3.386
0.161	3.565
0.125	3.544
0.149	3.596
0.161	3.590
0.129	3.324
0.155	3.564
0.066	2.046
0.081	2.103

Table C66—Experimental Pressure Drop – Flow rate Mixture Test 10 Temperature Average 99°F

Q (gal/min)	ΔP (psia)
0.497	8.843
0.498	8.856
0.497	8.835
0.495	8.835
0.496	8.851
0.494	8.845
0.495	8.830
0.493	8.834
0.493	8.836
0.491	8.824
0.490	8.834
0.491	8.848
0.490	8.843
0.492	8.845
0.489	8.841
0.490	8.851
0.489	8.844
0.488	8.860
0.488	8.856
0.489	8.861
0.407	7.174
0.431	7.715
0.409	7.230
0.459	7.601
0.428	7.686
0.439	7.321
0.438	7.564
0.442	7.563
0.448	7.755
0.395	7.015
0.417	7.151
0.428	7.243
0.416	7.426
0.448	7.388
0.420	7.028
0.412	6.995
0.425	7.149
0.440	7.260
0.422	6.984
0.183	3.051
0.191	2.970

Q (gal/min)	ΔP (psia)
0.134	2.568
0.155	2.790
0.149	2.805
0.170	2.858
0.154	2.804
0.183	2.729
0.148	2.605
0.188	2.915
0.070	0.999
0.057	0.991
0.044	1.005
0.045	1.029
0.058	0.999
0.067	0.978
0.068	0.954
0.051	0.924
0.047	0.904
0.051	0.869
0.047	0.908
0.046	0.886
0.055	0.918
0.049	0.895
0.045	0.890
0.056	0.851
0.048	0.858

Table C67—Experimental Pressure Drop – Flow rate Mixture Test 10 Temperature Average =99°F

Q (gal/min)	ΔP (psia)
0.570	8.370
0.570	8.380
0.570	8.391
0.569	8.383
0.569	8.384
0.570	8.396
0.569	8.386
0.570	8.400
0.567	8.391
0.570	8.390
0.569	8.389
0.569	8.400

Q (gal/min)	ΔP (psia)
0.570	8.411
0.570	8.413
0.567	8.398
0.568	8.401
0.569	8.409
0.567	8.421
0.564	8.423
0.564	8.438
0.563	8.430
0.562	8.429
0.560	8.429
0.560	8.438
0.562	8.435
0.501	6.984
0.493	7.011
0.518	7.240
0.493	6.894
0.504	7.039
0.497	6.893
0.513	7.123
0.526	7.143
0.504	6.989
0.530	7.125
0.537	7.176
0.457	6.219
0.439	6.039
0.453	6.215
0.427	5.976
0.446	6.194
0.426	6.279
0.454	6.396
0.462	6.431
0.432	6.121
0.365	5.136
0.367	5.191
0.390	5.374
0.370	5.296
0.257	3.679
0.383	5.219
0.299	4.214
0.430	5.774
0.422	5.591
0.352	5.315
0.394	5.405
0.397	5.398

Q (gal/min)	ΔP (psia)
0.371	5.264
0.396	5.484
0.401	5.444
0.241	3.808
0.288	3.840
0.268	3.694
0.148	2.235
0.161	2.358
0.169	2.330
0.412	5.711
0.557	8.204
0.152	1.873
0.598	8.323
0.565	8.443
0.567	8.433
0.565	8.428
0.567	8.436
0.562	8.419
0.564	8.419
0.565	8.425
0.564	8.423
0.563	8.430
0.563	8.438
0.562	8.446
0.564	8.459
0.561	8.444
0.563	8.454
0.560	8.470
0.563	8.459
0.561	8.464
0.559	8.461
0.556	8.464

Table C68—Experimental Pressure Drop – Flow rate Mixture Test 10 Temperature Average =99°F

Q (gal/min)	ΔP (psia)
0.647	7.881
0.649	7.853
0.652	7.858
0.651	7.848
0.650	7.835
0.651	7.825
0.653	7.824

0.654	7.819
0.656	7.824
0.656	7.813
0.272	3.454
0.645	7.851
0.644	7.810
0.535	6.165
0.556	6.400
0.580	6.484
0.563	6.508
0.579	6.434
0.582	6.474
0.583	6.510
0.596	6.541
0.580	6.493
0.583	6.554
0.419	5.433
0.483	5.440
0.498	5.441
0.458	5.556
0.463	5.398
0.414	4.824
0.382	4.859
0.371	4.009
0.198	2.599
0.215	2.458
0.514	5.469
0.315	4.019
0.369	4.193
0.164	2.270
0.255	2.476
0.199	2.455
0.127	1.961
0.216	1.986
0.149	1.553
0.079	1.238
0.103	1.224
0.113	1.370
0.112	1.314
0.198	2.103
0.172	2.538
0.682	7.538

Test 11

Table C69—Experimental Pressure Drop – Flow rate Mixture Test 11 Temperature Average 119°F

Q (gal/min)	ΔP (psia)
0.164	8.454
0.166	8.445
0.166	8.554
0.163	8.428
0.164	8.438
0.165	8.445
0.167	8.464
0.168	8.424
0.167	8.441
0.167	8.455
0.170	8.548
0.167	8.246
0.140	6.781
0.130	6.420
0.131	6.431
0.132	6.438
0.132	6.434
0.132	6.429
0.133	6.425
0.133	6.409
0.133	6.409
0.133	6.408
0.133	6.405
0.106	5.086
0.097	4.698
0.096	4.684
0.098	4.684
0.096	4.684
0.064	3.345
0.042	2.154
0.041	2.131
0.043	2.120
0.043	2.104
0.040	2.085
0.040	2.068
0.041	2.055

Table C70— Experimental Pressure Drop – Flow rate Mixture Test 11 Temperature Average =137°F

Q (gal/min)	ΔP (psia)
0.518	8.783
0.523	8.758
0.522	8.734
0.527	8.709
0.530	8.695
0.536	8.681
0.538	8.666
0.401	6.541
0.391	6.443
0.387	6.430
0.388	6.436
0.392	6.429
0.389	6.405
0.391	6.394
0.393	6.376
0.396	6.369
0.393	6.351
0.395	6.341
0.397	6.320
0.269	4.285
0.272	4.279
0.271	4.241
0.268	4.229
0.264	4.178
0.266	4.158
0.264	4.136
0.265	4.128
0.265	4.109
0.266	4.096
0.263	4.088
0.265	4.066
0.148	2.304
0.149	2.296
0.145	2.278
0.145	2.264
0.141	2.250
0.144	2.244
0.142	2.230
0.098	1.544
0.063	1.019
0.059	0.983
0.057	0.943

Q (gal/min)	ΔP (psia)
0.056	0.896

Table C71—Experimental Pressure Drop – Flow rate Mixture Test 11 Temperature Average 158°F

Q (gal/min)	ΔP (psia)
0.669	7.791
0.668	7.775
0.668	7.784
0.670	7.771
0.671	7.764
0.673	7.770
0.674	7.761
0.672	7.754
0.673	7.734
0.675	7.729
0.674	7.739
0.588	6.803
0.500	5.850
0.521	6.095
0.524	6.136
0.524	6.124
0.523	6.113
0.524	6.108
0.524	6.114
0.529	6.091
0.523	6.079
0.526	6.071
0.528	6.083
0.526	6.079
0.527	6.074
0.529	6.063
0.529	6.068
0.527	6.068
0.524	6.030
0.529	6.051
0.530	6.061
0.526	6.041
0.527	6.041
0.529	6.030
0.527	6.039
0.380	4.356
0.380	4.364

0.383	4.370
0.381	4.371
0.382	4.368
0.382	4.358
0.382	4.349
0.379	4.338
0.172	2.015
0.174	2.013
0.172	1.989
0.170	1.989
0.170	1.983
0.170	1.970
0.167	1.965
0.077	1.229
0.065	0.815

Table C72— Experimental Pressure Drop – Flow rate Mixture Test 11 Temperature Average 100°F

Q (gal/min)	ΔP (psia)
0.757	7.193
0.754	7.164
0.757	7.179
0.757	7.173
0.756	7.168
0.756	7.171
0.756	7.168
0.756	7.170
0.758	7.170
0.758	7.168
0.755	7.151
0.759	7.164
0.754	7.165
0.758	7.155
0.756	7.146
0.759	7.150
0.760	7.149
0.760	7.154
0.763	7.166
0.762	7.165
0.762	7.149
0.764	7.160
0.762	7.138
0.765	7.136
0.764	7.118

Q (gal/min)	ΔP (psia)
0.765	7.059
0.672	6.343
0.671	6.350
0.671	6.370
0.669	6.324
0.671	6.346
0.676	6.339
0.676	6.315
0.673	6.299
0.673	6.270
0.499	4.644
0.501	4.643
0.498	4.626
0.501	4.628
0.500	4.620
0.502	4.620
0.503	4.610
0.502	4.618
0.465	4.260
0.246	2.246
0.244	2.224
0.245	2.224
0.239	2.208
0.240	2.210
0.241	2.196
0.239	2.205
0.239	2.201
0.240	2.203
0.237	2.209
0.237	2.213
0.240	2.221
0.234	2.194
0.761	7.118

Table C73—Experimental Pressure Drop – Flow rate Mixture Test 12 Temperature Average 118°F

Q (gal/min)	ΔP (psia)
0.561	8.630
0.557	8.636
0.556	8.626
0.558	8.609

Q (gal/min)	ΔP (psia)
0.560	8.611
0.562	8.605
0.560	8.599
0.566	8.590
0.567	8.598
0.564	8.585
0.563	8.588
0.567	8.594
0.562	8.563
0.456	6.811
0.366	5.901
0.368	5.909
0.365	5.896
0.372	5.889
0.366	5.881
0.366	5.869
0.372	5.870
0.371	5.863
0.370	5.855
0.373	5.841
0.271	4.318
0.266	4.253
0.264	4.244
0.269	4.243
0.266	4.240
0.267	4.234
0.263	4.226
0.272	4.233
0.144	2.348
0.130	2.141
0.129	2.138
0.125	2.124
0.129	2.123
0.127	2.119
0.130	2.119
0.125	2.115
0.126	2.114
0.129	2.109
0.124	2.101
0.125	2.108
0.129	2.098
0.127	2.085
0.126	2.079
0.122	2.071
0.126	2.069

Table C74—Experimental Pressure Drop – Flow rate Mixture Test 12 Temperature Average 127°F

Q (gal/min)	ΔP (psia)
0.650	7.986
0.650	7.975
0.658	7.965
0.654	7.931
0.661	7.926
0.659	7.916
0.431	5.260
0.470	5.860
0.471	5.850
0.469	5.846
0.473	5.829
0.475	5.835
0.474	5.820
0.472	5.806
0.448	5.503
0.369	4.524
0.365	4.523
0.366	4.525
0.364	4.513
0.366	4.526
0.369	4.525
0.364	4.524
0.203	2.500
0.156	2.049
0.156	2.050
0.158	2.039
0.156	2.029
0.154	2.016
0.157	2.009
0.152	1.975
0.153	1.973
0.152	1.963
0.153	1.950
0.149	1.943
0.147	1.939
0.146	1.931

Table C75—Experimental Pressure Drop – Flow rate Mixture Test 12 Temperature Average 140°F

Q (gal/min)	ΔP (psia)
0.747	7.278
0.654	6.411
0.648	6.423
0.652	6.416
0.649	6.396
0.652	6.380
0.652	6.378
0.653	6.360
0.657	6.363
0.617	5.735
0.517	4.979
0.515	4.984
0.519	4.951
0.520	4.946
0.519	4.926
0.520	4.941
0.521	4.933
0.520	4.926
0.522	4.921
0.522	4.925
0.522	4.925
0.519	4.913
0.524	4.915
0.523	4.919
0.524	4.924
0.523	4.926
0.527	4.929
0.520	4.923
0.524	4.931
0.519	4.933
0.526	4.921
0.525	4.915
0.523	4.921
0.520	4.934
0.518	4.931
0.521	4.943
0.524	4.944
0.521	4.921
0.521	4.936
0.520	4.953
0.351	3.341

Q (gal/min)	ΔP (psia)
0.351	3.346
0.350	3.355
0.352	3.360
0.349	3.365
0.347	3.365
0.347	3.374
0.351	3.371
0.219	2.124
0.223	2.169
0.229	2.271
0.221	2.199
0.207	2.168
0.213	2.169
0.216	2.175
0.090	0.890
0.085	0.870
0.088	0.865
0.084	0.854
0.079	0.843
0.078	0.833
0.077	0.806
0.072	0.768
0.073	0.774
0.074	0.765
0.068	0.720
0.066	0.704
0.066	0.695
0.066	0.703
0.065	0.688
0.064	0.675

Table C76—Experimental Pressure Drop – Flow rate Mixture Test 12 Temperature Average 160°F

Q (gal/min)	ΔP (psia)
0.556	4.513
0.556	4.508
0.561	4.514
0.379	3.053
0.382	3.051
0.378	3.048
0.307	2.420
0.306	2.433

Q (gal/min)	ΔP (psia)
0.306	2.434
0.302	2.415
0.302	2.410
0.304	2.441
0.306	2.426
0.304	2.415
0.304	2.414
0.193	1.520
0.192	1.513
0.188	1.513
0.189	1.509
0.187	1.504
0.188	1.498
0.187	1.493
0.187	1.488
0.831	6.668
0.828	6.646
0.831	6.653

Table C77—Experimental Pressure Drop – Flow rate Mixture Test 12 Temperature Average 128°F

Q (gal/min)	ΔP (psia)
0.738	7.345
0.745	7.360
0.741	7.351
0.739	7.375
0.738	7.388
0.740	7.379
0.735	7.391
0.639	6.465
0.639	6.540
0.638	6.559
0.634	6.548
0.632	6.555
0.634	6.550
0.633	6.561
0.634	6.553
0.634	6.551
0.633	6.553
0.631	6.549
0.632	6.554
0.631	6.563
0.635	6.569

0.637	6.571
0.636	6.561
0.634	6.561
0.631	6.564
0.632	6.580
0.637	6.575
0.637	6.580
0.639	6.593
0.639	6.585
0.483	4.926
0.417	4.293
0.418	4.310
0.419	4.324
0.420	4.318
0.416	4.321
0.291	2.999
0.190	1.905

Table C78—Experimental Pressure Drop – Flow rate Mixture Test 13 Temperature Average 138°F

Q (gal/min)	ΔP (psia)
0.692	6.456
0.689	6.461
0.696	6.460
0.690	6.501
0.689	6.506
0.695	6.504
0.692	6.493
0.691	6.501
0.689	6.495
0.689	6.484
0.691	6.505
0.690	6.513
0.686	6.504
0.691	6.491
0.689	6.494
0.691	6.514
0.504	4.615
0.504	4.650
0.503	4.659
0.502	4.658
0.504	4.651
0.500	4.656
0.502	4.655
0.403	3.761

Q (gal/min)	ΔP (psia)
0.251	2.284
0.250	2.324
0.250	2.358
0.250	2.356
0.250	2.349
0.247	2.343
0.249	2.345
0.252	2.348
0.768	7.354
0.777	7.158
0.777	7.164
0.772	7.179

Table C79 —Experimental Pressure Drop – Flow rate Mixture Test 13 Temperature Average 160°F

Q (gal/min)	ΔP (psia)
0.843	6.655
0.842	6.655
0.845	6.636
0.844	6.633
0.846	6.628
0.849	6.628
0.745	5.770
0.542	4.256
0.545	4.269
0.546	4.263
0.418	3.125
0.295	2.289
0.292	2.293
0.293	2.289
0.290	2.294
0.136	1.063

APPENDIX D

Calculations using type curves

The use of the type curve shown in Chapter V is presented here:

Example 1

Fluid type 1.0 lb/bbl welan gum

Fluid density ρ=8.30 lb/gal

Flow power law index n=0.382

Consistency index K = 0.0180 lbf-s^n/ft^2

For the prototype we can estimate the behavior of this fluid in the prototype sensor using the curve types.

1) Enter with the appropriate length of the device. For the prototype, the length is 8 inches. Proceed horizontally to the line indicating the opening angle. (3°)
   Proceed vertically downwards towards the next plot

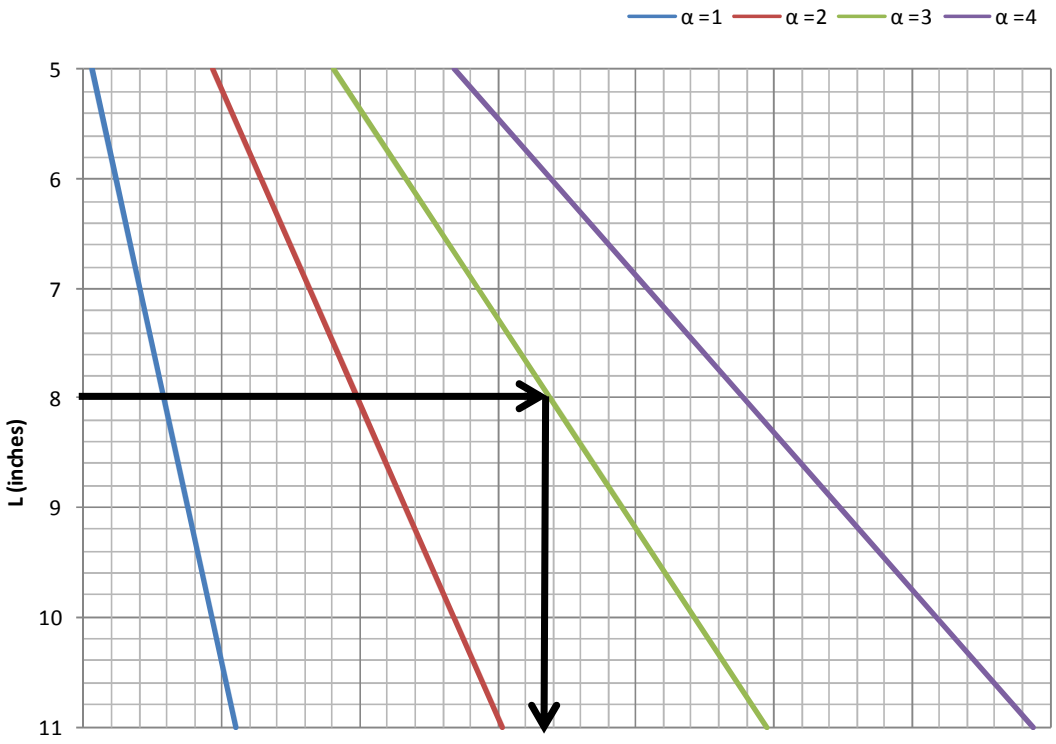

2) Continue drawing the line vertically until reaching the desired value of power-law index n (n= 0.387). Some visual interpolation is needed. Continue horizontally towards the next plot.

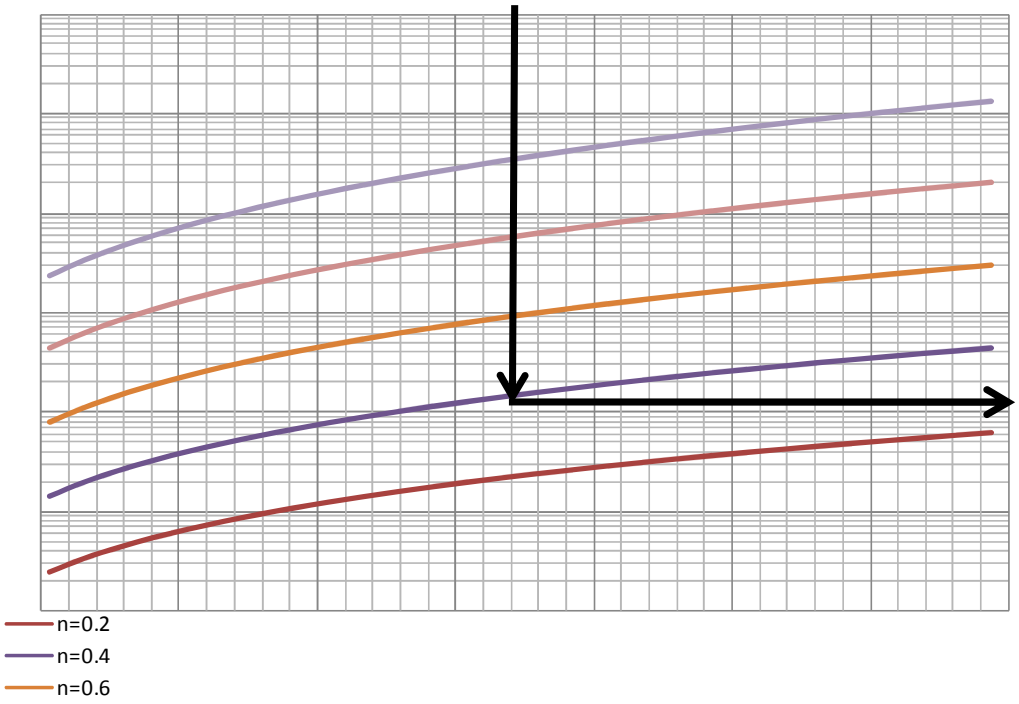

3) Proceed horizontally to the line indicating the opening angle. (3°) Proceed vertically downwards towards the next plot

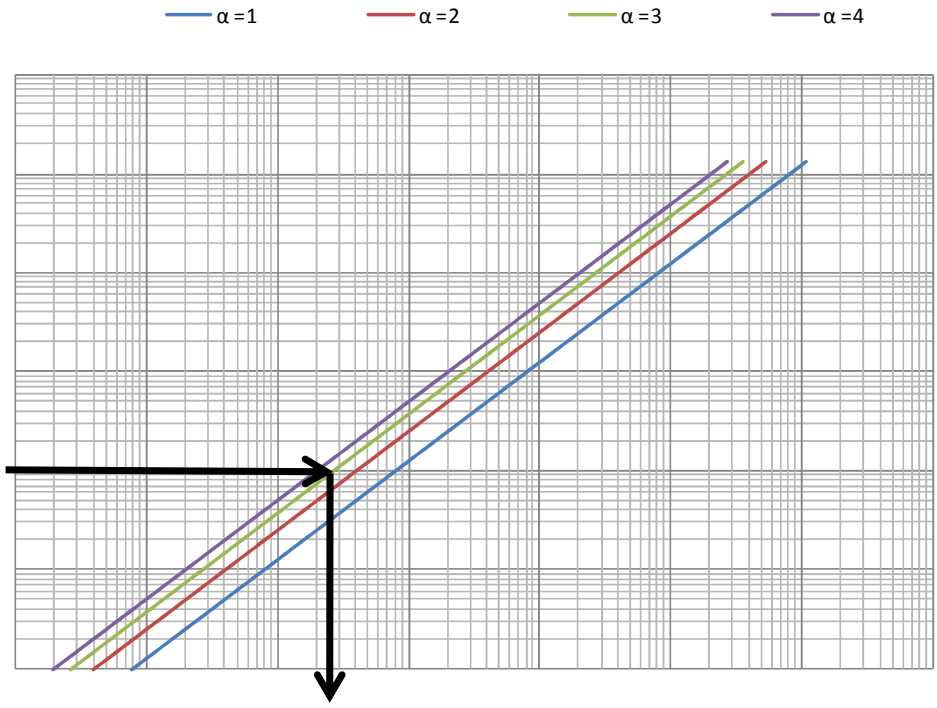

4) Proceed vertically until touching the sold black line. This line is a reference line.

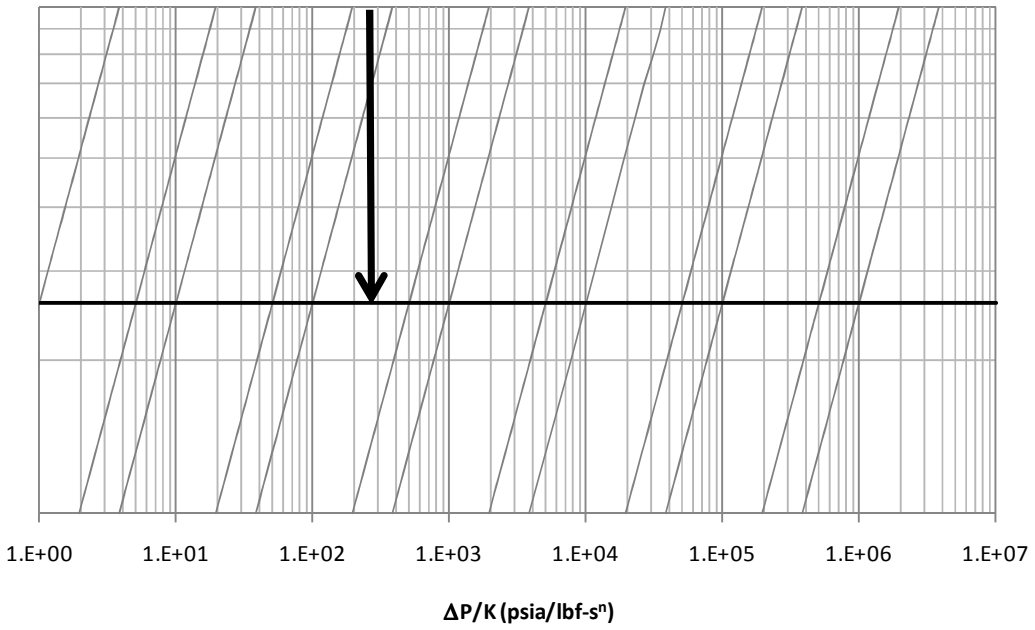

4) Draw a parallel line to the isolines in this plot. This line represents the range of $\frac{\Delta P}{K}$ for any flow rate Q.

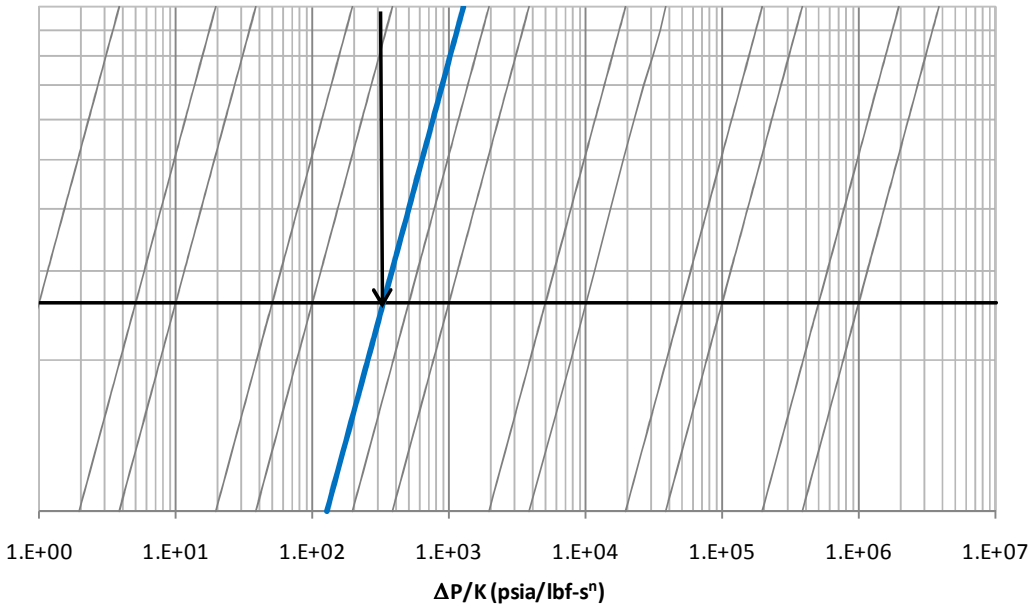

The range indicates that $100 < \frac{\Delta P}{K} < 1000$ approximately.

5) For example, for a flow rate of 0.5 gal/min, we enter vertically until we reach the isoline for the power law index n, (0.387). Some visual interpolation may be needed.

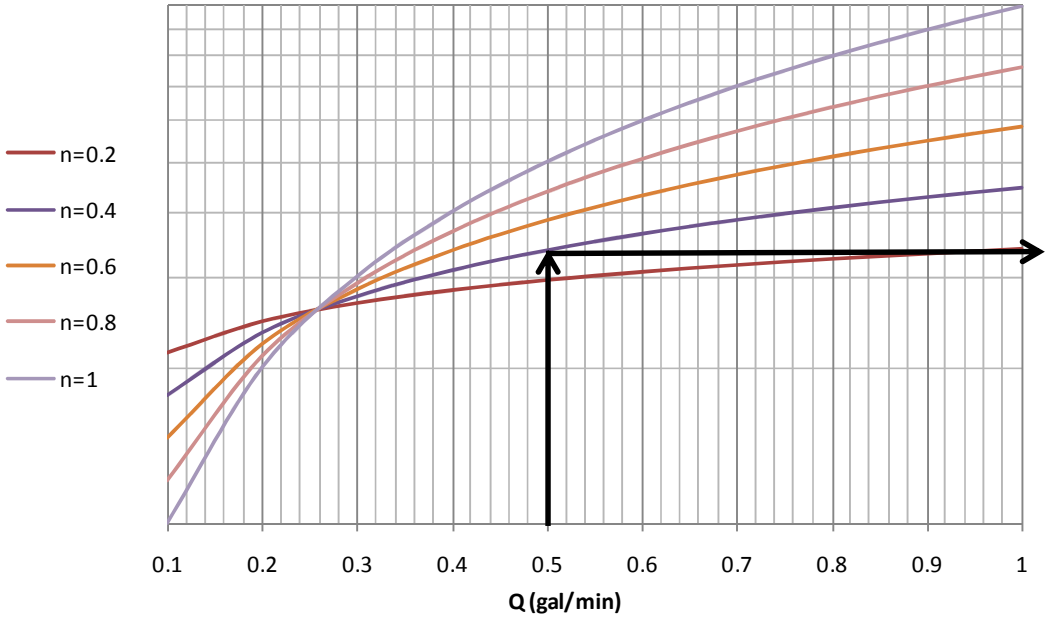

6). Continue the line horizontally until reaching the parallel line traced in step 4. proceed vertically and read the value $\frac{\Delta P}{K}$,

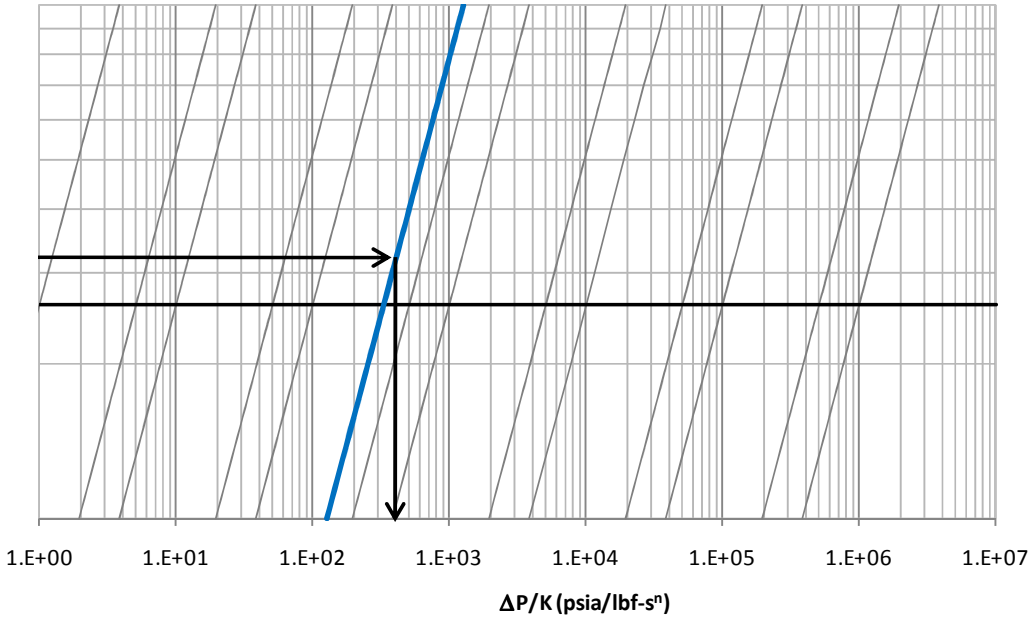

The value read from the scale is $\frac{\Delta P}{K}$

$$\frac{\Delta P}{K} = 400 \frac{\text{psi ft}^2}{\text{lbf - s}^n}$$

Since $K = 0.0180$ lbf-s^n/ft^2

At Q=0.5 gal/min → $\Delta P = 7.2$psi

The expected pressure drop is about 7 psi for this fluid in this prototype.

We can do the same for other flow rates and obtain a range of pressure drop. For example, at 0.1 gal/min and 1 gal/min

At Q=0.1 gal/min → $\frac{\Delta P}{K} = 220 \frac{\text{psi ft}^2}{\text{lbf - s}^n}$ $\Delta P = 3.96$psi

At Q=1 gal/min → $\frac{\Delta P}{K} = 600 \frac{\text{psi ft}^2}{\text{lbf - s}^n} \qquad \Delta P = 10.8\text{psi}$

Example 2

The RDT has a maximum flow rate of 1 gal/min at 500 psi differential.

What is the maximum viscosity that can be measured?

Recalling the expression for slot flow:

$$\Delta P = \frac{K}{72}(3.85Q)^n f_{slot}$$

At 1 gallon per minute and 500 psia

$$K = \frac{72 \times 500\text{psi}}{(3.85)^n f_{slot}}$$

f_{slot}, can be determined from the expressions provided.

For n=1

$$f_{slot} = 6.62074 \times 10^6 \frac{1}{\text{in}^{3n}}$$

Therefore

$$K = \frac{72 \times 500\text{psi}}{(3.85)^n \ 6.62074 \times 10^6 \frac{1}{\text{in}^{3n}}} = 1.4123 \times 10^{-3} \frac{\text{lbf} - \text{s}^n}{\text{ft}^2} = 67.62 \text{ cP}$$

For n=0.1

$$f_{slot} = 1627.23 \frac{1}{\text{in}^{3n}}$$

Therefore

$$K = \frac{72 \times 500\text{psi}}{(3.85)^n \, 1627..23} = 19.33 \frac{\text{lbf} - \text{s}^n}{\text{ft}^2}$$

If the device must be only 4 inches long, which dimensions r(0) or r_{fl} will result in the same maximum viscosity of 67 cp for a newtonian fluid?

Using the expressions for slot flow, and iterating with the $r_o(0)$, r_{fl}, We obtain the same factor for r_{fl} =0.11 ro(0) = 0.52 in

VITA

Name: Nolys Javier Rondon Alfonzo

Address: Department of Petroleum Engineering

Texas A&M University

3116 TAMU Richardson Building

College Station TX 77843

Education: Ph.D., Petroleum Engineering, Texas A&M, 2008

M.Eng., Petroleum Engineering, Texas A&M University, 2002

B.S., Petroleum Engineering, Universidad Central de Venezuela, 1999

Professional Affiliations: Society of Petroleum Engineers.